UNIVERSIDADE DE LISBOA

FACULDADE DE FARMÁCIA

NEW TARGETS AND THERAPEUTIC APPROACHES IN INHERITED METABOLIC DISORDERS

Sandra Dolores Arduim Brasil

DOUTORAMENTO EM FARMÁCIA

Biologia Celular e Molecular

2013

UNIVERSIDADE DE LISBOA

FACULDADE DE FARMÁCIA

NEW TARGETS AND THERAPEUTIC APPROACHES IN INHERITED METABOLIC DISORDERS

∞

NOVOS ALVOS E ABORDAGENS TERAPÊUTICAS EM DOENÇAS HEREDITÁRIAS DO METABOLISMO

Research Advisors: Professora Doutora Isabel Antolin Rivera,
Professora Doutora Paula Leandro e Professora Doutora Belén Pérez

Sandra Dolores Arduim Brasil

Lisboa

2013

Dissertação apresentada à Faculdade de Farmácia da Universidade de Lisboa para obtenção do grau de Doutor em Farmácia (Biologia Celular e Molecular).

De acordo com o disposto no ponto 1 do artigo nº41 do Regulamento de Estudos Pós-Graduados da Universidade de Lisboa, deliberação nº93/2006, publicada em Diário da República – II série nº153 – 5 de Julho de 2003, a autora desta dissertação declara que participou na conceção e execução do trabalho experimental, interpretação dos resultados obtidos e redação dos manuscritos.

The studies presented in this thesis were performed at Research Institute for Medicines and Pharmaceutical Sciences (iMed.UL), Faculty of Pharmacy, University of Lisbon – Portugal, and at Centro de Biología Molecular Severo Ochoa (CBMSO), Universidad Autónoma de Madrid – Spain, under the scientific supervision of Professor Isabel Antolin Rivera, Professor Paula Leandro and Professor Belén Pérez.

Sandra Dolores Arduim Brasil is the recipient of a Ph.D. fellowship (SFRH/BD/45753/2008) from Fundação para a Ciência e Tecnologia (FCT), Lisbon, Portugal.

“Somewhere, something incredible is waiting to be known.”

Carl Sagan

ACKNOWLEDGMENTS

Nesta secção gostaria de agradecer a todas as pessoas que de alguma forma contribuíram direta ou indiretamente para este trabalho que se realizou entre o iMed.UL em Lisboa e o Centro de Biología Molecular Severo Ochoa em Madrid.

Research Institute for Medicines and Pharmaceutical Sciences (iMed.UL):

Em primeiro lugar gostaria de agradecer à Professora Doutora Isabel Tavares de Almeida por me ter aceite no seu grupo de investigação e por me proporcionar todas as condições necessárias à realização deste trabalho.

Às minhas orientadoras, Isabel Rivera e Paula Leandro, a quem agradeço todo o apoio ao longo da realização desta tese. Professora Isabel, antes de mais, obrigado por me acompanhar desde os meus primeiros passos na vida de laboratório, por todo o seu apoio ao longo desta tese, por estar sempre presente e disponível mesmo longe, e por ter sempre uma palavra de carinho e amizade. Professora Paula, obrigado por todo o apoio, atenção e por ter sempre um sorriso.

Às Professoras Maria João Silva, Fátima Ventura, Rita Castro, Margarida Silva e Margarida Leite por me terem recebido no laboratório.

A todos os colegas que fizeram ou fazem parte do grupo Met&Gen: à Cátia, Inês, Mónica, Paula, Sara, Andreia, Ruben R, Marisa, Ruben S, Cristina, Madalena, Paulo, Fábio, Marco, Israel, João, Ana Serrão e Sílvia por todos os bons momentos no laboratório, pelo apoio, pelas gargalhadas, pelos cafés e lanches, amigos invisíveis e festas e, acima de tudo, por me acompanharem ao longo do tempo. Um obrigado especial à Ana Pinheiro por todo o apoio, amizade e todos os ensinamentos no meu ano de estágio e à Ana Isabel pelos bons momentos dentro e fora do laboratório, e por fazer da sua casa a minha casa.

Gostaria também de agradecer à Fundação para a Ciência e Tecnologia por me ter concedido a bolsa de doutoramento (SFRH/BD/45753/2008) sem a qual este trabalho não teria sido possível.

∞

Centro de Biología Molecular Severo Ochoa:

Me gustaría empezar por agradecer a la Profesora Magdalena Ugarte por darme la oportunidad de hacer parte de su grupo y trabajar en su laboratorio.

A mi coordinadora de tesis, Belén Pérez, por todo el apoyo en el laboratorio, por todos los consejos y por confiar en mí.

A Lourdes y Pilar por la ayuda y palabras de apoyo. A Alex y Eva por toda la ayuda, por contestar todas mis dudas, por tener siempre una sonrisa y palabras de apoyo.

A Fá por enseñarme, acogerme y nombrarme “su cobalamina”. Por ser tan dulce y por tener siempre una sonrisa. A Rosa, por haberme enseñado, por ser tan paciente y por todo el cariño. Gracias a las dos por todas las conversaciones, risas y momentos compartidos. A Ascen por toda la disponibilidad en contestar todas mis dudas y por ayudarme, especialmente en cultivos.

A todo el CEDEM. A Bego y Celia, por todo el apoyo. A Marga por la ayuda con el HPLC, a Pedro por la ayuda con el MS/MS, a María Jesús, Paloma, Fernando, Isaac, Charo, Leticia, Marina y Manu. A todos en secretaría, Isa, Ana, Paco, Susana, en especial a Eva y Julia, por tener siempre una sonrisa y a Gonzalo por toda la ayuda y por los buenos momentos fuera del labo. A Ana Vega y Ana Jorge por haber compartido mis primeros tiempos en el labo y por haberme enseñado.

A los lokis del 204. A Rocio, Patri, Lorena, Pachu, Alfonso, Celia, Raquel, Cristina y Pablo. Gracias por ser como sois, por acogerme, por compartir conmigo tantos momentos dentro y fuera del laboratorio. Por aturarme en mis malos días y hacerme reír, por ayudarme siempre, por toda la amistad y cariño. Sois únicos y os quiero MUCHO.

A Kristel por ser tan dulce como sus cupcakes y por todo el cariño demostrado desde el inicio. A Maja por toda la ayuda con la ATR, por las sugestiones de trabajo y por ser tan maja.

A todos los que han pasado por el labo. A Sven y Borja por toda la ayuda, a Paula por la tranquilidad, a Virginia, Elena y Ester por ser tan simpáticas y integrarse tan bien, a Liliana por compartir saudades conmigo, a Cristina, Ana, Irene y Ainhoa por llenar de vida el laboratorio.

∞

I would also like to thank Professor Beat Thöny and all in his lab for collaborating in a part of this work.

∞

A Pedro y Maria por toda la ayuda, el cariño y por tantos momentos buenos.

À Andreia, Catarina, Jaime e Rita, por quatro anos de faculdade com muitas noitadas de trabalho, mas cheios de bons momentos e por estarem sempre presentes apesar de geograficamente longe.

À gera de 85 e adotados. Eli, Vanda, Iolanda, Joana, Diana, Belisa, Hugo, Teixeira, obrigado por estarem sempre comigo desde que me lembro e por serem sempre um apoio constante. Este caminho não teria sido o mesmo sem vocês. Ao Fábio por ser meu “irmão”.

A toda a minha família, em especial os meus Pais a quem devo tudo o que sou e às minhas Irmãs que estão sempre ao meu lado. Obrigada por tudo!

Ao Helder, por tudo o que compartilhámos ao longo destes anos e para os quais não há palavras suficientes.

TABLE OF CONTENTS

INDEX

FIGURES

TABLES

ABBREVIATIONS

ABBREVIATIONS

A	adenosine
AdoCbl	adenosylcobalamin
Arg	arginine
ADP	adenosine diphosphate
AMO	antisense morpholino oligonucleotide
AON	antisense oligonucleotide
ATP	adenosine triphosphate
ATR	ATP:Cob(I)alamin adenosyltransferase
BBB	blood brain barrier
BDGP	Berkeley Drosophila Genome Project
BH_4	6R-L-erythro-5,6,7,8-tetrahydrobiopterin
bp	base pairs
BSA	bovine serum albumin
C	cytidine
Cbl	cobalamin
Ca^{2+}	calcium ion
cDNA	complementary DNA
Chr	chromosome
CNS	central nervous system
CoA	coenzyme A
Cys	cysteine
DMSO	dimethyl sulfoxide
DNA	deoxyribonucleic acid
DTT	dithiothreitol
EDTA	ethylenediamine tetraacetic acid
EURORDIS	European Organization for Rare Diseases
fs	frame-shift
G	guanosine
gDNA	genomic DNA
Gln	glutamine
Glu	glutamic acid
GS	gas chromatography
H_2DCFDA	2',7'-dichlorodihydrofluorescei diacetate
HGMD	Human Genome Mutation Database
His	histidine
HPLC	high-performance liquid chromatography
Ile	isoleucine
INFγ	interferon-gamma
LB	Luria Broth medium
Leu	leucine
LNA	locked nucleic acid

Lys	lysine
MeCbl	methylcobalamin
MEM	minimum essential medium
MMA	isolated methylmalonic acidúria
MMAA	methylmalonic aciduria cblA type
MMAB	methylmalonic aciduria cblB type
MMACHC	methylmalonic aciduria cblC type with homocystinuria
MMADHC	methylmalonic aciduria cblD type with homocystinuria
mPTP	mitochondrial permeability transition pore
mRNA	messenger RNA
MS/MS	tandem mass spectrometry
MUT	methylmalonic aciduria *mut* type
OCR	oxygen consumption rate
OHCbl	hydroxycobalamin
ORF	open reading frame
p53	cellular tumor antigen p53
PBS	saline phosphate buffer
PCR	polymerase chain reaction
PDB	Protein Data Bank
PTC	premature termination codon
RNA	ribonucleic acid
ROS	reactive oxygen species
SD	standard deviation
SDS	sodium dodecyl sulfate
SDS-PAGE	sodium dodecyl sulfate polyacrylamide gel electrophoresis
Ser	serine
T	thymidine
Thr	threonine
TNFα	tumor necrosis factor alpha
Trp	tryptophan
Val	valine

ABSTRACT

Inherited metabolic disorders (IMDs) are rare autosomal recessive disorders, showing a high allelic and phenotypic heterogeneity. The main therapeutic goal in these disorders is to restore the metabolic balance and, until now, most available therapies are not definitive and only alleviate the patients' symptoms.

In this work, three IMDs were analyzed, two organic acidurias, propionic and methylmalonic acidurias, and one aminoacidopathy, pyruvoyltetrahydropterin synthase.

Organic acid disorders or organic acidurias (OAs) are characterized by the excretion of non-amino organic acids in urine. Two of the most common OAs are propionic and methylmalonic acidurias. These two disorders are caused by defects in the oxidation pathway of propionyl-CoA into succinyl-CoA that enters the tricarboxylic acid cycle. Propionic aciduria is caused by mutations affecting the *PCCA* or *PCCB* genes that encode the subunits of the propionyl-CoA carboxylase enzyme, while methylmalonic aciduria is caused by mutations affecting not only the *MUT* gene but also the genes encoding the proteins involved in the trafficking and synthesis of the enzyme cofactor, adenosylcobalamin (AdoCbl). Until now, 9 different complementation groups have been identified, but only four, *mut*, *cblA*, *cblB* and *cblD* variant 2 are responsible for a phenotype of isolated methylmalonic aciduria. Pyruvoyltetrahydropterin synthase deficiency is caused by defects in the *PTS* gene that encodes the enzyme pyruvoyltetrahydropterin synthase (PTPS), which catalyzes the second step of the *de novo* tetrahydrobiopterin (BH_4) synthesis.

In this work four methylmalonic *cblD* variant 2 type, one methylmalonic *mut* type and two propionic patients of Spanish and Portuguese origin were genetically characterized, revealing the presence of three novel (c.165_166del2, c.170G>A and c.10-1G>C) and one already described (c.57_64del8) mutations in *cblD* variant 2 type patients, two novel mutations (c.244dupA and c.1408-10A>G) in the *mut* type patient and two already described mutations (c.1218del14ins12 and c.183+3G>C) in the propionic patients.

The functional analysis of three missense mutations (p.His183Leu, p.Arg186Trp and p.Glu193Lys), and two in-frame mutations (p.Ile117_Gln118del and p.Arg190dup) affecting the *MMAB* gene (*cblB* complementation group) revealed that all are disease causing, since the in-frame mutations are responsible for a complete lack of immunoreactive protein, while the missense mutations affect protein folding and stability.

The p.His183Leu and p.Arg190dup are novel mutations and were identified in two siblings presenting phenotypic differences. Analysis of these patients using a customized high-resolution comparative genomic hybridization assay (Metaboloarray®) and the analysis of the *MMAB* gene promoter regions did not reveal any other changes, while the analysis of fibroblasts derived from the patients revealed low protein levels when compared with

controls, and also differences in the protein levels between the siblings. The study of the mitochondrial protein quality control revealed elevated levels of mitochondrial Hsp70 in both patients and reduced Lon protease levels in one of the siblings.

Analysis of the mitochondrial function in these two *cblB* type patients, and also in two *mut* type patients, revealed mitochondrial impairment in all patients and, most importantly, a correlation between mitochondrial impairment and the phenotypic differences observed in the *cblB* type patients.

Finally, two different therapeutic approaches were assessed. The use of a pharmacological chaperone, *in vitro* upon missense mutations (p.His183Leu, p.Arg186Trp and p.Glu193Lys) affecting *MMAB* gene, and also *in vivo*, upon the wild-type protein. *In vitro* treatment with compound V increased the mutants' stability, and the *in vivo* treatment stabilized the wild-type protein in brain and liver without toxic effects.

A comparison of the stabilizing effect of the pharmacological chaperone and hydroxocobalamin (OHCbl) was also performed, showing a synergistic effect of both compounds upon the stability of wild-type and p.Ile96Thr mutant proteins in a cellular model.

The antisense therapy targeting pseudoexon inclusion in PTPS deficient patients was tested, and successfully restored the normal PTS splicing profile, immunoreactive protein levels, enzymatic activity and metabolic pathway in the three patients analyzed.

The results obtained with this work allowed the expansion of the known mutational spectrum in isolated methylmalonic aciduria, the characterization of novel mutants, as well as the identification of novel therapeutic targets.

Key words: Inherited metabolic disorders, mitochondrial impairment, pharmacological chaperone, antisense therapy.

RESUMO

As Doenças Metabólicas Hereditárias (DHMs) são doenças raras, transmitidas na sua maioria de forma autossómica recessiva, e que afetam o metabolismo intermediário. Embora a frequência individual de cada DHM seja baixa, quando analisadas no seu conjunto, estas doenças afetam cerca de 8% da população europeia.

As DHMs caracterizam-se por uma elevada heterogeneidade fenotípica e, até ao momento, as opções terapêuticas não corrigem as causas e apenas aliviam a sintomatologia dos doentes. Os recentes avanços científicos ampliaram o conhecimento das bases genéticas bem como da patofisiologia subjacente às DHMs, permitindo a procura e identificação de novas abordagens terapêuticas.

A classificação das DHMs é feita de acordo com a via metabólica afetada. Neste trabalho foram estudadas duas acidúrias orgânicas, acidúria propiónica e metilmalónica e uma aminoacidopatia, deficiência no enzima 6-piruvoil-tetrahidropterina sintase (PTPS).

As acidúrias propiónica e metilmalónica são duas das acidúrias orgânicas mais comuns e são causadas por defeitos na via metabólica que catalisa a oxidação do propionil-CoA em succinil-CoA, um intermediário do ciclo dos ácidos tricarboxílicos. A acidúria propiónica é causada por mutações nos genes *PCCA* ou *PCCB* que codificam as subunidades do enzima propionil-CoA carboxilase (PCC). Este enzima é responsável pela carboxilação do propionil-CoA em D-metilmalonil-CoA. Os doentes afetados apresentam um amplo espectro de manifestações clínicas caracterizado por acidose metabólica, cetose, hipoglicémia e hiperamonémia devido à acumulação de ácido propiónico e à depleção dos níveis de carnitina. O diagnóstico bioquímico consiste na deteção de níveis urinários elevados de 2-metilcitrato, ácido propiónico e 3-hidroxi-propionato, entre outros metabolitos, sendo a confirmação do diagnóstico realizada através de estudos enzimáticos ou de caracterização genética. O tratamento destes doentes passa pela restrição alimentar de aminoácidos percursores do propionil-CoA, administração de carnitina, biotina e cabamilglutamato, e também de metronidazol para reduzir a produção de propionato pela flora intestinal.

Por sua vez, a acidúria metilmalónica pode ter diversas causas: mutações no gene *MUT* que codifica o enzima metilmalonil-CoA mutase (MUT), responsável pela síntese de succinil-CoA a partir de L-metilmalonil-CoA, ou mutações em genes que codificam as proteínas responsáveis pela síntese e transporte do cofactor, adenosilcobalamina.

Até ao momento, foram identificados 9 grupos de complementação distintos, de acordo com as proteínas afetadas e o fenótipo apresentado pelos doentes, mas apenas quatro, *mut*, *cblA*, *cblB* e *cblD* variante 2, são responsáveis por um fenótipo de acidúria metilmalónica isolada. O grupo de complementação *cblA* é causado por mutações no gene *MMAA*, enquanto

mutações no gene *MMAB* são responsáveis pelo grupo *cblB*. O grupo de complementação *cblD* variant 2 é causado por mutações nos exões iniciais do gene *MMADHC*.

O diagnóstico de acidúria metilmalónica consiste na determinação de perfis metabólicos, em estudos enzimáticos e, finalmente, na caracterização genética. Estes doentes apresentam níveis elevados de ácido metilmalónico, 3-hidroxipropionato, 2-metilcitrato, lactato, propionilglicina e creatinina, tanto na urina como no plasma. O tratamento destes doentes passa também pela restrição alimentar, administração de vitamina B_{12} e carbamilglutamato, bem como suplementação com carnitina.

Mutações no gene *PTS* causam deficiência do enzima PTPS, responsável pela catálise do segundo passo da via de síntese *de novo* da tetrahidrobiopterina (BH_4). Estes doentes podem apresentar três fenótipos clínicos, classificados de acordo com a gravidade apresentada: central (deficit de BH_4 e neurotransmissores no sistema nervoso central e órgãos periféricos), periférico (deficit de BH_4 e neurotransmissores nos órgãos periféricos) e transitório.

Neste trabalho, realizou-se a caracterização molecular de vários doentes de origem espanhola e portuguesa: quatro doentes com acidúria metilmalónica pertencentes ao grupo *cblD* variante 2, um doente metilmalónico pertencente ao grupo *mut* e dois doentes com acidúria propiónica. Os resultados levaram à identificação de três mutações novas (c.165_166del2, c.170G>A e c.10-1G>C) e uma mutação já descrita (c.57_64del8) nos doentes tipo *cblD* variante 2, duas mutações novas (c.244dupA e c.1408-10A>G) no doente tipo *mut* e duas mutações já descritas (c.1218del14ins12 e c.183+3G>C) nos doentes propiónicos. Todas as mutações identificadas foram caracterizadas, tendo os resultados revelado que são muito provavelmente patogénicas e responsáveis pelo fenótipo clínico observado nos doentes.

A caracterização funcional das mutações no gene *MMAB*, que codifica o enzima adenosilcobalamina transferase (ATR), responsável pela síntese do cofactor do enzima MUT, adenosilcobalamina, revelou resultados dependentes do tipo de mutação. Assim, as três mutações *missense* (p.His183Leu, p.Arg186Trp e p.Glu193Lys) revelaram uma diminuição da estabilidade proteica, sugerindo uma possível deficiência no mecanismo de *folding*. As duas mutações *in-frame* (p.Ile117_Gln118del e p.Arg190dup) revelaram ser responsáveis por uma diminuição drástica dos níveis de proteína.

As mutações p.Arg183Leu e p.Arg190dup não se encontravam descritas na literatura e foram detetadas em dois irmãos pertencentes ao grupo *cblB* que, apesar do mesmo genótipo, apresentam diferenças fenotípicas significativas, sendo um deles assintomático e o outro apresentando níveis ligeiramente elevados de ácido metilmalónico. A sequenciação da região promotora do gene *MMAB*, bem como uma análise por hibridização genómica comparativa

(Metaboloarray®), não revelou nenhuma outra alteração genética. A análise dos níveis da proteína ATR nestes doentes revelou uma redução significativa em comparação com os controlos, bem como diferenças entre os dois irmãos. A análise indireta da atividade da proteína ATR em condições de stress (42°C) revelou uma redução significativa da mesma no irmão assintomático, indicando que as diferenças entre os dois irmãos poderiam estar relacionadas com diferenças na expressão de proteínas envolvidas no sistema de controlo de qualidade proteico. A análise posterior da expressão dos chaperones mitocondriais Hsp60, Hsp70 e da protease Lon, revelou níveis significativamente elevados do chaperone Hsp70 nos dois irmãos em comparação com o controlo e uma redução dos níveis da protease Lon foi observada no caso do irmão assintomático.

O conhecimento prévio da existência de disfunção mitocondrial em doentes com acidúria metilmalónica levou à análise da função mitocondrial nos dois irmãos tipo *cblB* e também em dois doentes pertencentes ao grupo de complementação *mut*. A análise dos níveis de espécies reativas de oxigénio (ROS), morfologia mitocondrial, função bioenergética e, por último, da formação/abertura do poro mitocondrial, revelou que todos os doentes apresentam uma redução da função mitocondrial quando comparados com os controlos. Observou-se uma correlação positiva entre a disfunção mitocondrial e as diferenças fenotípicas entre os dois irmãos, embora não se tenha detetado uma correlação entre os níveis de ácido metilmalónico e a diminuição da função mitocondrial.

Neste trabalho foram também estudadas duas abordagens terapêuticas diferentes, de acordo com o tipo de mutação presente. O uso de um chaperone farmacológico em doentes com acidúria metilmalónica tipo *cblB* causada por mutações missense, e de terapia *antisense* em doentes com deficiência no enzima PTPS causadas por mutações de *splicing*.

Estudos *in vitro* do efeito estabilizador de uma molécula, composto V, em mutantes *missense* (p.His183Leu, p.Arg186Trp e p.Glu193Lys), previamente caracterizados, revelaram um aumento da estabilidade proteica. O efeito do composto V foi também estudado *in vivo* sobre a proteína nativa, e observou-se um aumento dos níveis da proteína ATR em órgãos chave desta doença, como o fígado e o cérebro, e sem efeitos tóxicos aparentes. A comparação do efeito estabilizador obtido com o chaperone e o efeito estabilizador obtido com hidroxocobalamina (OHCbl), o cofator atualmente utilizado para tratamento, demonstrou um efeito sinergístico sobre a proteína nativa e o mutante *missense*, p.Ile96The, inicialmente utilizado para estudar o efeito do composto V.

A presença de mutações que afetam o mecanismo de *splicing* levando à introdução de pseudoexões, tal como se observou em doentes com deficit no enzima PTPS, levou ao uso de terapia *antisense* para recuperar o mecanismo normal de *splicing*. As abordagens passaram

pela utilização de vários tipos de sondas oligonucleotídicas antisense, tais como *antisense morfolino oligonucleotides* (AMOs), bem como *VIVO-morfolinos* e *locked antisense oligonucleotides* (LNAs), sendo o perfil normal de *splicing* recuperado com todos os oligonucleótidos utilizados. Para além da recuperação do perfil normal de *splicing*, foi possível recuperar ainda os níveis normais de proteína e atividade enzimática, bem como a normalização dos diversos compostos intermediários da via metabólica.

Os resultados obtidos com este trabalho permitiram, assim, a expansão do espectro mutacional da acidúria metilmalónica isolada, a caracterização funcional de novas proteínas mutantes, bem como a identificação de novas alternativas terapêuticas.

Palavras-chave: Doenças metabólicas hereditárias, disfunção mitocondrial, novas aproximações terapêuticas, chaperones, terapia antisense.

PART 1

INTRODUCTION and OBJECTIVES

1.1. INHERITED METABOLIC DISORDERS

Metabolism is the sum of all the biochemical processes and pathways in the body in which enzymes play a crucial role. Errors of metabolism are caused by congenital or acquired defects in the genes encoding those enzymes (genotype) causing an impaired function that leads to a disruption of the physiological homeostasis and, consequently, to clinical manifestations (phenotype). When the defect is hereditary we have inherited metabolic disorders (IMDs).

The term "inborn error of metabolism (IEM)" was coined more than a century ago by Sir Archibald E. Garrod during his studies on alkaptonuria (Garrod, 1975). The number of uncovered IEM has increased and, since then, more than five hundred different IEM have been identified (Martins, 1999).

The alterations found in hereditary metabolic disorders can be caused by substrate accumulation and/or its derivatives and also the shortage of a certain reaction product (Rao et al, 2009). The differences in the phenotypic manifestations observed depend on the severity of the alteration observed in the gene, the type and function of the affected enzyme, post translational mechanisms, cellular processes, genes in other *loci* that may also be affected and environmental factors. Due to all these factors, patients with IMD present a complex assembly of symptoms (Dipple and McCabe, 2000).

IMDs are considered rare disorders and, according to the European Organization for Rare Disease (EURORDIS), a disease is considered rare when 1 in every 2,000 inhabitants is affected (Orphan Drug Regulation 141/2,000). About 6,000 to 8,000 rare disorders are described and although the individual frequencies are low, collectively IMDs attain around 6 to 8% of the EU population.

IMDs are monogenic disorders with 67% displaying an autosomic recessive, 21% an autosomic dominant and 6% an X-linked pattern of inheritance; moreover, about 6% are related with defects in mitochondrial genome. In general, a high allelic heterogeneity is observed and the kind and intensity of clinical manifestations are related to the type of mutations detected (Pampols, 2010).

The major therapeutic goal in IMD is to re-establish the metabolic balance and, several strategies can be applied, either isolated or in combination. The first step is to either eliminate the accumulating substrate from the diet or to inhibit the enzymatic activity. The fast elimination of the toxic products from the body is also a common strategy. An increase of the residual enzymatic activity and the administration of the reaction end product in shortage are also therapeutic approaches (Raghuveer et al, 2006; Schwartz et al, 2008; Knerr et al, 2012).

In terms of medical care, treatment of IMD represents a significant challenge to the public health system and, until now, the majority of the available therapies are not definitive and only ameliorate the patient's symptoms.

The scientific achievements of the last years allowed uncovering more and more disorders, and also made possible a broader knowledge on the genetic and pathophysiological processes underlying IMD, thus paving the way to novel therapeutic strategies.

IMD can be classified according to the metabolic pathway in which the affected enzyme is involved. IMD can be divided into three major categories according to the pathophysiology; disorders that give rise to intoxication, disorders involving energy metabolism and disorders involving complex molecules (Saudubray et al, 2006a; Saudubray et al, 2006b). The first group is characterized by an acute or progressive intoxication due to a metabolic block and accumulation of toxic compounds, and includes inborn errors of amino acid metabolism, most organic acidurias, congenital urea cycle defects, sugar intolerances, metal intoxication and porphyrias (Saudubray et al, 2006a).

Organic acid disorders or organic acidurias (OAs) are characterized by the excretion of non-amino organic acids in urine. The majority of classic OAs are caused by abnormal amino acid catabolism of branched-chain amino acids or lysine (Deodato et al, 2006; Seashore, 2009).

The oxidation pathway of propionyl-CoA into succinyl-CoA is achieved by two mitochondrial enzymes, propionyl-CoA carboxylase and methylmalonyl-CoA mutase. Defects in the function of these enzymes are responsible for two of the most common OAs: propionic and methylmalonic acidurias (Figure 1) (Fenton et al, 2001; Pérez-Cerdá et al, 2004).

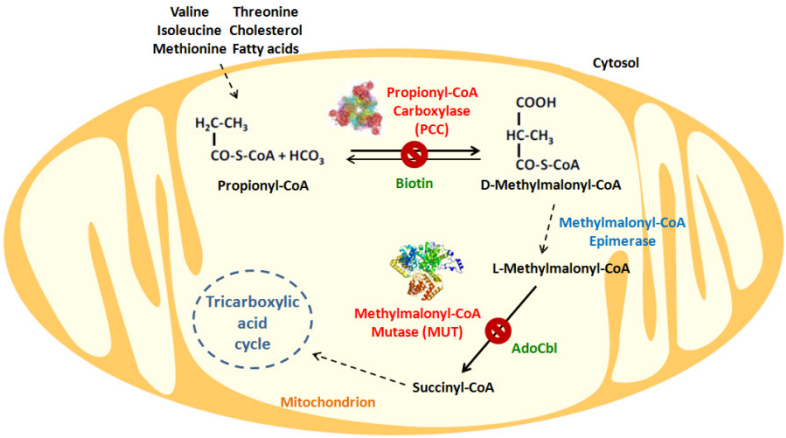

Figure 1– Oxidation pathway of propionyl-CoA into succinyl-CoA. Propionyl-CoA carboxylase catalyses the synthesis of D-methylmalonyl-CoA from propionyl-CoA and methylmalonyl-CoA converts L-methylmalonyl-Ca into succinyl-CoA. Methylmalonyl-CoA Epimerase catalyses the D to L dimerization. Defects in these enzymes are responsible for propionic and methylmalonic acidurias, respectively.

1.2. PROPIONIC ACIDURIA

Propionic aciduria (PA, MIM #606054) affects approximately one in every 30,000 new-borns around the world, although in some areas it can reach a higher incidence, and is caused by defects in the mitochondrial biotin-dependent enzyme propionyl-CoA carboxylase (PCC, E.C. 6.4.1.3) (Hofherr et al, 2009). Propionyl-CoA, originated from the catabolism of amino acids like valine, isoleucine, methionine and threonine, the catabolism of fatty acids and cholesterol, as well as from intestinal flora, is carboxylated to D-methylmalonil-CoA by propionyl-CoA carboxylase (Figure 1) (Campeau et al, 1999).

PCC is a heteropolimer composed of non-identical subunits α and β arranged in a α6β6 structure (Stankovics and Ledely, 1993). Each subunit is encoded by a different gene. The larger α subunit contains the union site to biotin and is synthesized by the *PCCA* gene (MIM *232000) located in chromosome 13q32 (Desviat et al, 2004; Ballhausen et al, 2009). This gene is composed of 24 exons ranging from 37 to 335 bp and the coding mRNA has an open reading frame of 2184 nucleotides that encodes a 728 amino acid protein (Kennerkcht et al, 1992; Campeau et al, 2001; Ballhausen et al, 2009).

The β subunit is encoded by the *PCCB* gene (MIM *232050) located in chromosome 3q13.3-q22 and is composed of 15 exons ranging from 57 to 183 bp. The coding mRNA has an open reading frame of 1617 nucleotides encoding a 539 amino acid protein (Ohura et al, 1993; Rodriguez-Pombo et al, 1998).

Mutations in any of the genes can cause PA and cells from patients with mutations in *PCCA* belong to the pccA complementation group, while those from patients with alterations in the *PCCB* gene belong to the pccB complementation group (Deodato et al, 2006). To date, 91 mutations have been described in *PCCA* and 95 different mutations in *PCCB* gene, being missense variants the prevalent type in both cases (HGMD® Professional 2013.1). Mutations are distributed along the gene sequence, although some clustering is observed in exon 13 in the *PCCA* gene and in exons 12 and 15 in *PCCB* gene, suggesting a hot spot for mutations (Desviat et al, 2004). None of the mutations detected in *PCCA* gene is predominant in Caucasians, while in *PCCB* gene a few mutations account for most cases and the mutation c.1218del14ins12 is the most common among Caucasians. Mutations c.1172_1173insT and p.Glu168Lys are also frequent, specifically in Spanish and Latin American populations (Desviat et al, 2004).

Clinical manifestations can present a neonatal-onset form or a late-onset form, but most of the affected individuals show a neonatal clinical onset of the disease (Pérez-Cerdá et

al, 2004; Deodato et al, 2006). Patients present a variable phenotype, characterized by mild to severe metabolic acidosis, ketosis, hyperlactacidemia, hypoglycemia and hyperammonemia due to the accumulation of propionate and low levels of free and total carnitine. Biochemical diagnosis is based on the characteristic profile of urinary organic acids that show elevations of 3-hydroxy-propionate, 2-methylcitrate and propionyl and tiglyl-glycine (Pérez-Cerdá et al, 2004; Desviat et al, 2004; Schwab et al, 2006).

Confirmation of the diagnosis can be achieved by enzymatic studies in lymphocytes and/or cultured fibroblasts or by molecular genetics (Pérez-Cerdá et al, 2004).

The treatment consists on dietary restriction of the precursor amino acids of propionyl-CoA, increase of caloric intake, avoidance of long-fasting periods, administration of carnitine to buffer intramitochondrial accumulation of propionyl-CoA, biotin and carbamylglutamate to improve hyperammonemia and metronidazole to reduce gut propionate produced by intestinal bacteria (Miyazaki et al, 2001; Deodato et al, 2006).

PA is a severe disorder with a poor survival rate on patients presenting an early-onset form and survivors may have developmental delay, nutritional problems and neurological impairment (Desviat et al, 2004).

1.3. ISOLATED METHYLMALONIC ACIDURIA

Methylmalonic aciduria (MMA) is caused by a complete or partial defect in the conversion of L-methylmalonyl-CoA into succinyl-CoA catalysed by the mitochondrial enzyme methylmalonyl-CoA mutase (MUT, EC 5.4.99.2), and also by defects in the genes encoding the proteins involved in the synthesis and transport of its cofactor, adenosylcobalamin (AdoCbl) (Figure 1) (Fowler et al, 2008; Takahashi-Iñiguez et al, 2012).

MUT is a dimer of identical subunits each containing two main functional domains. The amino terminal domain is composed by the leader sequence (residues 1 to 32) which targets the protein to the mitochondrion and a $(\beta\alpha)_8$ barrel (TIM-barrel) that spans residues 88 to 422 and contains the substrate binding site, and the carboxyl terminal domain that consists of a $(\beta\alpha)_5$ barrel, encompassing residues 578 to 750, and containing the cobalamin binding site. The two functional domains are connected by a linker region of 160 amino acids (Fenton et al, 2001; Acquaviva et al, 2005).

The MUT enzyme is encoded by the *MUT* gene (MIM *609058) located on chromosome 6p21 and is structured in 13 exons spanning more than 35 kb of genomic DNA (Jansen et al, 1989). The full-length messenger encodes a 750 amino acid protein with a

molecular weight of 88.2 kDa. The mature form of the protein lacks the mitochondrial leading sequence and has about 79 kDa (Thomä and Leadlay, 1996).

Until now, 242 different mutations have been described in the MUT gene being 68% of the missense type (HGMD® Professional 2013.1). Mutations have been found in all exons, but there seems to be a higher incidence in exons 2, 3, 6, 11 and 12, and some mutations have been found to be population specific. For example, the mutation p.Asn219Tyr is common in Caucasian patients and the c.671-678dup is found in many patients with Spanish origin (Acquaviva et al, 2005; Martinez, 2005; Worgan L et al, 2006).

As referred, MUT is dependent on adenosylcobalamin, a cofactor synthesized from cobalamin, an essential nutrient for cellular development (Padovani and Banerjee, 2009). Cobalamin is a complex organometallic cofactor with a corrin ring that donates four hydrogen atoms to a central cobalt atom and a bulky dimethylbenzimidazole (DMB) group. It can exist in the cell under three different conformational states: base-on or base-off according to the coordination state of the DMB group with cobalt, and base-off/His-on when the cobalt interacts with a histidine residue on the C-terminal of the MUT protein (Banerjee, 2006). The states base-off and base-off/His-on are the prevalent conformations and also the most physiologically relevant.

In mammals, only two proteins use cobalamin as cofactor, the mitochondrial MUT protein ,as already described, and the cytosolic enzyme, methionine synthase (MS EC 2.1.1.13) that uses methylcobalmin (MeCbl) to convert homocysteine into methionine (Yamanishi et al, 2005; Banerjee et al, 2009). Cobalamin is obtained from the diet and enters the cellular environment *via* a complex carrier-mediated import system that involves several different proteins. Somatic complementation studies using patients' cells allowed the establishment of nine different complementation groups: *cblA*, *cblB*, *cblC*, *cblD* (variant 1 and 2), *cblE*, *cblF*, *cblG*, *cblJ* and *mut* (Figure 2) (Gherasim et al, 2013a). The *mut* complementation group can be divided in two different categories according to the response to B_{12} supplementation by the patients' cells: mut^0 and mut^-. Patients belonging to the mut^0 group present very low or null MUT enzymatic activity and do not respond to B_{12} supplementation, while patients who belong to mut^- display some residual enzymatic activity and may respond to treatment with hydroxycobalamin (Fowler et al, 2008). Among the nine complementation defects, only four are responsible for a phenotype of isolated MMA: *mut*, *cblA*, *cblB* and *cblD* variant 2. Patients that belong to the *cblE*, *cblG* and *cblD* variant 1 present a biochemical phenotype of isolated homocysteinuria, while patients belonging to the *cblF*, *cblJ*, *cblC* and *cblD* groups present a combined phenotype of methylmalonic aciduria with homocysteinuria (Morel et al, 2005; Fowler et al, 2008; Kim et al, 2012).

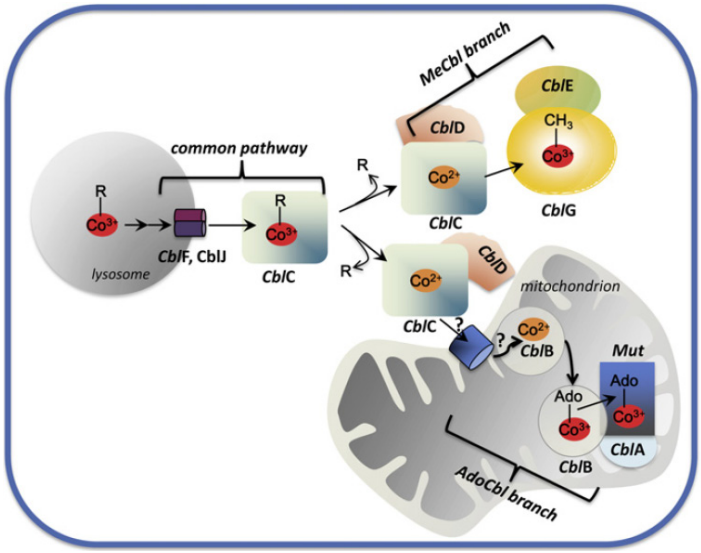

Figure 2 – Representation of the cobalamin trafficking pathway. The question marks denote the uncertainty of mechanism of cobalamin import to the mitochondrion and loading to the ATR protein. Adapted from Gherasim et al, 2013a.

1.3.1. Cobalamin defects causing isolated methylmalonic aciduria

Cellular cobalamin processing can be divided into two major pathways, cytosolic and mitochondrial. The protein responsible for cobalamin sorting for each of these pathways is MMADHC (for *M*ethyl*M*alonic *A*ciduria type *D* and *H*omo*C*ysteinuria) (Figure 2). The *MMADHC* cDNA has an ORF of 891 bp that is translated into a 296 amino acid protein with a predicted molecular mass of 32.8 kDa (Coelho et al, 2008). The protein presents a mitochondrial leader sequence (residues 1-11), a weakly conserved putative B_{12}-binding motif (GXXXHXD, residues 81-86) and a homologous region to the ATPase component of a bacterial ATP-binding cassette transporter (residues 78-168) (Coelho et al, 2008).

This protein is encoded by the *MMADHC* gene (MIM *611935), located in chromosome 2q23.2, and mutations affecting its function are responsible for the *cblD* complementation defect. This complementation group is the most complex of all because the patients present a clinical heterogeneity that can range from isolated homocystinuria (*cblD* variant 1), or isolated methylmalonic aciduria (*cblD* variant 2), to methylmalonic aciduria combined with homocystinuria (*cblD*) (Suormala et al, 2004). This heterogeneity provides strong evidence for its dual function in the cytoplasmatic and the mitochondrial pathways for cobalamin processing and assimilation, and is related with the location and type of the mutations affecting the gene (Coelho et al, 2008; Stucki et al, 2011). Mutations causing a premature translation stop codon toward the N-terminal of the protein are found in patients with *cblD*

variant 2, missense mutations located in the C-terminal of the protein are related to *cblD* variant 1, while nonsense and missense mutations affecting the middle and the C-terminal of the protein are related to *cblD* combined phenotype (Coelho et al, 2008; Stucki et al, 2011).

The observation of the three different phenotypes is explained by the existence of two additional initiation codons in the protein, located at positions 62 (methionine 62) and 116 (methionine 116). Therefore, mutations affecting residues located before Met62 or even Met116 only affect the protein region responsible for AdoCbl synthesis, originating a protein fully capable of MeCbl synthesis. Mutations downstream Met116 abolish the MeCbl synthesis, leaving AdoCbl synthesis intact. Mutations affecting patients with the combined phenotype are located in a short stretch of 14 amino acids towards the C-terminal of the protein. According to recent studies, this small region is one of the five putative sites of interaction between MMADHC and MMACHC protein (*cblC* complementation group) (Stucki et al, 2011).

It has been demonstrated that MMACHC interacts mainly with the C-terminal domain of MMADHC in the cytosol, indirectly assisting the transfer of cob(II)alamin to methionine synthase (Plesa et al, 2011).

The patients' clinical presentations are variable. Patients with the *cblD* combined phenotype present developmental delay, seizures, hypotonia, lethargy and megaloblastic anemia; patients with the *cblD* variant 1 present developmental delay, ataxia and megaloblastic anemia; and patients with the *cblD* variant 2 have respiratory distress, cranial hemorrhage, seizures and abnormal electroencephalograms (Miousse et al, 2009).

Until now, only 17 *cblD* patients have been described in the literature, making it the rarest complementation defect so far (Stucki et al, 2011).

The inactive cob(II)alamin then enters the mitochondrion and is adenosylated to its active AdoCbl form by ATP:Cob(I)alamin adenosyltransferase (ATR) (Maurice et al, 2008). ATR is encoded by the gene *MMAB* (for *M*ethyl*M*alonic *A*ciduria type *B*) located in chromosome 12q23.3 (Dobson et al, 2002a). Mutations affecting the correct processing of *MMAB* gene (MIM *607568) are responsible for the *cblB* defect (MIM #251110) (Dobson et al, 2002b). The most common mutation found in *MAAB* gene in European patients is p.R186W (about 33% of the mutant alleles) and is responsible for a severe clinical phenotype (Lerner-Ellis et al, 2006; Fowler et al, 2008).

ATR belongs to the PduO family and, in the presence of an electron supplied by a reductase, catalyses the reduction of bound cob(II)alamin to cob(I)alamin, which then displaces tri-phosphate (PPPi) from ATP to generate AboCbl. This reaction is

thermodynamically unfavourable but it is favoured by the base-off conformation which increases the redox potential (Yamanishi et al, 2005; Padovani and Banerjee, 2009).

ATR is a homotrimer where the monomer is a five-helix bundle. The α1 and α4 helices of each monomer associate to form the six-stranded coiled-coil core of the trimer, being the ATP-binding site at the interface between adjacent monomers. The active sites are located at the subunit interfaces and are distinctly different, since only two of them contain ATP and the other remains unlinked (Saridakis et al, 2004; Shubert et al, 2006; Fan et al, 2008).

Studies have shown that the binding of ATP to the N-terminus initiates the reaction by triggering a significant local reordering of the ATR structure. This forms a deep pocket that is postulated to be the cobalamin binding site. Next, cob(II)alamin binds to the enzyme's active site triggering the ordering of the C-terminus and the closure of a hinged lid, thus generating a four-coordinated cob(II)alamin intermediate. The final step is the electron transfer that generates the cob(I)alamin nucleophile, and AboCbl and PPi are formed in the active site (Maurice et al, 2008). The source of the electron used in the reduction reaction is still unknown (Mera et al, 2010).

The observation that ATR only uses two of the three active sites suggests a sequential rotary mechanism for the synthesis and delivery of AdoCbl (Figure 3). ATP binds to ATR sites 1 and 2 driving the catalysis of AdoCbl, while binding to site 3 provokes a conformational change in the adjacent subunit driving the cofactor transfer from site 1 to MUT, thus leaving one of the active sites empty in preparation for the next reaction (Padovani and Banerjee, 2009).

Based on these observations, ATR seems to serve both as an enzyme to synthesize AdoCbl and as an escort to deliver the cofactor to MUT, which presents a DXHXXG motif for base-off/His-on binding of cobalamin. The MUT histidine residue (His627), which serves as ligand, plays an essential role in the transfer of the cofactor and its mutation to another amino acid impairs the cofactor transfer (Yamanishi et al, 2005).

The assembly of AdoCbl to MUT is predicted to involve a GTP-dependent interaction with the MMAA protein. MMAA is coded by the *MMAA* gene (for *M*ethyl*M*alonic *A*ciduria type *A*) and, based on information from bacterial orthologs, belongs to the G3E family of P-loop GTPases. Mutations affecting the *MMAA* gene (MIM *607481) are responsible for the *cblA* complementation defect (MIM #251100) (Dobson et al, 2002b).

MMAA function is not completely clear. The observation that fibroblasts from *cblA* patients exhibit low AdoCbl content indicates that MMAA plays a role in the transfer of the cofactor from ATR to MUT and also in the maintenance of MUT's functional integrity, although the mechanism is not fully understood (Figure 3) (Banerjee et al, 2009; Froese et al, 2010).

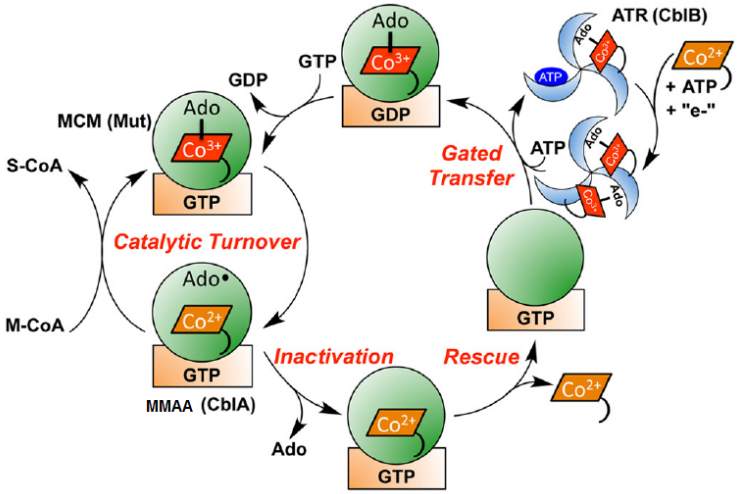

Figure 3 – Schematic model for the function of ATR, MMAA and MUT enzymes. ATR (blue wheel) synthesizes AdoCbl that is transferred to the MUT (green circle) active site in a reaction gated by the MMAA protein (orange rectangle). MMAA gating and rescue functions are highlighted. The loss of 5'-deoxyadenosine (Ado) from MUTs' active site leads to its inactivation and MMAA promotes the dissociation of cob(II)alamin, allowing the reconstitution of the mutase with the active cofactor. Adapted from Gherasim et al, 2013b.

The diagnostic approach to MMA involves metabolite analysis, genetic complementation and enzymatic studies and, finally, mutation analysis (Fowler et al, 2008). The first approach is the biochemical analysis of patients' urine or plasma, and elevated levels of methylmalonic acid, 3-hydroxypropionate, 2-methylcitrate, lactate, propionylglycine and creatinine are found (Morel, 2005; Fowler et al, 2008).

The treatment consists in dietary restriction, administration of vitamin B_{12}, *N*-carbamylglutamate, carnitine supplementation and, in the last years, liver or liver/kidney transplantation.

Patients that belong to the *cbl* complementation groups often respond to pharmacological doses of B_{12} vitamin, for instance *cblC*, *cblD* and *cblA* defects are treated with hydroxocobalamin, but patients belonging to *cblB* group show lower levels of positive response, with about only 40% of the *cblB* patients improving with B_{12} supplementation (Fowler et al, 2008).

Again, this treatment is not definite and it only ameliorates patient's symptoms, raising the need to search for new therapies and therapeutic targets.

1.4. MITOCHONDRIAL DYSFUNCTION IN ORGANIC ACIDURIAS

Mitochondria are essential organelles with a changing morphology and location in the cell. This phenomenon is dependent of fission and fusion processes that maintain structural integrity. Small spherical and oval mitochondria represent a fragmented or pro-fission state, whereas interconnected filamentous networks are a result of a pro-fusion phenotype (Galloway and Yoon, 2012; Shutt et al, 2012). They are involved in cellular bioenergetics and metabolic homeostasis, and the mitochondrial matrix contains a range of enzymes that play a role in the major metabolic pathways, like the tricarboxylic acid (TCA) cycle and the enzymatic machinery of oxidative phosphorylation (OXPHOS), responsible for adenosine triphosphate (ATP) production (Krauss, 2001; Kang and Pervaiz, 2012). Mitochondria are also involved in the regulation of redox and calcium (Ca^{2+}) signalling, fatty acid oxidation and iron metabolism (Wajner and Goodman, 2011).

OXPHOS relies on a series of respiratory complexes imbedded in the inner mitochondrial membrane: complex I (NADH-coenzyme Q reductase), complex III (coenzyme Q cytochrome c reductase), complex II (succinate-coenzyme Q reductase) and complex IV (cytochrome c oxidase) that catalyzes the last step of the electron transfer. Another component is ATP synthase (F_1F_0-ATPase) that uses the proton motive force to convert ADP and inorganic phosphate (Pi) to ATP which is then released into the matrix and can be transported to the cytosol by the adenine nucleotide translocase (ANT) (Figure 4).

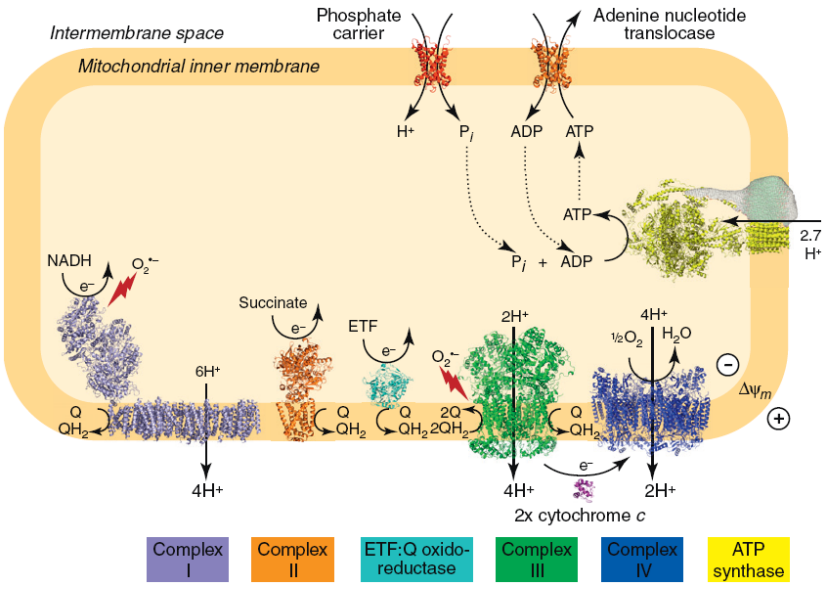

Figure 4– Mitochondrial respiratory chain. Q: oxidized ubiquinone, QH2: reduced ubiquinol, CoQ: coenzyme Q, Pi: phosphate, $\Delta\Psi m$: proton motive force. Adapted from Smith et al, 2012.

Side product of OXPHOS are reactive oxygen species (ROS), like hydroxyl radical (•OH), superoxide anion (O^{2-}) and hydrogen peroxide (H_2O_2), that are generated especially by complexes I and III, but also by complex II (Ma, 2010; Circu and Aw, 2010; Cardoso et al, 2012). These species are essential for a number of cellular reactions like inflammatory response, vascular function and oxygen sensing (Alfadda and Sallam, 2012), but show a high chemical reactivity and thus can cause non-specific cellular damage (Brieger et al, 2012). Therefore, cells have developed mechanisms for their neutralization like antioxidant enzymes and scavengers. The cell homeostasis is kept by a tight balance between the generation of ROS and the ability of protection systems to remove them. When this balance is disturbed, either by the overproduction of ROS or by a defect in the action of the antioxidant defence systems, damage is observed at protein, lipid and DNA levels constituting an important disease mechanism. When damage surpasses a threshold, cell is programmed to death by apoptosis, a mechanism central to homeostasis.

In an apoptotic event, and as a defence mechanism, mitochondria release apoptogenic signal molecules into the cytosol, a phenomenon called permeability transition (PT) that triggers the opening of a channel, the permeability transition pore (PTP), leading to loss of solutes with a molecular weight less than 1.5kDa (Wong et al, 2012; Brenner and Moulin, 2012).

Another trigger of PTP opening is the influx of Ca^{2+} into the cytosol, which leads to mitochondrial Ca^{2+} accumulation and consequent activation of respiratory dehydrogenases and oxidative phosphorylation (Kowaltowski et al, 2001).

Mitochondrial PTP (mPTP) structure is not clear and there have been many candidates, among them, adenine nucleotide translocase (ANT) and cyclophilin D (CyP-D). CyP-D is a hydrophobic protein capable of binding strongly to the inner mitochondrial membrane component and its activity is enhanced by the presence of ADP and reduced in the presence of Ca^{2+} ions. Cyclosporine-A (CsA) is an inhibitor of CyP-D and it has been shown to block mPTP formation. A set of studies have demonstrated that ANT and Cyp-D seem to act mainly as regulators rather than an integrant part of mPTP. It has also been postulated that the voltage-dependent anion channel (VDAC) plays an important role, but the observation that mitochondria from VDAC1 knockout mice possess a normal PTP has questioned this hypothesis (Javadov and Karmazyn, 2007; Arti et al, 2012).

mPTP seems to have a multiple and dynamic identity dependent on the cellular model, status and treatment, playing a key role in Ca^{2+} homeostasis in a conductance-dependent manner (Brenner and Moulin, 2012).

Oxidative stress caused by ROS has been implicated in the physiopathology of a palette of disorders, like cancer, autoimmune, neurodegenerative, mitochondrial and also organic acidurias, especially methylmalonic aciduria (Pieczenik and Neustadt, 2007; Richard et al, 2007; Chandler et al, 2009; Wajner and Goodman, 2011; Schapira, 2012; Gallego-Villar et al, 2012).

Mitochondrial dysfunction leading to high levels of ROS has been observed in liver, kidney and brain of MMA patients, and also in cultured skin tissues and mouse models, although the mechanism behind generation of ROS levels is not fully understood. The likeness of methylmalonic acid with the respiratory chain substrates lead to the hypothesis that methylmalonic acid was the main toxic metabolite in MMA, but it is now accepted that other metabolites, like 2-metylcitrate, may be involved (Richard et al, 2007; Mirandola et al, 2008; Chandler et al, 2009; Jafari et al, 2013).

1.5. PYRUVOYLTETRAHYDROPTERIN SYNTHASE DEFICIENCY

6*R*-L-erythro-5,6,7,8-tetrahydrobiopterin (BH_4) is an essential cofactor for several enzymes central to metabolic function, including four aromatic amino acid hydroxylases (phenylalanine hydroxylase, tyrosine hydroxylase, tryptophan hydroxylase type 1 and 2), alkyl glycerol mono-oxygenase and three NO synthase isoenzymes. It is also crucial in a number of biological and pathological processes associated with monoamine neurotransmitter formation, endothelial and cardiovascular dysfunction, immune response and pain sensitivity. It belongs to the pteridine family, specifically to the unconjugated pterin group that is characterized by a 2-amino-4-oxo structure. Biopterin is present in biological samples as biopterin, 7,8-dihydrobiopterin (BH_2) and BH_4 (Blau et al, 2008). BH_4 is synthesized *de novo* from GTP in a three steps, Mg^{2+}, Zn^{2+} and NADPH-dependent reaction. The first step is catalysed by GTP cyclohydrolase I (GTPCH). The second reaction, converting 7,8-dihydroneopterin triphosphate to 6-pyruvoyltetrahydropterin, is catalysed by pyruvoyltetrahydropterin synthase (PTPS) in a Mg^{2+} and Zn^{2+} dependent reaction. The final reaction is NADPH-dependent and is catalyzed by sepiapterin reductase (SR) that transforms 6-pyruvoyltetrahydropterin into BH_4 (Thöny and Blau, 2006).

BH_4 can also be obtained by two other pathways, the salvage and the alternative pathways that contribute to the BH_4 synthesis *in vivo* when SR activity is insufficient (Figure 5).

About 60% of all BH_4 deficiencies are caused by defects in the PTPS enzyme (Liu et al, 2008). PTPS is encoded by the *PTS* gene (MIM *612719) that maps to chromosome 11q22.3 – 11q23.3 and encompasses 6 exons with variable lengths. The messenger has an ORF of 662 bp with an ATG at position 10, coding a 145 amino acid protein with a molecular weight of 16.5

kDa. The stop codon is followed by a 198 bp untranslated region and an adjacent stretch of 17 adenines (Thöny et al, 1992; Nar et al, 1994).

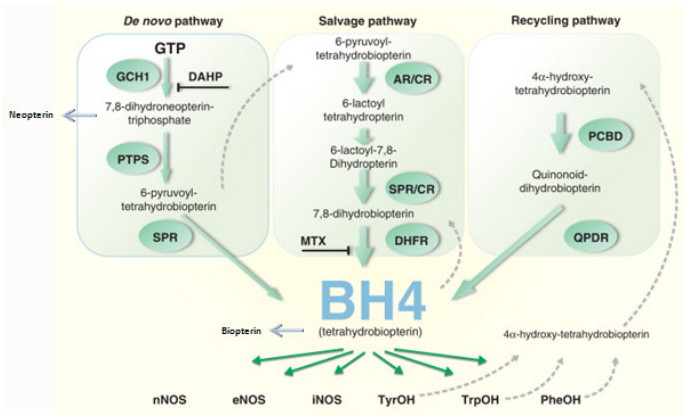

Figure 5 – Tetrahydrobiopterin synthesis, alternative and recycling pathways. nNOS, eNOS and iNOS: nitric oxide synthase enzymes, TyrOH: tyrosine hydroxylase, TrpOH: tryptophan hydroxylase, PheOH: phenylalanine hydroxylase, DAHP: 2,4-diamino-6-hydroxypyrimidine, MTX: methotrexate, GCH1: GTP cyclohydroxylase 1, PTS: 6-pyruvoyl tetrahydrobiopterin synthase, SPR: sepiapterin reductase, AR: aldose reductase, CR: carbonyl reductase, DHFR: dihydrofolate reductase, PCBD: pterin-4α-carbinolamine dehydratase, QDPR: quinonoid-dihydrobiopterin reductase. Adapted from Costigan et al, 2012.

PTPS is a hexamer of identical subunits, formed by the association of two trimers in a head-to-head association, leading to the active enzyme complex. The substrate-binding sites, six *per* active hexamer, are located close to the trimer interface. Each catalytic site is formed by two subunits from one trimer and by one subunit from the adjacent trimer, and contains a metal-binding site formed by three histidine residues (Oppliger et al, 2009).

PTPS deficiency presents an autosomic recessive mode of inheritance and is a phenotypically heterogeneous disorder. Patients with impaired PTPS activity can present three different clinical phenotypes, namely a central one presenting with a general lack of BH_4 in all organs and monoamine neurotransmitter shortage in the central nervous system (CNS); a peripheral one, where patients do not synthesize BH_4 in peripheral organs but have normal BH_4 and neurotransmitter levels in the CNS and, finally, a transient form that may disappear during infant thriving.

Until now, 52 different mutations have been identified, being missense the prevalent type. About 63% of all the mutant alleles identified so far are associated with the central phenotype (Thöny and Blau, 2006).

The patient's diagnosis consists in the measurement of phenylalanine and tyrosine levels in plasma or serum, before and after a BH_4 challenge to discriminate between classic

phenylketonuria and biopterin variants, analysis of pterin levels in urine, measurement of DHPR activity in blood, analysis of pterins, folates and neurotransmitter metabolites in cerebral spine fluid (CSF) and measurement of enzymatic activity. The first two tests are essential because they enable the differentiation of all BH_4 defects presenting with hyperphenylalaninemia (HPA) (Werner et al, 2011).

The treatment depends on the enzyme-defect phenotype. In the case of PTPS deficiency with the central phenotype, BH_4 supplementation and replacement therapy with neurotransmitter precursors such as levodopa, carbidopa and 5-hydroxytryptophan (5HT) are implemented. For the peripheral phenotype only BH_4 is administered, and for the transient form BH_4 is supplemented in the neonatal period (Laufs et al, 1998; Scheinfeld et al, 2010).

Although the treatment is effective in most cases, a few patients do not respond to the combined treatment, resulting in severe progressive illness (Laufs et al, 1998).

1.6. MUTATION SPECIFIC THERAPIES

Genetic disorders displaying high penetrance genetic are normally caused by mutations that result in either loss-of-function (LOF), characterized by the reduction of the levels and/or activity of a protein, or in gain-of-function (GOF), characterized by the increase in protein levels and/or activity with the introduction of a pathological function (Beaulieu Let al, 2012).

The growing understanding of the pathogenesis in IMD allied to the information obtained from the human genome sequencing and the comprehension of genotype-phenotype relationships has lead to the development of strategies based in the mutations nature, such as metabolic manipulation, protein augmentation and, more recently, genetic medicine (O'Connor and Crystal, 2006; Dietz, 2010).

1.6.1. Misfolding mutations and modulation of protein function

A correct three-dimensional structure is essential to normal protein function and is acquired by a correct folding mechanism. The folding process occurs in the cytosol in a spontaneous manner for small proteins, but larger peptides have to be assisted by a battery of folding catalysts, like cofactors, and small molecules called chaperones. Chaperones protect the nascent protein from the cytosol's crowded environment, shielding the proteins hydrophobic regions (Leandro and Gomes, 2008).

Although energetically favourable, the native state of a protein represents a very delicate equilibrium that can be disrupted by the presence of inherited or acquired mutations, various stress conditions, improper post-translation modifications and off-pathway folding, thus giving rise to misfolded proteins (Gregersen et al, 2006; Chen et al, 2011; Houck et al, 2012). Misfolded proteins can affect cellular homeostasis by two major mechanisms. The first, where misfolded proteins are degraded, is marked by a loss of function, while the other, in which the misfolded proteins accumulate leading to oligomer and aggregate formation, represent a gain of function (Gregersen, 2006).

To prevent protein unfolding, cells have an elaborate mechanism of defence called protein quality control (PQC) system (Figure 6). A system that seems to be spatially organized into compartments composed of molecular chaperones and proteases. Although vital for the correct folding of nascent protein's, PQC's main function is to be the first line of defence against the damage caused by the accumulation of misfolded proteins, which are marked by chaperones to be degraded by the ubiquitine-proteasome pathway if they cannot be correctly folded (Gregersen and Bross, 2010).

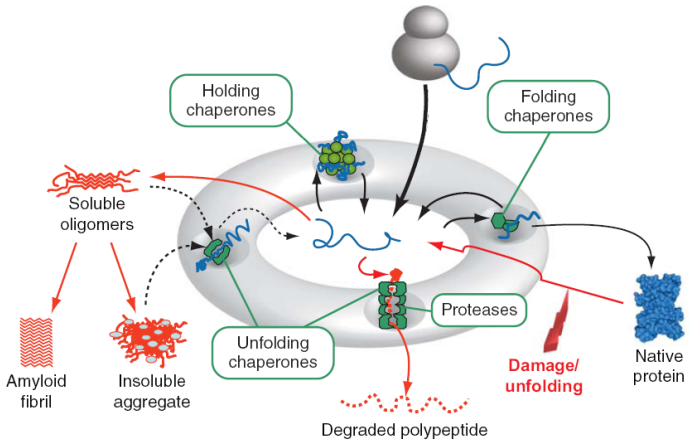

Figure 6 – Different protein quality control systems (PQC). Folding is promoted by folding chaperones, solubility is maintained by holding chaperones and unfolding chaperones dispose of disaggregate or misfolded proteins. Adapted from Gregersen N. et al, 2006.

The involvement of misfolded proteins in pathophysiological manifestations of several disorders has been proved and the list of the so-called "conformational diseases" is continuously growing (Leandro and Gomes, 2008).

Accordingly, misfolded proteins seem to be good candidates for therapies whose main goals are the rescue of the native conformation or the induction of stable intermediate protein states. In recent years, natural (cofactors), chemical and pharmacological chaperones have

been used as a possible therapeutic approach. Recently, the search for possible pharmacological chaperones in known compound libraries has proven to be successful (Pey et al, 2008).

1.6.2. Mutations affecting splicing process and disease

RNA plays a fundamental role in the transfer of information from DNA to proteins. When a protein-coding gene is transcribed, the pre-messenger RNA (pre-mRNA) must undergo a series of post-transcriptional processing events, mainly the removal of introns – pre-mRNA splicing – to obtain a mature mRNA that includes coding elements and appropriate signals for the translation of that information into functional proteins (Douglas and Wood, 2011). Pre-mRNA splicing relies in a series of signals that define intron-exon boundaries, and allow correct mRNA processing. These signals include the 5' and 3' splice sites (ss) that define the exon-intron and intron-exon junctions, respectively, the polypyrimidine (Py) tract and the branch-point sequence which aid in the 3'ss recognition (Wood et al, 2010; Pandya-Jones, 2011).

Splicing is carried out by the spliceosome, a large ribonucleoprotein (RNP) complex, consisting of five small nuclear RNPs (snRNPs) particles, U1, U2, U4, U5 and U6, that performs the two major functions of splicing: the recognition of the intron-exon boundaries and the catalysis of introns' removal and subsequent exons' union (Figure 7) (Faustino and Cooper, 2003; Jensen et al, 2009). Splicing initiation involves the recognition of the transcript 5' and 3' intronic splice sites by U1 and U2 auxiliary factor (U2AF), and of the branch point by splicing factor 1 (SF1) and mammalian branch-point binding protein (mBBP). This structure is called the early complex (E complex). In the next step, E complex recruits U2 which binds to the branch-point sequence and is converted to the A complex. The recruitment of U4, U5 and U6 snRNPs to complex A originates complex B, leading to a structural reordering to for the catalytic C complex (Jensen et al, 2009; Poulos et al, 2011).

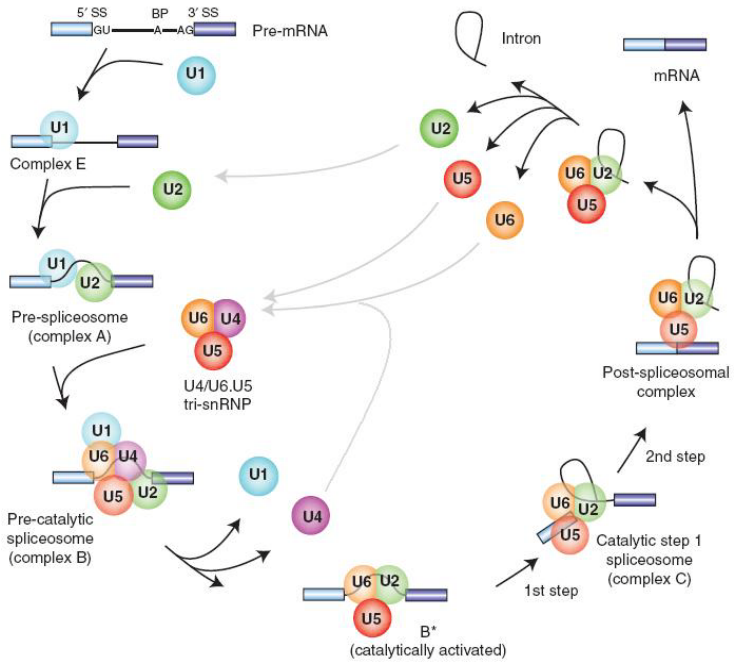

Figure 7 – **Pre-mRNA splicing by the spliceosome.** Exons and introns sequences are shown as boxes and lines, respectively. Adapted from Will and Lührmann, 2011.

The splicing process is also regulated by additional *cis*-acting sequences, located within both introns and exons, which recruit *trans*-acting splicing factors to ensure constitutive exons' inclusion and modulate splice site recognition's efficiency. These sequences have been classified in four functional categories: exonic splicing enhancers (ESEs), exonic splicing silencers (ESSs), intronic splicing enhancers (ISEs) and intronic splicing silencers (ISSs) (Garcia-Blanco et al, 2004; Ward and Cooper, 2010). ESEs and ISEs promote exon inclusion in mature transcripts by recruiting members of the serine/arginine-rich (SR) family of splicing factors. ESSs and ISSs promote the binding of splicing suppressors that include the members of the heterogeneous nuclear RNP family (hnRNP). ESSs located within exons can inhibit their inclusion and when located within and intron can promote its excision. ISSs inhibit exon definition and may also prevent inclusion of "pseudo" exons into mature mRNAs (Garcia-Blanco et al, 2004; Pozzoli and Sironi, 2005; Ward and Cooper, 2010).

About 10 to 30% of mutations associated with genetic disorder affect splicing process (Garcia-Blanco et al, 2004; Rincón et al, 2007) (HGMD® Professional 2013.1). These mutations can disrupt single gene expression by disruption of a splicing *cis*-element, or affect multiple genes by disrupting a component of the splicing machinery or a splicing regulatory complex in a *trans*-effect (Faustino and Cooper, 2003).

Most mutations that alter splicing pattern involve the invariant GT and AG dinucleotides at 5' and 3' splice sites, but can also affect other conserved sequences at the

intron-exon junction like the branch-point site and the Py tract, and also auxiliary splicing sequences. Splicing mutations can be considered gain-of-function or loss-of-function if a splicing element is enhanced or created or if a splicing element is weakened or destroyed, respectively, and they can lead to exon skipping, intron retention, introduction of new splice sites within exons or introns and cryptic splice sites activation (Garcia-Blanco et al, 2004).

The creation of new donor or acceptor splice sites within an intronic sequence, the creation of *de novo* acceptor sites and the deletion or creation of splicing regulatory elements can lead to the introduction of intronic sequences, called pseudoexons, that are flanked by apparently good acceptor and donor splice sites, which however are not normally recognized by the spliceosome (Pérez et al, 2009; Dhir and Buratti, 2010). The majority of the activated pseudoexon sequences belong to transposable elements (TEs). TEs are very frequent repetitive sequences, displaying chromosomal mobility, and that often replicate themselves through RNA (retrotransposons). Retrotransposons can be divided in long terminal repeats (LTRs) and in long and short interspersed nuclear elements (LINEs and SINEs). SINEs are the most abundant and, within SINEs, the most common (10% of the human genome) are *Alu* elements (Sorek, 2007; Vorechovsky, 2010). *Alu* are small primate-specific dimeric structures composed of left and right arms joined by an A-rich linker region that may serve as the Py tract required upstream the 3' splice site (Sorek, 2007).

With the increasing importance of splicing defects in human disorders came the realization that the splicing reactions and machinery are good targets for new therapeutic approaches (Garcia-Blanco et al, 2004).

1.6.3. Antisense oligonucleotide therapy

The first step in a therapeutic approach consists in the study of the molecular mechanism underlying the observed mutation's effect. The *in silico* analysis of the affected region, using the several available bioinformatic programs, is a good starting point and allows the identification of the affected splicing factors.

The subsequent study of the transcriptional profile of the patient's cells allows the comprehension of mutations functional effects upon the splicing mechanism. A splicing model system using specific splice reporter vectors, called minigenes, can be used. Minigenes are also known as exon-trapping vectors and consist of exonic portions of a gene with functional 5' and 3' splice sites separated by an intronic sequence that contains a polylinker. The exon and the respectively adjacent intronic regions of the mutant allele are cloned. The resulting construct is transfected into established cell lines and the splicing pattern is analysed. This system allows

the confirmation of the mutation's effect upon the splicing process and is also important to analyse the effect of a sole mutation in the case of heterozygous patients. (Desviat et al, 2012)

Upon the identification of the molecular mechanism of a given splicing mutation, the next step is to choose the therapeutic approach to modify the aberrant pattern and restore normal splicing. Agents designed to alter gene expression can act either at DNA level by inhibiting or activating transcription (antigene approach), or at RNA level to prevent translation (antisense approach) (Kaur et al, 2007). The last one can be achieved using various methods, like the over-expression of splicing factors, interference RNA (iRNA) or antisense oligonucleotides to selectively eliminate an aberrant mRNA. In this section, the focus will be centred on antisense oligonucleotides.

Antisense oligonucleotides (AONs) have proven to be an effective therapy in the exclusion of pseudoexons, but have also been used in the blockage of sequences involved in the control of RNA processing, like ISSs, ESEs and ribozyme catalytic sites (Morcos, 2007; Rincón et al, 2007; Pérez et al, 2009; Wood et al, 2010; Saonere, 2011).

AONs are simple oligonucleotides, oligonucleotide analogs or other polymers that bind to a sequence (sense strand) trough a Watson/Crick base-pairing mechanism and inhibit the transfer of genetic information from DNA to protein (Summerton and Weller, 1997; Dias and Stein, 2002; Summerton, 2007).

Since their first use, many chemical modifications have been made in order to improve resistance to nucleases and, consequently, to improve their function and to limit their toxicity. One of the most successful modifications was the substitution of ribose moieties by morpholino moieties, linked by uncharged phosphorodiamidate groups instead of phosphates. For that reason, morpholinos are also known as phosphorodiamidate morpholino oligos (PMOs). Morpholinos normally consist of a 25 nucleotides chain with high specificity, water solubility and resistance to a wide range of nucleases, especially RNase H, that bind to the target mRNA and sterically-block the translation machinery (Summerton and Weller, 1997; Morcos, 2007). The entry in the cell is made by endocytosis and needs to be aided by a delivery mechanism, either electroporation, conjugation with weakly-basic polyamine, ethoxylated polyethylenimine (EPEI) or the commercially available delivery agent Endo-Porter® (Morcos, 2001).

Because morpholinos do not freely cross the cells' membrane, they cannot be used in *in vivo* experiments. In order to circumvent this problem, another modification was made through the attachment of a morpholino molecule to a transporter; this one consists in a dendritic structure, assembled around a triazine core that serves to position eight guanidinium head groups in a correct conformation, thus allowing an effective cell membrane penetration.

This structure is called vivo-morpholino. Intravenous (i.v) injections in mice have shown an efficient delivery of vivo-morpholinos in a variety of tissues with special relevance to brain, lung and heart (Li and Morcos, 2008; Morcos et al, 2008).

Another type of oligonucleotides widely used is locked nucleic acids (LNAs). LNAs present a rigid structure due to a methylene bridge that connects the 2'-O atom and the 4'-C atom of the ribose ring, thus locking the nucleic acid in an ideal conformation for Watson-Crick binding (Campbell and Wengel, 2011). LNAs show structural resemblance with RNA, high affinity with complementary RNA, as well as with ssDNA, high specificity toward the target, high stability *in vivo*, lack of toxicity and good resistance to degradation by 3'-exonucleases. Another advantage is the possibility of synthesizing oligomers with lower sizes (6 to 20 nucleotides) and with varied ratios of LNA, allowing different mixtures like LNA/LNA, LNA/DNA and LNA/RNA. LNAs act mainly by recruiting RNase H to degrade the aberrant mRNA, although non-RNase H based mechanisms have also been reported (Veedu and Wengel, 2009).

Currently, the antisense oligonucleotide Vitravene® (ISIS Pharmaceuticals) has been approved for the treatment of cytomegalovirus infection, and other AONs are already in phase 1 and 2 of clinical trials (Kaur et al, 2007; Veedu and Wengel, 2009; Hua et al, 2011). These advances in antisense therapy are encouraging and open avenues to the use of antisense oligonucleotides in metabolic disorders.

1.7. OBJECTIVES

Inherited metabolic disorders are considered rare disorder, although collectively they affect about 6 to 8% of the European population. The advances in technology, in recent years, have contributed to the uncovering of more disorders and also to the broadening of the knowledge about genetic and pathophysiological processes underlying IMDs. Despite these advances, until now, there are no definitive available therapies for patients affected by these disorders and, in the majority of cases, their quality of life is severely impaired.

Recently, the concept of personalized therapy has emerged and the development of genome-based individualized medicine towards tailored treatments has become a goal in IMDs research field. In order to develop new therapeutic targets and treatment approaches, the structural and functional analysis of mutations and the physiopathological mechanisms underlying these disorders is crucial.

In this work the following objectives were set:

- ✓ Genetic analysis of isolated methylmalonic and propionic patients in Spanish and Portuguese populations.

- ✓ Structural and functional analysis of mutations found in isolated methylmalonic patients belonging to *cblB* and *mut* type complementation groups.

- ✓ Analysis of mitochondrial dysfunction in isolated methylmalonic patients belonging to *cblB* and *mut* type complementation groups.

- ✓ Study of new therapeutic options in inherited metabolic disorders. Assessment of the effect of pharmacological chaperones in isolated methylmalonic aciduria *cblB* type and the effect of antisense therapy in 6-pytuvoyltetrahydrobiopterin synthase deficiency.

PART 2

MATERIALS and METHODS

2.1. MATERIALS

2.1.1. CHEMICAL REAGENTS

Chemical reagents used in these studies were obtained from: Abnova (Heidelberg, Germany), Agilent Technologies Inc. (Santa Clara, CA, USA), American Radiolabeled Chemicals Inc. (St. Louis, MO, USA), Antibióticos SA (Alcobendas, Madrid, Spain), Bio-Rad Laboratories (München, Germany), Coriell Cell Repositories (Camden, NJ, USA), Difco Laboratories (Detroit. MI, USA), Exiqon (Vedbaek, Denmark), GE Healthcare Life Sciences – Amersham, Whatman (Township, NJ, USA), GeneTools (Philomath, OR, USA), Gentra Systems (Minneapolis, MN, USA), Life Technologies – Applied Biosystems, GibcoBRL, Invitrogen, Molecular Probes (Grand Island, NY, USA), Lonza Group (Basel, Switzerland), Mbiotech Inc. (Torrance, CA, USA), Polyplus-transfection SA (Illkirch, France), Promega (Madison, Wisconsin, USA), ProteinTech Group Inc. (Chicago, IL, USA), Qiagen (Düsseldorf, Germany), Roche Diagnostics (Basel, Switzerland), Santa Cruz Biotechnology Inc. (Santa Cruz, CA, USA), Seahorse Bioscience® (North Billerica, MA, USA), Serva Electrophoresis (Heidelberg, Germany), Sigma-Aldrich (St. Louis, MO, USA), Stratagene (Cedar Drive, TX, USA), Stressgen Bioreagents Inc. (Vitoria, British Columbia, Canada) and Thermo Fisher Scientific Inc. (Waltham, MA, USA).

2.1.2. BIOLOGIC MATERIAL

2.1.2.1. Patients' samples

In this work, three samples of pyruvoyltetrahydropterin synthase (PTPS) deficient patients, ten samples of isolated methylmalonic aciduria patients and two samples of patients with propionic aciduria were used.

PTPS deficient patients presented elevated levels of phenylalanine and biopterin, no detectable biopterin levels and low PTPS enzymatic activity in primary dermal fibroblasts. Low levels of homovalinic and 5-hydroxyindolacetic acids were also detected.

The biochemical parameters used for diagnosis of methylmalonic patients were the presence of elevated methylmalonic acid, 2-methylcitrate, low carnitine levels and absence of homocysteinuria in urine. Acylcarnitine levels in plasma were determined in some cases, confirming the presence of high levels of propionylcarnitine (C3) and methylmalonylcarnitine (C4DC). Propionic patients presented elevated levels of propionic acid and 2-methylcitrate.

Genetic material (skin biopsies and blood samples) from patients and controls was collected with the consent of parents and the hospitals where collections were performed. The experiments performed using this genetic material were authorized by Comité de Ética de la Investigación from Universidad Autónoma de Madrid, and the Comité de Ética da Universidade

de Lisboa, according to the fundamental principles of the World Medical Association (WMA) Declaration of Helsinki, to the UNESCO Universal Declaration on the Human Genome and Human Rights and also by the European Convention on Human Rights and Biomedicine.

2.1.2.2. Cell lines

For these studies, fibroblasts from the following control cell lines were used: GM09503, GM08680, GM08333, GM05756 and CC2509, purchased to the Coriell Cell Repositories and also from Lonza (Table 1). The studies of splicing profile with minigenes were performed on immortalized cell lines, Hep3B proceeding from human hepatoma and COS-1 proceeding from monkey kidney tissue.

Table 1 – Characteristic of the control cell lines used in this work.

Control	Cell line[a]	Age[b]	Sex	Race	Biopsy origin
C1	GM09503	10 y	M	Caucasian	Abdomen
C2	GM08680	5 m	M	Caucasian	Foreskin
C3	GM08333	5 m	M	Black	Foreskin
C4	GM05756	2 m	M	Caucasian	Inguinal region
C5	CC02509	-	M	Caucasian	Foreskin

[a] Identification number of the Coriell Repositories and Lonza
[b] Age of the individual at the moment of the sample collection.

The immortalized cell lines derived from cblB patients' fibroblasts, 19235-T (c.287T>C/c.584G>A – p.Ile96Thr/p.Ser174fs), 28040-T (p.Gly66fs/p.Ile117_Gln118del) and 27764-T (c.568-570dup/c.548A>T – p.Arg190dup/p.His183Leu) were used to study the effect of compound V upon ATR protein analyzing ^{14}C-propionate incorporation.

2.1.2.3. Bacterial strains

The following *E.coli* strains were used in this work:

- XL1-Blue (Stratagene): supE44, hsdR17, recA1, endA1, gyrA46, thi, relA1, lac$^-$, F'[proAB$^+$lacI^{q}lacZΔM15Tn10(tet^r)]
- TOPO One Shot Mach®1T1R (Invitrogen): lac ZΔM15, hsdR, lacX74, recA, endA, tonA
- BL21 Star™ DE3 (Invitrogen): F- ompT hsdSB (rB-mB-)gal, dcm,rne131(DE)
- BL21DE pLys (Promega): F-, ompT, hsdSb(rB-, mB-), dcm, gal, λ(DE3), pLysS, Cm^r

2.1.2.4. Vectors

The vectors used in this work were:

- TOPO TA Cloning PCR 2.1-Topo Vector (Invitrogen)
- pSPL3 (Life Technologies) gently given to our laboratory by Dr.Andersen (Buckler et al, 1991)
- pIV1 obtained from the introduction of a fragment of gDNA from patient MD335 (P14) into pCR3.1 (Invitrogen), gently given to our laboratory by Prof. Beat Thöny
- pET4.1 plasmid with MMAB wild-type cDNA, gently given to our laboratory by Dr. Ruma Banerjee (University of Michigan, Ann Arbor, USA)

2.2. METHODS

2.2.1. Isolation of genetic material

Genomic DNA (gDNA) was obtained from patients' or controls' cultured dermal fibroblasts, using the MagNa Pure Compact Nucleic Acid Isolation kit and the MagNa Pure Compact automated apparatus from Roche. gDNA from blood soaked paper was obtained using the Generation DNA Purification Systems kit from Gentra Systems.

Low amounts of plasmid DNA were obtained using Wizard* Plus SV Minipreps DNA Purification System from Promega and high amounts were obtained using the QIAGEN* Plasmid Maxi kit from Qiagen.

Total RNA was obtained from patients or control cultured dermal fibroblasts using Tripure Isolation Reagent from Invitrogen, RNeasy Mini kit from Qiagen or the MagNa Pure Compact RNA isolation kit from Roche.

2.2.2. DNA amplification

2.2.2.1. gDNA amplification

Specific primers for the different DNA fragments (Table 2) were designed using the reference sequences available at the Ensembl public data base (www.emsenbl.org/index.html) using the Primer3 software (frodo.wi.mit.edu/primer3). The DNA fragments were amplified using Fast Star (Roche) or Platinum (Invitrogen) polymerases and the corresponding buffers.

Table 2 – Primers used for gDNA amplification.

Gene	Oligonucleotide name	Sequence (5' - 3')
MUT	6 S	GCT ATT CTG AAG CTT AAT ATG G
MUT	6 AS	CTG AAT TTT TTT TGC AAA CAT CG
MMADHC	2 S	ACC TTC GAA GAG TGG ACG TT
MMADHC	2AS	ATA CCA CCC AAT GCC ATC AT
MMADHC	3 AS	CCA AAA GGA GAT TTG TTT CAG G
MMADHC	4 S	AAC GGA CTT GCC TGT GAT CT
MMADHC	4 AS	GGA CAA TGC CAA GTT TTC CA
PCCB	ex1a	CGT ACC CAC GCT TTA GCA CAT
PCCB	ex1b	GGG CAC GCA GTG ATA GGT C
PCCB	184A	CTT CAA GCC CTC CCA TGA ACA GC
PCCB	184B	GGT AGG CCA GCT GAG CCA CAC CT
PCCB	304A	GGC ATA GTG GCC AAA CTC ATT AG
PCCB	304B	AGT TTT CAT TCC CCA AGA TTG GC
PCCB	373A	CAC TGG GTT TTC ATC TCT AGC
PCCB	373B	GTA CCT AGC TCA GTG TCT TGT
PCCB	5An	TGT GGT ATT TTG TGA ATG TCG TT
PCCB	5BN	AGG CCA TGG CTT AGA GAA CTT A
PCCB	6A	TAT CTT TCC ACA GAT AAT GCC TC
PCCB	6B	GGT AAC AAC CTA GAT CTG GGT CAG
PCCB	764A	GAA GCA GCA ACT TTG GGC TGG C
PCCB	764B	CCT GTC AGG GCA GAG AAA GGC AA
PCCB	885A	AAG CCC AGC AGG GAC AGA ACT GG
PCCB	885B	CAA GTG GTC CAG TGC TTC CTC AC
PCCB	965A	GAA ATG TCA TTC TGT AGT GTC AT
PCCB	965B	GAC AGA AAG GAT ACC ATG GAC C
PCCB	1091A	GGA TGG CTG CTG AGG ACA AA
PCCB	1199B	TCC CAC CAC GGC TAT GCT GTA G
PCCB	AvaII	GCC AAG CTT CTC TAC GCA TTT G
PCCB	1300B	AGC TAT GCC TTG AGC TCT CGC
PCCB	1398A	CAG TTC CTC CCT CTA TGC TAT G
PCCB	1399B	CAC TAG TCA ACA GAT TAG ACT GC
PCCB	14Anew	GCA CCC ACA CAC AGT GAT AAT G
PCCB	1399B	CAC TAG TCA ACA GAT TAG ACT GC
PCCB	1499	CTA CCA TCT CTG TAT CAG GTT G
PCCB	cDNA2	GCT CTA GAC TTG GTT TCT TTT CCT TTG ATT T

2.2.2.2. cDNA amplification

cDNA was obtained by retrotranscription of total RNA from controls' and patients' skin fibroblasts using the SuperScript III First-Stand Synthesis System from Invitrogen, or the AMV Reverse Transcription System kit from Promega. Full-length cDNA was amplified using specific primers (Table 3) designed as described for gDNA.

Table 3 – Primers used for cDNA amplification

Gene	Oligonucleotide Name	Sequence (5' - 3')
PTS	PTPS-53	TTT CAA TAA ATA GGC ACT CC
PTS	PTPS-54	ATG AGC ACG GAA GGT GGT
MMADHC	cblD cDNA S	GTT CTG GGA CAG CTG GAG AC
MMADHC	cblD cDNA AS	CAA TGT GGA TGT GTT CAA CG

2.2.3. PCR products purification

Single fragments obtained by PCR amplification were directly purified using SpinClean PCR Purification kit from MBiotech. PCR products containing more than one transcript were loaded into an agarose gel (GibcoBRL), separated and purified using QIAEX® II Gel Extraction kit (Qiagen).

2.2.4. DNA sequencing

Direct sequencing analysis was performed by the termination chain reaction with 2',3'-dideoxynucleotides (ddNTPs) incorporation (Sanger et al, 1977). The reactions were performed with BigDye Termination v3.1 Cycle Sequencing kit on an *ABI* Prism 3730 automated sequencer, both from Applied Biosystems. The sequence analyses were performed at the genomic department of Parque Científico de Madrid.

Mutations found were designated according to the official mutation nomenclature (Human Genome Variation Society at www.hgvs.org).

2.2.5. Cloning and bacterial transformation

MUT patient – Exon 6 and the corresponding flanking intronic regions of patient (P5) with isolated methylmalonic aciduria were amplified using the primers *MUT* 6 S and *MUT* 6 AS described in table 2. After sequence confirmation, the purified PCR product was cloned into TOPO TA vector according to manufacture instructions. The inserted sequence was excised, using restriction enzyme EcoRI, and the insert was subcloned into pSPL3 vector (Figure 8A)

after prior vector linearization with EcoRI. The resulting construct was transformed into XL1-Blue or TOPO One Shot® supercompetent bacteria by thermal shock (30 minutes at 4°C, 45 seconds at 42°C and 2 minutes at 4°C) and platted on LB-agar plates supplemented with ampicillin. The resulting colonies were isolated and grown in LB medium supplemented with ampicillin and plasmidic DNA was isolated as described in section 2.2.1.

PTPS patient – A DNA fragment encompassing *PTS* exons 2 to 4 from a control individual was amplified using a mixture of *Taq* and *Pfu* polymerases (Promega), cloned into pCR3.1 vector (Invitrogen) (Figure 8B) and used as a template (pIV1). The mutation c.164-712A>T from patient P14 was introduced using the QuikChange II XL kit (Agilent Technologies) and the primer 5' – CCT CCC AGG TTC TGT CGA TTC TCC AGC – 3' and its reverse complement (pDM2).

Using the vector pIV1 as template, variant minigenes containing the mutations c.164-714C>A and c.164-715T>A were generated by site-directed mutagenesis using the primers 5' – CTC CAC CTC CCA GGT ACG AGC GAT TCT CC – 3' and 5' – CTC CAC CTC CCA GGT ACG TAG AGC GAT TCT CC – 3', respectively, and their reverse complement. The resulting constructs were transformed into XL1-Blue supercompetent bacteria, as described for MUT patient, and the positive clones were selected by direct sequencing.

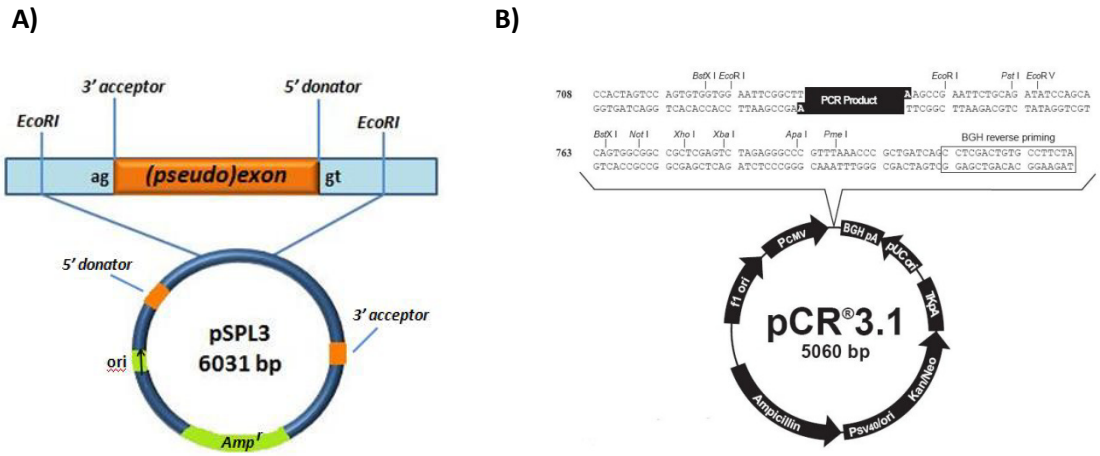

Figure 8 – Vectors used in cloning and bacterial transformation. A) pSPL3 structure representation. 5' and 3' splice sites are indicated in orange. Amp^r is the ampicilin resistance gene. **B)** pCR3.1 structure adapted from Invitrogen Technologies.
(http://tools.invitrogen.com/content/sfs/manuals/pcdna3_1_man.pdf)

2.2.6. Site directed mutagenesis

Site directed mutagenesis was performed by PCR using the Quickchange™ Site Directed Mutagenesis kit from Stratagene. Primers were designed using Primer3 and Agilent Primer designer software and are listed in (Table 4).

To obtain the different allelic variants of the *MMAB* gene, the prokaryote pET4.1 plasmid containing the *MMAB* wild-type cDNA (without the mitochondrial leader sequence) was used as template. The presence of the desired mutation was assessed by direct sequencing of the clone's DNA.

Table 4 – Sequence of the different primers used for site directed mutagenesis. The underlined nucleotide represents the location of the mutation and [] defines the sequence deleted by the p.Ile117_Gln118del mutation.

Gene	Protein change	Oligonucleotide name	Sequence (5' - 3')
MMAB	ATR p.His183Leu	MMAB H183L S	AGC TCG GCG CTG CTT TTC TGC CGG
MMAB	ATR p.His183Leu	MMAB H183L AS	CCG GCA GAA AAG CAG CGC CGA GCT
MMAB	ATR p.Arg186Trp	MMAB R186W S	CAT TTC TGC TGG GCC GTG TGC
MMAB	ATR p.Arg186Trp	MMAB R186W AS	GCA CAC GGC CCA GCA GAA ATG
MMAB	ATR p.Glu193Lys	MMAB E193K S	CCG GGC CAA GAG ACG TGT GGT G
MMAB	ATR p.Glu193Lys	MMAB E193K AS	CAC CAC ACG TCT CTT GGC CCG G
MMAB	ATR p.Arg190dup	MMAB R190dup S	CGG GCC GTG TGC CGC CGC CGG GCC GAG AGA CG
MMAB	ATR p.Arg190dup	MMAB R190dup AS	ACG TCT CTC GGC CCG GCG GCG GCA CAC GGC CCG
MMAB	ATR p.Ile117-Gln118del	MMAB c.349-1G>A S	GAG CTT CAG AAA [ATC CAG] TGC ACA TTG CAG
MMAB	ATR p.Ile117-Gln118del	MMAB c.349-1G>A AS	CTG CAA TGT GCA [CTG GAT] TTT CTG AAG CTC

2.2.7. Mitochondrial isolation

For mitochondrial isolation, Anti-TOM22 MicroBeads (Mitochondrial isolation kit, Miltenyi Biotec, Bergisch Gladbach, Germany) were used.

$8.0x10^5$ cells of control and patients' immortalized fibroblasts were seeded in T75 flasks and incubated overnight at 37˚C. The cells were treated with 80µM of compound V, 1µM of OHCbl, or with the combination of compound V and OHCbl, and incubated for 72 hours. Two flasks were used for each treatment.

The cells were harvested by trypsinization and the pellets were re-suspended in 1mL of lysis buffer (Miltenyi Biotec) and homogenized with a 25g needle using 15 stokes. The resulting solution was transferred to a 15 mL conical tube and 9 mL of ice-cold 1x separation buffer and 50 µL of anti-TOM22 MicroBeads were added. This solution was incubated for 1 hour at 4˚C

with gentle shaking. Subsequently, the suspension was loaded onto a pre-equilibrated MACS Column (Miltenyi Biotec), which was placed in the magnetic field of a MACS Separator (Miltenyi Biotec). Columns were washed three times with 3 mL of separation buffer and, after removing the column from the magnetic field, retained mitochondria were eluted with 1.5 mL of separation buffer (Miltenyi Biotec). Following centrifugation at 13,000 rpm for 1 min, mitochondrial pellet was washed with 300 µL of storage buffer (Miltenyi Biotec) and was finally resuspended in 50 µL of storage buffer.

2.2.8. Protein quantification

Total amount of protein obtained from skin fibroblast cell pellets, Hep3B cell or bacterial cell pellets were quantified using the Bradford reagent (BioRad) according to the manufacturer's instructions or the method described by Lowry (Lowry et al, 1951), using bovine serum albumin (BSA) as calibration standard.

2.2.9. SDS-PAGE and Western Blot analysis

Total protein extracts, obtained from skin fibroblasts and Hep3B pellets, were re-suspended in PBS and a protease inhibitor cocktail (Complete mini EDTA free – Roche) and ruptured by three 5 minutes cycles of freezing and thawing and centrifuged for 5 minutes at 13,000 rpm.

Total amount of protein was assessed as described in section 2.2.8. and aliquots containing equal amount of protein were prepared in a buffer containing β-mercaptoethanol, glycerol and bromophenol blue, or DTT 1mM and NuPAGE LDS sample buffer 4x (Invitrogen).

Samples were separated by SDS-PAGE in 10, 12 or 15% acrylamide/bis-acrylamide gels (Serva). 10% or 4-12% NuPAGE Bis-Tris gels and 4-morpholineethanesulfonic acid (MES) electrophoresis buffer from Invitrogen were also used.

After SDS-PAGE, samples were transferred to Whatman nitrocellulose membranes using Mini Protean III (BioRad) at 100 V for 1 hour or the iBlot gel TransferStacks Nitrocellulose Regular and the iBlot system from Invitrogen (Life Technologies) at 20V for 7 minutes. Protein equal loading was accessed using Ponseau S staining. Nitrocellulose membranes were incubated with 5% skinny milk in PBS with 0.1% Tween for 1 to 2 hours. The following step was the incubation with primary antibodies according to assay:

- Wild-type ATR and mutant proteins: rabbit anti-human ATR polyclonal antibody (1:1,000 – ProteinTech);

- PTPS protein: rabbit anti-human polyclonal antibody SZ28 (1:500), gently provided by Prof. Beat Thöny;
- Lon protease: anti-LONP1 polyclonal antibody (1:1,000 – Abnova);
- Mitochondrial chaperones Hsp-60 and Hsp-70: anti-hsp60 and anti-hsp70 monoclonal antibodies (1:1,000 – Stressgen and Thermo Fisher Scientific respectively);
- Tubulin: anti-αtubulin monoclonal antibody (1:5,000 – Santa Cruz)
- Citrate synthase: anti-citrate synthase polyclonal antibody (1:5,000 – Sigma Aldrich)

After incubation with primary antibodies, membranes were washed with PBS Tween 0.1 % for 10 minutes for three times, and then incubated with the following secondary antibodies: conjugated goat-anti rabbit IgG-horseradish peroxidase (1:5,000 – Santa Cruz) and conjugated goat-anti mouse IgG-horseradish peroxidase (1:10,000 – Santa Cruz). Protein was detected using Enhanced Chemiluminescense System (ECL) (Amersham) and the relative amount of protein was determined using a calibrated densitometer GS-800 from BioRad.

2.2.10. Cell culture, transfection and treatments

Primary fibroblast cultures were grown in MEM medium supplemented with 1 % glutamine 200 mM, 10 % foetal calf serum (FCS) and antibiotics (penicillin 100 U/mL and streptomycin 100 µg/mL) in a humidified atmosphere containing 5 % CO_2 at 37 ^oC, in T25, T75 flasks or in six-wells (p6) and p100 plates, according to the experiment.

Cultures of immortalized primary fibroblast and of Hep3B and COS-1 were grown in MEM medium supplemented with 1 % glutamine 200 mM, 5 % foetal calf serum (FCS) and antibiotics (penicillin 100 U/mL and streptomycin 100 µg/mL) and puromycin (0.5 µg/mL) in a humidified atmosphere containing 5 % CO_2 at 37 ^oC, in T25 flasks or in p6 and p100 plates according to the experiment.

2.2.10.1. MUT minigene

For these experiments, $4x10^5$ COS-1 cells were plated on a six well plate – p6. The experiments were performed in MEM complete medium using 8 µL of JetPei (Polyplus Transfection) and 2 µg of plasmid DNA from the empty pSPL3 vector and the minigene bearing the wild-type or the mutant sequences of *MUT's* exon 6. The cells were incubated at 37 °C for 48 hours. After this period, cells were harvested by trypsinization and RNA was extracted as

previously described. The transcriptional profile was studied by PCR amplification of the cDNA using the pSPL3 vector specific primers (Table 5):

Table 5 – pSPL3 vector specific primers.

Oligonucleotide name	Sequence (5' - 3')
SD6 (sense)	TCT GAG TCA CCT GGA CAA CC
SA2 (antisense)	ATC TCA GTG GTA TTT GTG AGC

2.2.10.2. Antisense oligonucleotide treatment

For these experiments, $5x10^5$ dermal fibroblasts of patients and controls were cultured as described. Cells were passaged by trypsinization and studied at a passage number ranging from 6-23.

The 25-mer AMO were designed, synthesized and purified by Gene Tools and were targeted to donor or acceptor cryptic splice sites in the pre-mRNA. The sequences of the three AMOs PTS-AMO1, PTS-AMO2, and PTS-AMO3 used are shown in Table 6.

As a negative control, a standard 25-mer Morpholino control oligonucleotide provided by Gene Tools was used. As a delivery reagent, Endo-Porter® was used following the manufacturer's recommendations.

Table 6 – Sequence of the AMOs used for the treatment of PTPS patients' cells.

Oligonucleotide name	Sequence (5' - 3')
PTPS AMO1	AGT GCC TAC AAT GTA ACA GGC AAG T
PTPS AMO2	AGG CTG GAG AAT CGC TCG AAC CTG G
PTPS AMO3	AGG CTG GAG AAT CGC TCG CAC CTG G
Negative control	CCT CTT ACC TCA GTT ACA ATT TAT A

After transfection with 0, 20 and 30 µM of the corresponding AMO, cells were harvested at 24 hours and mRNA was isolated using the MagnaPure system following the manufacturer's protocol. The cell lines were incubated with cycloheximide 0.75-1 mg/mL, 4 to 6 hours prior to cell harvest. PCR amplification of transcripts derived from patient P12 and patient P13 cell lines was performed using 5´-TAT GGA GGA GGC GAT TAT GC-3´ and 5'-TTT CAA TAA ATA GGC ACT CC-3´ as forward and reverse primer, respectively. To exclude amplification from the allele bearing the c.163+2T>G mutation in patient P14 sample, a specific forward primer located in the exon 1 and exon 2 junction was used (5´-CCG ATT GTA CAG TAA ATT TCT AA-3´).

Antisense Vivo-Morpholinos (AMOs) that were covalently linked to Vivo-Porter (also supplied by Gene Tools) were added directly to the primary dermal fibroblast cell cultures. After 24 hour incubation, cells were harvested and conventional RT-PCR for splice analysis was performed as described in section 2.2.2.2.

LNAs were designed, synthesized and purified by Exiqon against the target sequence for patients patient P12 and patient P14, as shown in Table 7. For this experiment, $2x10^5$ cells were plated on p6 plates and were treated with different doses of LNA (1, 5, 25, 50 nM and 5 µM) and 10 µL of Lipofectamin 2000, for 24 hours.

The cells were collected by trypsinization and the pellet was stored at -70°C prior to use. Total RNA was extracted using the Tripure Isolation Reagent (Invitrogen).

Table 7 – LNA sequences used in PTPS patients.

Name	5' - 3' Sequence	Target mutation
***PTS*-LNA1**	CAAACAAACCTTAACT	c.84-322A>T
***PTS*-LNA2**	TCGCTCGAACCTGGGA	c.164-712A>T

2.2.11. PTPS enzymatic activity assay

For these experiments, $1x10^6$ non-stimulated patients' skin fibroblast cells were grown in 75-cm^2 plates in MEM, treated with 30 µM of AMO and incubated for 48 or 72 hours. The cells were harvested by trypzinization and the pellets were stored at -70°C until analyzed. The pellets were re-suspended in 150 µL of lysis buffer (10 nmol/L Tris-HCl, pH 7.4, containing 10 mL/L Triton X-100) and lysed by freezing and thawing six times. After centrifugation at 15,000g for 5 minutes, 50 µL of the supernatant was added to 60 µL of reaction mixture containing 100 mmol/L Tris-HCl, pH 7.4, 10 mmol/L $MgCl_2$, 1mmol/L NADPH, 1 mmol/L NADH, 3 mU of SR, 220 mU of DHPR and 60 µmol/L of dihydroneopterin triphosphate, in a final volume of 110 µL. A 50 µL aliquot was incubated at 37 °C for 120 minutes and another aliquot was used as blank. The reaction was stopped by cooling the samples on ice and adding 15 µL of 300 g/L trichloroacetic acid (TCA) for protein precipitation. The samples were centrifuged at 15,000 g for 5 minutes and oxidized by incubating 50 µL of the supernatant with 10 µL of 10 g/L iodine for 60 minutes, at room temperature, in the dark. The oxidation reaction was stopped by adding 15 µL of 10 g/L of ascorbic acid. The samples were then diluted (1:4 by volume) with water and heated at 60 °C for 2 hours before being deproteinized using an Ultrafree-MC filter and analysed by HPLC. One unit of PTPS produces 1 µmol of biopterin *per* minute at 37 °C. (Bonafé et al, 2001)

2.2.12. Pterin quantification

For pterin quantification, $1x10^6$ patients' skin fibroblasts and Hep3B immortalized cells were grown in 75-cm^2 plates in MEM. When the patients cells reached a confluent monolayer, the expression of the GTPCH enzyme was stimulated with a cytokine cocktail containing 1250 U of recombinant human interferon-γ (IFN-γ) and 500 U of tumour necrosis factor α (TNF-α), and incubated for 24 to 96 hours. At the same time, the cells were treated with 30 µM of the corresponding AMO and harvested at 48, 72 or 96 hours after transfection. Cells grown for 96 hours were transfected twice with the AMOs. After incubation, cells were washed with PBS, harvested by trypsinization, counted to determine the cell number, washed again with PBS, and kept at -70 °C until analyzed for neopterin and biopterin. All the harvesting procedure was done in low light conditions.

Cytokine-stimulated patients' cells and non-stimulated Hep3B cell pellets were lysed in 150 µL of lysis buffer (100 mM Tris-HCl, pH 8.0, 2.5 mM EDTA, 300 mM KCl and 10 % glycerin) by freezing and thawing six times. Lysate was centrifuged at 15,000 g for 15 min at 4 °C. A volume of 100 µL of supernatant was oxidized with 6 µL of 1 M HCl and 20 µL of a 10 g/L iodine solution for 30 minutes, at room temperature, in the dark. The remaining supernatant was used for determination of protein concentration using the Bradford reagent (Bio-Rad). The oxidation reaction was stopped by the addition of 20 µL of 10 g/L ascorbic acid (freshly prepared). To adjust the pH to 8.0-9.0, 10 µL of dephosphorylation buffer (1 M Tris-HCl pH 9.6 containing 80 mM $MgCl_2$) was added to the sample with alkaline phosphatase (20 U) to dephosphorylate the neopterin triphosphate. The sample was incubated at 37 °C for 60 min. The reaction was stopped by acidification to pH 2.0 with 7 µL of 2 M HCl. The sample was deproteinized using a low protein binding centrifugal filter (Whatman) and analyzed by HPLC. The intracellular concentrations of neopterin and biopterin after cytokine stimulation are expressed as pmol *per* mg of total protein (Werner et al., 1996; Bonafé et al, 2001).

2.2.13. Prokaryotic expression and purification of wild-type and mutant ATR proteins

Human *ATR* gene mutations, p.Ile117-Gln118 p.His183Leu p.Arg186Trp, p.Arg190dup, and p. Glu193Lys were introduced by site directed mutagenesis as previously described. Wild-type and mutant ATR proteins were expressed in BL21Star™DE3 One Shot cells and incubated at 37 °C until optimum optical density (about 0.6-0.8 absorbance units) was reached and protein expression was induced with 1mM IPTG. The bacterial cultures were re-incubated at 37°C for five hours and pellets were collected by centrifugation at 6,000 rpm for 10 minutes at 4 °C and frozen at -70°C until further use. Cell pellets were re-suspended at 4 °C in 50 mM

potassium phosphate buffer pH 8, 100 mM NaCl, 1 mM DTT, 1 mM EDTA, 0.05 mg/mL DNase I, 0.03 mg/mL lysozyme and a protease inhibitor cocktail (Complete Mini, EDTA-free Protease Inhibitor Cocktail Tablets®, Roche) and incubated for 1 hour with agitation at 4 °C. After, the cell suspension was sonicated and centrifuged to obtain the crude soluble cell extract. At this point, total protein concentration was assessed using the Bradford reagent (Bio-Rad) and samples containing 1 mg/mL were prepared to perform protein stability assays. The remaining protein extract was precipitated with ammonium sulphate, dialysed and separated by anion-exchange chromatography using a HiTrap Sepharose Q column (GE Healthcare), as previously described (Leal et al, 2004; Jorge-Finnigan et al, 2010). Fractions eluted from the HiTrap Sepharose Q column were subjected to SDS-PAGE to identify those enriched in ATR protein and, before the ATR enzymatic assay, wild-type and mutant ATR proteins were further purified by molecular exclusion chromatography in Tris-HCl pH 8 buffer using a HiLoad Superdex 200 60/10 column (GE Healthcare) at 4 °C, as described. (Jorge-Finnigan et al, 2010).

2.2.14. ATR protein stability studies

The stability of the wild-type and mutant ATR proteins (p.Ile117-Gln118del, p.His183Leu, p.Arg190dup, p.Arg186Trp and p.Glu193Lys), expressed in a prokaryotic system, was measured by incubation at 37 °C following IPTG induction. The wild-type and mutant p.His183Leu were also incubated at 27 °C. Soluble supernatant was incubated at 37 or 27 °C and aliquots were removed at different time points. The cell extracts were subjected to SDS-PAGE. Western blot analysis was performed as described above. Following densitometric analysis, relative protein levels were expressed as percentage referred to time zero.

2.2.15. Effect of ligands upon mutant and wild-type ATR proteins

2.2.15.1. Stabilization of wild-type and mutant ATR proteins in a prokaryotic system

As described in section 2.2.13., the prokaryotic expression of wild-type and mutant forms of ATR protein were induced over night in LB medium in the presence of 80 µM of compound V for the wild-type and p.His183Leu, p.Arg186Trp and p.Glu193Lys mutant forms. Since compound V is suspended in DMSO, bacteria were also incubated with the corresponding DMSO concentration (0.1 % or 0.2 %) as control.

The wild-type ATR and mutant p.Ile96Thr proteins, previously used for compound V studies, were also incubated in the presence of 1 µg/mL of hydroxocobalamin and the combination of the two compounds, compound V and hydroxocobalamin.

The bacterial extracts were obtained as described in section 2.2.13 and analysed by SDS-PAGE and Western-Blot as described in section 2.2.9.

2.2.15.2. Analysis of in vivo effect of ligands upon wild-type ATR protein

Seventeen 12 weeks old wild-type (wt) female mice (C57BL/6J) were bought from Harlan Laboratories (Harlan Laboratories Inc., Indianapolis, IN, USA). The animals were housed at Centro de Biología Molecular Severo Ochoa at 22 ± 1°C on a 12/12h light/dark cycle with *ad libitum* access to food and water. Mice were kept under standard laboratory conditions in accordance with European Community Guidelines (directive 86/609/EEC). All animals were handled in strict accordance with good animal practice as defined by the national animal welfare bodies and institutional guidelines. The mice (23-25g) were treated with 25 µL suspension containing (a) 0.25 mg/mL (about 0.7 mM and (b) 5mg/mL (about 14 mM) of compound V in 10 %DMSO and 9 % glucose for 12 days. The loading was made using a pipette and letting the animals drink the solution. Each treatment group was composed by 6 animals. The control group was loaded with DMSO and glucose and was composed by 5 animals due to the death of one of them before the beginning of treatment.

Approximately 30 minutes after the last dose, the animals were sacrificed with CO_2 and liver and brain were removed. The brain and liver samples were divided in three equal parts and one was frozen in liquid nitrogen for further studies. Liver extracts were prepared in phosphate saline buffer (PBS) with a protease inhibitors cocktail (Roche), and brain extracts were prepared in modified RIPPA buffer (50 mM Tris-HCl pH 7.4, 1 %Triton, 150 mM NaCl, 1 mM EDTA, 1 mM NaF, 1 mM Na_3VO_4, 1 µg/mL protease inhibitor cocktail and 0,25 % Na-deoxycholate). Liver samples were homogenized using a TissueLyser II (Qiagen) and brain samples were prepared using a glass tissue grind tube SZ 20 (Kimble Chase, Vineland, NJ, USA). Extracts were clarified by centrifugation at 13,000 rpm for 30 minutes at 4°C and the supernatants were stored at -70 °C prior to use.

2.2.15.3. Analysis of the effect of ligands in vivo by MS/MS

The control and treated mouse livers were divided in three equal parts. Two parts were homogenized using a glass tissue grind tube SZ 20 (Kimble Chase) in 1 mL of methanol (MeOH) or DMSO, respectively. The homogenate was centrifuged at 4 °C at 13,000 rpm for 10 minutes, and the liquid phase was collected. Samples in MeOH and DMSO were completely dried under a stream of nitrogen at 40 °C and re-suspended in 150 µL of the mixture, DMSO, H_2O and formic acid (100:50:0.2 %). An external calibration was made using different

concentrations of compound V (0 to 75 µmol/L). No internal calibration was used. The samples were analyzed by HPLC-MS/MS.

Analyses were performed in a HPLC 1100 series (Agilent Technologies) coupled to a MS/MS QTrap (Applied Biosystems) using a mobile phase consisting in a solution of H_2O, MeOH and formic acid (25:75:0.1) in an isocratic mode, running for 16 minutes. The flow rate was established at 150 µL/min and 10 µL of each sample were loaded into a Symmetry® C18 column (2.1x100 mm, 3.5 µm particle size, Waters Corp, Milford, MA, USA).

The MS/MS acquisition consisted of a multiple reaction monitoring from the ion par m/z 320≥91, after the method's optimization, where molecular ion 320 corresponds to $[M+H^+]$ (the molecular weight of the compound V plus one proton) and 91 corresponds to the ion weight of an abundant fragment of the compound.

2.2.16. Propionate Incorporation

$4x10^5$ skin fibroblasts of *cblB* patients and controls, both normal or immortalized, were plated on p6 plates and incubated in 1 mL of Puck's saline solution containing glucose (0,5 mM), fetal calf serum (15 %), propionate (1 mM) and 1 µCi/mL of ^{14}C Propionate for 18 hours. Then, cells were washed with PBS, harvested by trypsinization and centrifuged at maximum speed for 10 minutes. The pellet was re-suspended and allowed to stand in a 5 % TCA solution at 4 °C. After centrifugation, TCA-precipitated material was re-suspended in NaOH 0.5 N, as described (Perez-Cerdá et al, 1989). Incorporation of ^{14}C into TCA precipitate was estimated by re-suspending the samples in scintillation liquid and radioactivity quantification was performed in a Wallac RackBeta 1219 liquid scintillation counter (PerkinElmer, Waltham, MA, USA). The obtained data was divided by the corresponding amount of protein that was assessed using the Lowry method. This experiment was performed at 37 °C or 42 °C for some assays.

2.2.17. Analysis of mitochondrial profile

2.2.17.1. ROS analysis

For analysis of reactive oxygen species (ROS), $3x10^5$ skin fibroblasts from three control and the patients' cell lines were cultured in a p6 plate, as previously described in section 2.2.10. One auto-fluorescence, one negative and one positive control were included in each assay. The cells were washed with PBS and detached by trypsinization for 1 minute; the reaction was immediately stopped by adding 1 mL of complete culture medium. 500 µL of a mixture of H_2DCFDA fluorescence probe (2,7-dichlorodihydrofluorecence diacetate; Molecular Probes) at a final concentration of 5 µM and PBS was added to the controls and patients' cells.

The auto-fluorescence control was treated only with PBS, a mixture of PBS and 4 M NaCl was added to the negative control, and the positive control was treated with a mixture of PBS with fluorescent probe and 4 M NaCl. The cells were incubated at 37 °C in the dark for 30 min. After centrifugation, cells were re-suspended in 0.001 % propidium iodide (Sigma-Aldrich) and PBS mixture to detect cell death. ROS levels (H_20_2) were monitored by flow cytometry and samples were analysed using a FACSCalibur apparatus with two solid-state lasers (λ 488 and λ 633 nm) (Becton Dickinson & Comp., Franklin Lakes, NJ, USA). A minimum of 10,000 individual events were recorded and the data was acquired using Cell Quest-Pro (Becton Dickinson, New Jersey, USA) and analysed using FlowJo software.

2.2.17.2. Bioenergetic Profile

An XF24 Analyser (Seahorse Biosciences) was used to measure bioenergetic function. Control and patients skin fibroblasts were seeded to a density of 50,000 cells in 24-well tissue culture microplates and incubated with 100 µL of DMEM or DMEM lacking D-glucose and supplemented with galactose respectively, and incubated at 37 °C for 3 to 5 hours. After the incubation period, another 250 µL of the corresponding medium was added and incubated overnight at 37 °C. The next day the medium was removed and the cells were washed with PBS and 700µL of the corresponding medium (DMEM or DMEM lacking D-glucose and supplemented with galactose) lacking sodium bicarbonate was added. Then the plates were incubated at 37 °C in a non-CO_2 incubator for 1 hour. To assess the bioenergetic profile, we used modulating compounds, like oligomycin (6 µM), carbonyl cyanide p-(trifluoromethoxy)-phenylhydrazone (FCCP) (50 µM), rotenone (1 µM) and actinomycin A (1µM). The calibration plate, containing these compounds, was prepared according to manufacture's protocol. The oxygen consumption rate (OCR) and the extracellular acidification rate (ECAR) were monitored in real time. After the completion of the assay, the number of viable cells was assessed and the results were normalized using those values (Dranka et al, 2011).

2.2.17.3. Mitochondrial morphology analysis

The mitochondrial morphology of patients' and controls' derived-fibroblast was observed using the Mitotracker® Red CM-H2Ros probe (Molecular Probes). Fibroblasts were seeded at a density of $1x10^5$ cells over a 10 mm glass coverslip placed inside a 24-well tissue culture plate and incubated with 1mL of MEM at 37 °C overnight. Afterwards, cells were incubated at 37 °C for 40 minutes with 500nM Mitotracker® in MEM media, and then fixed in 0.5 mL 10 % formalin at room temperature for 20 minutes. Cells were washed with PBS for three times and mounted with the cells facing down in a microscope slide in mounting media.

Images were taken one day after fixation, using an Axiovert200 inverted microscope (Zeiss, Jena, Germany) with a DsRED filter and 63x magnification.

2.2.17.4. Mitochondrial Ca^{2+} uptake in permeabilized cells

Mitochondrial Ca^{2+} uptake from patients and control fibroblast cell lines was measured in the presence of the Ca^{2+} - sensitive fluorescent probe Calcium-Green 5N (Invitrogen) at a final concentration of 0.1 μM (excitation λ 506 nm, emission λ 532 nm) using digitonin permeabilized cells. A minimum of $2x10^6$ cells were harvested by trypsinization, followed by centrifugation on MEM medium. Cells were washed and re-suspended in MSK buffer (125 mM KCl, 2 mM potassium phosphate, 3 mM $MgCl_2$, 20 mM Hepes, pH 7.4) and kept on ice for 18 hours. An AMINCO-Bowman (series 2) spectrofluorometer (Thermo Fisher Scientific), provided with temperature control and continuous stirring was used to perform the experiments carried out at 30 °C in the presence of the respiratory substrates succinate (5mM) and rotenone (1 μM), and also in the presence of ATP and cyclosporine A (5 μM). Digitonin (80 μM) was added to permeabilize the cells and, after 3 to 5 min of incubation, $CaCl_2$ was added repeatedly to the cuvette until mPTP opening.

2.2.18. *In silico* analysis

All cDNA and gDNA sequences of genes studied in this work were obtained using the public databases Ensembl (http://www.ensembl.org/index.html) and GenBank from NCBI (http://www.ncbi.nih.gov/). For mutation nomenclature the Human Genome Variation Society (HGVS, http://www.hgvs.org/) guide lines were followed, and all the mutations found were consulted on the Human Gene Mutation Database Professional release (HGMD Professional 2013.1, http://www.hgmd.cf.ac.uk).

The program BLAST (http://ncbi.nlm.nih.gov/BLAST/) was used to search public databases for sequence homology.

Analysis of DNA sequences was performed using the Chromas 1.45 software (Griffith University, Australia).

As previously described, the oligonucleotides used for DNA amplification were designed using the Primer3 (v. 0.4.0) program (Rozen and Skaletsky, 2000).

The location of possible exonic splicing enhancers (ESEs) was assessed using the programs for prediction of splicing factors recognition sequences, ESE Finder (v 3.0, http://rulai.cshl.edu/tools/ESE) (Cartegni et al, 2003) and HSFinder (v 2.4, http://www.umd.be/HSF/) (Desmet et al, 2009). The Berkeley Drosophila Genome Project (BGDP, http://www.fruitfly.org/seq.tools/splice) server and the Alternative Splice Site

Predictor (ASSP, http://wangcomputing.com/assp/index.html) were used to predict the effect of mutation upon splicing sites.

The pathogenesis and possible functional effect of missense mutations was evaluated using the Polymorphism Phenotyping (PolyPhen-2) software (http://genetics.bwh.harvard.edu/pph2/) and also the SIFT software (http://sift.jcvi.org/).

Protein sequences were obtained from the Protein Data Bank (PDB, http://www.rcsb.org/pdb/home/) and from SWISS-PROT (http://www.expasy.org/sprot/).

The entropy levels from wild-type and mutant hATR proteins were calculated using the CAFFE bioinformatic program which calculates the entropy levels necessary to form the correctly folded protein (Bastolla et al, 2001; Bastolla et al, 2004).

PART 3

RESULTS

3.1. MOLECULAR CHARACTERIZATION OF PATIENTS WITH ORGANIC ACIDEMIAS

In this section, seven patients were studied, five of them presenting biochemical and clinical symptoms of isolated methylmalonic aciduria, while the remaining two presented symptoms of propionic academia. The results revealed that four patients (P1, P2, P3 and P4) carried mutations in the gene *MMADHC*, one patient (P5) presented a mutation in the *MUT* gene and two patients (P6 and P7) presented mutations in the *PCCB* gene.

In Table 8 are depicted the biochemical and enzymatic data, as well as the clinical phenotype and the clinical outcome of the four *cblD* patients analyzed. The biochemical analysis of these four patients suggested they presented isolated methylmalonic aciduria (Table 8). However, analysis of MUT enzymatic activity of patients P1, P2 and P3 showed levels in the control range, discarding the possibility of mutations affecting the *MUT* gene. For P4 only gDNA was available hence, the enzymatic and response to hydroxycobalamin data were not available.

Patients P1, P2 and P3 presented a clear response to treatment with hydroxycobalamin, which could indicate a defect in *MMAA* or *MMAB* genes. Both were analyzed by direct sequencing, but no mutations were found. The identification of the *MMADHC* gene as responsible for the *cblD* complementation defect (Coelho et al, 2008) during the time of this work, led to the search of mutations in this gene for these four methylmalonic patients, whose genotypes remained unidentified. Direct sequence analysis of cDNA and/or gDNA from these four patients allowed their full molecular characterization. Three new mutations, **c.165_166del2**, **c.170G>A**, **c.10-1G>C**, as well as one already described mutation, c.57_64del8, were identified in homozygosity (Figure 9).

Patient P1 revealed to be homozygous for the previously described mutation c. 57_64del8 (p.Cys19fs) (Coelho et al, 2008). This mutation leads to the deletion of 8 nucleotides in exon 2, causing an out-of frame deletion of the protein C-terminal end.

Patient P2 was homozygous for the novel mutation c.165_166del2 (p.Thr55fs). This mutation leads to the exclusion of two nucleotides in exon 3 and, just like the previous mutation, to the production of an out-frame mutation.

In Patient P3 a novel point mutation, c.170G>A (p.Trp57X) in exon 3, was identified. This is, probably, a severe pathogenic mutation, since it leads to the introduction of a premature stop codon (PTC), putatively leading to a truncated protein.

Patient P4 presented also a novel point mutation, c.10-1G>C. This mutation affects the guanosine residue of the original 3' splice site of intron 1. *In silico* analysis revealed that the deletion of the original acceptor splice site results in the increase of the score of an AG

dinucleotide located inside exon 2, which probably leads to the activation of this new splice site (Figure 10). Hence, 14 exonic nucleotides are, probably, eliminated, resulting in a disruption of the ORF. This mutation is also responsible for the creation of a new binding site for the serine/arginine-rich splicing factor 6 (SRSF6), which plays an important role in determination of alternative splicing events.

All the novel mutations are likely pathogenic since all produce, most probably, a truncated protein.

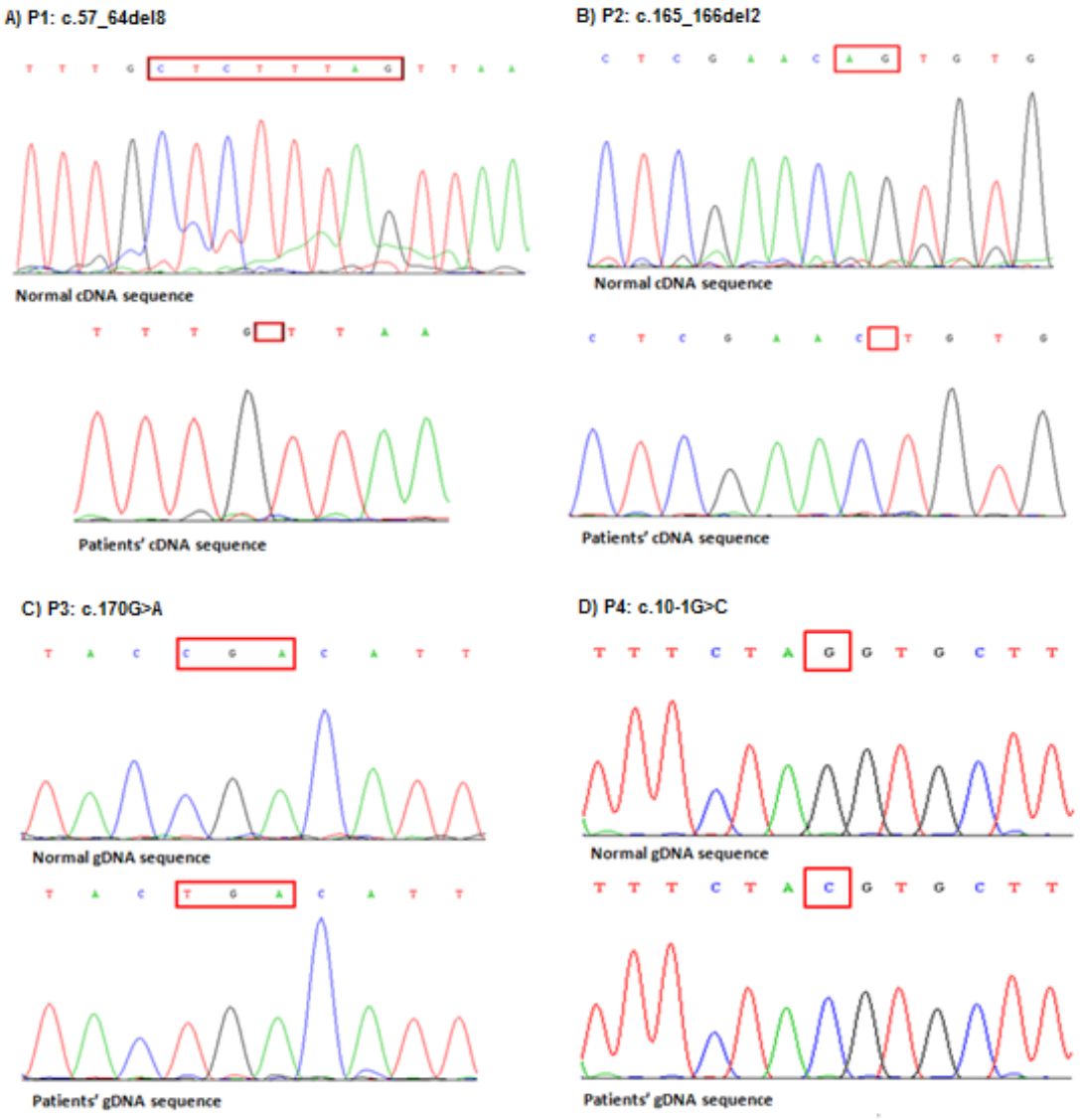

Figure 9 – Mutations identified by direct Sanger sequencing of the *MMADHC* gene. A) P1 presented a deletion of 8 nucleotides in exon 2. **B)** P2 presented a small deletion of 2 nucleotides in exon 3. **C)** P3 presented a C>T change in exon 3 and **D)** P4 presented a G>C change in the first nucleotide upstream exon 2. Mutations according to NM_000532.3.

Table 8 – Genetic, biochemical and clinical parameters of the methylmalonic *cblD* type patients studied.

Patiente	Mutation (cDNA/gDNA/protein)*	MUT Enzimatic Activity**	[14C]-Propionate Incorporation *ex vivo* -OHCbl / +OHCbl (Fold change)	Clinical Onset	Treatment	Outcome
P1	c.57_64del8/c.57_64del8 Chr2(hg19):g.150438731_150438738del8 p.Cys19fs/p.Cys19fs	0.96	0.13 / 2.30 (17.7)	Severe onset on 4th day of live with hypotonia and a severe metabolic acidosis. At 6th day clinical worsening with coma and elevated hyperammonemia (>400µmol/L)	Hypoproteic diet, vitamin B_{12} (1mg/day) and L-carnitine	Mild delay in motor performances and normal mental development with very mild cerebral MRI abnormalities. Very good clinical evolution.
P2	c.165_166del2/c.165_166del2 p.Thr55fs/p.Thr55fs Chr2(hg19):g.150436151_150436152del2	3.03	0.15 / 4.97 (33.1)	Elevated levels of cystein, methylmalonic and butyric acid.	Vitamin B_{12}	Good evolution.
P3	c.170G>A/c.170G>A p.Trp57*/p.Trp57* Chr2(hg19):g.150436147C>T	2.86	0.17 / 8.2 (48.2)	Convulsions in 1st year of life, no fever, severe muscular hypotonia and psychomotor delay. At age of two presented polyuria, polydipsia and progressive degeneration of height and height growth. Renal failure and elevated ammonia levels in plasma Positive screening for creatinine and methylmalonic acid	Injections of vitamin B_{12} (1mg) twice a week and L-carnitine	Good evolution.
P4	c.10-1G>C/c.10-1G>C Ch2(hg19):g.150438786C>G	ND	ND	Vomiting and anorexia since 15 months old. Metabolic decompensations associated with neurological signs. Severe high anion gap metabolic acidosis, ketosis and ketonuria, hyperammonemia and hyperglycinemia. Also presented thrombocytopenia and neutropenia.	**1st treatment:** Carbalu and dialysis for hyper ammonemia **2nd treatment:** vitamin B_{12} and L-carnitine	Good evolution. Normal aminoacid levels in urine, elevated glycine, lysine and metylmalonic acid levels in plasma.
C	—	0.89±0.43	1.94±1.2/ 2.29±1.5 (1.18)	—	—	—

ND: Non determined. *Mutations according to NM_015702.2 and NC_000002.11 (*MMADHC*) obtained using the Mutalyzer 2.0 beta 26 version software according to hg19 (https://mutalyzer.nl/positionConverter). **Mutase activity (nmol/min per mg protein) measured with 36 µM AdoCbl. ***[14C]-Propionate incorporation (nmol/10h/mg protein) in the absence or presence of 1µg/mL of hydroxocobalamin.

Table 9 – Genetic and biochemical data from propionic and methylmalonic *mut* type patients.

Patient	Gene	Mutation*(cDNA/gDNA/protein)	Propionic acid at diagnostics (mmol/mol creatinine)	Methylmalonic acid at diagnostics (mmol/mol creatinine)	Outcome
P5	*MUT*	c.1408-10A>G/ c.244dupA Chr6(hg19):g.49416575T>C/g.49426936dup p.?/p.Leu81fs	–	378	Good evolution with no developmental delays.
P6	*PCCB*	c.1218del14ins12/ c.183+3G>C Chr3(hg19):g.136045712delins12/g.135969403G>C p.Gly405fs/p.Arg61fs	3795	–	NA
P7	*PCCB*	c.1218del14ins12/ c.1218del14ins12 Chr3(hg19):g.136045712delins12 p.Gly405fs	2185,2	–	NA

NA: Non available

*Mutations according to NM_000532.3 and NC_000003.11 (*PCCB*) and NM_000255.3 and NC_000006.11 (*MUT*). The genomic coordinates were obtained from the Mutalyzer 2.0 beta 26 software according to hg19 (https://mutalyzer.nl/positionConverter).

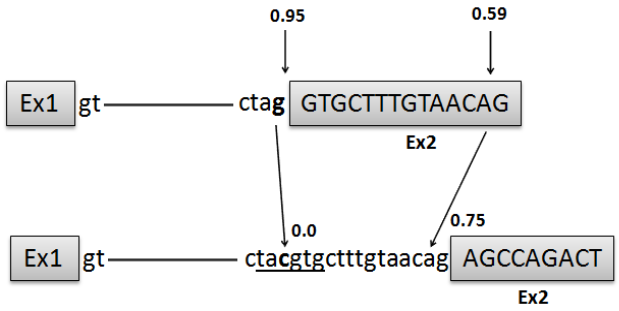

Figure 10 – Prediction of the effect of mutation c-10-1G>C (bold letters) in P4 splicing profile from *in silico* data. The upper part represents the normal splicing profile while the lower part represents the possible mutation effect**.** Splicing scores were calculated with the BDGP software (www.fruitfly.org) and the underlined sequence represents a new binding site for the SRSF6 protein.

Patient P5 is a female born of non consanguineous parents who presents a mild methylmalonic phenotype. Only gDNA was available from this patient, hence, no enzymatic analysis was performed. Since the presence of mutations in *MUT* gene is responsible for the majority of the isolated methylmalonic deficits described until now, the analysis started with the amplification and sequencing of the 13 exons of this gene, which lead to the identification of two novel mutations, **c.244dupA** and **c.1408-10A>G**. None of the mutations was described in the Exome Variant Server (http://evs.gs.washington.edu/EVS). For further characterization, exon 1, bearing mutation c.244dupA, and its intronic flanking regions were cloned into the TOPO® TA vector and sequenced.

The c.244dupA is a frameshift mutation that leads to the insertion of an adenosine nucleotide in exon 1. This mutation is predicted to be pathogenic since it probably originates a truncated protein, p.Leu81fs (Figure 11).

The mutation c.1408-10A>G is responsible for the substitution of an adenosine nucleotide for a guanosine in the position -10 of intron 5 (Figure 11). The functional analysis of this mutation is presented in the next section.

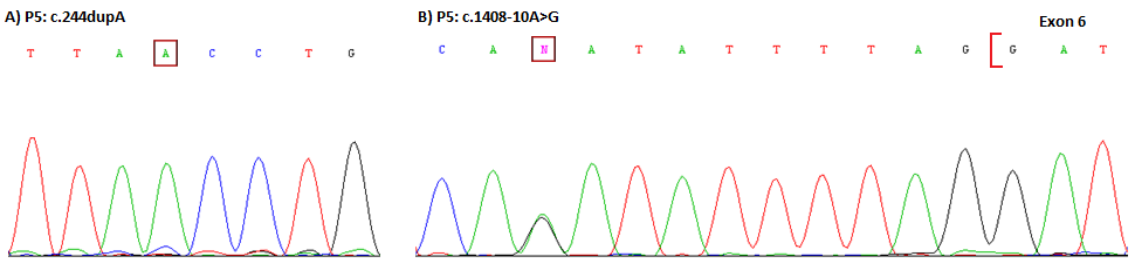

Figure 11 – Mutational profile of patient P5. A) Mutation c.244dupA in exon 1 was cloned into the TOPO® TA vector and analyzed. **B)** Splicing mutation, c.1408-10A>G in intron 5.

Regarding the propionic patients, P6 and P7, and since the mutations incidence is higher in the *PCCB* gene, their molecular characterization started with the amplification and direct sequencing of this gene. This strategy revealed to be appropriate, because it allowed the full characterization of the two patients and revealed the presence of two known mutations, c.1218del14ins12 and c.183+3G>C.

Patient P6 revealed to be a compound heterozygote for the two known mutations, c.1812del14ins12 and c.183+3G>C (Figure 12). Mutation c.183+3G>C affects the guanosine residue in position +3 in the 5' donor site of exon 1. This transversion weakens the wild-type donor splice site and may induce the selection of another GT in position +21 which presents a naturally elevated splice score (0,96). Segregation analysis was performed and it was possible to establish the parental origin of both mutations.

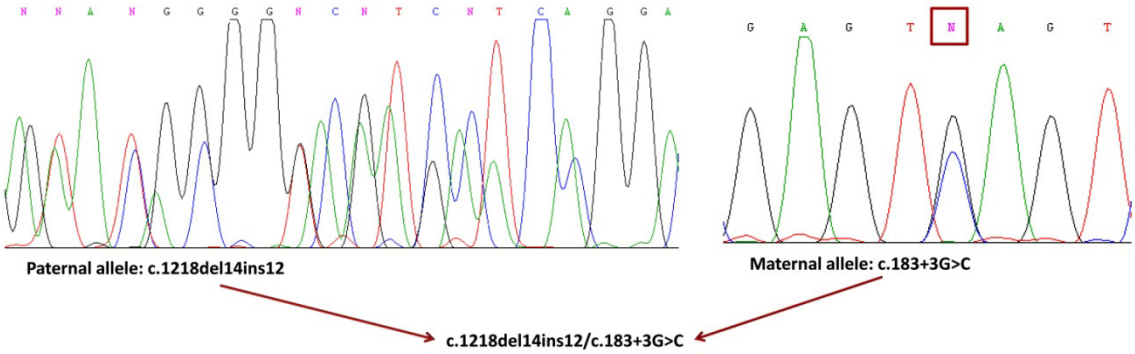

Figure 12 – Mutational profile of patient P6. This patient is a compound heterozygous for the mutations c.1218del14ins12 and c.183+3G>C (down panel). In the upper panel are the mutations found in the parental study.

Patient P7 was homozygous for the mutation c.1218del14ins12 (Figure 13). This mutation affects codon 406 in exon 12 of *PCCB* gene and consists in the deletion of 14 nucleotides and the simultaneous insertion of 12 nucleotides in the place occupied by the deleted nucleotides. This mutation is fairly common and is associated with a premature stop codon and, consequently, a truncated protein.

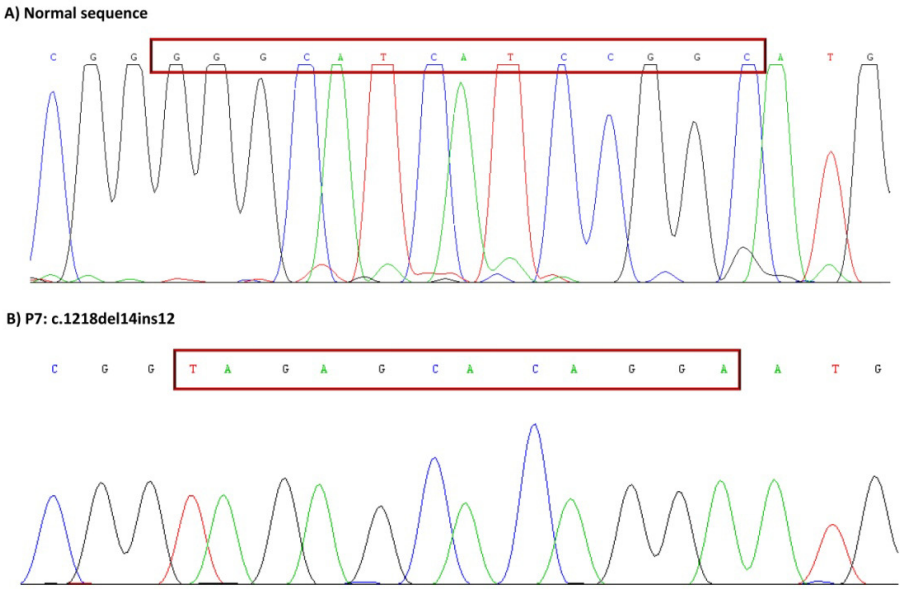

Figure 13 – Sequence profile of patient P7 genomic DNA. A) Wild-type sequence where the deleted nucleotides are highlighted. **B)** Sequence bearing the mutation found in P5. The inserted sequence is highlighted in red.

3.2. FUNCTIONAL ANALYSIS OF MUTATIONS IN ORGANIC ACIDURIAS

In this section we analyzed the functional effect of the splicing mutation found in *MUT* gene and of missense mutations found in *MMAB* gene.

Mutations are important genetic factors of human diseases and their role is determined by the diversity of their impact on molecular function. The analysis of mutations effect upon protein structure and function allows the elucidation of the effect of the allelic variants upon the MUT and ATR proteins, respectively, in order to find the best therapeutic option based on mutations specific mechanism of action.

3.2.1. Characterization of a splicing mutation in methylmalonic aciduria *mut* type

Since mutation c.1408-10A>G has not been previously described in the literature, we proceeded to analyze its possible effect upon the splicing profile and the resulting protein, in order to elucidate if this is a disease causing mutation and the pathogenic mechanism to address therapeutic strategies.

The *in silico* analysis of the sequence encompassing the mutation, using the human splicing finder software (www.umd.be/HSF/), indicated that this mutation might create a new acceptor splice site with a higher score (87.81), upstream the natural acceptor splice site. This analysis showed also that the natural splice site presents a low score (75.58), which might favor the possibility of activation of another splice site.

In order to study the effects of this new mutation, and since it was not possible to obtain patients' cells, an *ex vivo* minigene assay was performed to analyze the transcriptional profile. In this assay, exon 6 of *MUT* gene and the respective intronic flanking regions were amplified from P5 and from a control sample, and cloned into the pSPL3 vector. After the transfection of a COS cell line and a 24 hour incubation period, total RNA was extracted and analyzed by RT-PCR (Figure 14).

Direct sequencing analysis showed that the mutation creates a new splicing site upstream the original splice site for exon 6, which presents a low splicing score, as previously predicted by *in silico* analysis, leading to the introduction of nine additional nucleotides. The final result should be the introduction of three additional amino acids into the protein sequence. The corresponding band (band number 4, Figure 14) was a heteroduplex of the sequence containing nine additional nucleotides and also the normal sequence.

We also observed the presence of a lower molecular weight band, resulting from the elimination of 135 nucleotides from exon 6, which might translate into the elimination of 45 amino acid residues from the protein. The *in silico* analysis of the sequence corresponding to the wild-type exon 6, using the Alternative Splice Site Predictor (ASSP - http://wangcomputing.com) software, revealed the presence of a cryptic acceptor site (gaattgccagGAACACACAA), located inside exon 6, with a higher score (3.505) when compared with the one observed for the constitutive acceptor site (2.278).

We observed the presence of the same band in the control profile, and also a band corresponding to the heteroduplex formed between the normal sequence and the sequence lacking the 135 nucleotides, what suggests that this may be a normal event in control individuals.

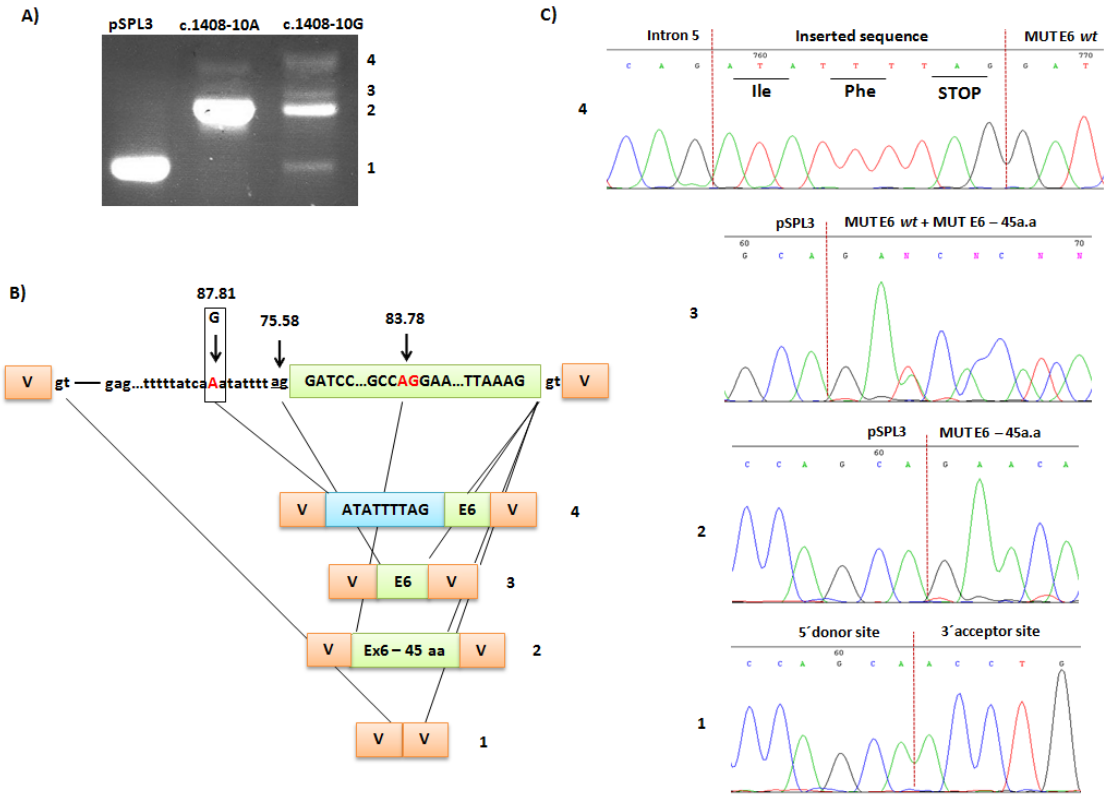

Figure 14 – Transcriptional profile obtained with the minigene ex vivo assay for the c.1408-10A>G mutation. A) RT-PCR profile, **B)** schematic representation of the different fragments obtained, **C)** Sequences of each fragment obtained. Splicing scores were calculated using the Human Splicing Finder software (http://www.umd.be/HSF).

3.2.2. Structural and functional analysis of allelic variants identified in methylmalonic *cblB* type patients

Five mutations were studied, two new mutations (p.His183Leu and p.Arg190dup), and three previously described mutations (p.Ile117_Gln118del, p.Arg186Trp and p.Glu193Lys). (HGMD® Professional 2013.1)

The new mutations (p.His183Leu and p.Arg190dup) were previously identified in two siblings with isolated methylmalonic *cblB* type phenotype (P8 and P9 – Table 10). Patient P8 was detected by expanded newborn screening and the phenotype of isolated methylmalonic aciduria was confirmed by the analysis of metabolites in urine by GS/MS, which showed elevated methylmalonic acid levels. Family genetic studies were performed and his sibling, P9 was later characterized and presented a small increase in methylmalonic acid levels. Both patients present a positive response to hydroxocobalamin treatment.

Table 10 – Biochemical, clinical and genetic data from isolated methylmalonic *cblB* type patients.

Patient	Gene	MMA levels at diagnosis (mmol/molcreat)	[14C]-Propionate incorporation -OHCbl/+OHCbl* (Fold change)	Genotype**(cDNA/gDNA/protein)	Clinical Outcome
P8	*MMAB*	830	0.63/1.19 (2X)	c.548A>T/c.568_570dup Chr12(hg19):g.109998881T>A/g.109998859_109998861dup p.His183Leu/p.Arg190dup	One month. Asymptomatic
P9	*MMAB*	58	1.06/2.59 (3X)	c.548A>T/c.568_570dup Chr12(hg19):g.109998881T>A/g.109998859_109998861dup p.His183Leu/p.Arg190dup	9y. Asymptomatic. Studied due to previous affected sibling
Control	-	1 – 13	1.90±1.18/2.34±1.61	-	-

NS: Not studied.

* [14C]-Propionate incorporation (nmol/10h/mg protein) in the absence or presence of 1µg/mL of hydroxocobalamin.

**Mutations according to NM_052845.3 (*MMAB*) and the genomic coordinates were obtained using the Mutalyzer 2.0 beta-26 software according to hg19 (https://mutalyzer.nl/positionConverter).

Further analysis revealed that p.His183Leu and p.Arg190dup variants were not described in the exome variant database (evs.gs.washington.edu). To identify genetic background variances that could explain the biochemical differences between the siblings, the promoter was sequenced and analysis of genomic rearrangements was performed. The genomic rearrangements were studied using a customized high-resolution comparative genomic hybridization assay (Metaboloarray°) and no changes or copy number variations were found.

The levels of immunoreactive ATR protein were analyzed by western blot in control and patients' derived fibroblasts and, as shown in Figure 15, both patients presented lower protein levels than the control, although P8 presents decreased levels when compared with his sibling P9.

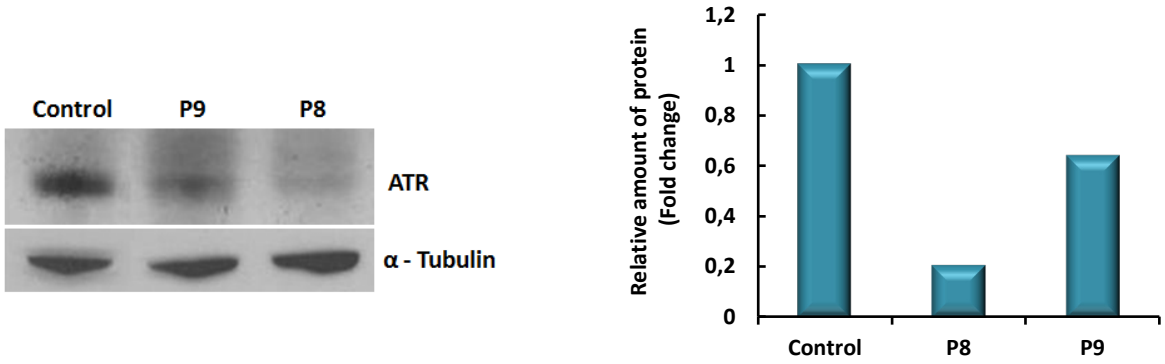

Figure 15 – Analysis of the immunoreactive ATR protein. ATR protein levels were assessed in control and methylmalonic *cblB* type patients, P8 and P9, by western blot.

To further assess the effect of these mutations upon the protein function of the *cblB* type patients, the metabolic pathway function was assessed by an indirect measure of [^{14}C]-propionate incorporation levels at physiological conditions (37 °C) and also under stress conditions (42 °C) (Figure 16).

The results of the [^{14}C]-propionate incorporation show a significant decreased rate at physiological conditions for patient P8, when compared with the control and with his sibling, patient P9 who, in the same conditions, presented levels comparable to the control. When the cells were incubated at 42 °C, the incorporation rate for P9 was decreased, indicating that, in a stress situation, the fibroblasts derived from this patient have the same behaviour as those of his affected sibling.

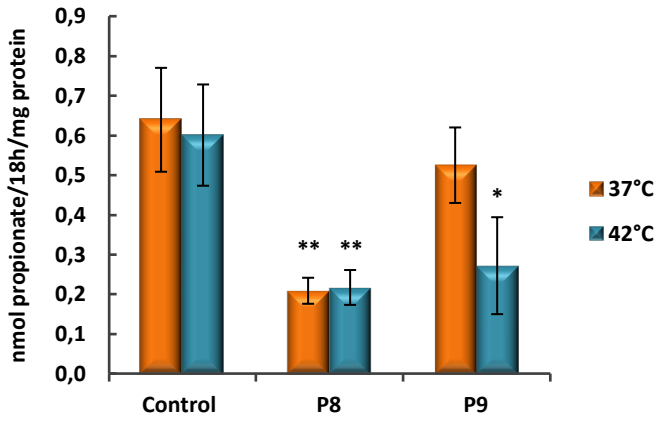

Figure 16 – Effect of stress conditions upon the ATR protein function. [^{14}C]-propionate incorporation of control and patients' dermal fibroblasts at 37 °C or 42 °C in the absence of hydroxocobalamin (OHCbl) to provide an indirect quantification of ATR activity. Results are the means ± SD for three independent experiments. (*P<0.05, **P<0.01)

3.2.3. Stability analysis of the p.His183Leu and p.Arg190dup allelic variants using a prokaryotic expression system

To further assess the effect of p.His183Leu and p.Arg190dup mutants found in patients P8 and P9, both were studied using a prokaryotic expression system. The human wild-type and the different mutant ATR proteins were expressed in an *E.coli* strain at physiological temperature (37 °C), and crude protein extracts were loaded into a SDS-PAGE gel. The results are shown in Figure 17 and, as can be observed, no soluble protein was obtained for the p.R190dup mutation, even when high amounts of crude extract were loaded.

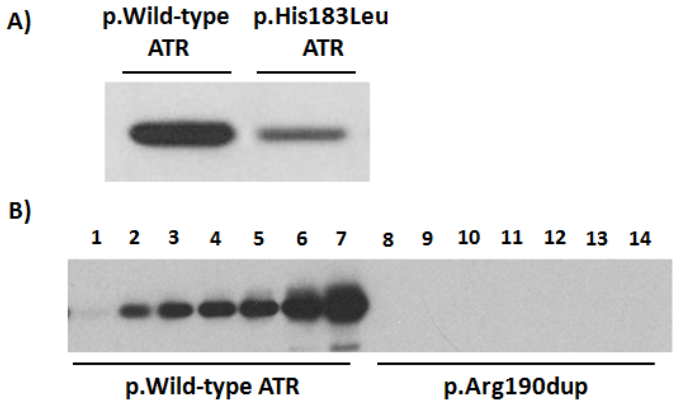

Figure 17 – Western blot of wild-type and mutant ATR proteins. A) Wild-type and p.His183Leu crude protein extracts obtained from an *E.coli* strain. **B)** Lanes 1 to 7 – different amounts of crude soluble bacteria extract of wild-type ATR, lanes 8 to 14 – different amounts of crude soluble bacteria extract of p.Arg190dup mutant.

Since it was not possible to obtain enough amount of protein for the p.Arg190dup mutant, no stability studies could be performed.

The mutation p.His183Leu was further studied in order to assess its impact upon the ATR protein folding stability. The wild-type and the mutant were expressed using the same prokaryotic system, both at physiological temperature (37 °C) and permissive folding conditions (27 °C) and samples were collected at different times. The crude extracts were analyzed by SDS-PAGE followed by immunodetection, and the amount of reactive protein was quantified by laser densitometry (Figure 18).

The results obtained at physiological temperature showed that the mutant p.His183Leu is more unstable than the wild-type protein, presenting about 58 % decrease in stability when compared with the wild-type, which indicates that this could be a destabilizing mutation (Table 11).

When p.His183Leu and wild-type proteins were incubated in permissive folding conditions (27 °C), *in vitro* stability was increased for both proteins, but especially for the p.His183Leu mutant that presented a 3.3 fold increase reaching the wild-type levels. This indicates that most probably p.His183Leu is a folding mutant (Figure 18).

Table 11 – Relative protein stability for wild-type and p.His183Leu mutant at physiological and folding permissive temperatures.

	Relative protein stability (hours)		Fold change
	37°C	27°C	
Wild-type ATR	5.4	6.1	1.13
p.His183Leu ATR	2.28	7.6	3.3

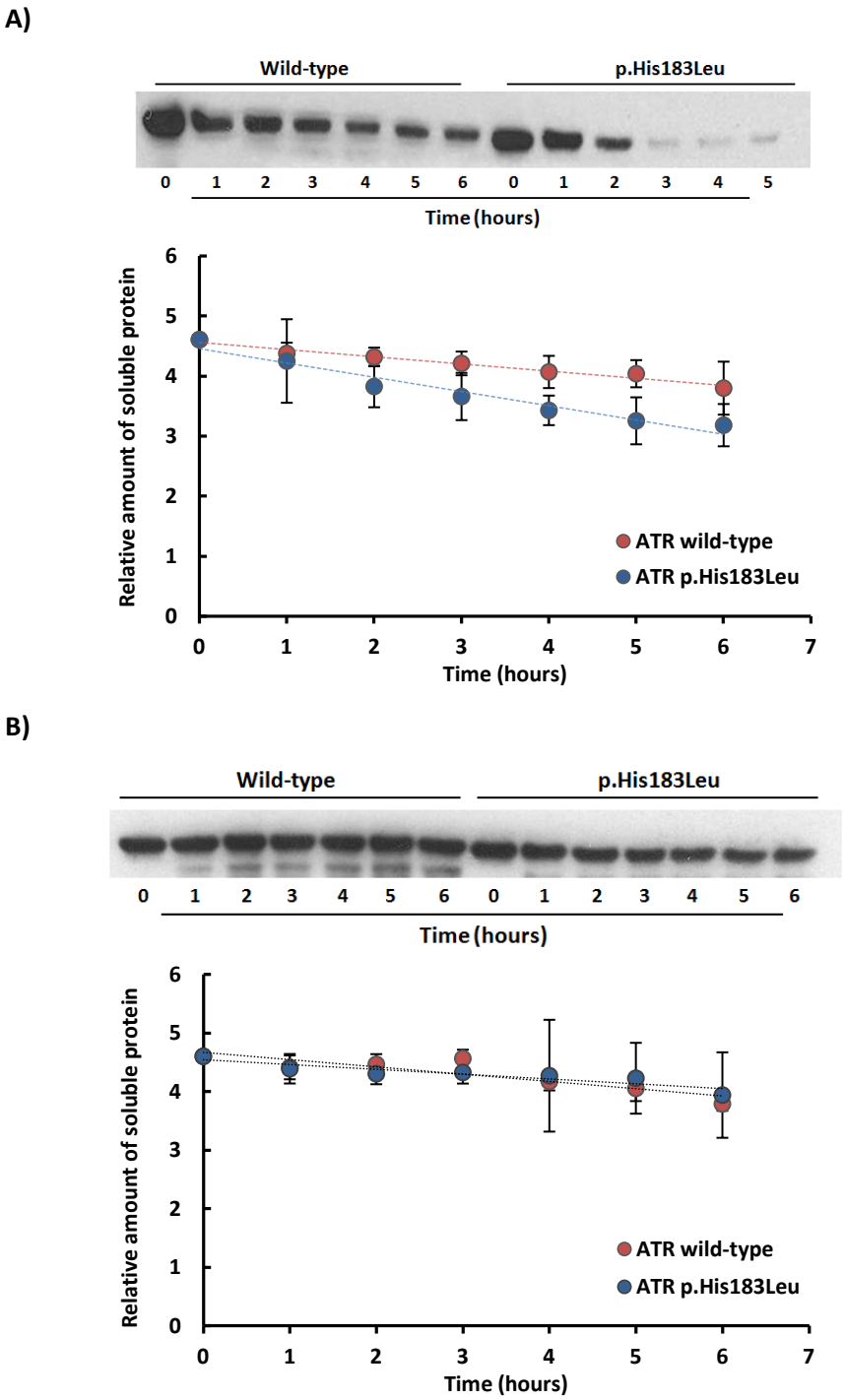

Figure 18– Degradation profile of the wild-type and mutant p.His183Leu at A) physiological (37 °C) and B) permissive conditions (27 °C). The crude extracts were incubated over time at 37 °C and aliquots were collected and analyzed by western-blot. The data show the mean value ± SD (n=6) and represent the percentage of the density of each protein compared to time zero.

3.2.4. Chaperone and protease profile in *cblB* type patients bearing p.His183Leu and p.Arg190dup mutations

Since patients P8 and P9 have the same genotype but different phenotypes, and both mutations (p.His183Leu and p.Arg190dup) are responsible for a decrease in protein stability, the mitochondrial protein quality control system (mtPQC) was studied. The levels of mitochondrial chaperones, Hsp60 and Hsp70, and the protease Lon protein, were analyzed by western blot in fibroblasts derived from control and *cblB* patients, P8 and P9.

Figure 19 shows an increase on the immunoreactive protein levels of the mitochondrial protein Hsp70 in both patients when compared to control, although patient P8 presents higher levels than his sibling P9. Mitochondrial chaperone Hsp60 levels seem normal in patient P8 cells, while a slight decrease was observed in patient P9.

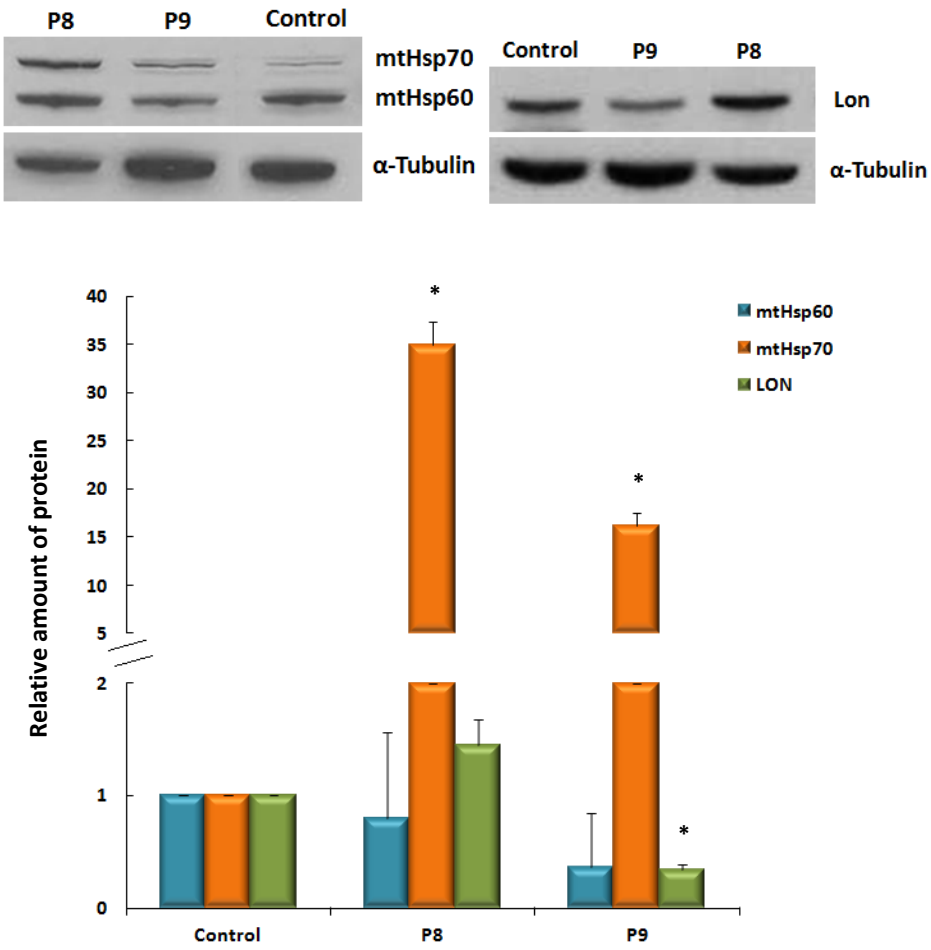

Figure 19 – Mitochondrial protein quality control analysis. Western blotting of soluble crude extract from patients´ fibroblasts using anti mtHsp70, mtHsp60 and Lon antibodies is shown.αThe -tubulin protein was used as control loading protein. Protein amount was quantified by laser densitometry and data represent the mean quantification values ± SD of three independent experiments (*P<0.05).

The analysis of immunoreactive levels of Lon protease (Figure 19) showed an increase in protein levels for patient P8, while his sibling P9 showed a markedly decrease in the amount of reactive protein.

3.2.5. Stability analysis of allelic variants affecting the ATR protein using a prokaryotic expression system

The effect of other allelic variants affecting ATR protein was also analyzed. The previously described mutations, p.Ile117_Gln118del, p.Arg186Trp and p.Glu193Lys were studied. The p.Ile117_Gln118del was identified in a *cblB* type patient diagnosed in the laboratory, and the p.Arg186Trp and p.Glu193Lys variants were analyzed due not only to their high incidence in the *cblB* type patients population (p.Arg186Trp) and also due to their characterization as folding mutants, and hence, as interesting targets for therapeutic approach using chaperones (Fan and Bobik, 2008).

As described before, human wild-type ATR and the different mutants were expressed in an *E.coli* strain at physiologic temperature (37 °C), and crude protein extracts were loaded into a SDS-PAGE gel. The results are shown in Figure 20 and, as can be observed, no soluble protein was obtained for p.Ile117_Gln118del mutation.

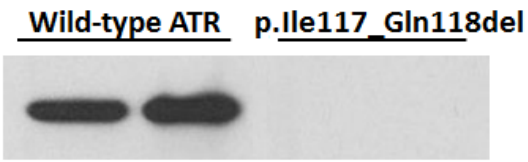

Figure 20 – Western blot of wild-type ATR and p.Ile117_Gln118del mutant. Crude protein extracts obtained from an *E.coli* strain were analyzed at physiological temperature (37 °C).

The p Ile117_Gln118del was also expressed at permissive folding conditions (27 °C), but no differences in the expression of the mutant were observed.

Stability studies were performed at 37 °C for both p.Arg186Trp and p.Glu193Lys mutants, as described before and a decrease in stability was observed for the two mutant proteins, especially for p.Glu193Lys mutant (Figure 21).

The p.Arg186Trp mutant present a reduction in stability of about 37 % when compared to the wild-type, while the p.Glu193Lys mutant presents a 93 % reduction of stability in the same conditions (Table 12).

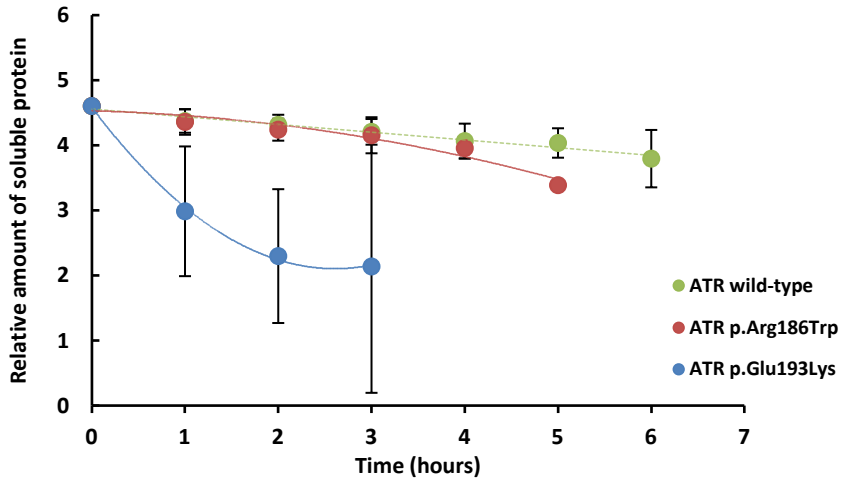

Figure 21– Degradation profile of the wild-type and the p.Arg186Trp and p.Glu193Lys mutant ATR proteins at physiological conditions (37 °C). The crude extracts were incubated over time at 37 °C and aliquots were collected and analyzed by western-blot. The data show the mean value ± SD (n=3) and represent the percentage of the density of each protein compared to time zero.

Table 12 – Relative protein stability for wild-type ATR and p.Arg186Trp and p.Glu193Lys mutants at physiological temperature.

	Relative protein stability at 37 °C (hours)	Relative protein stability reduction (%)
Wild-type ATR	5.4	100
p.Arg186Trp ATR	3.4	37
p.Glu193Lys ATR	0.38	93

3.2.6. Structural analysis of missense changes affecting ATR protein

The ATR protein is a homotrimer, being each subunit composed of five α-helices with the active site located at the monomers interface, and mutations affecting protein residues are responsible for structural and functional defects. In order to analyze the effect of the p.Ile117_Gln118del, p.His183Leu, p.Arg186Trp, p. Arg190dup and p.Glu193Lys mutations upon the trimeric ATR protein structure, the crystallographic structure (2IDX) available at the public database *Protein Data Bank* (PDB – *www.pdb.org*) was used.

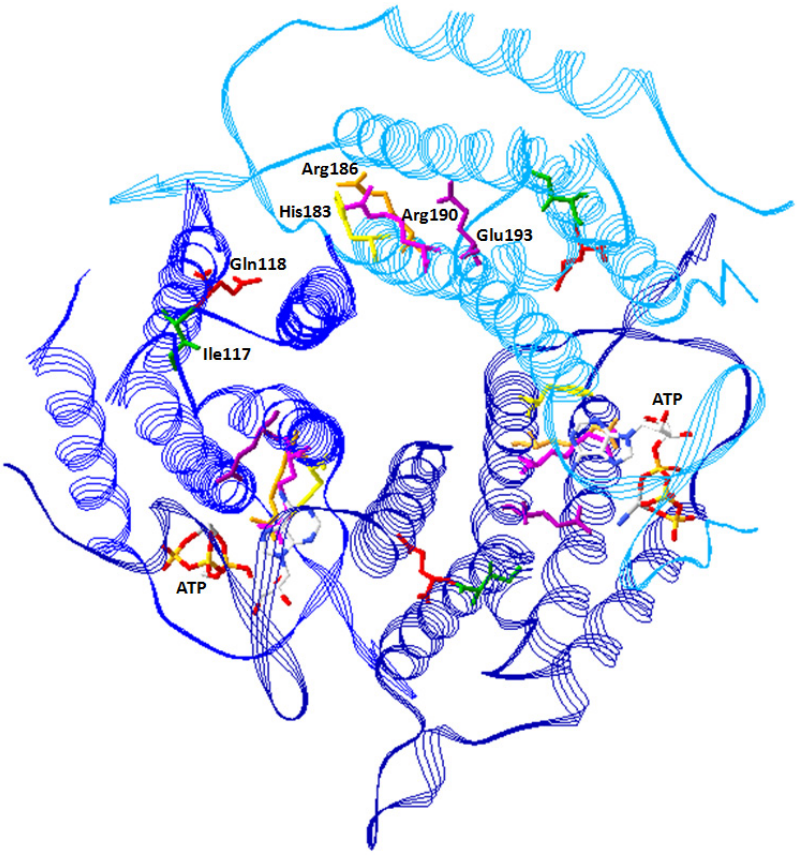

Figure 22 – Tridimensional trimeric ATR structure and localization of the mutated residues. All three monomers are represented in blue and the residuesIle117 in green, Gln118 in red, His183 in yellow, the Arg186 in orange, Arg190dup in pink and the Glu193 in purple. This image was obtained using the SPDB software and the protein structure available at PDB database (2IDX).

The residues Ile117 and Gln118 are located on the 2α-helix of the ATR protein. The Gln118 is an invariant residue that establishes hydrogen bonds with the 3α – 4α helices loop (Schubert and Hill, 2006), hence its elimination probably disrupts the protein structure leading to a severe effect.

The Arg190 residue is located in the 4α-helix of the ATR protein and establishes hydrogen bonds with ATP (Schubert and Hill, 2006). The duplication of this residue probably has a severe impact on the protein structure, leading to its complete loss-of-function.

The effect of the missense mutations, p.His183Leu, p.Arg186Trp and p.Glu193Lys, was also analyzed *in silico* using the bioinformatic program CAFFE. This computational method is based on a fold recognition algorithm that uses an effective free energy function, instead of relying on sequence similarity and derived energy parameters for simplified models of protein folding. This program analyzes the entropy energy lost to form the protein complex. It sets a minimum threshold of 2.3 for the inter-chain energy and if all the three ATR chains (A, B and C) present a value above 2.3, the complex is formed (Bastolla et al, 2001; Bastolla et al, 2004).

The three missense mutations were analyzed and the values obtained were compared to the wild-type protein and are depicted in Table 13. The p.Glu193Lys mutation is the most unstable and none of the values obtained for the three chains was above 2.3, indicating that this mutant does not assembles correctly. The complex assembly is also compromised for mutation p.His183Leu although two of the chains (A and C) may interact. Mutation p.Arg186Trp presents the same inter-chain values as the wild-type but a slightly higher total energy value. This suggests the change of an arginine residue for a tryptophan makes the molecular structure more rigid, thus affecting the protein mobility and stability.

Table 13 – Amount of entropy necessary to form the three stable chains (A, B and C) observed in the wild-type ATR protein and mutants, p.His183Leu, p.Arg168Trp and p.Glu193Lys. The values showed were obtained using the CAFFE program which uses a minimum of 2.3 (3RT) threshold for a stable formation.

	Inter-chain energy	Total chain energy
Wild-type ATR	-2.43 A -2.36 B -2.56 C	-24.0 (ABC)
p. His183Leu ATR	-2.32 A -2.25 B -2.45 C	-16.2 (AC) -6.5 (B)
p. Arg186Trp ATR	-2.43 A -2.36 B -2.56 C	-24.7 (ABC)
p. Glu193Lys ATR	-2.26 A -2.19 B -2.22 C	-8.2 (A) -6.1 (B) -6.3 (C)

The results obtained with the *in silico* analysis corroborate the data obtained with the stability assays performed, and are also in accordance with the data available in the literature for the p.Arg186Trp and p.Glu193Lys mutants.

3.3. MITOCHONDRIAL DYSFUNCTION IN ISOLATED METHYLMALONIC ACIDURIA

Organic acidurias have been related with mitochondrial dysfunction, which can be translated in high reactive oxygen species (ROS) levels, impaired bioenergetic function, defective mitochondrial morphology and, ultimately, apoptosis. In order to assess if the phenotypic differences observed in the previously described *cblB* type patients could be

related to defects in mitochondrial function, ROS levels, mitochondrial morphology and bioenergetics function was assessed in patients P8 and P9. Mitochondrial dysfunction was also analyzed in two methylmalonic *mut* type patients, patients P10 and P11 (Table 14).

Table 14 – Biochemical, clinical and genetic data from isolated methylmalonic *mut* type patients.

Patient	Gene	MMA levels (mmol/molcreat)	Genotype (cDNA/gDNA/protein)*	Outcome
P10	*MUT*	3032	c.1808G>A/c.1957-892C>A Chr6(hg19)g.49409553C>T/g.49404227G>T p.Val583fs/p.Gln652fs	Deceased
P11	*MUT*	4159	c.1850T>G+c.205A>G/c.1957-898A>G Chr6(hg19):g.49408025A>C+g.49426975T>C /g.49404234T>C p.Leu617Arg+p.Ile69Val/p.Gln652fs	Deceased
Control	-	1 – 13	-	-

NS: Not studied.

ND: Non determined.

* Mutations according to NM_052845.3 (MMAB) and NM_000255.3 (MUT) and the genomic coordinates were obtained using the Mutalyzer 2.0 beta-26 software (https://mutalyzer.nl/positionConverter).

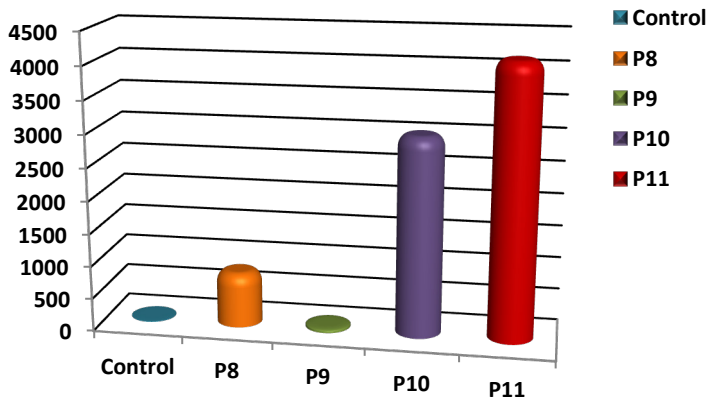

Figure 23 – Methylmalonic acid levels of *cblB* and *mut* type patients.

These patients were included in this study for comparison with *cblB* type patients, since they present higher methylmalonic acid levels (Figure 23), which have been related to mitochondrial dysfunction.

3.3.1. Analysis of ROS and mitochondrial morphology in isolated methylmalonic patients

Total ROS levels were analyzed by flow cytometry in *cblB* type patients (P8 and P9) and control samples, using a H_2DCFDA fluorescence probe to measure hydrogen peroxide (H_2O_2)

levels and propidium iodide to quantify the number of death cells. The ROS levels of patient P10 were previously measured (Richard et al, 2007) and were also included in the graph for comparison.

As shown in Figure 24, both *cblB* type patients present significant elevated ROS levels when compared with control, and patient P8 present higher ROS levels than his sibling, P9. Patient P10 also present significantly high ROS levels when compared with control.

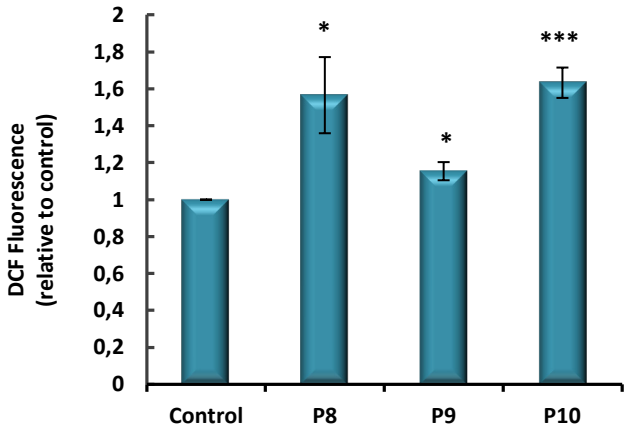

Figure 24 – Analysis of intracellular ROS content in isolated methylmalonic patients. Control and *cblB* patients´ fibroblasts were analyzed. Cells were incubated with the H_2DCFDA fluorescence probe and propidium iodide. ROS levels were accessed by flow cytometry. The X axis represents patients´ cell lines and the Y axis represents the fluorescence levels. Data represent the mean ± SD levels of five independent experiments each performed in triplicate. (*P<0.05, ***P<0.001).

Elevated ROS levels have been related to altered mitochondrial morphology, hence, a specific mitochondrial probe, MitoTracker® Red CM-H2Ros, was used to stain control, *cblB* type (P8 and P9) and *mut* (P10 and P11) patients' mitochondria and the cells were analyzed by confocal microscopy (Figure 25).

The thread-like mitochondria morphology is associated with mitochondrial fusion, while the dotted or grain-like morphology is associated with mitochondrial fission and mitochondrial dysfunction.

As can be observed in Figure 25, the mitochondria in control-derived fibroblasts present a low percentage of grain-like morphology, while both *cblB* and *mut* type patients present a higher percentage. Although the levels of grain-like mitochondria are also elevated in patient P9 when compared with control, they are lower than the ones displayed by his sibling, P8, and the *mut* type patients, P10 and P11.

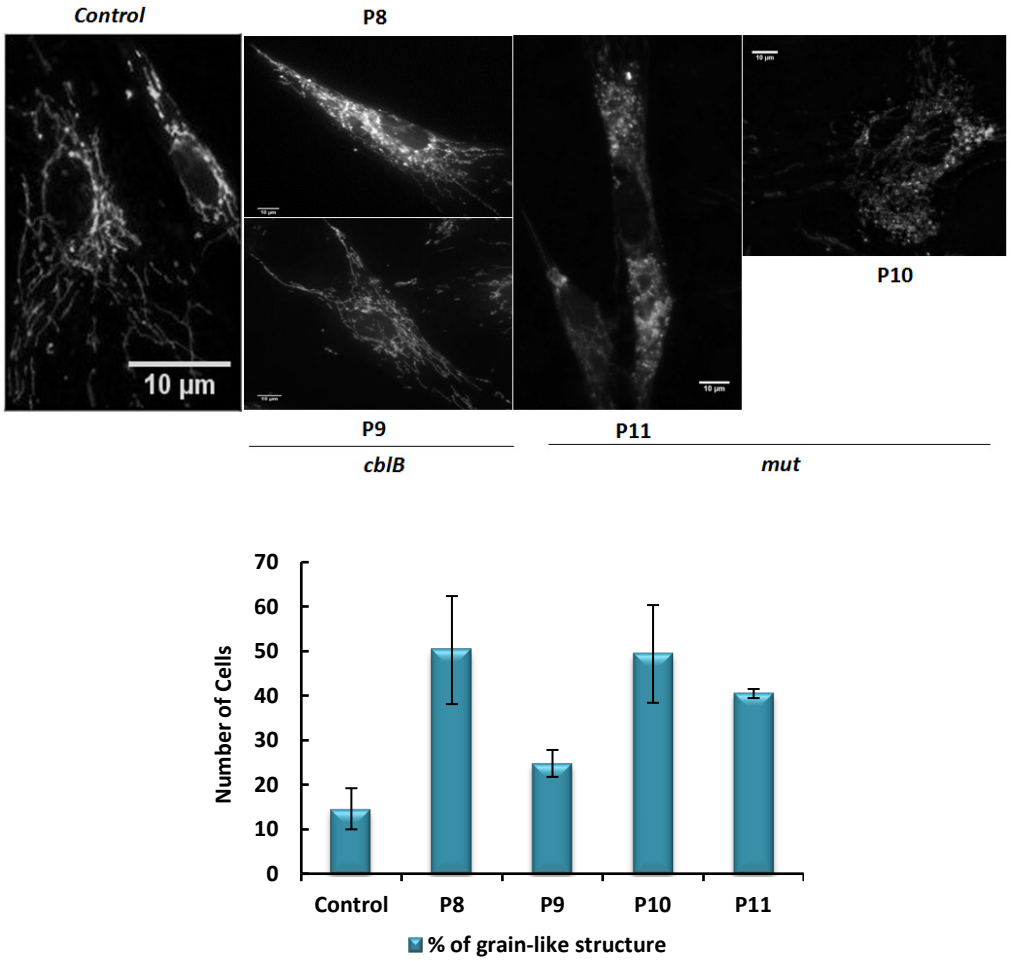

Figure 25 – Mitochondrial morphology in control, *cblB* type (P8, P9) and *mut* type patients (P10 and P11). Cells labeled with MitoTracker®Red CM-H2Ros lead to two distinct phenotypes: thread (Control, P9) and grain (P8, P10 and P11), being the last associated with mitochondria fission. The results are shown as means ± SD of three independent experiments.

The bioenergetic function was analyzed in *cblB* and *mut* type patients and also in controls. The cells were incubated in culture medium supplemented with glucose or galactose and the mitochondrial function was assessed in adherent cells using a SeaHorse® extracellular flux analyzer.

A series of respiratory chain inhibitors and uncouplers [oligomycin, carbonyl cyanide 4-(trifluoromethoxy) phenyl-hydrazone – FCCP, antimycin and rotenone] were added throughout the experiment and the oxygen consumption rate (OCR) levels were assessed.

The profile obtained for this assay is represented in Figure 26. The first three values represent the cells basal respiration rate. When the ATP synthase inhibitor, oligomycin, is added, the OCR rate decreases representing the ATP-linked respiration. The addition of the uncoupler, FCCP, leads to an increase in OCR due to the cells intent to produce ATP and represents the maximal respiration rate. Finally, the addition of antimycin, a cytochrome c

reductase inhibitor, and rotenone, a complex I inhibitor, leads to the complete inhibition of oxidative phosphorylation.

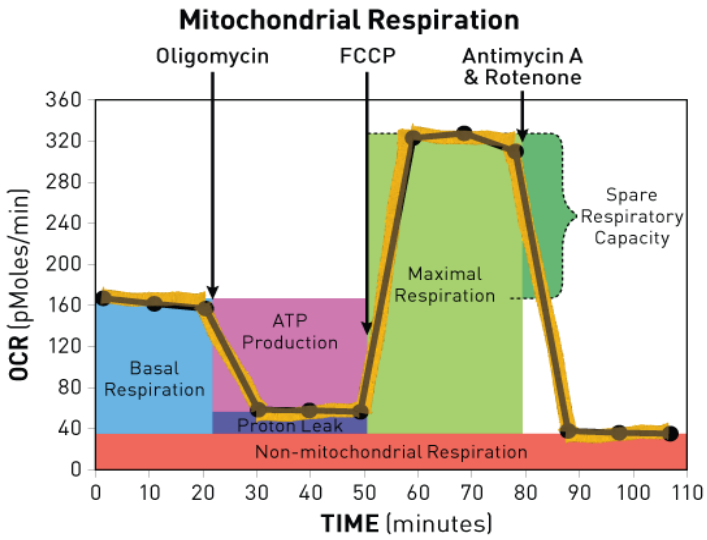

Figure 26 – Representation of the fundamental parameters of mitochondrial respiration obtained with this experiment. Basal respiration, ATP-linked respiration, proton leak, maximal respiration, reserve capacity (spare respiratory capacity) and non-mitochondrial respiration. (www.seahorsebio.com).

The results obtained for the patients and control cells incubated in a glucose rich medium are shown in Figure 27. A decrease in the general OCR levels is observed for all the patients when compared with the control. Regarding the *cblB* type patients, the OCR levels of patient P8 are lower than the ones of the sibling, P9. Comparing the OCR levels among the *mut* type patients, the general OCR levels of patient P10 are much lower when compared with those of patient P11.

When the control and patients' cells were incubated in a galactose rich medium, an increase in general OCR levels was observed for control and patients (Figure 27). The respiration levels were also decreased for all patients when compared with the control levels.

The maximum OCR levels (the OCR value obtained after the addition of FCCP), the reserve capacity (maximum OCR minus basal OCR value), ATP-linked respiration (OCR after the addition of oligomycin minus the basal OCR), and non-mitochondrial respiration (OCR obtained after the addition of rotenone and antimycin) were calculated using the data obtained and the results are shown in Figure 28.

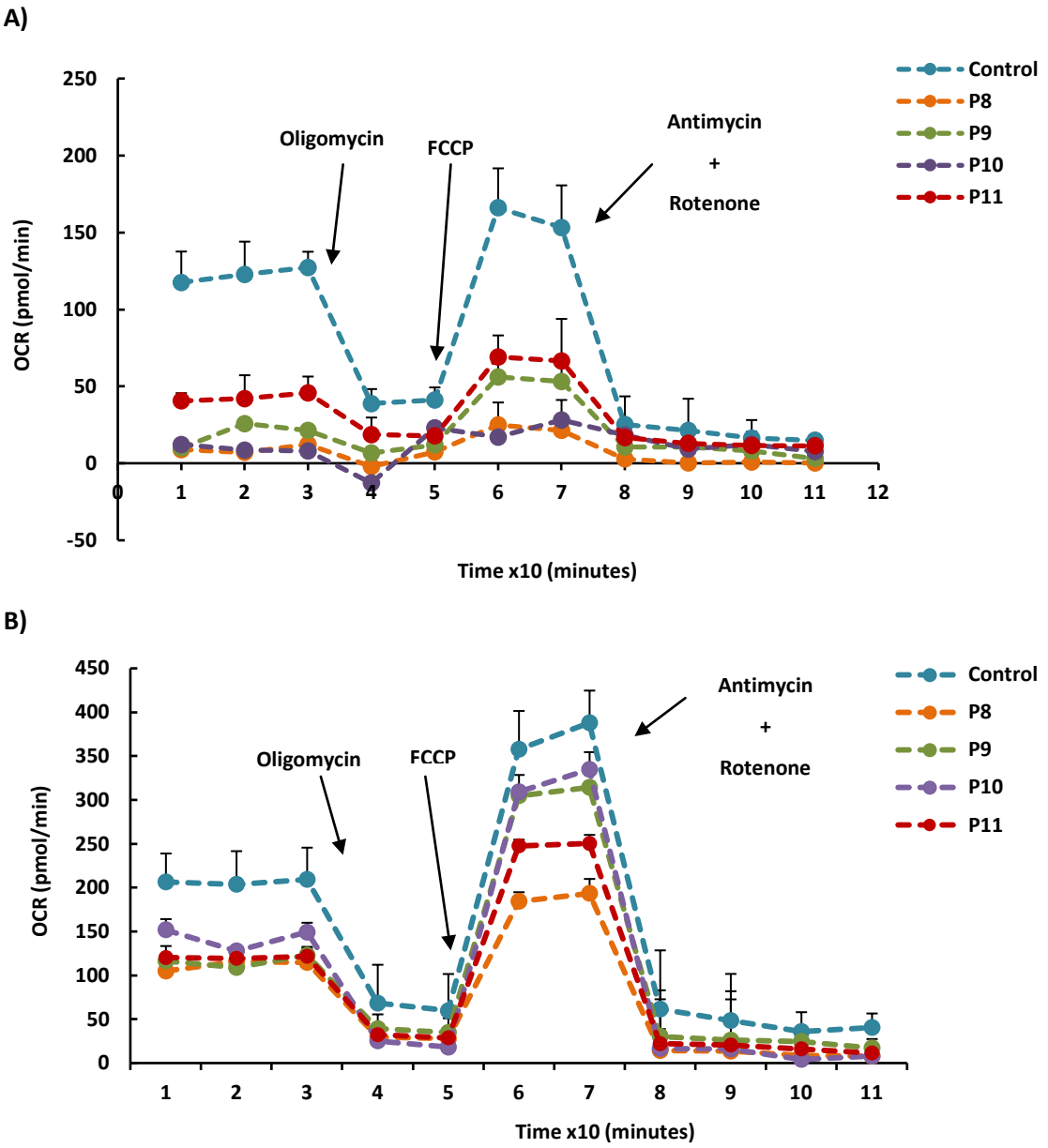

Figure 27 – Bioenergetic profile of control and *cblB* and *mut* type patient fibroblasts. Cells were treated with DMEM supplemented with glucose **A)** or galactose **B)** and the OCR profile for each was measured. Data are means ± SD for one independent experiment, performed in triplicate.

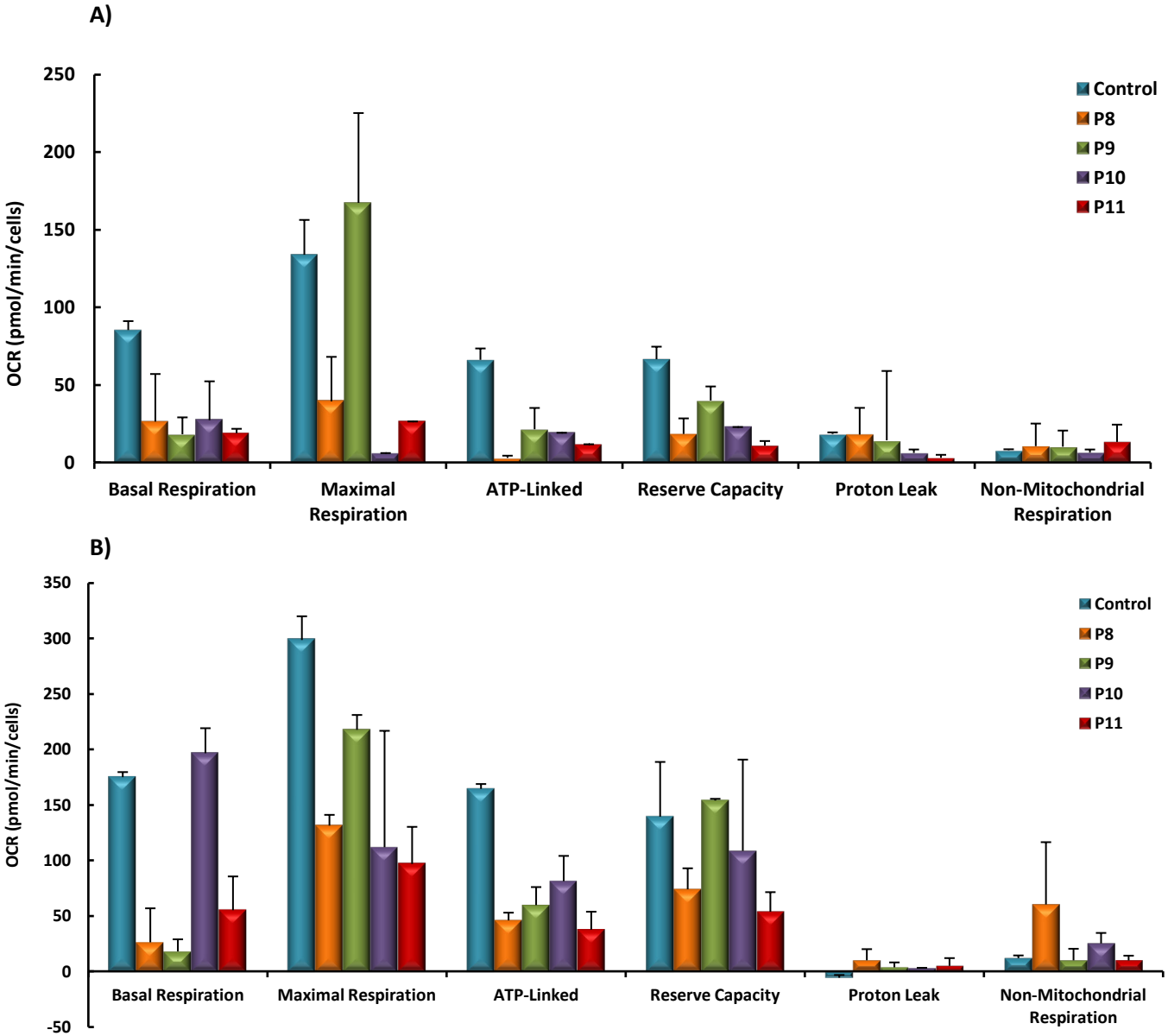

Figure 28 – Bioenergetic profile of control and *cblB* and *mut* type patient fibroblasts. Cells were treated with DMEM supplemented with glucose **A)** or galactose **B)** and the OCR profile for each was measured. Maximum OCR (the OCR value obtained after the addition of FCCP), reserve capacity (maximum OCR minus basal OCR value), ATP-linked respiration (OCR after the addition of oligomycin minus the basal OCR), and non-mitochondrial respiration (OCR obtained after the addition of rotenone and antimycin) were calculated using the data obtained. Data are means ± SD for three independent experiments, each performed in triplicate.

Isolated methylmalonic patients, *cblB* and *mut* type, derived fibroblasts incubated in glucose rich medium (Figure 28) presented markedly lower basal respiration levels, ATP-linked respiration and reserve capacity when compared with the control levels. Patient P9 presents higher maximal respiration and reserve capacity levels, but also proton leak levels, when compared with patients P8, P10 and P11. All patients' cells present slightly higher non-mitochondrial respiration levels than the control.

When the cells were incubated in a galactose rich medium, patients P8, P9 and P11 derived fibroblasts presented lower basal respiration levels when compared with control and also with patient P10. All the patients present decreased maximal respiration and ATP-linked respiration levels when compared to the control, although patients P9 and P10 present higher OCR levels than patients P8 and P11, respectively. Patients P9 and P10 showed reserve capacity levels in the control range, while P8 and P11 showed decreased levels. It is to note that in galactose rich medium, patient P8 displayed increased non-mitochondrial respiration levels.

Finally, the velocity of formation/opening of the mitochondrial permeability transition pore (mPTP) was also determined in fibroblasts derived from *cblB* and *mut* type patients and control. Velocity of mPTP formation/opening can be measured by following the ability of mitochondria to take up and retain Ca^{2+}.

The control and patients-derived fibroblasts were incubated in the reaction medium for 18 hours and the formation/opening of the pore was assessed by a fluorimetry assay. A Ca^{2+} specific fluorescent probe was used, the cells were permeabilized and Ca^{2+} insults were performed over time. Fluorescence increases from baseline value with each Ca^{2+} addition and, as the mitochondria takes up the Ca^{2+}, a decrease in fluorescence is observed until mitochondria takes up enough Ca^{2+} for the mPTP formation/opening occur and an increase of fluorescence is observed due to the intramitochondrial Ca^{2+} release. The experiment was performed in the presence of adenine nucleotide, ADP, and the results are shown in Figure 29.

The formation/opening of the mPTP is premature for *cblB* type patients, P8 and P9, when compared with control and especially for patient P8 who presented a higher formation/opening rate than his sibling P9. The *mut* type patients presented an mPTP formation/opening rate similar to the control, although in patient P10 the mPTP formation/opening rate was slightly premature when compared with control and patient P11.

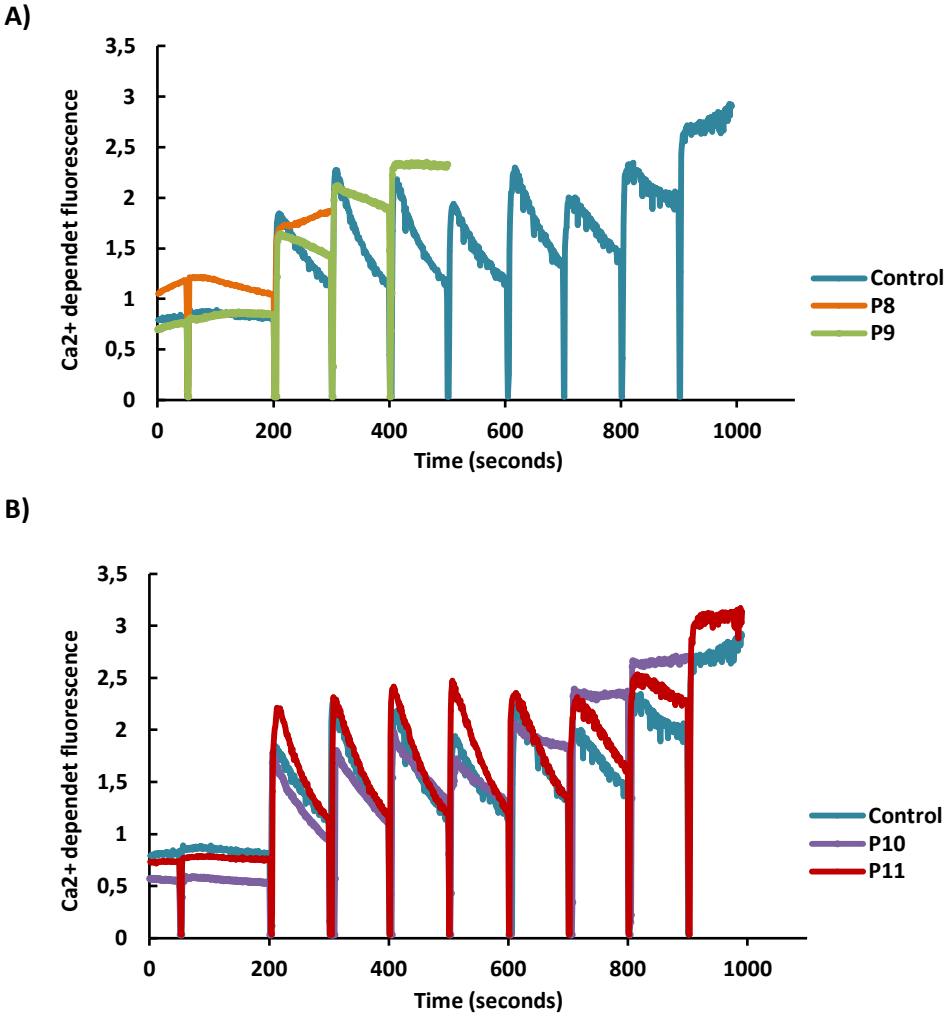

Figure 29 – Mitochondrial permeability transition pore formation/opening profile for *cblB* A) and *mut* B) type patients. The data are representative of the profile obtained in one experiment although at least three independent experiments were performed. The maintenance of the same profile for each patient and control was taken into account.

3.4. SPECIFIC THERAPY STRATEGIES IN INHERITED METABOLIC DISORDERS

3.4.1. Effect of pharmacological chaperones on ATR protein

Some patients respond to treatment with hydroxocobalamin, but the majority does not present biochemical and/or clinical improvements. Most of the mutations affecting *cblB* type patients are of missense type and hence, chaperone therapy is a good therapeutic option.

In order to find new pharmacological chaperones, a set of 2,000 compounds, from a commercially available library (MyriaScreen Diversity Collection) bearing a total of 10,000 compounds, has been previously analyzed in the laboratory by differential scanning fluorimetry (DSF) and circular dichroism (CD), and a total of six compounds were selected.

The effect of these six compounds was also previously analyzed in the laboratory using a prokaryotic expression system and a cellular line bearing the missense mutation p.Ile96Thr. Two different concentrations of the compounds, 40 µM and 80 µM, and also the corresponding amount of DMSO, since the compounds are suspended in that solvent, were used. Of these six compounds, one was selected as the most efficient at the highest concentration (80 µM): compound V (N-{[(4-chlorophenyl)carbamothioyl]amino}-2-phenylacetamid) (Figure 30).

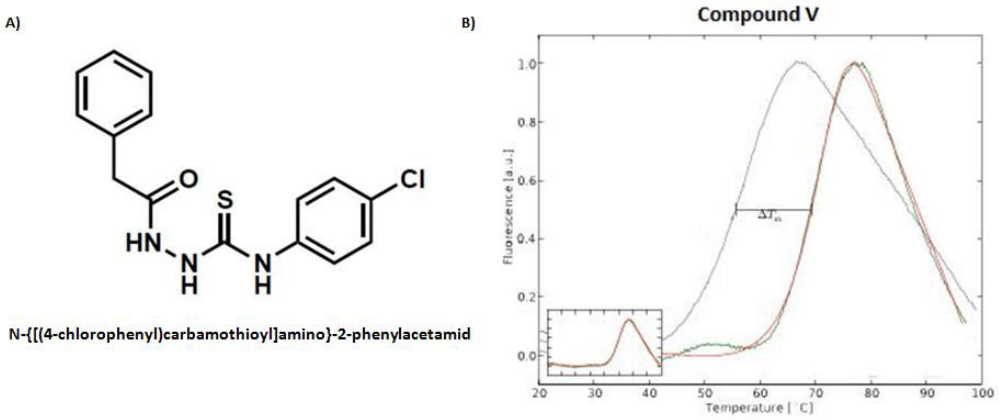

Figure 30 – Compound V structure (A) and DSF profile (B). The DSF profile was obtained using the purified ATR protein and a shift to the right (red line), indicating a stabilizing effect was observed. In the left lower part of the figure, a representation of the crude results is also showen.

3.4.2. Evaluation of the pharmacological effect of compound V upon missense mutations affecting *MMAB* gene using a prokaryotic expression system

The effect of compound V upon the p.Ile96Thr mutant was previously study in the laboratory and, to widen the study of this pharmacological compound upon other missense mutations found in *cblB* patients, the mutant variants p.His183Leu, p.Arg186Trp and p.Glu193Lys were also studied. The mutant and wild-type ATR proteins were expressed in a prokaryotic expression system and incubated with 80 µM of compound V and the results are depicted in Figure 31.

An increase in the *in vitro* stability of all proteins, both wild-type and mutants, was observed and is presented in Table 15. The stability of the wild-type ATR protein was slightly increased (about 1.1 fold) while the highest increase (about 15 fold) was observed for the p.Glu193Lys mutant. The incubation with compound V had the same stabilizing effect on p.His183Leu and p.Arg186Trp mutants. The p.His183Leu showed an increase of 2.8 fold and the p.Arg186Trp mutant revealed an increase of about 2.5 fold when compared with the

respective mutants without treatment. The increase in the stability observed for mutants p.His183Leu and p.Arg186Trp is in the same range of the increase in stability previously observed for the p.Ile96Thr mutant (3.24 fold).

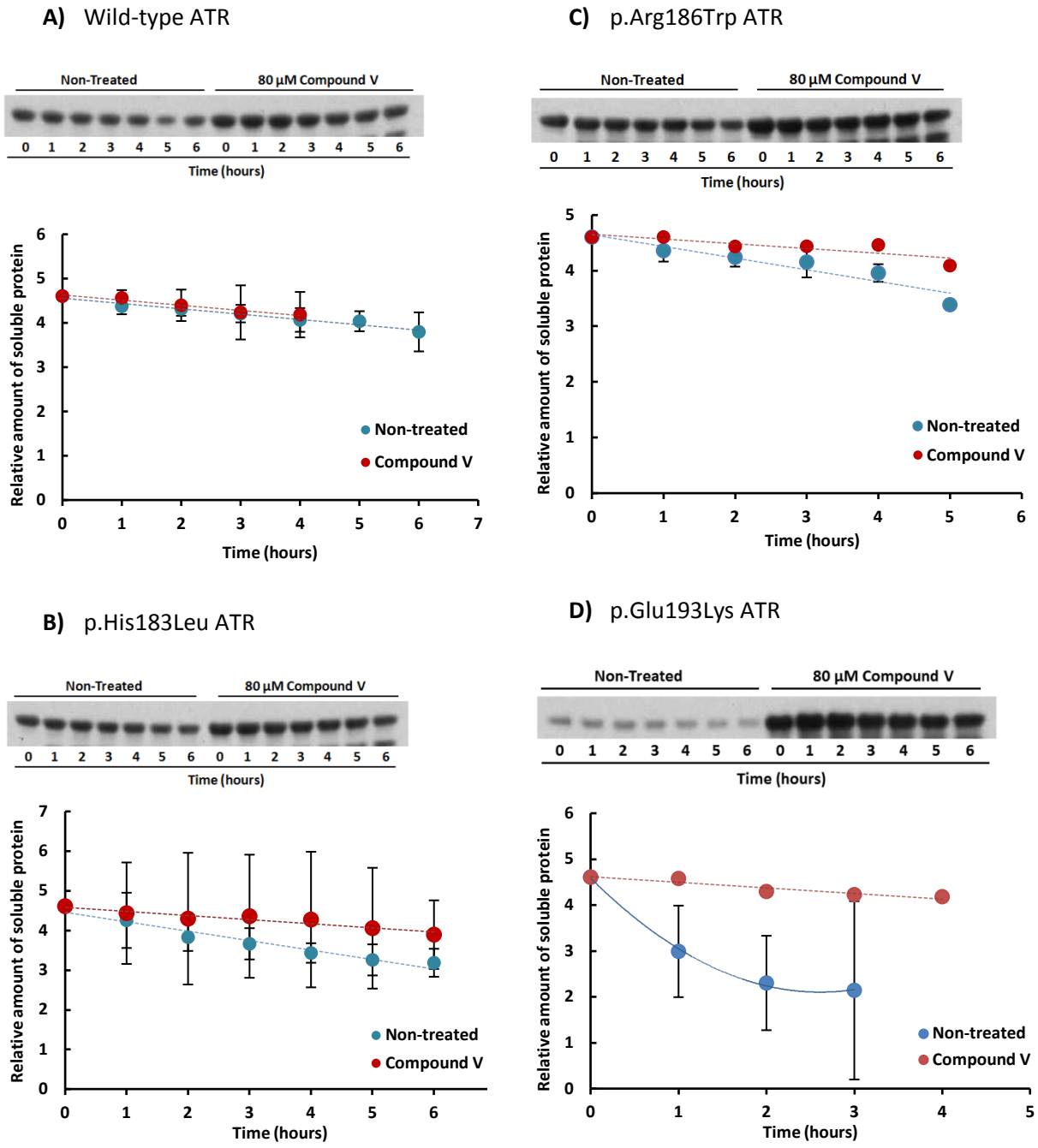

Figure 31 – Degradation profile of the A) wild-type ATR and B) p.His183Leu, C) p.Arg186Trp and D) p.Glu193Lys mutant ATR proteins at physiological conditions (37 °C) treated with 80 µM of compound V. The crude extracts were incubated over time at 37 °C and aliquots were collected and analyzed by western-blot. The data show the mean value ± SD (n=3) and represent the percentage of the density of each protein compared to time zero.

Table 15 – Relative protein stability for wild-type ATR and p.His183Leu, p.Arg186Trp and p.Glu193Lys mutants at physiological temperature before and after compound V treatment.

	Relative protein stability at 37°C (hours)		Fold change
	Non-treated	80 µM compound V	
Wild-type ATR	5.4	6.1	1.1
p.His183Leu ATR	2.28	6.4	2.8
p.Arg186Trp ATR	3.4	8.6	2.6
p.Glu193Lys ATR	0.38	5.8	15.2

These results indicate that compound V is a promising pharmacological chaperone for treating *cblB* patients carrying diverse missense mutations.

3.4.3. Study of the stabilizing effect of compound V upon p.His183Leu mutant using a cellular model

In order to assess the effect of compound V upon the p.His183Leu mutant, an immortalized fibroblast-derived cell line harboring this mutation was used. Since the effect of compound V upon p.Ile96Thr mutant had been previously characterized, an immortalized cell line harboring this mutation was used as positive control. An immortalized cell line harboring the mutation p.Ile117_Gln118del was used as a negative control.

The cells were incubated with 80 µM of compound V, or the corresponding amount of DMSO for 72 hours and the ATR activity was indirectly assessed by measuring the propionate incorporation into acid-precipitable material (Figure 32).

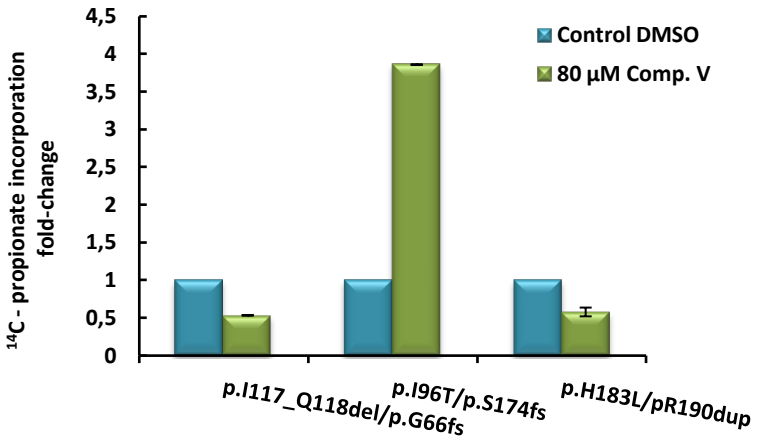

Figure 32 – Effect of compound V upon p.His183Leu mutant studied in a cellular disease model. Immortalized patient-derived fibroblasts harboring the missense mutations p.Ile117_Gln118del, p.Ile96Thr and p.His183Leu were incubated with 80 µM of compound V for 72 hours. The ATR activity was indirectly measured via [^{14}C]-propionate incorporation into acid-precipitable material in intact cells.

Nevertheless, as observed in Figure 32, the treatment with compound V was not effective since the propionate incorporation levels were not increased.

3.4.4. Comparison of OHCbl and compound V stabilizing effect upon p.Ile96Thr mutant

Hydroxocobalamin (OHCbl) is administered to *cblB* patients as therapy, with positive results in some cases. In this context, the stabilizing effect of compound V was compared with the effect obtained with OHCbl administration. In these experiments, cultures of *cblB* patients' fibroblasts were supplemented with 1 µg/mL of OHCbl, corresponding to the amount normally administered to patients.

The p.Ile96Thr mutant, previously used for compound V analysis, and the wild-type protein were expressed in a prokaryotic expression system and incubated overnight at 37 °C with 80 µM of compound V, 1 µg/mL of OHCbl or the combination of the two compounds. The soluble protein extract was obtained and incubated again at 37 °C. Aliquots were removed at different times, loaded onto SDS-PAGE gels and ATR protein was detected by western immunobloting.

As shown in Figure 33, the stabilizing effect afforded by compound V is markedly higher when compared with OHCbl, while the combination of the two compounds seems to have an even higher stabilizing effect, which could indicate a synergistic effect. This implies that, *in vitro*, compound V is a more efficient pharmacological chaperone than OHCbl. Moreover, the combination of both compounds may be profitably used in mutants that do not respond to OHCbl administration.

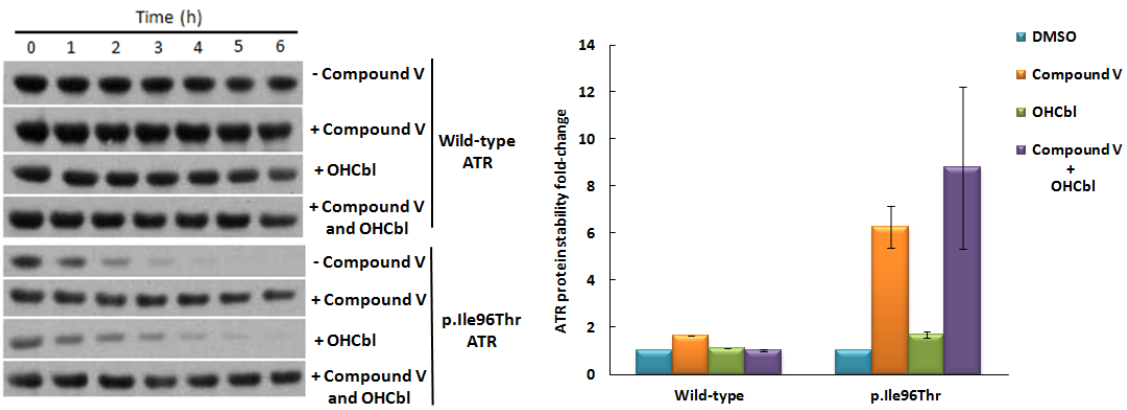

Figure 33 – Effect of compound V and OHCbl on wild-type and p.Ile96Thr ATR proteins. Cells were treated over time with 80 µM of compound V, 1 µg/mL OHCbl and compound V with OHCbl at physiological conditions (37 °C). The crude extracts were incubated over time at 37 °C and aliquots were collected and analyzed by western-blot. The data show the mean value ± SD (n=3) and represent the percentage of the density of each protein compared to time zero.

To assess if the stabilizing effect observed over bacteria extracts was reproducible in a eukaryotic cell system, immortalized fibroblast-cell lines, derived from a control and from a patient bearing the p.Ile96Thr/p.Ser174fs mutations, were incubated for 72 hours with the same amounts of compound V (80 µM) or OHCbl (1 µg/mL) and also with the combination of the two compounds. The restoration of the metabolic pathway was indirectly evaluated by measuring the incorporation of radiolabeled propionate into acid-precipitable material of intact cells. The reactive ATR protein levels, in control and patients' cell lines, were also measured by western blot. So, immortalized fibroblasts were treated as previously described, mitochondria were extracted and loaded into a SDS-PAGE gel.

As observed in Figure 34, the propionate incorporation levels in the control cell line were not altered by the treatment with either compound V, OHCbl or the combination of both compounds. In the cell line harboring the missense p.Ile96Thr mutation, an increase in the propionate incorporation was observed when the cells were treated with OHCbl, as expected. Moreover, the cells treated with 80 µM of compound V showed an even higher incorporation level, which rose again upon treatment with compound V and OHCbl. This observation indicates that compound V, and especially its combination with OHCbl, displays *ex vivo* a high stabilizing effect upon this missense mutation.

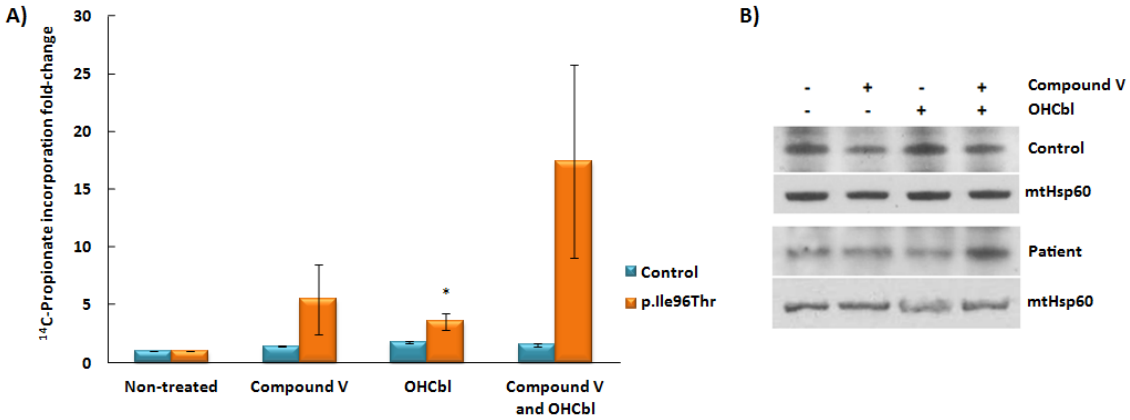

Figure 34 – Effect of compound V and OHCbl in a cellular disease model. Immortalized cell lines, derived either from control or a patient harboring the mutations p.Ile96Thr/Ser174fs were incubated with 80 µM of compound V, 1 µg/mL of OHCbl and the combination of the two compounds, for 72 hours. A) The ATR activity was indirectly measured via [^{14}C]-propionate incorporation into acid-precipitable material in intact cells and B) the amount of immunoreactive ATR protein from isolated mitochondria was analyzed by western blot. Mitochondrial Hsp60 was used as loading control. The data show the mean value ± SD (n=3) (*P<0.05).

When the ATR protein levels were analyzed by western blot, the obtained results for the patients' cell line harboring the p.Ile96Thr mutation also indicate that the highest stabilizing effect is obtained under the combined effect of compound V and OHCbl.

Concerning the control cell line, the incubation with compound V and the combination of compound V and OHCbl showed a less stabilizing effect when compared with the incubation with OHCbl alone.

3.4.5. Analysis of the *in vivo* pharmacological effect and toxicity of compound V

In order to establish the chaperone effect of compound V upon the stability of endogenous ATR protein, and also to assess its pharmacokinetics, toxicity and absorption, distribution and excretion levels, an *in vivo* system was used. Since a *cblB* mouse model is not available, a wild-type C57BL/6 mouse strain was used.

Two doses (0.25 mg/kg/d and 5 mg/kg/d) of compound V were orally administered every day for a 12 day period. No secondary effects of compound exposure (weight loss, automutilation, tumors, abnormal movements, etc.) were observed in any of the animals tested. One mouse, belonging to the control group, was deceased previously to treatment administration. After treatment, the animals were sacrificed and brains and livers were divided into three sections. One was used for analyzing the amount of ATR protein by immunoblotting and the other two were frozen in liquid nitrogen for further experiments.

Brain and liver extracts were prepared and the soluble protein was loaded into a SDS-PAGE gel and analyzed by western blot. The results are shown in Figure 35, where an increase in the amount of ATR protein can be observed, both in liver and brain extracts of mice treated with the highest compound V concentration (5 mg/kg/d). These two organs are disease-relevant in *cblB* patients and, accordingly, these results indicate that compound V has an ATR stabilizing effect *in vivo*.

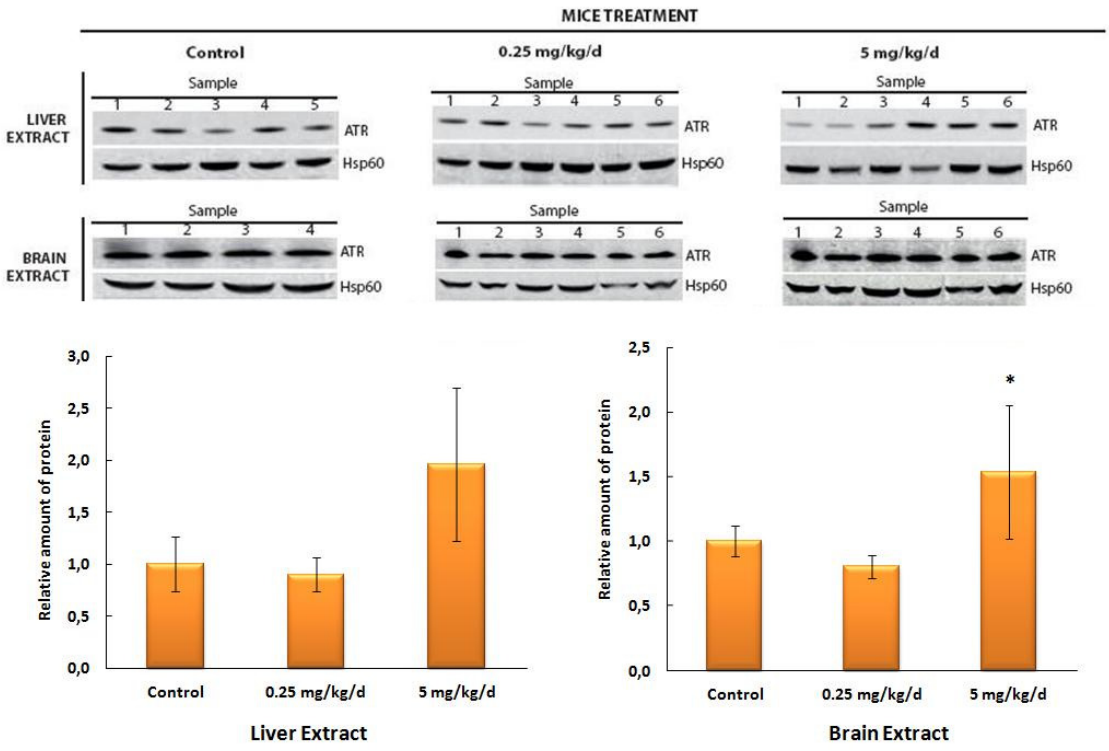

Figure 35 – Effect of compound V in wild-type mice. Two groups of six wild-type C57BL/6 mice were orally treated for 12 days with 0.25 mg/kg/d or 5 mg/kg/d of compound V. The control animals (5 mice) were treated with 10 % DMSO in a 9 % glucose solution used for vehicle for compound V administration. After treatment, whole liver and brain extracts were prepared and ATR protein levels were detected by immunoblotting. The results represent the mean ± SD for each group (n=3).

Since ATR protein is responsible for the synthesis of AdoCbl, the cofactor of the MUT enzyme, western blot analyses were performed to assess if compound V also had an effect upon MUT protein. Experiments were performed as described for ATR protein, only differing in sample number: five liver samples treated with 5mg/kg/d and three and five samples of control and brain extracts treated with 0.25mg/kg/d, respectively. The results are shown in Figure 36 and a slight increase in the amount of immunoreactive MUT protein was observed, both in liver and brain extracts treated with 0.25 mg/kg/d. No increase in the amount of MUT protein was observed in the samples treated with the higher concentration of compound V.

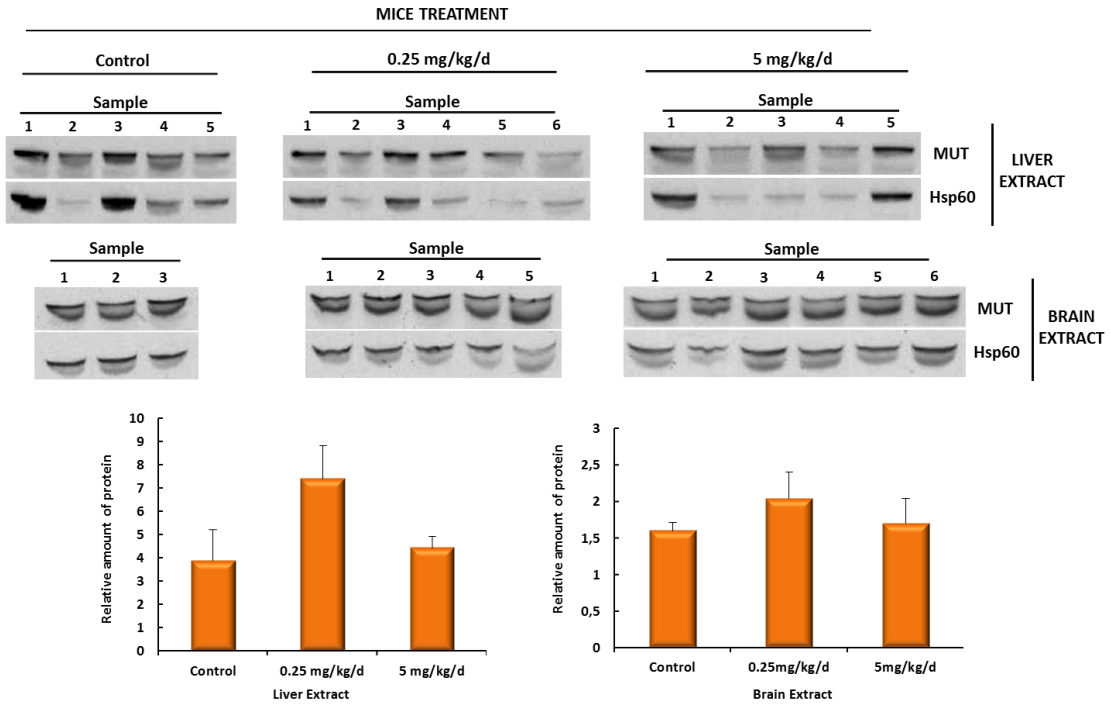

Figure 36 – Effect of compound V in wild-type mice. Two groups of six wild-type C57BL/6 mice were orally treated for 12 days with 0.25 mg/kg/d or 5 mg/kg/d of compound V. The control animals (5 mice) were treated with 10 % DMSO in a 9 % glucose solution used for vehicle for compound V administration. After treatment, whole liver and brain extracts were prepared and MUT protein levels were detected by immunoblotting. The results represent the mean ± SD for each group (n=3).

To assess the metabolization rate of compound V by the wild-type mice, liver extracts from the control and treated mice groups were suspended in DMSO or methanol to dissolve compound V, and analyzed by HPLC-MS/MS Figure 37). The best results were obtained when DMSO was used, since the compound is more soluble in such solvent.

Figure 37 shows an example of the external calibration using 40 µmol/L of compound V, which has a retention time of about 11.5/11.6 minutes. As can be observed, the liver extracts belonging to the control group did not reveal any amount of compound V, while the samples corresponding to the two treated groups showed the presence of the drug.

The liver extracts of mice treated with 5 mg/kg/d of compound V presented the highest amount of compound V but also other chromatographic peaks, not observed in the liver extracts of mice treated with 0.25 mg/kd/d. These peaks may probably correspond to metabolization and/or degradation products of compound V, when present in higher amounts.

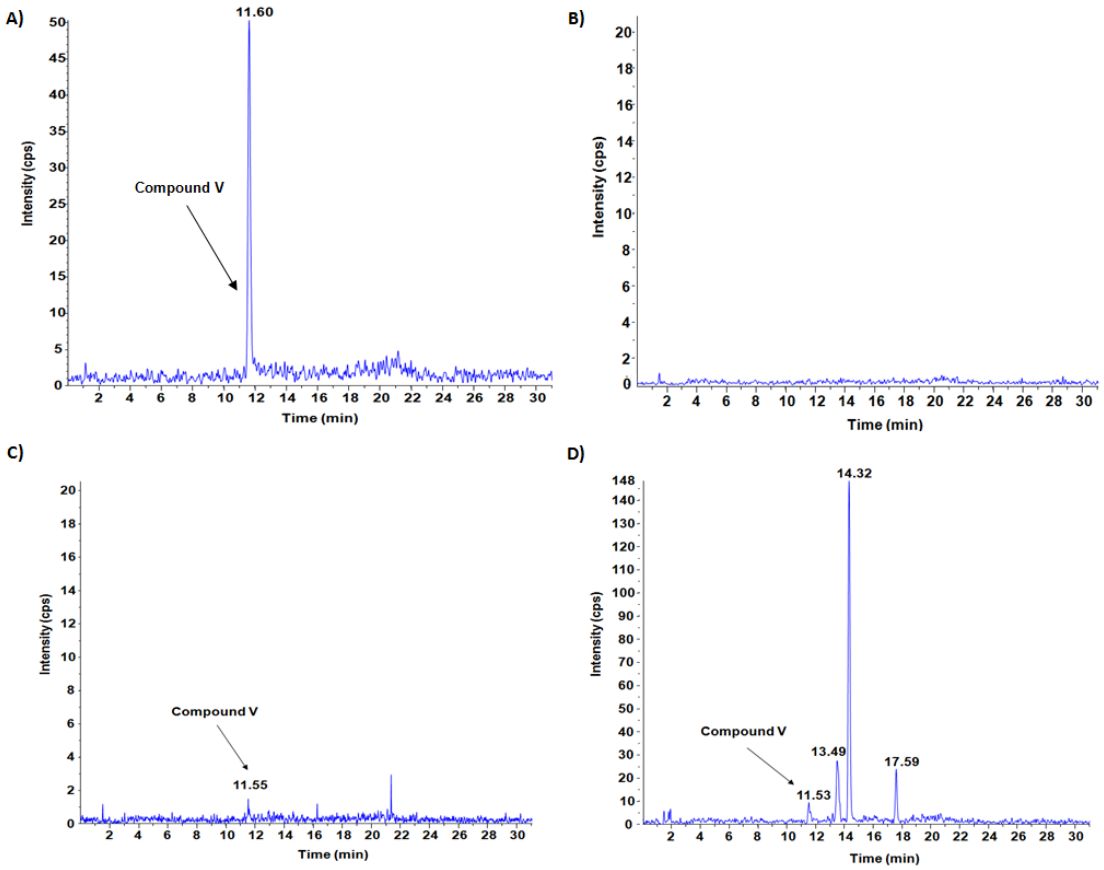

Figure 37 – Quantification of the amount of compound V detected in the liver of treated mice.
A) Profile of the pike corresponding to compound V at a concentration of 40 µmol/L. **B)** Profile of liver extracts obtained from mice treated with the mixture of glucose 9 % and DMSO 10 %. **C)** Profile of liver extracts obtained from the mice treated with 0.25 mg/Kg/d. **D)** Profile of liver extracts obtained from mice treated with the higher concentration, 5 mg/Kg/d. The peak corresponding to compound V has a retention time of 11.5 minutes and in the profile obtained for the higher concentration we can also observe other peaks that may correspond to metabolization and/or degradation products.

3.5. ANTISENSE THERAPY IN TETRAHYDROBIOPTERIN DEFICIENCY

3.5.1. Biochemical and genetic analysis of PTPS deficient patients

Three tetrahydrobiopterin deficient patients (P12, P13 and P14) identified by Prof. Beat Thöny group (Meili et al, 2009), following newborn screening for hyperphenylalaninemia, were studied. Patient P12 presented a severe form of PTPS, P13 was born from first cousins of Moroccan origin and presented a mild form of PTPS and P14 also presented a severe form of PTPS deficiency.

Mutation analysis was carried out in the laboratory of Prof. Beat Thöny, using gDNA and cDNA samples prepared from primary dermal fibroblasts and/or whole blood samples, and the results revealed that P12 was homozygous for the nucleotide transversion c.84-322A>T,

P13 was compound heterozygous for the changes c.163+695_163+751del57 and c.393delA and P14 was also compound heterozygous for the transversions c.163+2T>G and c.164-712A>T (Table 17).

Analysis of the primary dermal fibroblast from P12 revealed an insertion of a LINE2 sequence of 79 bp between exon 1 and 2 (r.83_84ins79), while in primary cells of P13 the maternal deletion of 57 nucleotides, located 20 nucleotides upstream an antisense *Alu* sequence, originated the introduction of 45 intronic nucleotides. In P14, the intronic mutation c.163+2T>G is located in the 5'splice site of intron 2 and generates three distinct shorter cDNA fragments corresponding to the skipping of exon 2, of exons 2-3 and of exons 2-4. The intronic mutation c.164-712A>T is located in the "putative exonic splicing silencer" site (PESS), 5' from the antisense *Alu* sequence in intron 2 of the *PTS* gene, and leads to the inclusion of a similar antisense *Alu* exon found in P13. P14 also presents a 70 nucleotide longer fragment that corresponds to the 45 nucleotide fragment found in P9 extended by 25 nucleotides at the 5' side (Figure 38).

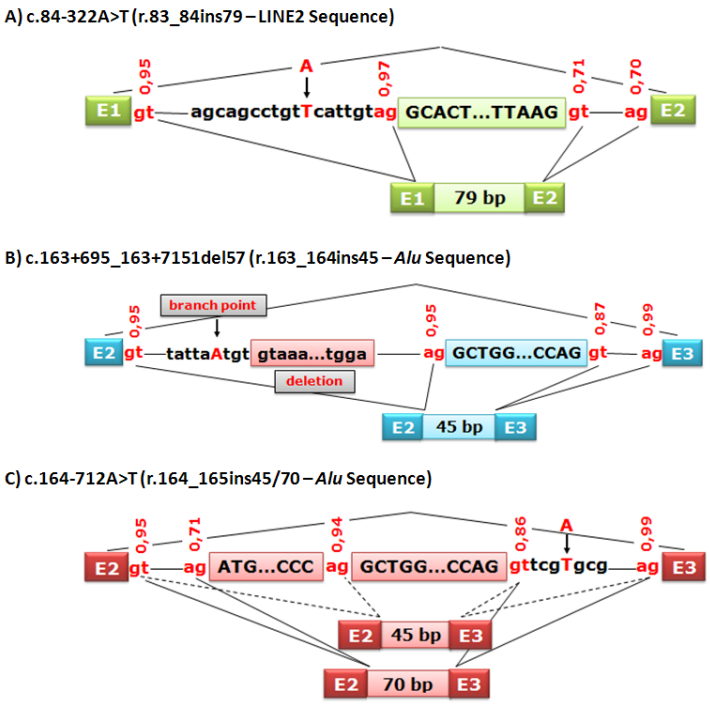

Figure 38 – Deep intronic mutations found in PTPS deficient patients. Splicing patterns showing the regions of the *PTS* gene where the splicing mutations were found. The numbers indicate the splicing scores calculated using the BDGP software available at fruitfly site (http://www.fruitfly.org/).

Table 16 – Biochemical and phenotypical data from PTPS deficient patients.

Patient	Phe (µM)	Neop. (U)*	Biop. (U)*	Neop. (CSF) nM	Biop. (CSF) nM	5-HIAA (CSF) nM	HVA (CSF) nM	PTPS (RBC) µU/g Hb	PTPS (FB) µU/mg protein
P12**	1694	38.0	<0.01	69.0	8.05	31	81	0.34	0.21
P13**	1100	5.04	<0.01	10.1	34.7	527	1023	0.41	0.05
P14	668	50	<0.01	N.A.	N.A.	85.1	56	N.A.	0.22
Reference***	<120	1.40-18.71	0.89-7.60	15-35	20-70	150-800	300-1100	11-29	0.4-1.6

*mmol/mol creatinine

**Described in Meili et al, 2009.

***Reference values in unaffected controls (BIODEF). Phe: phenylalanine levels in blood, Neop.: neopterin, Biop.: biopterin, 5-HIAA: 5-hydroxyindoleactic acid, HVA: homovanillic acid, CFS: cerebrospinal fluid, RBC: red blood cells, FB: skin fibroblasts.

Table 17 – Genetical and treatment data for the PTPS deficient patients analyzed.

Patient	Gene	Mutation*(cDNA/gDNA/RNA)	Treatment
P12	*PTS*	c.84-322A>T/c.84-322A>T Chr11(hg19):g.112098995A>T/g.112098995A>T r.83_84ins79/r.83_84ins79	BH_4 (5 mg/kg/d) followed by treatment with L-Dopa/Carbidopa, 5-OH-tryptophan and folinic acid. The dosage of BH4, L-Dopa/Carbidopa and 5-OH-tryptophan was increased to 6 mg/kg/d, 10 mg/kg/d and 6 mg/kg/d, respectively due to the development of tremor and mild hypertonia of the limbs.
P13	*PTS*	c.163+695_163+751del57/c.393delA Chr11(hg19):g.112100091_112100147del57/g.112104233delA r.163_164ins45/ –	Treated with BH_4 (1 mg/kg/d), L-Dopa/Carbidopa (10 mg/kg/d) and 5-OH-tryptophan (10 mg/kg/d).
P14	*PTS*	c.163+2T>G/c.164-712A>T Chr11(hg19): g.112099398T>G/g.112100219A>T – /r.164_165ins45/70	NA

NA: Non available.

* Mutations according to NM_000317.2 and NC_000011.8 and the genomic coordinates were obtained using the Mutalyzer 2.0 beta-26 software according to hg19. (https://mutalyzer.nl/positionConverter).

The region of the *Alu* sequence is located between exons 2 and 3 and contains a putative 5' splice site and at least two 3' splice acceptor sites, being the most upstream predicted to define the "natural" *Alu* exon, which is located 70 nucleotides downstream the corresponding 5'GT splice site, identical to the pseudoexon 5' site of P13.

It has been reported that complementarity to U1 snRNA exerts, to some extent, a dominant effect on 5' splice site selection (Roca et al, 2005). Mutation c.164-712A>T, found in patient P14, is located near the exon-intron boundary and might affect the complementarity to U1 snRNA. In order to analyze more extensively this 5'GT splice site and the effect of c.164-712A>T mutation, an *ex vivo* minigene assay was used (Figure 39).

The 5' splice site motif consists of nine partially conserved nucleotides at the exon-intron boundary, corresponding to the last 3 nucleotides of the upstream exon and the first 6 intronic nucleotides. The effect of the original mutation c.164-712A>T found in P14, as well as two additional changes (c.164-714C>A and c.164-715T>A) upon U1 snRNA complementarity was also tested. As shown in Figure 39, both these last changes, c.164-714C>A and c.164-715T>A, activate pseudoexon splicing insertion, although c.164-714C>A shows a profile more similar to the wild-type construct, activating the pseudoexon to a much lesser extent.

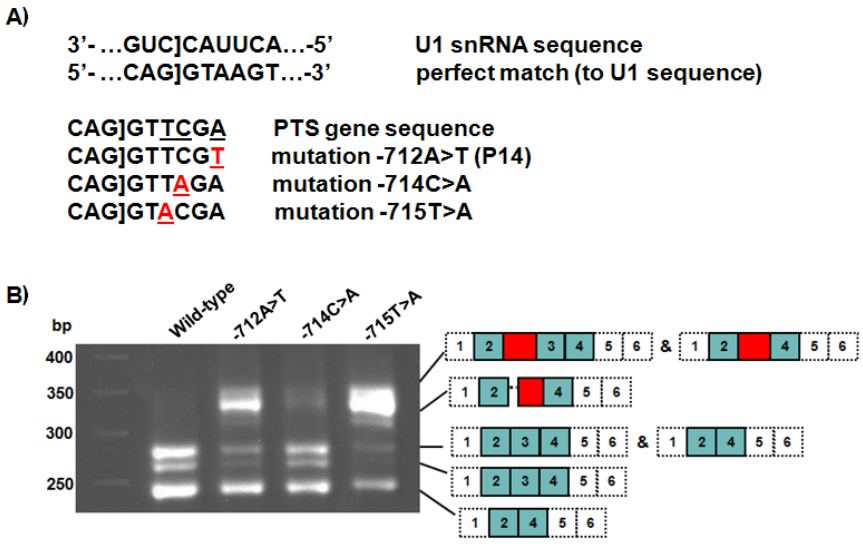

Figure 39 – Ex vivo splicing assay for patient P14 using a minigene bearing the wild-type sequence, the mutation c.164-712A>T found in P14 and the two additional changes c.164-714C>A and c.164-715T >A. A) Schematic representation of the base pairing between the 5' splice site of the pseudoexon and the U1 snRNA sequence, plus the different minigene constructs. The 5' splice sequence consists of nine partially conserved nucleotides at the exon-intron boundary and the differences between the *PTS* gene sequence and the perfect match to the U1 sequence are underlined. The changes to the perfect match sequence are in red and also underlined. **B)** RT-PCR profile of the ex vivo splicing assay obtained for the different minigene constructs.

Mutation c.164-715T>A appears to be more efficient in the 70 nucleotide pseudoexon activation when compared with mutation c.164-712A>T, found in P14. This mutation also activates the insertion of the 45 nucleotide pseudoexon, although to a minor extent.

These results show that, by changing the nucleotides found in positions +3 (-715T>A) or +6 (-712A>T) downstream the pseudoexon, the complementary to U1 snRNA was improved and the 5' splice site was strengthened, unequivocally proving that the c.164-712A>T is located in the site of U1 snRNA union.

3.5.2. Antisense therapy in PTPS patients

Since antisense therapy has been successfully used in other disorders to rescue aberrant splicing, antisense oligonucleotides (AONs), particularly antisense morpholino oligonucleotides (AMOs) were used in order to investigate if the pathological insertions, activated by the mutations found in patients P12, P13 and P14, could be suppressed.

Cell cultures of patient-derived fibroblast were treated with specific AMO targeted to the 3' (PTS-AMO1) and 5' cryptic splice sites (PTS-AMO2 and PTS-AMO3), aiming to block the access of the splicing machinery to the pseudoexonic regions in the pre-mRNA (Table 18).

Although patients P13 and P14 show the activation of the same pseudoexon, the AMO sequences used are different according to the patient's mutation. The PTPS AMO2 sequence hybridizes with the normal sequence of the exon-intron junction sequence, while the PTPS AMO3 sequence hybridizes with the sequence of the exon-intron junction sequence of patient P14 that bears an A>T transversion at position +6.

Table 18 – AMO sequence and target used for antisense therapy on PTPS deficient patients.

Name	5' - 3' Sequence	Target mutation
PTPS AMO1	AGT GCC TAC AAT GTA ACA GGC AAG T	r.83_84ins79
PTPS AMO2	AGG CTG GAG AAT CGC TCG AAC CTG G	r.163_164ins45
PTPS AMO3	AGG CTG GAG AAT CGC ACG AAC CTG G	r.164_165ins45/70

Patients' fibroblasts were transfected with two different concentrations of the corresponding AMO, 20 µM and 30 µM, for a 24 hour period, followed by transcriptional profiling analysis. The results depicted in Figure 40 show that the splicing profile was restored in all three cases and in a dose dependent manner. For all patients, the upper band corresponding to the intronic insertion disappeared, even though cells were cultured in the presence of cycloheximide to avoid mRNA degradation. The obtained cDNA fragments were subjected to direct sequence analysis, and in patient P13 the presence of the c.393delA

mutation was confirmed in heterozygous state after AMO treatment as can be seen in Figure 41.

Furthermore, and to demonstrate AMO specificity, the three patients' fibroblasts were treated with a scrambled AMO and, as shown in the right panel of Figure 40, the correct splicing profile was not restored.

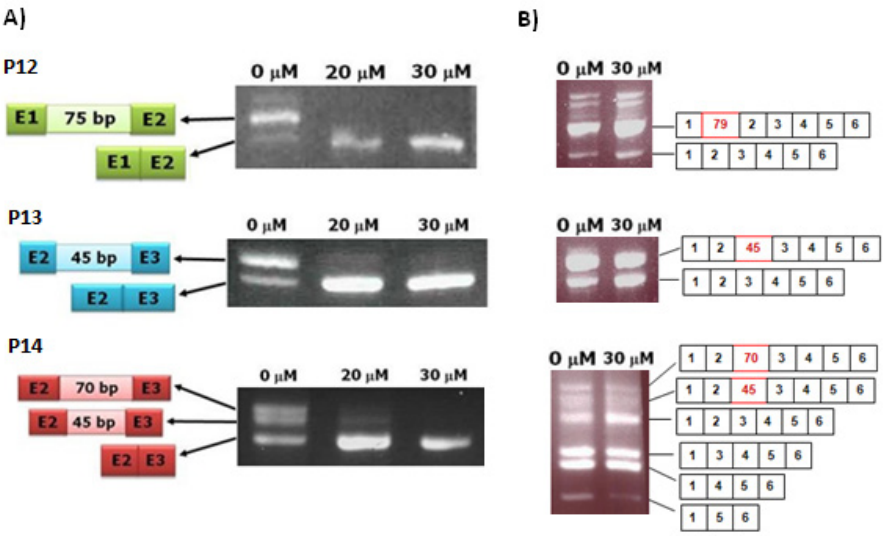

Figure 40 – Splicing therapy using antisense AMO to avoid pseudoexon inclusion in primary dermal fibroblasts from PTPS-deficient patients. A) Transcriptional analysis by conventional RT-PCR of fibroblasts derived from patients P12, P13 and P14 untreated (0 µM) or treated (20 µM and 30 µM) with the corresponding AMO. **B)** Transcriptional analysis by conventional RT-PCR of fibroblasts derived from patients P12, P13 and P14 untreated (0 µM) or treated (30 µM) with scrambled AMO sequence.

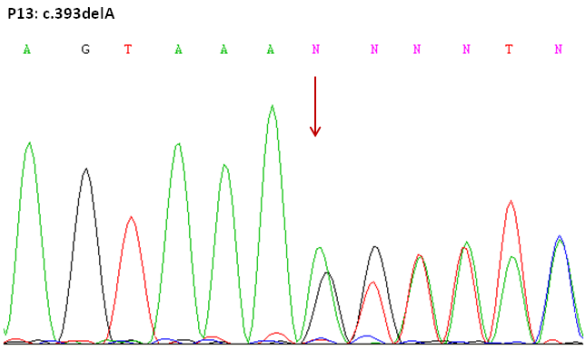

Figure 41 – Patient P13 cDNA analysis by direct sequence. The cDNA obtained after AMO treatment was sequenced and the presence of the mutation c.393delA can be observed in heterozygosis.

VIVO-morpholino complexes have a new transporter structure that provides effective *in vivo* delivery of morpholino antisense oligomers into a variety of tissues. VIVO-morpholinos are conjugates resulting from the covalently linkage between an octa-guanidine dendrimer

and the morpholino oligo. Moreover, a new class of shorter and more stable oligonucleotides called LNA (locked nucleic acid) was proven to be effective in the prevention of pseudoexon inclusion. Taken these two facts into account, both these approaches were tested to averiguate if the splicing correction was comparable to AMO treatment under cell culture conditions. Due to poor growth behavior of the primary dermal fibroblasts from patient P13, only P12 and P14 were used in this analysis.

The VIVO-morpholino sequence was similar to the already used AMO sequence and the sequence of the LNAs is shown in Table 19.

Table 19 – LNA sequence used for antisense therapy.

Name	5' - 3' Sequence	Target mutation
***PTS*-LNA1**	CAAACAAACCTTAACT	r.83_84ins79
***PTS*-LNA2**	TCGCTCGAACCTGGGA	r.164_165ins45/70

The LNAs were designed to target the 5' splice donor site of both pseudoexon sequences. Figure 42 shows the results obtained with both treatments. For the LNA treatment, the oligonucleotide delivery is performed using a powerful transfection agent and, consequently, lower oligonucleotide doses were used (1nM, 5nM, 25nM, 50nM and 5µM). These doses were obtained from positive results described in the literature (Beane et al, 2007; Gupta et al, 2010). The treatment with VIVO-morpholino was performed using the same concentrations used for AMO treatment and showed that the aberrant splicing profile was reversed using both concentrations.

The treatment using LNA was more efficient for patient P14 than for patient P12. In P12 the treatment was dose dependent and a higher dose (5 µM) was used for this patient in comparison with P14.

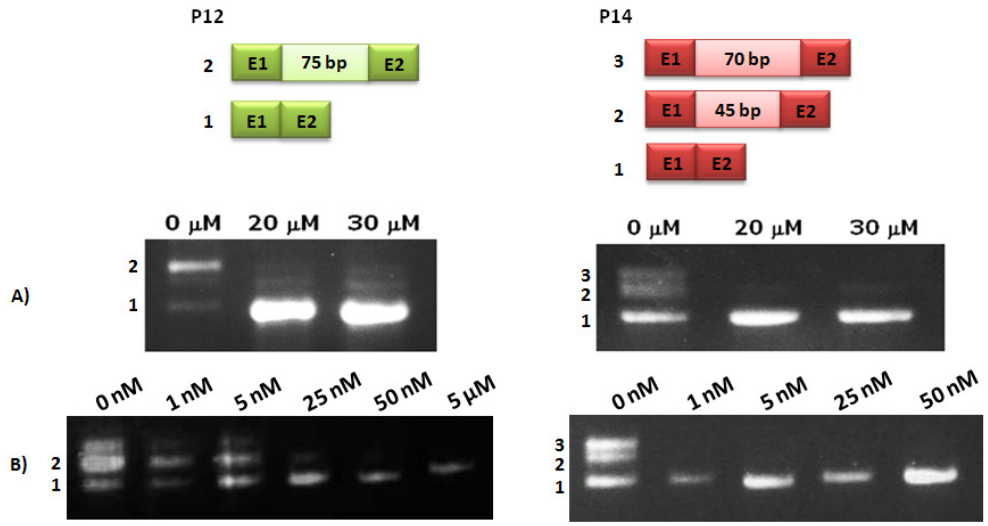

Figure 42 – Treatment with VIVO-morpholino and LNA oligonucleotides. Transcriptional profile analysis by RT-PCR of patients P12 and P14 derived fibroblast upon the treatment with different concentrations of **A)** VIVO-morpholino and **B)** LNA.

3.5.3. Effect of AMO antisense therapy upon protein and metabolites

After the successful recovery of the normal splicing pattern with AMO, we investigated the effect of treatment upon the amount of PTPS reactive protein and also upon enzymatic activity. Primary dermal fibroblasts were treated with the higher dose of AMO, 30 µM, during 48 hours to assess the amount of protein, and during 48 and 72 hours for evaluation of enzymatic activity

As shown in Figure 43, after treatment all patients' cells showed a recovery in protein production, almost reaching control levels in patient P14. In P13, the recovery level was much lower, but still a band corresponding to the PTPS protein was observed.

The recovered protein, observed in the western blot, was shown to be functional. In Figure 43, an increase in activity in the range of normal levels was observed in all patients' cells after treatment. The highest activity levels were obtained after a 48 hours treatment, being the levels slightly lowered after 72 hours of treatment. Primary dermal fibroblasts of patients P12 and P13 reached normal activity levels, which are between 0.4 and 1.6 µU/mg (Bonafé et al, 2001). It is interesting to notice that, although the level of reactive protein was lower in patient P13, the enzymatic activity levels were higher than the observed in patients P12 and P14, who showed the highest levels of reactive protein.

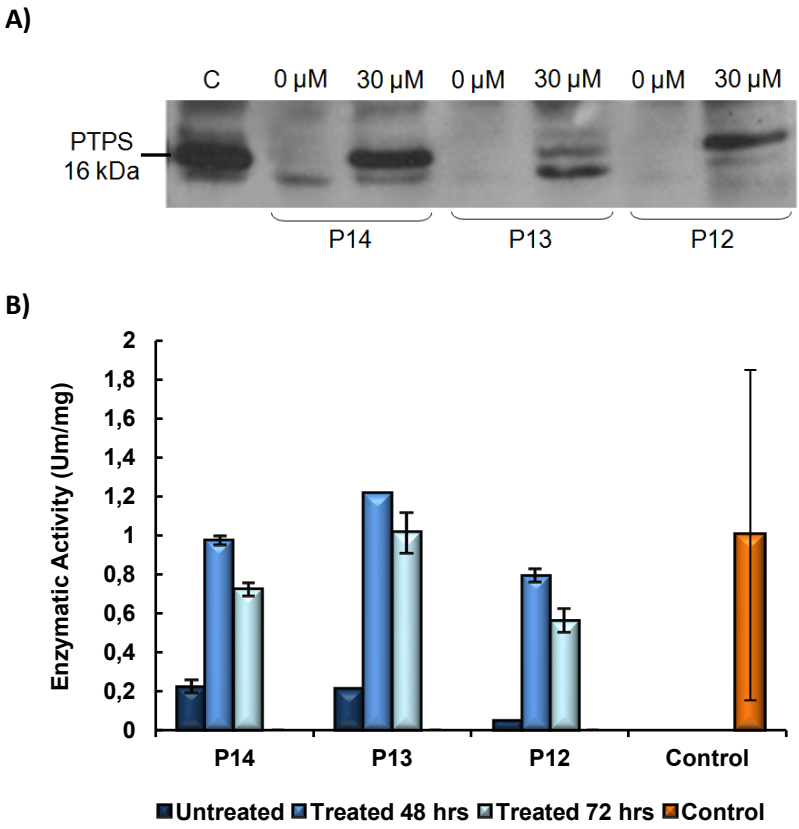

Figure 43 – Protein expression and PTPS enzymatic activity analysis in primary patients' fibroblasts after AMO treatment. **A)** PTPS protein expression in control and patients' derived fibroblast untreated or treated with 30 µM of the corresponding AMO. **B)** Functional correction of PTPS enzymatic activity after treatment. The activity was assayed in a control cell line and in primary dermal fibroblasts derived from the patients treated at different times with 30 µM of the corresponding AMO.

PTPS patients always present an altered pterin profile, showing an increase in neopterin and a decrease in biopterin levels. Since GTPCH is not expressed in dermal fibroblasts, the metabolic pathway must be induced upon co-treatment with TNFα and INFγ (Ionova et al, 2008). Pterin levels were quantified in patients' fibroblasts after treatment with 30 µM of the corresponding AMO and simultaneous cytokine stimulation.

The cells were treated for 48, 72 and 96 hours and, as shown in Table 20, the neopterin levels were decreased and the biopterin levels increased to variable degrees, depending on the cell line. Nevertheless, and in general, the neopterin-biopterin ratio was decreased in all patients' cells in a time dependent manner. During the 96 hour treatment, cells were transfected twice, the first at time 0 and the second after 48 hours.

For both patients, P12 and P14, the best results were obtained after 96 hours of treatment, although patient P12 presented the best recovery, once a decrease of more than 1,000 fold in the neopterin/biopterin ration was observed. This must probably be due to the

fact that P12 is homozygous for the splicing allele, while the other two patients carry a second mutation that cannot be corrected by the pseudoexon exclusion therapy.

Due to the poor growth rate of P13 fibroblasts, positive results were only obtained after 48 hours of treatment, though a significant decreased was also observed.

Table 20 – Neopterin and biopterin levels in PTPS patients P12, P13 and P14 before and after treatment with 30 µM AMO for 48, 72 and 96 hours.

Patient	Time of treatment (h)	Neopterin (pmol/mg)	Biopterin (pmol/mg)	Neopterin Fold Activation	Biopterin Fold Activation	N/B ratio
P12	0	281.16	0.40	-	-	703
	48	75.88	14.17	3.71	35.05	5.35
	72	57.84	32.91	1.31	2.32	1.76
	96	15.61	26.86	3.71	0.82	0.58
P13 **	0	378.23	0.51	-	-	741.60
	48	243.32	5.53	1.55	10.84	44.00
P14	0	235.37	1.48	-	-	159.49
	48	123.23	8.98	1.91	6.09	13.72
	72	38.46	9.52	3.20	1.06	4.04
	96	6.50	2.09	5.92	0.22	3.12
Control *	48 - 72	11.42	45.85	-	-	0.25
Patient (U) ***	Untreated	45 nmol/L	0 nmol/L	-	-	-
	Treated	34 nmol/L	25 nmol/L	-	-	1.36

* Neopterin and biopterin in control fibroblasts.

**The assay was performed only at 48 hours post-transfection due to the poor growth behavior of the primary fibroblasts.

***Neopterin and biopterin in patient's urine before and 24 hours after an oral loading test with 20 mg/Kg synthetic BH_4. Neopterin and biopterin in control urine are 5-22 nmol/L and 4-10 nmol/L, respectively; ratio: 1.25-2.2 (Blau et al, 2003).

PART 4

DISCUSSION

In this work we performed the description and characterization of mutations found in isolated methylmalonic and propionic patients, we have elucidated the pathophysiological mechanism of mitochondrial dysfunction in *cblB* type patients and, finally, we have demonstrated the application of two different therapeutical approaches, chaperone and antisense therapy, in isolated methylmalonic aciduria and 6-pyruvoyl-tetrahydropterin synthase deficiency, respectively.

4.1. MOLECULAR CHARACTERIZATION OF PATIENTS WITH ORGANIC ACIDEMIAS

In this section, isolated methylmalonic and propionic patients from Spanish and Portuguese origin were characterized allowing the identification of the mutations causing these disorders and, consequently, familiar genetic counseling of the patients' families, prenatal diagnosis and also genotype-phenotype correlation.

Patients with isolated methylmalonic aciduria belong to the *cblD* variant 2 and *mut* complementation groups, while the propionic patients belonged to the *pccB* complementation group.

The characterization of the *cblD* variant 2 type patients, the first done in our laboratory, allowed the expansion of the known *MMADHC* gene mutational spectrum, since three new mutations (c.165_166del2, c.170G>A and c.10-1G>C) were identified. Moreover, one already described mutation, c.57_64del8, was also identified (Coelho et al, 2008; Stucki et al, 2011).

Until now, only three mutations responsible for a *cblD* variant 2 type had been described in the literature, representing 25 % of the mutations found in the *MMADHC* gene, and the mutational spectrum is heterogeneous with no prevalent mutation type (Coelho et al, 2008; HGMD® Professional 2013.1). This mutational heterogeneity has also been described for other genes such as *MMAA* and *MUT*, also responsible for an isolated methylmalonic phenotype, although ethnic-specific mutations have been described (Acquaviva et al, 2005; Martinez et al, 2005; Worgan et al, 2006; Merinero et al, 2008).

The novel mutation c.10-1G>C affects the original acceptor splice site of intron 1. *In silico* analysis revealed that this mutation is responsible for the inactivation of the constitutive acceptor splice site and for the increase of the splicing score of an AG dinucleotide located inside the exon, creating a new acceptor splice site and consequently, the deletion of the first five amino acids of the protein. Exon 2 starts at the Val4 residue, located in the proposed mitochondrial leader sequence (residues 1-11) (Coelho et al, 2008; Plesa et al, 2011). This is a conserved residue among several species and the disruption of this sequence impairs the transfer of cobalamin to its mitochondrial metabolization pathway.

The novel mutations c.165_166del2 and c.170G>A also affect conserved protein residues, Thr55 and Trp57, respectively. Mutation c.165_166del2 eliminates 2 nucleotides, disrupting the ORF and may lead to the introduction of a premature stop codon, while mutation c.170G>A introduces a premature stop codon, putatively leading to a truncated protein.

The *cblD* complementation group is the most heterogeneous within the cobalamin complementation defects, since the affected patients can present three different phenotypes; isolated methylmalonic aciduria (*cblD* variant 2), isolated homocystinuria (*cblD* variant 1) and the combination of methylmalonic aciduria and homocystinuria (*cblD*) (Suormala et al, 2004). The MMADHC protein function is not fully understood, but it seems to interact with the MMACHC protein in order to direct cobalamin to the cytosol or to the mitochondrion (Coelho et al, 2008; Stucki et al, 2011). A study revealed that MMADHC protein has several interaction domains with MMACHC protein, all of them located towards the C-terminal end (Plesa et al, 2011).

All the four mutations identified in our patients are located in the N-terminal end of the protein and, most importantly, before the Met62 residue. It has been described that residues Met62 and Met116 are located within a sequence compatible with the Kozak consensus one, and that they might be used as second initiation codons. This fact could explain why *cblD* variant 2 patients have a normal MeCbl synthesis in spite of an AdoCbl impaired synthesis (Coelho et al, 2008; Stucki et al, 2011).

The characterization of mutations within a population allows genetic counseling and also the possibility to establish genotype-phenotype correlations. All the studied *cblD* variant 2 type patients presented severe clinical symptoms within the first two years of life, and carry mutations that are normally associated with a severe effect upon the protein. Nevertheless, all the patients show a positive response to B_{12} treatment and a good clinical evolution. This positive response is not fully understood since the AdoCbl synthesis requires an intact mitochondrial leader sequence and also the sequence downstream Met62 (Stucki et al, 2011). The observation that the interaction between MMADHC and MMACHC proteins increased the levels of AdoCbl synthesis with low effect on MeCbl synthesis (Stucki et al, 2011), and the fact that none of the mutations described in this work affects the weakly conserved putative B_{12}-binding motif, GXXXHXD, located between residues 81 and 86, could indicate that the complex formed by these two proteins is stabilized by the excess of vitamin B_{12}, shifting the balance towards AdoCbl synthesis. Another hypothesis is the stabilization of the truncated protein by cobalamin that could act as a natural chaperone, as described for other disorders (Rodrigues et al, 2012).

The characterization of the propionic patients allowed the identification of two previously described mutations in *PCCB* gene, a small indel mutation (c.1218del14ins12) and a splicing mutation (c.183+3G>C) (Gravel el al, 1994; Rodrígues-Pombo et al, 1998). The c.1218del14ins12 is the most common mutation among Caucasians, being present in 32 % of white origin alleles. A study involving 29 patients of Spanish and Latin American heritage led to a similar result. This is a complex mutation, resulting from a deletion of 14 nucleotides and their replacement by 12 nucleotides that are unrelated to the deleted nucleotides. This leads to the generation of a frameshift, arising in a stop codon about 100 amino acids proximal to the normal protein C-terminal, thus possibly originating a truncated and unstable protein. The origin of this indel is not clear, but it might derive from the duplication of nine nucleotides upstream the mutation site, with random filling of three more nucleotides. Hybridization studies, using mutant allele-specific oligonucleotides, showed that the inserted 12 nucleotides did not originate in a 1Kb region around the mutation (Tahara et al, 1990; Rodríguez-Pombo et al, 1998; Fenton et al, 2001). The identification in unrelated patients of another in-frame deletion in the same region suggests that this region of *PCCB* gene may be prone to undergo this type of mutation (Tahara et al, 1990).

The c.183+3G>C mutation affects intron 1 donor splice site, disrupting the normal splicing profile. The *in silico* analysis using the Human Slicing Finder software shows that the substitution of a guanosine residue by a cytidine at position +3, leads to the decrease of the 5' donor splice site score from 83.41 to 79.54 and, possibly, the activation of a cryptic donor splice site located downstream which presents a higher splice site score, 86.28. The c.183+2T>C mutation was described in propionic patients and already characterized (Desviat et al, 2006). This mutation also affects the 5' donor splice site of intron 1 and activates a cryptic donor splice site located downstream, which leads to the insertion of 20 nucleotides of intron 1 between exons 1 and 2 and probably originate a frameshift and, consequently an aberrant protein. Since these two mutations are located in the same region, their effect could be similar and the insertion of the additional 20 nucleotides from intron 1 observed for c.183+2T>C mutation could also occur in the patient affected by the c.183+3G>C mutation. Functional analysis should be performed in order to confirm this hypothesis.

Due to the lack of patient cells, the effect of this mutation could not be fully elucidated, although a good approach could be the use of an *ex vivo* minigene assay to confirm the effect of this mutation (Desviat et al, 2012; Morse et al, 2012). The recognition of the exon-intron junction by the spliceosome is essential for the splicing process and the spliceosome assembly is initiated by the binding of U1snRNP to the donor splice site. It is postulated that, in a functional donor site, there is a minimal number of 5 or 6 base pairing to U1 snRNA and that

the disruption of any of these bases could affect normal splicing (De Conti et al, 2012). Overexpression of a mutant U1snRNA, engineered to bind specifically to the mutant donor splice site, has been used successfully to correct the aberrant splicing profile and thus, by analogy, could be a good therapeutical approach for this type of mutations (Zhuang et al, 1986; Sanchez-Alcudia et al, 2011; Glaus et al, 2011).

4.2. FUNCTIONAL ANALYSIS OF MUTATIONS IN ORGANIC ACIDURIAS

Mutations are responsible for diverse effects upon the protein function, leading to either a loss or a gain of function. The majority of IMD is caused by loss of function of a particular protein, which can be complete, originating a protein with null function, or a reduction of the protein's ability to work. The analysis of the mutation effects upon protein function allows the identification of the molecular mechanisms responsible for these disorders. In this section, the functional effect of six allelic variants, one identified in *MUT* gene and five identified in *MMAB* gene, was assessed using appropriate models. The knowledge of the molecular mechanism underlying the pathogenic effect of these mutations allows the identification of new therapeutic targets and the development of alternative treatments based in individual genotypes.

The results indicate that the identified allelic variants are pathogenic; one mutation affects the correct mRNA processing (c.1480-10A>G in the *MUT* gene), while two in frame mutations (p.I117_Q118del and p.R190dup in *MMAB* gene) and three missense mutations (p.H183L, p.R186W, and p.E193K in *MMAB* gene) are responsible for the destabilization of the ATR protein residual activity.

Transcriptional analysis of the patient bearing the c.1480-10A>G mutation in the *MUT* gene confirmed the results anticipated by the *ex vivo* minigene splicing assay.

Direct transcriptional analysis of the *MUT* gene patient bearing the c.1480-10A>G mutation was not possible because DNA was the only biological material available from the patient. This problem was circumvented by using an *ex vivo* minigene splicing assay which revealed that this mutation is responsible for the creation of a new acceptor 3' splice site with a higher splice score that the original site, which leads to the insertion of 9 additional nucleotides in the beginning of exon 6. This mutation also leads to the activation of a cryptic acceptor splice site within exon 6 and the consequent elimination of its first 135 nucleotides. The presence in the control individuals' profile of the smaller transcript, lacking the 135 nucleotides, indicates that this splicing event may also occur in physiological conditions and that it may be due to the fact that the constitutive acceptor splice site of exon 6 has a low

splice score. Furthermore, the minigene profile analysis also revealed the simultaneous presence of the normal *MUT* transcript.

The patient's phenotype is mild, even though a small duplication, c.244dupA, responsible for the disruption of the normal ORF, was also found in the other allele. The presence of these two mutations should be associated with a severe effect, but the presence of the normal transcript, even in small amounts, may be responsible for the amelioration of the phenotype. An RT-PCR should be performed using the patient's derived fibroblasts or linfoblasts in order to demonstrate the presence of the normal transcript. Although the 9 nucleotides inserted do not disrupt the ORF, one of the triplets encodes a stop codon, which could lead to a truncated protein. In this case, in which the original splice site is not altered, one therapeutical option could be the use of AONs specifically designed to block the recognition of the mutant transcript by the splicing machinery. Since this mutation is located in close proximity to the constitutive acceptor splice site, small and highly specific oligonucleotides, like locked nucleic acids (LNAs), might ensure better results.

The analysis of the variants identified in *MMAB* gene, p.Ile117_Gln118del, p.His183Leu, p.Arg186Trp, p.Arg190dup and p.Glu193Lys, indicates they affect the stability and function of the ATR protein.

The novel variants, p.His183Leu and p.Arg190dup were found in two siblings (P8 and P9) who presented different phenotypic manifestations while bearing the same genotype. Both changes were absent from the Exome Variant data base (evs.gs.washington.edu) and were classified as probably damaging by PolyPhen2 (genetics.bwh.harvard.edu/pph2). No other variants were found in the promoter sequence of these patients and no exonic copy number variations were detected by genomic rearrangements (Metaboloarray®). The analysis of the immunoreactive ATR protein, in patients' derived-fibroblasts, revealed low protein levels when compared to controls. The comparison of the ATR protein levels between siblings revealed that patient P8 present lower levels than P9. When compared to controls, the analysis of the protein function at physiological temperature revealed lower propionate incorporation levels for P8 fibroblasts and normal levels for P9 fibroblasts, when compared to controls, but when the cells were incubated at 42 ˚C, the propionate incorporation levels of P9 fibroblasts were impaired and reached patient P8 levels. This indicates that, in a stress situation such as a fever episode, patient P9, normally asymptomatic, could present the same phenotype as his sibling P8.

A prokaryotic system was used to perform *in vitro* expression analysis of the mutants p.His183Leu and p.Arg190dup, and for the last mutation, no detectable amount of protein was produced. The Arg190 residue is located in the protein α4-helix, which is involved in the

formation of the active site cleft. The main carboxyl chain of Arg190 establishes hydrogen bonds with the five-member ring of ATP and also with the ribose oxygen molecule (Schubert and Hill, 2006). The p.Arg190His mutant has been reported in methylmalonic *cblB* type patients and although the study of this mutant revealed a similar affinity for cobalamin when compared to the wild-type protein, it also revealed a decreased affinity for the ATP molecule, confirming the role of this residue in ATP binding (Zhang et al, 2009). These data indicate that the in-frame deletion affecting this residue probably has a severe impact on the protein structure and, consequently, a complete loss-of-function as shown by the functional analysis.

The new p.His183Leu mutant was studied more thoroughly. The expression of the mutant variant, using a prokaryotic system at physiological temperature, showed a reduced stability of about 58 % when compared with the wild-type protein, while the expression of the mutant in permissive folding conditions (27 °C) increased the mutant stability to wild-type levels. The stabilization of missense mutations by permissive folding conditions is a trait of folding mutants and has been described for other disorders, like phenylketonuria (Gámez et al, 2000). Residue His183 is located inside the ATR α4-helix, distant from the active site, but nevertheless it is postulated that the local conformation of single amino acid residues at one site of the protein can control the structure of more distant regions (Muntau and Gersting, 2010). The proximity to a hydrophobic loop between α3 and α4, that may be involved in dimethylbenzimidizole (DMB) binding, suggests that mutations in this residue may affect DMB-off transition *in vivo* (Fan and Bobik, 2008). *In silico* analysis was performed, revealing that the substitution of an aromatic histidine residue by a branched-chain leucine residue was responsible for the destabilization of the protein structure with the impairment of the trimer functionality.

A mutation in the same residue, p.His183Tyr, has been described and western blot analysis revealed protein levels near wild-type *in vivo* and a positive response to vitamin B_{12} treatment. The authors postulated that this mutation could interfere with the *in vivo* reduction of cob(II)alamin to cob(I)alamin, thus impairing ATR activity (Fan and Bobik, 2008). These results are similar to the ones obtained in the present work, what indicates that the p.H183L mutant could exert a similar effect.

Since this mutation is responsible for a folding defect, the levels of mitochondrial Hsp60 and Hsp70 chaperones, and also Lon protease, were analysed by western blot in patients P8 and P9 derived-fibroblasts and high levels of Hsp70 chaperone were detected. Although normal mtHsp60 levels were obtained for patient P8, patient P9 presented slightly impaired mtHsp60 levels when compared to controls and also low levels of Lon protease.

Hsp70 family of chaperones is highly conserved in evolution and mitochondrial Hsp70 (mtHsp70) is essential for *de novo* protein folding and suppression of protein aggregation under stress conditions (Richter et al, 2010; Hageman et al, 2011). mtHsp70 is also involved in the translocation of mitochondrial precursor proteins across the mitochondrial membrane, and maintains the proteins in an unfolded state until they are assembled in their tertiary structures. It is also implicated in the efficient degradation of damaged proteins by proteases (Luce et al, 2010; Gregersen and Bross, 2010; Baker et al, 2011). Mitochondrial Hsp60 (mtHsp60) is also involved in the proper folding of proteins after their import into the mitochondrion, in an ATP-dependent process (Stuart et al, 1994). mtHsp70 levels are induced under stress conditions, such as high temperatures or unfolded proteins, and hence the high levels observed in patients P8 and P9 can be related to the folding defect of ATR protein caused by the p.His183Leu mutation (Stuart et al, 1994; Callahan et al, 2002). The low stability levels of this variant could induce the expression of mtHsp70 in an attempt to refold the mutant protein and establish normal cellular homeostasis.

The interaction between mtHsp70 and matrix proteases has been described (Luce et al, 2010). One of the most important mitochondrial matrix soluble proteases is the Lon protein, an ATP-dependent serine/lysine protease of the AAA^+ family (Luce et al, 2010). Apart from its proteolytic role, Lon is also important for protein complex assembly and maintenance of mitochondrial DNA integrity (Gottesman et al, 1997; Lu et al, 2007). Lon is up-regulated under stress conditions and low levels of this protease have been described in patients with hereditary spastic paraplegia (Hansen et al, 2008). The slightly high levels of Lon protease observed in P8 may indicate that this protein is activated by the stress conditions induced by the folding mutant p.His183Leu and also by the high levels of mtHsp70. Interestingly, patient P9 presented low Lon immunoreactive protein levels, which could indicate that, in this patient, the protease system is less activated when compared to control and to his sibling P8, allowing the misfolded ATR protein to undergo more folding attempts, instead of being prematurely degraded. This has been observed for patients with reduced mtHsp60 levels, a situation also observed in patient P9 (Hansen et al, 2008).

Regarding the other ATR mutant proteins (p.Ile117_Gln118del, p.Arg186Trp and p.Glu193Lys), *in vitro* expression analysis was also performed using a prokaryotic system and, as for mutant p.Arg190dup, no detectable amount of protein was found for p.Ile117_Gln118del mutation at physiological conditions. The Ile117 and Gln118 residues are located on the α2-helix and the Gln118 residue establishes hydrogen bonds with the α3-α4 loop and with the α1-helix. The α3-α4 loop is involved in the active site cleft formation and the

elimination of these two residues may impair the formation of the active site and, consequently, impair the protein function (Schubert and Hill, 2006).

The prokaryotic expression of missense p.Arg186Trp and p.Glu193Lys mutants, at physiological temperature, revealed a decreased stability of 36 % and 93 %, respectively, when compared to the wild-type. These results confirm the *in silico* analysis of these mutants, using the CAFFE bioinformatic software, that showed that the p.Glu193Lys mutant was more unstable than the wild-type, with a total inability to form the active trimer, while the p.Arg186Trp mutant presented a higher degree of stability. These two variants have already been described and studied in the literature. The Arg186 residue is located in the α4 helix and forms, along with the Arg90, Phe170 and Phe221 residues, the surface of the active site cleft. The invariant side chain of Arg186 residue projects below the ATP molecule, although not directly interacting with it; instead, it could interact with the cobalamin molecule. Studies performed with the bacterial L*r*PduO revealed that Arg186 (Arg128 in L*r*PduO) forms a salt bridge with a conserved aspartate residue (Asp35) from the adjacent unit, being this salt bridge essential for the formation of the enzyme/ATP complex. The Arg186 is highly conserved and its substitution for a tryptophan residue is the most common missense mutation affecting *MMAB* gene. The expression of this mutant rendered low amount of soluble protein indicating an impairment of protein folding and rapid degradation, while enzymatic studies revealed that this mutant present a null activity, even in the presence of high amounts of ATP and cobalamin (Schubert and Hill, 2006; Maurice et al, 2008; Mera and Escalante-Semerana, 2010).

The Glu193 residue is located on the ATR α4-helix and establishes hydrogen bonds with the Mg^{2+} and the Lys78 residue, which is important for the *in vivo* binding of MgATP/cobalamin to the ATR protein. This mutant is enzymatically inactive and probably affects cobalamin binding, since it is unable to mediate the base-off transition of AdoCbl (Schubert and Hill, 2006; Fan and Bobik, 2008). These results support our findings of an impaired protein function in these mutants.

Taken together, our data and the data available in the literature indicate that the *MMAB* missense mutants, p.His183Leu, p.Arg186Trp and p.Glu193Lys, are responsible for folding defects and, consequently, a decreased stability of the ATR protein. Hence, these mutants could be good candidates for treatment with pharmacological chaperones.

4.3. MITOCHONDRIAL DYSFUNCTION IN ISOLATED METHYLMALONIC ACIDURIA

Mitochondrial dysfunction has been described to be involved directly or indirectly in the pathogenesis of inherited metabolic disorders and also in organic acidurias (Wajner and Goodman, 2011). It is postulated that the impairment of OXPHOS and other pathways involved in energy production is due to the accumulation of toxic intermediates in the mitochondrion (secondary mitochondrial dysfunction). The accumulation of these intermediates affects organs such as liver, heart, skeletal muscle, kidney, pancreas and brain (Wajner and Goodman, 2011). The impairment of mitochondrial function has been described in methylmalonic aciduria and is translated into decreased levels of NADH-cytochrome *c* reductase (complex I+III), succinate cytochrome *c* reductase (complex II+III) and COX (complex IV). Lower GSH and GSSG levels were also observed in liver extracts. These findings were described in patients' cells, liver extracts and also in a $Mut^{-/-}$ mouse model (Cosson et al, 2008; Keyzer et al, 2009; Chandler et al, 2009). Since high ROS and apoptosis levels, as well as MnSOD levels, were described in *cblB* type methylmalonic patients (Richard et al, 2005; Richard et al, 2007; Jorge-Finnigan et al, 2010), and a correlation between protein aggregation and mitochondrial dysfunction has been demonstrated, mitochondrial function was assessed in patients P8 and P9 bearing the destabilizing mutants, p.H183L and p.R190dup. In this section, two methylmalonic *mut* type patients (P10 and P11) were also analyzed.

Analysis of total ROS levels revealed an increase for both patients, when compared to controls, although P9 presented lower levels than his sibling P8. ROS levels are influenced by diverse factors, including perturbations in the respiratory chain, lipid oxidation and toxic accumulation of metabolites, related to loss of enzyme function due to misfolding mutations (Gregersen and Bross, 2010).

All patients also presented an altered mitochondrial physiology, characterized by an increase in mitochondria presenting a grain-like structure, although exhibiting differences among them. Patients P8 (*cblB* type), P10 and P11 (*mut* type) presented similar values while P9 (*cblB* type*)* presented lower levels of altered mitochondria. Mitochondria are dynamic organelles which constantly change shape and location inside the cell (Galloway and Yoon, 2012). Mitochondrial morphology is dependent on two processes, fusion and fission, that are in equilibrium in normal conditions. Fusion is activated for mitochondrial rescue, since the affected mitochondria can exchange damaged proteins and lipids with other mitochondria and, although it is not essential for cell maintenance *in vitro*, it is required for embryogenesis development. Fission is essential for maintenance of normal mitochondria number in growing and dividing cells and has been related to quality control, since it segregates damaged

mitochondria parts, targeting them to mitophagy (Youle and van der Bliek, 2012). In fibroblasts, mitochondria are usually long filaments and this morphology is associated with fusion events, while a grain-like morphology is associated with fission events (Youle and van der Bliek, 2012). A grain-like morphology has also been associated with elevated ROS levels due to accumulation of a misfolded protein in short-chain acyl-CoA dehydrogenase deficiency (SCAD) (Schmidt et al, 2010; Schmidt et al, 2011). These results are similar to the ones observed in the patients analyzed in this work, since high grain-like structure levels are observed in patients who also present elevated total ROS levels.

The analysis of the oxygen consumption rates (OCR) in the four patients revealed differences between *cblB* and *mut* type patients. The patients' cells were incubated in glucose or galactose rich medium and, in both environments, *cblB* and *mut* patients derived fibroblasts presented lower oxygen consumption rates when compared to controls. In glucose rich medium, all patients presented lower basal and ATP-linked respiration rates, but also an impaired reserve capacity, which indicates that in a stress or high ATP demand situation, patients' cells have a poor response. Regarding maximal respiration, all patients but P9 presented lower levels than the controls. When the cells were incubated in a galactose rich medium, an increase in the oxygen consumption rate was observed for all cell lines because cells are forced to rely on OXPHOS instead of glycolysis (Marroquin et al, 2007). In this situation, the differences in OCR levels were emphasized between patients, as well as the underlying OXPHOS defects (Aguer et al, 2011). In this case, all patients, but P10, presented lower basal respiration levels, while all four patients showed low maximal and ATP-linked respiration levels. Differences in the reserve capacity were also observed, since both P9 (*cblB*) and P10 (*mut*) patients presented levels similar to the controls. An increase in non-mitochondrial respiration was observed in patient P8, indicating that the fibroblasts derived from this patient are not able to completely rely on OXPHOS, even when its use is forced upon the cells. Comparing the data among the four patients, P8 (*cblB*) and P10 (*mut*), seem to have a decreased bioenergetic function when compared to P9 (*cblB*) and P11 (*mut*). The differences observed between the two siblings, P8 and P9, can be related to the differences also observed in ROS levels and mitochondrial morphology.

Another mitochondrial structure influenced by elevated ROS levels is the permeability transition pore. Mitochondrial permeability transition pore (mPTP) is responsible for mitochondrial permeability transition, a phenomenon that results in the modification of the permeability properties of the mitochondrial inner membrane (Brenner and Moulin, 2012). mPTP is a structure formed in the mitochondria, due to an increase in Ca^{2+} levels, which enhances the permeability across the mitochondrial membrane of solutes with molecular mass

under 1.5 kDa. This drives to loss of proton-motive force, mitochondrial swelling and reduced Ca^{2+} retention ability (Siemen and Ziemer, 2013). mPTP can also be triggered by oxidative damage and adenine nucleotides depletion (Brookes et al, 2004). The mPTP opening represents a point of no return and is associated with apoptosis, although some studies suggest that this event may be reversible (Rasola and Bernardi, 2011; Siemen and Ziemer, 2013). The analysis of the *cblB* type patients, P8 and P9, revealed that both patients' derived fibroblasts presented a high velocity of formation/opening of the mPTP when compared to controls' derived fibroblasts, especially in P8, whose fibroblasts showed the fastest velocity of mPTP formation. The same was not observed in fibroblasts of *mut* type patients, P10 and P11, which presented a velocity of formation/opening of the mPTP similar to controls' derived fibroblasts. The profile of mPTP opening observed in *cblB* patients can be related to the oxidative damage observed in these two patients but, since *mut* type patients also presented oxidative damage, this parameter alone is not enough to justify the differences observed in mPTP opening/formation. The mPTP components have not been fully characterized and there are conflicting data in the literature about mPTP structure (Elrod et al, 2013; Siemen and Ziemer, 2013). Nevertheless, it has been postulated that mPTP formation can be influenced by other factors, such as cyclophilin D (CypD), inorganic phosphate (P_i), Complement Component 1, q Subcomponent Binding Protein (C1QBP) and p53 protein levels. ADP, adenine nucleotides and divalent cations such as Mg^{2+}, Sr^{2+}, Ba^{2+} and Mn^{2+} have been shown to inhibit mPTP formation (Vaseva et al, 2012; Elrod et al, 2013). Differences in any of these parameters, observed between the *cblB* and *mut* type patients' cells, could account for the differences observed in the opening/formation of the mPTP.

The analysis of all the mitochondrial parameters (ROS levels, mitochondrial morphology, bioenergetic function and mPTP formation/opening) in *cblB* and *mut* type patients indicates the existence of mitochondrial dysfunction in fibroblasts derived from these methylmalonic patients. The phenotypic variation between the two *cblB* type siblings could be explained by the differences observed in the mitochondrial function, since patient P8, also presented a higher mitochondrial impairment when compared with his sibling, P9.

Mitochondrial impairment has been related to high levels of methylmalonic acid due to the similarity of this metabolite to complex II inhibitors, such as malonate (Ballhausen et al, 2009). The mitochondrial dysfunction observed in these patients does not correlate with methylmalonic acid levels, since *mut* type patients (P10 and P11) presented significantly higher levels than *cblB* type patients (P8 and P9). Patients P8 and P11 showed similar bioenergetic function, and no premature opening/formation of mPTP was observed for *mut* type patients. These results are in accordance with data obtained from the analysis of the effect of

methylmalonic acid in brain, which indicate that other metabolites derived from the alternative oxidation of propionyl-CoA, such as 2-methylcytrate and malonate, are also involved in mitochondrial dysfunction of methylmalonic patients (Kölker et al, 2003; Kölker and Okun, 2005). Further studies involving tissues of peripheral organs, such as liver and kidney, could shed light on the metabolites involved in mitochondrial dysfunction and the mechanism underlying that effect.

Ultimately, these results indicate that methylmalonic acid alone is not responsible for the mitochondrial impairment observed in these patients, and that mitochondrial dysfunction can be considered, not only a phenotypic modifier for these methylmalonic *cblB* type patients, but also a therapeutic target. Further studies with a wide range of patients with the same genotype and phenotype inconsistencies should be performed in order to confirm these results in other mutants.

4.4. SPECIFIC THERAPEUTIC STRATEGIES IN INHERITED METABOLIC DISORDERS

In this work two different therapeutical approaches have been tested: the effect of pharmacological chaperones upon missense mutations affecting ATR protein, and also, antisense therapy targeted to pseudoexon exclusion in 6-pyruvoyltetrahidropterin synthase deficiency.

The first therapeutical approach in this work was the use of a pharmacological chaperone, named as compound V (N-{[(4-chlorophenyl)carbamothioyl]amino}-2-phenylacetamid), which had been previously selected from a commercially library (MyriaScreen Diversity Collection) of 2,000 compounds. Its effect was tested, in our laboratory, in the wild-type ATR protein and in the missense mutant p.Ile96Thr, using both prokaryotic and eukaryotic expression systems, and a stabilizing effect was observed for wild-type and mutant proteins in either systems.

Missense mutations represent 58 % of the mutations identified in the *MMAB* gene (HGMD® Professional 2013.1) and, hence, the pharmacological effect of compound V was further assessed upon other missense mutations described in patients diagnosed in the laboratory, and also upon variants described in the literature as folding mutants, p.His183Leu, p.Arg186Trp and p.Glu193Lys (Schubert and Hill, 2006; Fan and Bobik, 2008). The production of these mutants in a prokaryotic expression system supplemented with 80 µM of compound V, at physiological conditions, revealed a significant stabilizing effect upon all mutant proteins.

In order to compare the chaperone effect of compound V with the one exerted by hydroxocobalamin, one of the current treatments for responsive patients, a prokaryotic

system was used to test the effect of compound V, OHCbl or the combination of both upon the wild-type protein and the p.Ile96Thr mutant. A slight stabilizing effect was observed when both wild-type and p.I96T mutant were expressed in the presence of OHCbl, although the stabilizing effect was much higher when compound V was used. The combination of the two compounds was responsible for a higher stabilizing effect when compared with the effect of isolated compound V or OHCbl.

These experiments were also performed *ex vivo*, using a control cell line and an ATR $^{-/-}$ cellular model derived from fibroblasts bearing the p.Ile96Thr/p.Ser174fs genotype. Propionate incorporation levels were measured upon cell treatment and the incorporation rates observed in the wild-type cell line were not influenced by compound V, OHCbl or the combination of both; however, in the cell line bearing the missense p.Ile96Thr mutation, propionate incorporation rate was higher when the cells were incubated in the presence of compound V when compared with OHCbl treatment, but the higher incorporation rate was reached when the cells were incubated in the presence of both, compound V and OHCbl. This synergistic effect between compound V and OHCbl was also observed upon production of immunoreactive protein, suggesting that both compounds probably bind to different sites in the protein, but also that both sites must be in close proximity, since the union of one of the compounds could stabilize the binding site of the other compound.

It has been described that, for mice bearing defects in *PCCA* gene, enzymatic activities around 10-15% of the wild-type are responsible for a significant improvement on the biochemical parameters (Miyazaki et al, 2001). Accordingly, the high stabilizing effect displayed by compound V alone is very significant. Moreover, the pharmacological effect of compound V seems to be mutation dependent, once p.Glu193Lys is more stabilized in the prokaryotic system than p.His183Leu and p.Arg186Trp mutants. Accordingly, the combined effect of compound V and OHCbl could be a good approach for those mutants less responsive to isolated compound V. The combination of compounds for treatment of inherited metabolic disorders, or even the combination of different approaches, has been described for lysosomal storage disorders (Porto et al, 2009; Parenti, 2009) and, hence, could be applied in the treatment of *cblB* type isolated methylmalonic aciduria.

The results obtained during this work also indicate that, although 40 % of *cblB* type patients are responsive to vitamin B_{12} treatment, this last compound is not a natural chaperone. The positive response to vitamin B_{12} is not completely understood and it may rely on factors such as mRNA stabilization or expression regulation (Linscheid et al, 1998; Erlandsen et al, 2004). The mechanism underlying the response to pharmacological doses of vitamin B_{12} could also be related to a reduced affinity of the mutant enzyme to hydroxocobalamin,

translated in an elevated Michaelis-Menten constant (Km). Nevertheless, p.His183Leu displays similar Km values when compared to the wild-type protein (laboratory data) and the p.Arg186Trp and Glu193Lys mutants have a complete impaired enzymatic activity (Fan and Bobik, 2008). Another possible explanation would be the stabilization of the complex formed by ATR, MUT and MMAA proteins in the mitochondrion, which could be affected by ATR mutants (Banerjee et al, 2009).

Toxicity, absorption, distribution and metabolization of compound V was assessed using wild-type C57BL/6 mice, since no animal model is available for methylmalonic aciduria *cblB* type. This approach has also been used in other disorders (Pey et al, 2008; Calvo et al, 2010). No alterations in animal normal behavior (food and water intake, socialization, sleep cycles, etc.) were observed, indicating no apparent toxic effects for both concentrations used (0.25 mg/kg/d and 5 mg/kg/d) (Sloman and McNeil, 2012). The stabilizing effect was assessed in liver and brain, central organs in this disorder, and western blot analysis revealed an increase in the relative amount of wild-type ATR protein in both organs. The stabilization of this protein in brain extracts is of great importance, since it indicates that compound V could be crossing the blood brain barrier. The literature shows conflicting data about methylmalonic acid effects in the brain (Kölker and Okun, 2005), but the persistence of neurological effects in patients that undergo liver or liver/kidney transplantation suggests that the presence of methylmalonic acid or other toxic metabolites, such as 2-methylcytrate or propionic acid, is responsible for the neurotoxicity observed in these patients (Kaplan et al, 2006; Kasahara et al, 2006).

The metabolization rate of compound V was analyzed in liver extracts and HPLC-MS/MS analysis revealed the presence of the compound in the liver, for both concentrations used. This indicates that compound V is successfully absorbed and metabolized.

Experimental evidences show that some pharmacological chaperones can stabilize one mutant protein while acting as inhibitors over other proteins (Calvo et al, 2010). Because ATR protein interacts in the mitochondrion with the MUT protein, it prompted us to investigate if compound V might have any effect upon MUT protein. The same methodological approach was used and no apparent stabilizing effect was observed, indicating that compound V acts, effectively, as a pharmacological chaperone aiding the folding of ATR protein.

The analysis of the stabilizing effect of compound V upon p.His183Leu mutant was performed in cell cultures of immortalized fibroblasts from patient P8 (p.His183Leu/p.Arg190dup) and no recovery of the propionate incorporation rate was observed. This could be due to the destabilizing effect of the other mutation, p.Arg190dup, which, as shown before, is responsible for the complete impairment of ATR protein

production. Cells from patient P8 presented the same incorporation profile as the cells bearing the p.Ile117_Gln118del, also a very destabilizing mutation. These results are important since they indicate that, despite a positive effect upon the isolated missense mutant is observed, for patient treatment purposes the complete genotype profile has to be taken into account. In this patient P8, the synergistic effect observed for compound V and OHCbl could be beneficial, and further assays should be performed to assess if recovery is achieved in those conditions.

Taken together, our data indicate that compound V is capable of stabilizing different missense mutants affecting the ATR protein, both *in vitro* and *ex vivo*. *In vivo* experiments indicate that its oral administration is well tolerated and no toxic effects are associated with a 12 day period of treatment. The successful absorption and metabolization of compound V, allied to the stabilizing effect observed upon the wild-type ATR protein in key organs such as liver and brain, indicate that this compound is a good candidate for future studies upon other missense mutants and also for clinical trials in *cblB* type patients.

The second therapeutic approach was the use of antisense therapy for pseudoexon exclusion. Mutations affecting the normal splicing process account for about 9 % of all mutations described in Human Genome Mutation Database (HGMD® Professional 2013.1), although this percentage may vary among the different disorders. One of the effects of defective splicing is the inclusion of intronic regions that resemble normal exons. These regions are called pseudoexons and the aberrant inclusion of pseudoexons are emerging as a common cause of human disorders (Dhir and Buratti, 2010) The use of antisense therapy based on antisense oligonucleotides (AON) has become widely accepted as a promising treatment strategy (Saonere, 2011), and has been successfully used in disorders such as propionic and methylmalonic aciduria (Rincón et al, 2007; Perez et al, 2010), Duchenne muscular dystrophy (Wood et al, 2010), and spinal muscular atrophy (SMA)(Hua et al, 2010), among others.

Cell cultures from three PTPS deficient patients (P12, P13 and P14) bearing deep intronic splicing mutations were treated with antisense therapy, particularly, antisense morpholino oligos (AMOs). Patients P12 and P13 had been previously described (Meili et al, 2009). P12 is homozygous for the c.84-322A>T mutation that leads to the insertion of a 79 nucleotides LINE2 (long-interspersed element) sequence between exon 1 and 2 (r.83_84ins79), while P13 is heterozygous for the c.163+695_163+751del57 mutation, responsible for the insertion of 45 nucleotides between exons 2 and 3 (r.163_164ins45). Patient P14 is also heterozygous for the c.164-712A>T mutation that leads to the introduction of the same 45 nucleotide sequence observed in patient P13 and of another sequence of 45 nucleotides plus 25 adjacent nucleotides (r.164_165ins45/70). In both patients P13 and P14, the inserted

sequences belong to an antisense *Alu* sequence (Meili et al, 2009). LINEs are transposon or transposon-derived elements, which consist of repetitive sequences, and account for more than 50 % of the human genome and about 4% of human genes contain repetitive sequences in their coding regions (Keren et al, 2010; Poulos et al, 2011). *Alu* elements are the most abundant repetitive element found in the human genome and the inclusion of these repetitive elements in the mRNA, as internal exons, has been described in several disorders (Varon et al, 2003; Keren et al, 2010).

Mutation c.164-712A>T was found in patient P14 and is responsible for the inclusion of a pseudoexon sequence. This mutation affects the coupling of the splice site sequence to the U1 snRNA, and it has been observed that the complementarity between the 5' splice site sequence and the last eleven nucleotides of the 5' U1 snRNA site is one of the most important steps in the splicing process. It has also been demonstrated that the higher the complementarity between these two sequences, the higher is the splicing efficiency and pre-mRNA stability (Freund et al, 2005). In higher eukaryotes, consensus 5' splice site consists of nine partially conserved nucleotides, located at the exon-intron boundary: NAG|GTRAGT in which N is A or C and R is A or G. These positions are numbered spanning from -3 to +6 (De Conti et al, 2012). Most splicing mutations located near the exon-intron junction affect the GT dinucleotide. Mutations affecting other nucleotides beside the GT dinucleotide, are mostly 8located between the +3 and +6 nucleotides of the adjacent intron and the most common affect positions +1, +2 and +5 (Krawczak et al, 2007; De Conti et al, 2012). Hence, the effect of the mutation c.164-712A>T (position +6) upon the possible U1 snRNA union sequence was studied using an *ex vivo* minigene system. The effect of two additional changes, c.164-714C>A (position +4) and c.164-715T>A (position +3), upon U1 snRNA complementarity were also studied. The pseudoexon activation was observed for the c.164-712A>T (position + 6), as expected, and to a higher extent for the c.164-715T>A (position +3). The c.164-714C>A mutation also activated the insertion of the pseudoexon, although to a much lesser extent. These results shown that the c.164-712A>T is in fact influencing the U1 snRNA binding and that changing the nucleotides that are involved in the interaction with the U1 snRNA binding sequence, the complementarity of this protein to the pre-mRNA can be increased or decreased.

For the antisense therapy, three different types of oligonucleotides were used. Morpholino oligos (AMOs), VIVO-morpholinos oligos (VIVO-AMOs) and locked nucleic acids (LNAs). AMOs have been used successfully for pseudoexon exclusion in other disorders (Rincón et al, 2007; Moulton and Jiang, 2009). In this study, morpholino oligos were designed to hybridize specifically to each inserted sequence and two different concentrations, 20 µM and

30 µM were used. Recovery of the normal splicing profile was obtained in cell cultures of all patients and at both concentrations. We have demonstrated AMO specificity, since no recovery of the normal splicing profile was observed for any of the patients when the experiment was performed with scrambled AMOs.

The treatment of the patients-derived fibroblasts with AMO also recovered the immunoreactive PTPS protein levels and enzymatic activity. The pterin levels, specially the neopterin/biopterin ration were also analyzed by HPLC and a significant decrease was observed, indicating a restoration of the normal metabolic pathway.

Although the efficiency of morpholino oligonucleotides has been extensively proven, its use on *in vivo* systems has only been successful with leaky tissues, such as muscle. To increase transport and delivery efficiency, VIVO-morpholinos (VIVO-AMOs) were designed (Morcos et al, 2008). These oligonucleotides are AMOs coupled to an eight guanidinium head group in a dendrimer scaffold, and this structure enables the oligonucleotide entry into the cell without any type of aid (Li and Morcos, 2008; Morcos et al, 2008; Moulton and Jiang, 2009). It has been demonstrated that these oligonucleotides can cross the blood brain barrier, although to a minor extent when compared with organs like liver, kidney or small intestine (Morcos et al, 2008). Since PTPS deficient patients usually present neurological symptoms and because AMOs enter the cells by aid of a transfection agent, which molecules do not cross the blood brain barrier, the antisense effect of VIVO-morpholinos was analyzed. These oligonucleotides are specifically designed for *in vivo* experiments, but since an animal model is not available to test the effect of antisense therapy in this disorder, patient-derived fibroblasts were used and the normal splicing profile was recovered in patients P12 and P14.

The effect of LNAs was also tested for patients P12 and P14. LNAs are smaller oligonucleoties with a locked ribose ring, which confers greater stability (Veedu and Wengel, 2009; Campbell and Wengel, 2011). The use of LNAs has been reported in several disorders and their effect has been tested in different organs (Beane et al, 2007; Gupta et al, 2010; Obad et al, 2011; Moschos et al, 2011).

Specific LNA sequences were designed against the pseudoexon sequence and the treatment of the patients-derived fibroblasts was successful, with a dose dependent recovery of the normal splicing profile. Although LNAs normally have to enter the cell through a carrier system (transfection agent), reports on the positive effect of “naked” LNAs have been described using process called gymnosis (Stein et al, 2010; Soifer et al, 2012). This is of great importance for disorders like PTPS deficiency where the antisense oligonucleotides must be able to reach the brain. Nevertheless, for gymnosis to occur, LNAs have to be chemically modified (Soifer et al, 2012). The conjugation of LNAs with nanoparticles has also been

described and could be another approach (Preiss and Bothun, 2011; Griveau et al, 2013). Future experiments should be performed using chemically modified LNAs to assess the efficacy of the treatment without transfection agents.

The data obtained with these studies indicate that antisense therapy using different types of antisense oligonucleotides has successfully eliminated pseudoexon inclusion in three different splicing mutations found in PTPS deficient patients.

The effective targeting of pseudoexon sequences using antisense therapy, and the full recovery of the normal splicing profiles, is of great importance since repetitive elements are probably the major source of pseudoexon sequences, and the inclusion of such sequences in the pre-mRNA is emerging as an important disease-causing effect.

PART 5

CONCLUDING REMARKS

This work has contributed to the description and characterization of mutations found in isolated methylmalonic *mut*, *cblD* and *cblB* and propionic patients, broadening the knowledge of the molecular basis of these disorders, to the elucidation of the pathophysiological mechanisms of mitochondrial dysfunction in *cblB* type patients and, finally, represents the proof of concept for the use of two different therapeutical approaches, chaperone and antisense therapy, in isolated methylmalonic aciduria and 6-pyruvoyltetrahydropterin synthase deficiency, respectively.

First, the identification of the *MMADHC* gene, responsible for the *cblD* complementation group allowed the characterization, for the first time in our laboratory, of four isolated methylmalonic *cblD* variant 2 type patients who had remained uncharacterized until then and, moreover, the identification of three novel mutations, which contributed to the expansion of the known mutational spectrum of *cblD* variant 2 type deficiency.

Additionally, the characterization of one *mut* type methylmalonic patient and two propionic patients of Portuguese origin revealed the presence of two novel mutations in the *MUT* gene and two already described mutations in *PCCB* gene, respectively. The two novel mutations, c.244dupA and c.1408-10A>G found in the *MUT* gene are disease causing and the functional characterization of the splicing mutation revealed that, due to its effect, antisense therapy might be a good therapeutic approach.

Functional analysis of two novel (p.His183Leu and p.Arg190dup) and three already described (p.Ile117_Gln118, p.Arg186Trp, and p.Glu193Lys) mutations affecting the *MMAB* gene (*cblB* complementation group) revealed that all are destabilizing mutations. Both p.Ile117_Gln118 and p.Arg190dup are highly destabilizing mutations and are probably responsible for a complete lack of ATR protein, while the p.His183Leu, p.Arg186Trp, and p.Glu193Lys mutants affect the ATR folding and produce an unstable protein. These results indicate that these three mutants are probable candidates for chaperone therapy.

The two novel mutations (p.His183Leu and p.Arg190dup) were described in two siblings (patients P8 and P9) who presented phenotypic differences, in spite of the same genotype. Analysis of the propionate incorporation rates revealed a decrease in protein activity for one of the siblings, only in a stress situation. This is important because asymptomatic patients can manifest a disease phenotype in stress situations, such as fever episodes, possibly leading to neurological affectations. Moreover, it indicates that the phenotypical differences between the siblings could be explained by differential expression of proteins implicated in the protein quality control system, since they bear folding mutants.

The analysis of mitochondrial dysfunction in both siblings and two other *mut* type patients confirmed that isolated methylmalonic patients present mitochondrial impairment.

Moreover, a correlation between the mitochondrial dysfunction and the phenotypic differences between the *cblB* type siblings was observed, since the sibling with the worst phenotype (patient P8) presented higher mitochondrial impairment.

We can also conclude that for the *cblB* type patients, mitochondrial dysfunction could be a phenotype modifier. Furthermore, it could be considered as a future therapeutical target. This opens the door to further studies using specific pharmacological strategies targeting the mitochondria and also to the administration of antioxidants (vitamin C, vitamin E and MitoQ), as a complementary treatment option.

Moreover, in organic acidurias, mitochondrial impairment has been related with high methylmalonic acid levels but, in this work, that correlation was not observed. This suggests that although methylmalonic acid is a hallmark of methylmalonic aciduria and may be responsible for mitochondrial impairment, other factors like other toxic metabolites, differences in control systems, such as the mtPQC, but also mutations affecting genes encoding free radicals scavengers, can contribute to mitochondrial dysfunction.

The *in vitro* and *in vivo* analysis of compound V confirmed its effect as a pharmacological chaperone upon different missense mutations and, its effective metabolization and delivery to key organs in these disorders, such as liver and brain, with no apparent toxic effects. Hence, this work is the proof of concept for the use of pharmacological chaperones in methylmalonic aciduria *cblB* type.

Most importantly, in this work we have demonstrated that OHCbl is not a natural chaperone of the ATR protein. We have also demonstrated that the combination of OHCbl and compound V is responsible for a synergistic action and the recovery of protein activity in a control cell line. This observation is of great importance since it opens the possibility to other treatment strategies in these patients and also to further studies with chaperones.

This work represents also the proof of concept that antisense oligonucleotide therapy can be used to exclude pseudoexon sequences affecting the *PTS* gene. The use of other antisense oligonucleotides, such as LNAs and VIVO-morpholinos has also recovered of the normal splicing profile. The successful use of VIVO-morpholinos is of great importance, since this type of oligonucleotides allows a higher stability and delivery efficiency of the morpholino molecule *in vivo*. Further studies using nanoparticles should be performed in order to increase delivery efficiency in a key organ such as the brain.

In conclusion, this work allowed the identification and characterization of novel mutations identified in isolated methylmalonic patients, the identification of mitochondrial dysfunction as a phenotypic modifier in isolated methylmalonic aciduria and, finally, the assessment of specific therapeutical strategies in metabolic disorders.

REFERENCES

Acquaviva, C., J. F. Benoist, S. Pereira, I. Callebaut, T. Koskas, D. Porquet and J. Elion (2005). "Molecular basis of methylmalonyl-CoA mutase apoenzyme defect in 40 European patients affected by mut(o) and mut- forms of methylmalonic acidemia: identification of 29 novel mutations in the MUT gene." Hum Mutat 25(2): 167-176.

Aguer, C., D. Gambarotta, R. J. Mailloux, C. Moffat, R. Dent, R. McPherson and M. E. Harper (2011). "Galactose enhances oxidative metabolism and reveals mitochondrial dysfunction in human primary muscle cells." PLoS One **6**(12): e28536.

Alfadda, A. A. and R. M. Sallam (2012). "Reactive oxygen species in health and disease." J Biomed Biotechnol **2012**: 936486.

Arti M., R. Ankur, R. Seema, D. Amarjeet, K. Ashok (2012). "Mitochondrial permeability transition pores: another view." IRJP **3**(5): 106-08.

Baker, M. J., T. Tatsuta and T. Langer (2011). "Quality control of mitochondrial proteostasis." Cold Spring Harb Perspect Biol **3**(7).

Ballhausen, D., L. Mittaz, O. Boulat, L. Bonafe and O. Braissant (2009). "Evidence for catabolic pathway of propionate metabolism in CNS: expression pattern of methylmalonyl-CoA mutase and propionyl-CoA carboxylase alpha-subunit in developing and adult rat brain." Neuroscience **164**(2): 578-587.

Banerjee, R., C. Gherasim and D. Padovani (2009). "The tinker, tailor, soldier in intracellular B12 trafficking." Curr Opin Chem Biol **13**(4): 484-491.

Banerjee, R. (2006). "B12 trafficking in mammals: A for coenzyme escort service." ACS Chem Biol **1**(3): 149-159.

Bastolla, U., A. Moya, E. Viguera and R. C. van Ham (2004). "Genomic determinants of protein folding thermodynamics in prokaryotic organisms." J Mol Biol **343**(5): 1451-1466.

Bastolla, U., J. Farwer, E. W. Knapp and M. Vendruscolo (2001). "How to guarantee optimal stability for most representative structures in the Protein Data Bank." Proteins **44**(2): 79-96.

Beane, R. L., R. Ram, S. Gabillet, K. Arar, B. P. Monia and D. R. Corey (2007). "Inhibiting gene expression with locked nucleic acids (LNAs) that target chromosomal DNA." Biochemistry **46**(25): 7572-7580.

Beaulieu, C. L., M. E. Samuels, S. Ekins, C. R. McMaster, A. M. Edwards, A. R. Krainer, G. G. Hicks, B. J. Frey, K. M. Boycott and A. E. Mackenzie (2012). "A generalizable pre-clinical research approach for orphan disease therapy." Orphanet J Rare Dis **7**: 39.

Birben, E., U. M. Sahiner, C. Sackesen, S. Erzurum and O. Kalayci (2012). "Oxidative stress and antioxidant defense." World Allergy Organ J **5**(1): 9-19.

Blau, N. Duran M., Blaskovics ME., Gibson KM. (2003). Physician's guide to the laboratory diagnosis of metabolic disorders. 2nd ed. Berlin: Springer. pp.89-106.

Blau, N. (2008). "Defining tetrahydrobiopterin (BH4)-responsiveness in PKU." J Inherit Metab Dis **31**(1): 2-3.

Bonafe, L., B. Thony, W. Leimbacher, L. Kierat and N. Blau (2001). "Diagnosis of dopa-responsive dystonia and other tetrahydrobiopterin disorders by the study of biopterin metabolism in fibroblasts." Clin Chem **47**(3): 477-485.

Brenner, C. and M. Moulin (2012). "Physiological roles of the permeability transition pore." Circ Res **111**(9): 1237-1247.

Brieger, K., S. Schiavone, F. J. Miller, Jr. and K. H. Krause (2012). "Reactive oxygen species: from health to disease." Swiss Med Wkly **142**: w13659.

Brookes, P. S., Y. Yoon, J. L. Robotham, M. W. Anders and S. S. Sheu (2004). "Calcium, ATP, and ROS: a mitochondrial love-hate triangle." Am J Physiol Cell Physiol **287**(4): C817-833.

Callahan, M. K., D. Chaillot, C. Jacquin, P. R. Clark and A. Menoret (2002). "Differential acquisition of antigenic peptides by Hsp70 and Hsc70 under oxidative conditions." J Biol Chem **277**(37): 33604-33609.

Calvo, A. C., T. Scherer, A. L. Pey, M. Ying, I. Winge, J. McKinney, J. Haavik, B. Thony and A. Martinez (2010). "Effect of pharmacological chaperones on brain tyrosine hydroxylase and tryptophan hydroxylase 2." J Neurochem **114**(3): 853-863.

Campbell, M. A. and J. Wengel (2011). "Locked vs. unlocked nucleic acids (LNA vs. UNA): contrasting structures work towards common therapeutic goals." Chem Soc Rev **40**(12): 5680-5689.

Campeau, E., L. Dupuis, A. Leon-Del-Rio and R. Gravel (1999). "Coding sequence mutations in the alpha subunit of propionyl-CoA carboxylase in patients with propionic acidemia." Mol Genet Metab **67**(1): 11-22.

Campeau, E., L. R. Desviat, D. Leclerc, X. Wu, B. Perez, M. Ugarte and R. A. Gravel (2001). "Structure of the PCCA gene and distribution of mutations causing propionic acidemia." Mol Genet Metab **74**(1-2): 238-247.

Cardoso, A. R., B. Chausse, F. M. da Cunha, L. A. Luevano-Martinez, T. B. Marazzi, P. S. Pessoa, B. B. Queliconi and A. J. Kowaltowski (2012). "Mitochondrial compartmentalization of redox processes." Free Radic Biol Med **52**(11-12): 2201-2208.

Cartegni, L., J. Wang, Z. Zhu, M. Q. Zhang and A. R. Krainer (2003). "ESEfinder: A web resource to identify exonic splicing enhancers." Nucleic Acids Res **31**(13): 3568-3571.

Circu, M. L. and T. Y. Aw (2010). "Reactive oxygen species, cellular redox systems, and apoptosis." Free Radic Biol Med **48**(6): 749-762.

Chandler, R. J., P. M. Zerfas, S. Shanske, J. Sloan, V. Hoffmann, S. DiMauro and C. P. Venditti (2009). "Mitochondrial dysfunction in mut methylmalonic acidemia." FASEB J **23**(4): 1252-1261.

Chen, B., M. Retzlaff, T. Roos and J. Frydman (2011). "Cellular strategies of protein quality control." Cold Spring Harb Perspect Biol **3**(8): a004374.

Coelho, D., T. Suormala, M. Stucki, J. P. Lerner-Ellis, D. S. Rosenblatt, R. F. Newbold, M. R. Baumgartner and B. Fowler (2008). "Gene identification for the cblD defect of vitamin B12 metabolism." N Engl J Med **358**(14): 1454-1464.

Costigan, M., A. Latremoliere and C. J. Woolf (2012). "Analgesia by inhibiting tetrahydrobiopterin synthesis." Curr Opin Pharmacol **12**(1): 92-99.

Cosson, M. A., G. Touati, F. Lacaille, V. Valayannnopoulos, C. Guyot, G. Guest, V. Verkarre, D. Chretien, D. Rabier, A. Munnich, J. F. Benoist, Y. de Keyzer, P. Niaudet and P. de Lonlay (2008). "Liver hepatoblastoma and multiple OXPHOS deficiency in the follow-up of a patient with methylmalonic aciduria." Mol Genet Metab **95**(1-2): 107-109.

De Conti, L., M. Baralle and E. Buratti (2013). "Exon and intron definition in pre-mRNA splicing." Wiley Interdiscip Rev RNA **4**(1): 49-60.

de Keyzer, Y., V. Valayannopoulos, J. F. Benoist, F. Batteux, F. Lacaille, L. Hubert, D. Chretien, B. Chadefeaux-Vekemans, P. Niaudet, G. Touati, A. Munnich and P. de Lonlay (2009). "Multiple OXPHOS deficiency in the liver, kidney, heart, and skeletal muscle of patients with methylmalonic aciduria and propionic aciduria." Pediatr Res **66**(1): 91-95.

Deodato, F., S. Boenzi, F. M. Santorelli and C. Dionisi-Vici (2006). "Methylmalonic and propionic aciduria." Am J Med Genet C Semin Med Genet **142C**(2): 104-112.

Desmet, F. O., D. Hamroun, M. Lalande, G. Collod-Beroud, M. Claustres and C. Beroud (2009). "Human Splicing Finder: an online bioinformatics tool to predict splicing signals." Nucleic Acids Res **37**(9): e67.

Desviat, L. R., B. Perez, C. Perez-Cerda, P. Rodriguez-Pombo, S. Clavero and M. Ugarte (2004). "Propionic acidemia: mutation update and functional and structural effects of the variant alleles." Mol Genet Metab **83**(1-2): 28-37.

Desviat, L. R., S. Clavero, et al. (2006). "New splicing mutations in propionic acidemia." J Hum Genet **51**(11): 992-7.

Desviat, L. R., B. Perez and M. Ugarte (2012). "Minigenes to confirm exon skipping mutations." Methods Mol Biol **867**: 37-47.

Dias, N. and C. A. Stein (2002). "Antisense oligonucleotides: basic concepts and mechanisms." Mol Cancer Ther **1**(5): 347-355.

Dietz, H. C. (2010). "New therapeutic approaches to mendelian disorders." N Engl J Med **363**(9): 852-863.

Dipple, K. M. and E. R. McCabe (2000). "Modifier genes convert "simple" Mendelian disorders to complex traits." Mol Genet Metab **71**(1-2): 43-50.

Dhir, A. and E. Buratti (2010). "Alternative splicing: role of pseudoexons in human disease and potential therapeutic strategies." FEBS J **277**(4): 841-855.

Dobson, C. M., T. Wai, D. Leclerc, H. Kadir, M. Narang, J. P. Lerner-Ellis, T. J. Hudson, D. S. Rosenblatt and R. A. Gravel (2002a). "Identification of the gene responsible for the cblB complementation group of vitamin B12-dependent methylmalonic aciduria." Hum Mol Genet **11**(26): 3361-3369.

Dobson, C. M., T. Wai, D. Leclerc, A. Wilson, X. Wu, C. Dore, T. Hudson, D. S. Rosenblatt and R. A. Gravel (2002b). "Identification of the gene responsible for the cblA complementation group of vitamin B12-responsive methylmalonic acidemia based on analysis of prokaryotic gene arrangements." Proc Natl Acad Sci U S A **99**(24): 15554-15559.

Douglas, A. G. and M. J. Wood (2011). "RNA splicing: disease and therapy." Brief Funct Genomics **10**(3): 151-164.

Dranka, B. P., G. A. Benavides, A. R. Diers, S. Giordano, B. R. Zelickson, C. Reily, L. Zou, J. C. Chatham, B. G. Hill, J. Zhang, A. Landar and V. M. Darley-Usmar (2011). "Assessing bioenergetic function in response to oxidative stress by metabolic profiling." Free Radic Biol Med **51**(9): 1621-1635.

Elrod, J. W. and J. D. Molkentin (2013). "Physiologic functions of cyclophilin D and the mitochondrial permeability transition pore." Circ J **77**(5): 1111-1122.

Erlandsen, H., A. L. Pey, A. Gamez, B. Perez, L. R. Desviat, C. Aguado, R. Koch, S. Surendran, S. Tyring, R. Matalon, C. R. Scriver, M. Ugarte, A. Martinez and R. C. Stevens (2004). "Correction of kinetic and stability defects by tetrahydrobiopterin in phenylketonuria patients with certain phenylalanine hydroxylase mutations." Proc Natl Acad Sci U S A **101**(48): 16903-16908.

Fan, C. and T. A. Bobik (2008). "Functional characterization and mutation analysis of human ATP:Cob(I)alamin adenosyltransferase." Biochemistry **47**(9): 2806-2813.

Faustino, N. A. and T. A. Cooper (2003). "Pre-mRNA splicing and human disease." Genes Dev **17**(4): 419-437.

Fowler, B., J. V. Leonard and M. R. Baumgartner (2008). "Causes of and diagnostic approach to methylmalonic acidurias." J Inherit Metab Dis **31**(3): 350-360.

Fenton, W. A., Gravel, R. A. and Rosenberg, L. E. (2001). “Disorders of propionate and methylmalonate metabolism.” In Scriver, C R., Beaudet, A. L., Sly, W. and Valle, D., editors. The Metabolic and Molecular Bases of Inherited Disease., New York: McGraw-Hill. pp. 2165-2190.

Fortes, P., Y. Cuevas, F. Guan, P. Liu, S. Pentlicky, S. P. Jung, M. L. Martinez-Chantar, J. Prieto, D. Rowe and S. I. Gunderson (2003). "Inhibiting expression of specific genes in mammalian cells with 5' end-mutated U1 small nuclear RNAs targeted to terminal exons of pre-mRNA." Proc Natl Acad Sci U S A **100**(14): 8264-8269.

Freund, M., M. J. Hicks, C. Konermann, M. Otte, K. J. Hertel and H. Schaal (2005). "Extended base pair complementarity between U1 snRNA and the 5' splice site does not inhibit splicing in higher eukaryotes, but rather increases 5' splice site recognition." Nucleic Acids Res **33**(16): 5112-5119.

Froese, D. S. and R. A. Gravel (2010). "Genetic disorders of vitamin B(1)(2) metabolism: eight complementation groups--eight genes." Expert Rev Mol Med **12**: e37.

Gallego-Villar, L., C. Perez-Cerda, B. Perez, D. Abia, M. Ugarte, E. Richard and L. R. Desviat (2012). "Functional characterization of novel genotypes and cellular oxidative stress studies in propionic acidemia." J Inherit Metab Dis [Epub ahead of print].

Galloway, C. A. and Y. Yoon (2012). "Mitochondrial Morphology in Metabolic Diseases." Antioxid Redox Signal **19**(4): 415-30.

Gamez, A., B. Perez, M. Ugarte and L. R. Desviat (2000). "Expression analysis of phenylketonuria mutations. Effect on folding and stability of the phenylalanine hydroxylase protein." J Biol Chem **275**(38): 29737-29742.

Garcia-Blanco, M. A., A. P. Baraniak and E. L. Lasda (2004). "Alternative splicing in disease and therapy." Nat Biotechnol **22**(5): 535-546.

Garrod, A. E. (1975). "The Lancet. The incidence of alkaptonuria: a study in chemical individuality." Nutr Rev **33**(3): 81-83.

Gherasim, C., L. Hannibal, D. Rajagopalan, D. W. Jacobsen and R. Banerjee (2013a). "The C-terminal domain of CblD interacts with CblC and influences intracellular cobalamin partitioning." Biochimie **95**(5): 1023-1032.

Gherasim, C., M. Lofgren and R. Banerjee (2013b). "Navigating the B(12) road: assimilation, delivery, and disorders of cobalamin." J Biol Chem **288**(19): 13186-13193.

Glaus, E., F. Schmid, R. Da Costa, W. Berger and J. Neidhardt (2011). "Gene therapeutic approach using mutation-adapted U1 snRNA to correct a RPGR splice defect in patient-derived cells." Mol Ther **19**(5): 936-941.

Gravel, R. A., B. R. Akerman, A. M. Lamhonwah, M. Loyer, A. Leon-del-Rio and I. Italiano (1994). "Mutations participating in interallelic complementation in propionic acidemia." Am J Hum Genet **55**(1): 51-58.

Gregersen, N. (2006). "Protein misfolding disorders: pathogenesis and intervention." J Inherit Metab Dis **29**(2-3): 456-470.

Gregersen, N., P. Bross, S. Vang and J. H. Christensen (2006). "Protein misfolding and human disease." Annu Rev Genomics Hum Genet **7**: 103-124.

Gregersen, N. and P. Bross (2010). "Protein misfolding and cellular stress: an overview." Methods Mol Biol **648**: 3-23.

Griveau, A., J. Bejaud, S. Anthiya, S. Avril, D. Autret and E. Garcion (2013). "Silencing of miR-21 by locked nucleic acid-lipid nanocapsule complexes sensitize human glioblastoma cells to radiation-induced cell death." Int J Pharm [Epub ahead of print].

Gottesman, S., S. Wickner and M. R. Maurizi (1997). "Protein quality control: triage by chaperones and proteases." Genes Dev **11**(7): 815-823.

Gupta, N., N. Fisker, M. C. Asselin, M. Lindholm, C. Rosenbohm, H. Orum, J. Elmen, N. G. Seidah and E. M. Straarup (2010). "A locked nucleic acid antisense oligonucleotide (LNA) silences PCSK9 and enhances LDLR expression in vitro and in vivo." PLoS One **5**(5): e10682.

Hansen, J., T. J. Corydon, J. Palmfeldt, A. Durr, B. Fontaine, M. N. Nielsen, J. H. Christensen, N. Gregersen and P. Bross (2008). "Decreased expression of the mitochondrial matrix proteases Lon and ClpP in cells from a patient with hereditary spastic paraplegia (SPG13)." Neuroscience **153**(2): 474-482.

Hageman, J., M. A. van Waarde, A. Zylicz, D. Walerych and H. H. Kampinga (2011). "The diverse members of the mammalian HSP70 machine show distinct chaperone-like activities." Biochem J **435**(1): 127-142.

Hua, Y., K. Sahashi, G. Hung, F. Rigo, M. A. Passini, C. F. Bennett and A. R. Krainer (2010). "Antisense correction of SMN2 splicing in the CNS rescues necrosis in a type III SMA mouse model." Genes Dev **24**(15): 1634-1644.

Hofherr, S. E., J. S. Senac, C. Y. Chen, D. J. Palmer, P. Ng and M. A. Barry (2009). "Short-term rescue of neonatal lethality in a mouse model of propionic acidemia by gene therapy." Hum Gene Ther **20**(2): 169-180.

Houck, S. A., S. Singh and D. M. Cyr (2012). "Cellular responses to misfolded proteins and protein aggregates." Methods Mol Biol **832**: 455-461.

Jafari, P., O. Braissant, P. Zavadakova, H. Henry, L. Bonafe and D. Ballhausen (2013). "Brain damage in methylmalonic aciduria: 2-methylcitrate induces cerebral ammonium accumulation and apoptosis in 3D organotypic brain cell cultures." Orphanet J Rare Dis **8**: 4.

Jansen, R., F. Kalousek, W. A. Fenton, L. E. Rosenberg and F. D. Ledley (1989). "Cloning of full-length methylmalonyl-CoA mutase from a cDNA library using the polymerase chain reaction." Genomics **4**(2): 198-205.

Javadov, S. and M. Karmazyn (2007). "Mitochondrial permeability transition pore opening as an endpoint to initiate cell death and as a putative target for cardioprotection." Cell Physiol Biochem **20**(1-4): 1-22.

Jensen, C. J., B. J. Oldfield and J. P. Rubio (2009). "Splicing, cis genetic variation and disease." Biochem Soc Trans **37**(Pt 6): 1311-1315.

Jorge-Finnigan, A., C. Aguado, R. Sanchez-Alcudia, D. Abia, E. Richard, B. Merinero, A. Gamez, R. Banerjee, L. R. Desviat, M. Ugarte and B. Perez (2010). "Functional and structural analysis of five mutations identified in methylmalonic aciduria cblB type." Hum Mutat **31**(9): 1033-1042.

Kang, J. and S. Pervaiz (2012). "Mitochondria: redox metabolism and dysfunction." Biochem Res Int **2012**: 896751.

Kaplan, P., C. Ficicioglu, A. T. Mazur, M. J. Palmieri and G. T. Berry (2006). "Liver transplantation is not curative for methylmalonic acidopathy caused by methylmalonyl-CoA mutase deficiency." Mol Genet Metab **88**(4): 322-326.

Kasahara, M., R. Horikawa, M. Tagawa, S. Uemoto, S. Yokoyama, Y. Shibata, T. Kawano, T. Kuroda, T. Honna, K. Tanaka and M. Saeki (2006). "Current role of liver transplantation for methylmalonic acidemia: a review of the literature." Pediatr Transplant **10**(8): 943-947.

Kaur, H., B. R. Babu and S. Maiti (2007). "Perspectives on chemistry and therapeutic applications of Locked Nucleic Acid (LNA)." Chem Rev **107**(11): 4672-4697.

Kennerknecht I., et al. (1992). “Assignment of the human gene propionyl coenzyme A carboxylase, alpha-chain, (PCCA) to chromosome 13q32 by in situ hybridization.” Genomics **14**(2): 550-1

Keren, H., G. Lev-Maor and G. Ast (2010). "Alternative splicing and evolution: diversification, exon definition and function." Nat Rev Genet **11**(5): 345-355.

Kim, J. C., N. C. Lee, P. W. Hwu, Y. H. Chien, S. Fahiminiya, J. Majewski, D. Watkins and D. S. Rosenblatt (2012). "Late onset of symptoms in an atypical patient with the cblJ inborn error of vitamin B12 metabolism: diagnosis and novel mutation revealed by exome sequencing." Mol Genet Metab **107**(4): 664-668.

Knerr, I., N. Weinhold, J. Vockley and K. M. Gibson (2012). "Advances and challenges in the treatment of branched-chain amino/keto acid metabolic defects." J Inherit Metab Dis **35**(1): 29-40.

Kolker, S., M. Schwab, F. Horster, S. Sauer, A. Hinz, N. I. Wolf, E. Mayatepek, G. F. Hoffmann, J. A. Smeitink and J. G. Okun (2003). "Methylmalonic acid, a biochemical hallmark of methylmalonic acidurias but no inhibitor of mitochondrial respiratory chain." J Biol Chem **278**(48): 47388-47393.

Kolker, S. and J. G. Okun (2005). "Methylmalonic acid--an endogenous toxin?" Cell Mol Life Sci **62**(6): 621-624.

Kowaltowski, A. J., R. F. Castilho and A. E. Vercesi (2001). "Mitochondrial permeability transition and oxidative stress." FEBS Lett **495**(1-2): 12-15.

Krauss, S., M. D. Brand and F. Buttgereit (2001). "Signaling takes a breath--new quantitative perspectives on bioenergetics and signal transduction." Immunity **15**(4): 497-502.

Krawczak, M., N. S. Thomas, B. Hundrieser, M. Mort, M. Wittig, J. Hampe and D. N. Cooper (2007). "Single base-pair substitutions in exon-intron junctions of human genes: nature, distribution, and consequences for mRNA splicing." Hum Mutat **28**(2): 150-158.

Laufs, S., N. Blau and B. Thony (1998). "Retrovirus-mediated double transduction of the GTPCH and PTPS genes allows 6-pyruvoyltetrahydropterin synthase-deficient human fibroblasts to synthesize and release tetrahydrobiopterin." J Neurochem **71**(1): 33-40.

Leal, N. A., H. Olteanu, R. Banerjee and T. A. Bobik (2004). "Human ATP:Cob(I)alamin adenosyltransferase and its interaction with methionine synthase reductase." J Biol Chem **279**(46): 47536-47542.

Leandro, P. and C. M. Gomes (2008). "Protein misfolding in conformational disorders: rescue of folding defects and chemical chaperoning." Mini Rev Med Chem **8**(9): 901-911.

Lerner-Ellis, J. P., A. B. Gradinger, D. Watkins, J. C. Tirone, A. Villeneuve, C. M. Dobson, A. Montpetit, P. Lepage, R. A. Gravel and D. S. Rosenblatt (2006). "Mutation and biochemical analysis of patients belonging to the cblB complementation class of vitamin B12-dependent methylmalonic aciduria." Mol Genet Metab **87**(3): 219-225.

Li, Y. F. and P. A. Morcos (2008). "Design and synthesis of dendritic molecular transporter that achieves efficient in vivo delivery of morpholino antisense oligo." Bioconjug Chem **19**(7): 1464-1470.

Linscheid, P., A. Schaffner, N. Blau and G. Schoedon (1998). "Regulation of 6-pyruvoyltetrahydropterin synthase activity and messenger RNA abundance in human vascular endothelial cells." Circulation **98**(17): 1703-1706.

Liu, K. M., T. T. Liu, N. C. Lee, L. Y. Cheng, K. J. Hsiao and D. M. Niu (2008). "Long-term follow-up of Taiwanese Chinese patients treated early for 6-pyruvoyl-tetrahydropterin synthase deficiency." Arch Neurol **65**(3): 387-392.

Lowry, O. H., N. J. Rosebrough, A. L. Farr and R. J. Randall (1951). "Protein measurement with the Folin phenol reagent." J Biol Chem **193**(1): 265-275.

Lu, B., S. Yadav, P. G. Shah, T. Liu, B. Tian, S. Pukszta, N. Villaluna, E. Kutejova, C. S. Newlon, J. H. Santos and C. K. Suzuki (2007). "Roles for the human ATP-dependent Lon protease in mitochondrial DNA maintenance." J Biol Chem **282**(24): 17363-17374.

Luce, K., A. C. Weil and H. D. Osiewacz (2010). "Mitochondrial protein quality control systems in aging and disease." Adv Exp Med Biol **694**: 108-125.

Ma, Q. (2010). "Transcriptional responses to oxidative stress: pathological and toxicological implications." Pharmacol Ther **125**(3): 376-393.

Marroquin, L. D., J. Hynes, J. A. Dykens, J. D. Jamieson and Y. Will (2007). "Circumventing the Crabtree effect: replacing media glucose with galactose increases susceptibility of HepG2 cells to mitochondrial toxicants." Toxicol Sci **97**(2): 539-547.

Martinez, M. A., A. Rincon, L. R. Desviat, B. Merinero, M. Ugarte and B. Perez (2005). "Genetic analysis of three genes causing isolated methylmalonic acidemia: identification of 21 novel allelic variants." Mol Genet Metab **84**(4): 317-325.

Martins, A. M. (1999). "Inborn errors of metabolism: a clinical overview." Sao Paulo Med J **117**(6): 251-265.

Maurice, M., P. Mera, K. Park, T.C. Brunold, J.C. Escalante-Semerena and I. Rayment (2008). "Structural characterization of a human-type corrinoid adenosyltransferase confirms that coenzyme B_{12} is synthesized through a four-coordinate intermediate." Biochemistry **47**: 5755-5766.

Meili, D., J. Kralovicova, J. Zagalak, L. Bonafe, L. Fiori, N. Blau, B. Thony and I. Vorechovsky (2009). "Disease-causing mutations improving the branch site and polypyrimidine tract: pseudoexon activation of LINE-2 and antisense Alu lacking the poly(T)-tail." Hum Mutat **30**(5): 823-831.

Mera, P. E. and J. C. Escalante-Semerena (2010). "Multiple roles of ATP:cob(I)alamin adenosyltransferases in the conversion of B_{12} to coenzyme B12." Appl Microbiol Biotechnol **88**(1): 41-48.

Merinero, B., B. Perez, C. Perez-Cerda, A. Rincon, L. R. Desviat, M. A. Martinez, P. R. Sala, M. J. Garcia, L. Aldamiz-Echevarria, J. Campos, V. Cornejo, M. Del Toro, A. Mahfoud, M. Martinez-Pardo, R. Parini, C. Pedron, L. Pena-Quintana, M. Perez, M. Pourfarzam and M. Ugarte (2008). "Methylmalonic acidaemia: examination of genotype and biochemical data in 32 patients belonging to mut, cblA or cblB complementation group." J Inherit Metab Dis **31**(1): 55-66.

Miousse, I. R., D. Watkins, D. Coelho, T. Rupar, E. A. Crombez, E. Vilain, J. A. Bernstein, T. Cowan, C. Lee-Messer, G. M. Enns, B. Fowler and D. S. Rosenblatt (2009). "Clinical and molecular heterogeneity in patients with the cblD inborn error of cobalamin metabolism." J Pediatr **154**(4): 551-556.

Mirandola, S. R., D. R. Melo, P. F. Schuck, G. C. Ferreira, M. Wajner and R. F. Castilho (2008). "Methylmalonate inhibits succinate-supported oxygen consumption by interfering with mitochondrial succinate uptake." J Inherit Metab Dis **31**(1): 44-54.

Miyazaki, T., T. Ohura, M. Kobayashi, Y. Shigematsu, S. Yamaguchi, Y. Suzuki, I. Hata, Y. Aoki, X. Yang, C. Minjares, I. Haruta, H. Uto, Y. Ito and U. Muller (2001). "Fatal propionic acidemia in mice lacking propionyl-CoA carboxylase and its rescue by postnatal, liver-specific supplementation via a transgene." J Biol Chem **276**(38): 35995-35999.

Morse, R., A. G. Todd and P. J. Young (2012). "Using mini-genes to identify factors that modulate alternative splicing." Methods Mol Biol **867**: 349-362.

Morcos, P. A. (2001). "Achieving efficient delivery of morpholino oligos in cultured cells." Genesis **30**(3): 94-102.

Morcos, P. A. (2007). "Achieving targeted and quantifiable alteration of mRNA splicing with Morpholino oligos." Biochem Biophys Res Commun **358**(2): 521-527.

Morcos, P. A., Y. Li and S. Jiang (2008). "Vivo-Morpholinos: a non-peptide transporter delivers Morpholinos into a wide array of mouse tissues." Biotechniques **45**(6): 613-614, 616, 618 passim.

Morel, C.F., D. Watkins, P. Scott, P. Rinaldo, D.S. Rosenblatt (2005). "Prenatal diagnosis for methylmalonic acidemia and inborn errors of vitamin B12 metabolism and transport." Mol Genet Metab **86**(1-2): 160-71.

Moschos, S. A., M. Frick, B. Taylor, P. Turnpenny, H. Graves, K. G. Spink, K. Brady, D. Lamb, D. Collins, T. D. Rockel, M. Weber, O. Lazari, L. Perez-Tosar, S. A. Fancy, C. Lapthorn, M. X. Green, S. Evans, M. Selby, G. Jones, L. Jones, S. Kearney, H. Mechiche, D. Gikunju, R. Subramanian, E. Uhlmann, M. Jurk, J. Vollmer, G. Ciaramella and M. Yeadon (2011). "Uptake, efficacy, and systemic distribution of naked, inhaled short interfering RNA (siRNA) and locked nucleic acid (LNA) antisense." Mol Ther **19**(12): 2163-2168.

Moulton, J. D. and S. Jiang (2009). "Gene knockdowns in adult animals: PPMOs and vivo-morpholinos." Molecules **14**(3): 1304-1323.

Muntau, A. C. and S. W. Gersting (2010). "Phenylketonuria as a model for protein misfolding diseases and for the development of next generation orphan drugs for patients with inborn errors of metabolism." J Inherit Metab Dis **33**(6): 649-658.

Nar, H., R. Huber, C. W. Heizmann, B. Thony and D. Burgisser (1994). "Three-dimensional structure of 6-pyruvoyl tetrahydropterin synthase, an enzyme involved in tetrahydrobiopterin biosynthesis." EMBO J **13**(6): 1255-1262.

O'Connor, T. P. and R. G. Crystal (2006). "Genetic medicines: treatment strategies for hereditary disorders." Nat Rev Genet **7**(4): 261-276.

Obad, S., C. O. dos Santos, A. Petri, M. Heidenblad, O. Broom, C. Ruse, C. Fu, M. Lindow, J. Stenvang, E. M. Straarup, H. F. Hansen, T. Koch, D. Pappin, G. J. Hannon and S. Kauppinen (2011). "Silencing of microRNA families by seed-targeting tiny LNAs." Nat Genet **43**(4): 371-378.

Ohura, T., M. Ogasawara, H. Ikeda, K. Narisawa and K. Tada (1993). "The molecular defect in propionic acidemia: exon skipping caused by an 8-bp deletion from an intron in the PCCB allele." Hum Genet **92**(4): 397-402.

Ohura, T., K. Narisawa and K. Tada (1993). "Propionic acidaemia: sequence analysis of mutant mRNAs from Japanese beta subunit-deficient patients." J Inherit Metab Dis **16**(5): 863-867.

Oppliger T., B. Thony, H. Nar, D. Burgisser, R. Huber, C.W. Heizmann and N. Blau (1995). “Structural and functional consequences of mutations in 6-pyruvoyltetrahydropterin synthase causing hyperphenylalaninemia in humans. Phosphorylation is a requirement for in vivo activity.” J Biol Chem **270**(49): 29498-506.

Pandya-Jones, A. (2011). "Pre-mRNA splicing during transcription in the mammalian system." Wiley Interdiscip Rev RNA **2**(5): 700-717.

Padovani, D. and R. Banerjee (2009). "A rotary mechanism for coenzyme B(12) synthesis by adenosyltransferase." Biochemistry **48**(23): 5350-5357.

Padovani, D. and R. Banerjee (2009). "A G-protein editor gates coenzyme B12 loading and is corrupted in methylmalonic aciduria." Proc Natl Acad Sci U S A **106**(51): 21567-21572.

Pampols, T. (2010). "Inherited metabolic rare disease." Adv Exp Med Biol **686**: 397-431.

Parenti, G. (2009). "Treating lysosomal storage diseases with pharmacological chaperones: from concept to clinics." EMBO Mol Med **1**(5): 268-279.

Perez-Cerda, C., B. Perez, B. Merinero, L. R. Desviat, P. Rodriguez-Pombo and M. Ugarte (2004). "Prenatal diagnosis of propionic acidemia." Prenat Diagn **24**(12): 962-964.

Perez, B., A. Rincon, A. Jorge-Finnigan, E. Richard, B. Merinero, M. Ugarte and L. R. Desviat (2009). "Pseudoexon exclusion by antisense therapy in methylmalonic aciduria (MMAuria)." Hum Mutat **30**(12): 1676-1682.

Pey, A. L., M. Ying, N. Cremades, A. Velazquez-Campoy, T. Scherer, B. Thony, J. Sancho and A. Martinez (2008). "Identification of pharmacological chaperones as potential therapeutic agents to treat phenylketonuria." J Clin Invest **118**(8): 2858-2867.

Plesa, M., J. Kim, S. G. Paquette, H. Gagnon, C. Ng-Thow-Hing, B. F. Gibbs, M. A. Hancock, D. S. Rosenblatt and J. W. Coulton (2011). "Interaction between MMACHC and MMADHC, two human proteins participating in intracellular vitamin B(1)(2) metabolism." Mol Genet Metab **102**(2): 139-148.

Pieczenik, S. R. and J. Neustadt (2007). "Mitochondrial dysfunction and molecular pathways of disease." Exp Mol Pathol **83**(1): 84-92.

Poulos, M. G., R. Batra, K. Charizanis and M. S. Swanson (2011). "Developments in RNA splicing and disease." Cold Spring Harb Perspect Biol **3**(1): a000778.

Porto, C., M. Cardone, F. Fontana, B. Rossi, M. R. Tuzzi, A. Tarallo, M. V. Barone, G. Andria and G. Parenti (2009). "The pharmacological chaperone N-butyldeoxynojirimycin enhances enzyme replacement therapy in Pompe disease fibroblasts." Mol Ther **17**(6): 964-971.

Pozzoli, U. and M. Sironi (2005). "Silencers regulate both constitutive and alternative splicing events in mammals." Cell Mol Life Sci **62**(14): 1579-1604.

Preiss, M. R. and G. D. Bothun (2011). "Stimuli-responsive liposome-nanoparticle assemblies." Expert Opin Drug Deliv **8**(8): 1025-1040.

Raghuveer, T. S., U. Garg and W. D. Graf (2006). "Inborn errors of metabolism in infancy and early childhood: an update." Am Fam Physician **73**(11): 1981-1990.

Rao, A. N., J. Kavitha, M. Koch and V. Suresh Kumar (2009). "Inborn errors of metabolism: Review and data from a tertiary care center." Indian J Clin Biochem **24**(3): 215-222.

Rasola, A. and P. Bernardi (2011). "Mitochondrial permeability transition in Ca(2+)-dependent apoptosis and necrosis." Cell Calcium **50**(3): 222-233.

Richard, E., A. Alvarez-Barrientos, B. Perez, L. R. Desviat and M. Ugarte (2007). "Methylmalonic acidaemia leads to increased production of reactive oxygen species and induction of apoptosis through the mitochondrial/caspase pathway." J Pathol **213**(4): 453-461.

Richard, E., L. Monteoliva, S. Juarez, B. Perez, L. R. Desviat, M. Ugarte and J. P. Albar (2006). "Quantitative analysis of mitochondrial protein expression in methylmalonic acidemia by two-dimensional difference gel electrophoresis." J Proteome Res **5**(7): 1602-1610.

Richter, K., M. Haslbeck and J. Buchner (2010). "The heat shock response: life on the verge of death." Mol Cell **40**(2): 253-266.

Rincon, A., C. Aguado, L. R. Desviat, R. Sanchez-Alcudia, M. Ugarte and B. Perez (2007). "Propionic and methylmalonic acidemia: antisense therapeutics for intronic variations causing aberrantly spliced messenger RNA." Am J Hum Genet **81**(6): 1262-1270.

Rodrigues, J. V., B. J. Henriques, T. G. Lucas and C. M. Gomes (2012). "Cofactors and metabolites as protein folding helpers in metabolic diseases." Curr Top Med Chem **12**(22): 2546-2559.

Rodriguez-Pombo, P., J. Hoenicka, S. Muro, B. Perez, C. Perez-Cerda, E. Richard, L. R. Desviat and M. Ugarte (1998). "Human propionyl-CoA carboxylase beta subunit gene: exon-intron definition and mutation spectrum in Spanish and Latin American propionic acidemia patients." Am J Hum Genet **63**(2): 360-369.

Rozen, S. and H. Skaletsky (2000). "Primer3 on the WWW for general users and for biologist programmers." Methods Mol Biol **132**: 365-386.

Sanger, F., S. Nicklen and A. R. Coulson (1977). "DNA sequencing with chain-terminating inhibitors." Proc Natl Acad Sci U S A **74**(12): 5463-5467.

Sanchez-Alcudia, R., B. Perez, C. Perez-Cerda, M. Ugarte and L. R. Desviat (2011). "Overexpression of adapted U1snRNA in patients' cells to correct a 5' splice site mutation in propionic acidemia." Mol Genet Metab **102**(2): 134-138.

Saonere J. A. (2011). "Antisense therapy, a magic bullet for the treatment of various diseases: Present and future prospects." J Med Genet Genomics **3**(5): 77-83.

Saridakis, V., A. Yakunin, X. Xu, P. Anandakumar, M. Pennycooke, J. Gu, F. Cheung, J. M. Lew, R. Sanishvili, A. Joachimiak, C. H. Arrowsmith, D. Christendat and A. M. Edwards (2004). "The structural basis for methylmalonic aciduria. The crystal structure of archaeal ATP:cobalamin adenosyltransferase." J Biol Chem **279**(22): 23646-23653.

Saudubray, J. M., F. Sedel and J. H. Walter (2006a). "Clinical approach to treatable inborn metabolic diseases: an introduction." J Inherit Metab Dis **29**(2-3): 261-274.

Saudubray, J. M., I. Desguerre, F. Sedel and C. Charpentier (2006b). "A Clinical Approach to Inherited Metabolic Diseases" In Fernandes J., Saudubray J. M., van den Berghe G. and Walter J., editors. Inborn Metabolis Diseases: Diagnosis and Treatment. 4th ed. Germany: Springer. p. 5-47.

Schapira, A. H. (2012). "Mitochondrial diseases." Lancet **379**(9828): 1825-1834.

Schapira, A. H. (2012). "Targeting mitochondria for neuroprotection in Parkinson's disease." Antioxid Redox Signal **16**(9): 965-973.

Scheinfeld, N., E. Jones. Tetrahydrobiopterin Deficiency. eMedicine Pediatrics: Genetics and Metabolism [Internet]. [Updated 2010 Aug 9; cited 2013 Apr 23]; Available from: http://emedicine.medscape.com/article/949470-print.

Seashore MR. (2009). "The Organic Acidemias: An Overview." In Pagon RA, Adam MP, Bird TD, Dolan CR, Fong CT, Stephens K, editors. GeneReviews™ [Internet]. Seattle (WA): University of Washington, Seattle; 1993-2013. 2001 Jun 27 [updated 2009 Dec 22].

Schmidt, S. P., T. J. Corydon, C. B. Pedersen, P. Bross and N. Gregersen (2010). "Misfolding of short-chain acyl-CoA dehydrogenase leads to mitochondrial fission and oxidative stress." Mol Genet Metab **100**(2): 155-162.

Schmidt, S. P., T. J. Corydon, C. B. Pedersen, S. Vang, J. Palmfeldt, V. Stenbroen, R. J. Wanders, J. P. Ruiter and N. Gregersen (2011). "Toxic response caused by a misfolding variant of the mitochondrial protein short-chain acyl-CoA dehydrogenase." J Inherit Metab Dis **34**(2): 465-475.

Schubert, H. L. and C. P. Hill (2006). "Structure of ATP-bound human ATP:cobalamin adenosyltransferase." Biochemistry **45**(51): 15188-15196.

Schwab, M. A., S. W. Sauer, J. G. Okun, L. G. Nijtmans, R. J. Rodenburg, L. P. van den Heuvel, S. Drose, U. Brandt, G. F. Hoffmann, H. Ter Laak, S. Kolker and J. A. Smeitink (2006). "Secondary mitochondrial dysfunction in propionic aciduria: a pathogenic role for endogenous mitochondrial toxins." Biochem J **398**(1): 107-112.

Schwartz, I. V., C. F. Souza and R. Giugliani (2008). "Treatment of inborn errors of metabolism." J Pediatr (Rio J) **84**(4 Suppl): S8-19.

Siemen, D. and M. Ziemer (2013). "What is the nature of the mitochondrial permeability transition pore and what is it not?" IUBMB Life **65**(3): 255-262.

Sloman, K. A. and P. L. McNeil (2012). "Using physiology and behaviour to understand the responses of fish early life stages to toxicants." J Fish Biol **81**(7): 2175-2198.

Soifer, H. S., T. Koch, J. Lai, B. Hansen, A. Hoeg, H. Oerum and C. A. Stein (2012). "Silencing of gene expression by gymnotic delivery of antisense oligonucleotides." Methods Mol Biol **815**: 333-346.

Sorek, R. (2007). "The birth of new exons: mechanisms and evolutionary consequences." RNA **13**(10): 1603-1608.

Stankovics, J. and F. D. Ledley (1993). "Cloning of functional alpha propionyl CoA carboxylase and correction of enzyme deficiency in pccA fibroblasts." Am J Hum Genet **52**(1): 144-151.

Stefan Kolker, M. S., Friederike Horster, Sven Sauer, Angela Hinz, Nicole I. Wolf, Ertan Mayatepek, Georg F. Hoffmann, Jan A.M. Smeitink, and Jurgen G. Okun (2003). "Methylmalonic acid, a biochemical hallmark of methylmalonic acidurias but no inhibitor of mitochondrial respiratory chain." The journal of biological chemistry **278**(48): 47388-47393.

Stein, C. A., J. B. Hansen, J. Lai, S. Wu, A. Voskresenskiy, A. Hog, J. Worm, M. Hedtjarn, N. Souleimanian, P. Miller, H. S. Soifer, D. Castanotto, L. Benimetskaya, H. Orum and T. Koch (2010). "Efficient gene silencing by delivery of locked nucleic acid antisense oligonucleotides, unassisted by transfection reagents." Nucleic Acids Res **38**(1): e3.

Stuart, R. A., D. M. Cyr and W. Neupert (1994). "Hsp70 in mitochondrial biogenesis: from chaperoning nascent polypeptide chains to facilitation of protein degradation." Experientia **50**(11-12): 1002-1011.

Stuart, R. A., D. M. Cyr, E. A. Craig and W. Neupert (1994). "Mitochondrial molecular chaperones: their role in protein translocation." Trends Biochem Sci **19**(2): 87-92.

Stucki, M., D. Coelho, T. Suormala, P. Burda, B. Fowler and M. R. Baumgartner (2012). "Molecular mechanisms leading to three different phenotypes in the cblD defect of intracellular cobalamin metabolism." Hum Mol Genet **21**(6): 1410-1418.

Summerton, J. E. (2007). "Morpholino, siRNA, and S-DNA compared: impact of structure and mechanism of action on off-target effects and sequence specificity." Curr Top Med Chem **7**(7): 651-660.

Summerton, J. and D. Weller (1997). "Morpholino antisense oligomers: design, preparation, and properties." Antisense Nucleic Acid Drug Dev **7**(3): 187-195.

Suormala, T., M. R. Baumgartner, D. Coelho, P. Zavadakova, V. Kozich, H. G. Koch, M. Berghauser, J. E. Wraith, A. Burlina, A. Sewell, J. Herwig and B. Fowler (2004). "The cblD defect causes either isolated or combined deficiency of methylcobalamin and adenosylcobalamin synthesis." J Biol Chem **279**(41): 42742-42749.

Shutt, T., M. Geoffrion, R. Milne and H. M. McBride (2012). "The intracellular redox state is a core determinant of mitochondrial fusion." EMBO Rep **13**(10): 909-915.

Tahara, T., J. P. Kraus and L. E. Rosenberg (1990). "An unusual insertion/deletion in the gene encoding the beta-subunit of propionyl-CoA carboxylase is a frequent mutation in Caucasian propionic acidemia." Proc Natl Acad Sci U S A **87**(4): 1372-1376.

Takahashi-Iniguez, T., E. Garcia-Hernandez, R. Arreguin-Espinosa and M. E. Flores (2012). "Role of vitamin B12 on methylmalonyl-CoA mutase activity." J Zhejiang Univ Sci B **13**(6): 423-437.

Thoma, N. H. and P. F. Leadlay (1996). "Homology modeling of human methylmalonyl-CoA mutase: a structural basis for point mutations causing methylmalonic aciduria." Protein Sci **5**(9): 1922-1927.

Thony, B. and N. Blau (2006). "Mutations in the BH4-metabolizing genes GTP cyclohydrolase I, 6-pyruvoyl-tetrahydropterin synthase, sepiapterin reductase, carbinolamine-4a-dehydratase, and dihydropteridine reductase." Hum Mutat **27**(9): 870-878.

Thony, B., W. Leimbacher, D. Burgisser and C. W. Heizmann (1992). "Human 6-pyruvoyltetrahydropterin synthase: cDNA cloning and heterologous expression of the recombinant enzyme." Biochem Biophys Res Commun **189**(3): 1437-1443.

Vaseva, A. V., N. D. Marchenko, K. Ji, S. E. Tsirka, S. Holzmann and U. M. Moll (2012). "p53 opens the mitochondrial permeability transition pore to trigger necrosis." Cell **149**(7): 1536-1548.

Veedu, R. N. and J. Wengel (2009). "Locked nucleic acid as a novel class of therapeutic agents." RNA Biol **6**(3): 321-323.

Vorechovsky, I. (2010). "Transposable elements in disease-associated cryptic exons." Hum Genet **127**(2): 135-154.

Wajner, M. and S. I. Goodman (2011). "Disruption of mitochondrial homeostasis in organic acidurias: insights from human and animal studies." J Bioenerg Biomembr **43**(1): 31-38.

Ward, A. J. and T. A. Cooper (2010). "The pathobiology of splicing." J Pathol **220**(2): 152-163.

Werner, E. R., N. Blau and B. Thony (2011). "Tetrahydrobiopterin: biochemistry and pathophysiology." Biochem J **438**(3): 397-414.

Werner, E. R., G. Werner-Felmayer and H. Wachter (1996). "High-performance liquid chromatographic methods for the quantification of tetrahydrobiopterin biosynthetic enzymes." J Chromatogr B Biomed Appl **684**(1-2): 51-58.

Will, C. L. and R. Luhrmann (2011). "Spliceosome structure and function." Cold Spring Harb Perspect Biol **3**(7).

Wood, M. J., M. J. Gait and H. Yin (2010). "RNA-targeted splice-correction therapy for neuromuscular disease." Brain **133**(Pt 4): 957-972.

Wong R., C. Steenbergen, E. Murphy (2012). “Mitochondrial permeability transition pore and calcium handling.” Methods Mol Biol **810**: 235-42.

Worgan, L. C., K. Niles, J. C. Tirone, A. Hofmann, A. Verner, A. Sammak, T. Kucic, P. Lepage and D. S. Rosenblatt (2006). "Spectrum of mutations in mut methylmalonic acidemia and identification of a common Hispanic mutation and haplotype." Hum Mutat **27**(1): 31-43.

Yamanishi, M., M. Vlasie and R. Banerjee (2005). "Adenosyltransferase: an enzyme and an escort for coenzyme B12?" Trends Biochem Sci **30**(6): 304-308.

Youle, R. J. and A. M. van der Bliek (2012). "Mitochondrial fission, fusion, and stress." Science **337**(6098): 1062-1065.

Zhang, J., X. Wu, D. Padovani, H. L. Schubert and R. A. Gravel (2009). "Ligand-binding by catalytically inactive mutants of the cblB complementation group defective in human ATP:cob(I)alamin adenosyltransferase." Mol Genet Metab **98**(3): 278-284.

Zhuang, Y. and A. M. Weiner (1986). "A compensatory base change in U1 snRNA suppresses a 5' splice site mutation." Cell **46**(6): 827-835.

PAPERS

Part of this work is presented in the following scientific publications:

1. **Brasil S**, Richard E, Jorge-Finnigan A, Leal F, Merinero B, Banerjee R, Desviat LR, Ugarte M, Pérez B. (2013), Mitochondrial dysfunction studies in families with discordant phenotypes of methylmalonic aciduria *cblB* type, (submitted).

2. Jorge-Finnigan A*, **Brasil S***, Underhaug J, Ruíz-Sala P, Merinero B, Banerjee R, Desviat LR, Ugarte M, Martinez A, Pérez B. (2013), Pharmacological chaperones as a potential therapeutic option in methylmalonic aciduria cblB type, Hum Mol Genet [Epub ahead of print] $IF_{(2013)}$ = 7.692 (* both authors contributed equally to this work)

3. **Brasil S**, Viecelli HM, Meili D, Rassi A, Desviat LR, Pérez B, Ugarte M, Thöny B. (2011), Pseudoexon exclusion by antisense therapy in 6-pyruvoyl-tetrahydropterin synthase deficiency, Hum.Mutation **32**(9):1019-1027. $IF_{(2011)}$ = 5.686

HMG Advance Access published May 30, 2013

Human Molecular Genetics, 2013 ***1–10***
doi:10.1093/hmg/ddt217

Pharmacological chaperones as a potential therapeutic option in methylmalonic aciduria cblB type

Ana Jorge-Finnigan[1,2,†], Sandra Brasil[1,3,†], Jarl Underhaug[2], Pedro Ruíz-Sala[1], Begoña Merinero[1], Ruma Banerjee[4], Lourdes R. Desviat[1], Magdalena Ugarte[1], Aurora Martinez[2,*] and Belén Pérez[1,*]

[1]Centro de Diagnóstico de Enfermedades Moleculares, Centro de Biología Molecular-SO, UAM-CSIC, Universidad Autónoma de Madrid, Campus de Cantoblanco, 28049 Madrid/Centro de Investigación Biomédica en Red de Enfermedades Raras (CIBERER), IDIPAZ, Madrid, Spain [2]Department of Biomedicine, University of Bergen, Norway [3]Metabolism & Genetics Group, Research Institute for Medicines and Pharmaceuticals Sciences (iMed.UL), Faculty of Pharmacy, University of Lisbon, Portugal [4]Department of Biological Chemistry, University of Michigan Medical Center, Ann Arbor, MI, USA

Received February 8, 2013; Revised April 15, 2013; Accepted May 8, 2013

Methylmalonic aciduria (MMA) *cblB* type is caused by mutations in the *MMAB* gene. This encodes the enzyme ATP:cob(I)alamin adenosyltransferase (ATR), which converts reduced cob(I)alamin to an active adenosylcobalamin cofactor. We recently reported the presence of destabilizing pathogenic mutations that retain some residual ATR activity. The aim of the present study was to seek pharmacological chaperones as a tailored therapy for stabilizing the ATR protein. High-throughput ligand screening of over 2000 compounds was performed; six were found to enhance the thermal stability of purified recombinant ATR. Further studies using a well-established bacterial system in which the recombinant ATR protein was expressed in the presence of these six compounds, showed them all to increase the stability of the wild-type ATR and the p.Ile96Thr mutant proteins. Compound V (*N*-{[(4-chlorophenyl)carbamothioyl]amino}-2-phenylacetamide) significantly increased this stability and did not act as an inhibitor of the purified protein. Importantly, compound V increased the activity of ATR in patient-derived fibroblasts harboring the destabilizing p.Ile96Thr mutation in a hemizygous state to within control range. When cobalamin was coadministrated with compound V, mutant ATR activity further improved. Oral administration of low doses of compound V to C57BL/6J mice for 12 days, led to increase in steady-state levels of ATR protein in liver and brain (disease-relevant organs). These results hold promise for the clinical use of pharmacological chaperones in MMA *cblB* type patients harboring chaperone-responsive mutations.

INTRODUCTION

Cobalamin, or vitamin B_{12}, is an essential micronutrient that mammals must obtain from their diet. It is then processed via a complex pathway for the biosynthesis of methylcobalamin and adenosylcobalamin (AdoCbl), which, respectively, serve as cofactors of the cytosolic enzyme methionine synthase (MS, EC_2.1.1.13) and the mitochondrial enzyme methylmalonyl-CoA mutase (MUT, EC_5.4.99.2). The study of inborn defects of cobalamin metabolism has revealed nine complementation groups: *cblA to cblJ* and *mut* (1–4). In particular, defects in the mitochondrial enzyme methylmalonyl-CoA mutase (*mut* group) or in the synthesis of the AdoCbl cofactor (complementation groups *cblA*, *cblB* or *cblD variant2*) lead to isolated methylmalonic aciduria (MMA, MIM 251 000) (5).

The synthesis and transfer of AdoCbl to MUT involves three proteins, ATP:adenosylcobalamin transferase (ATR, EC_2.5.1.17), the *cblA* protein and the *cblD* protein (5–7). ATR is a homotrimer encoded by the *MMAB* gene (8,9). MUT is responsible for the isomerization of L-methylmalonyl-CoA into succinyl-CoA, which can enter the Krebs cycle, and MMA *cblB* type is caused by mutations in the gene encoding ATR (10).

MMA *cblB* patients suffer either a severe early-onset form of the disease, with neonatal ketoacidosis, lethargy, failure to thrive

*To whom correspondence should be addressed. E-mail: bperez@cbm.uam.es (B.P.); Aurora.Martinez@biomed.uib.no (A.M.)
†These authors contributed equally to this work.

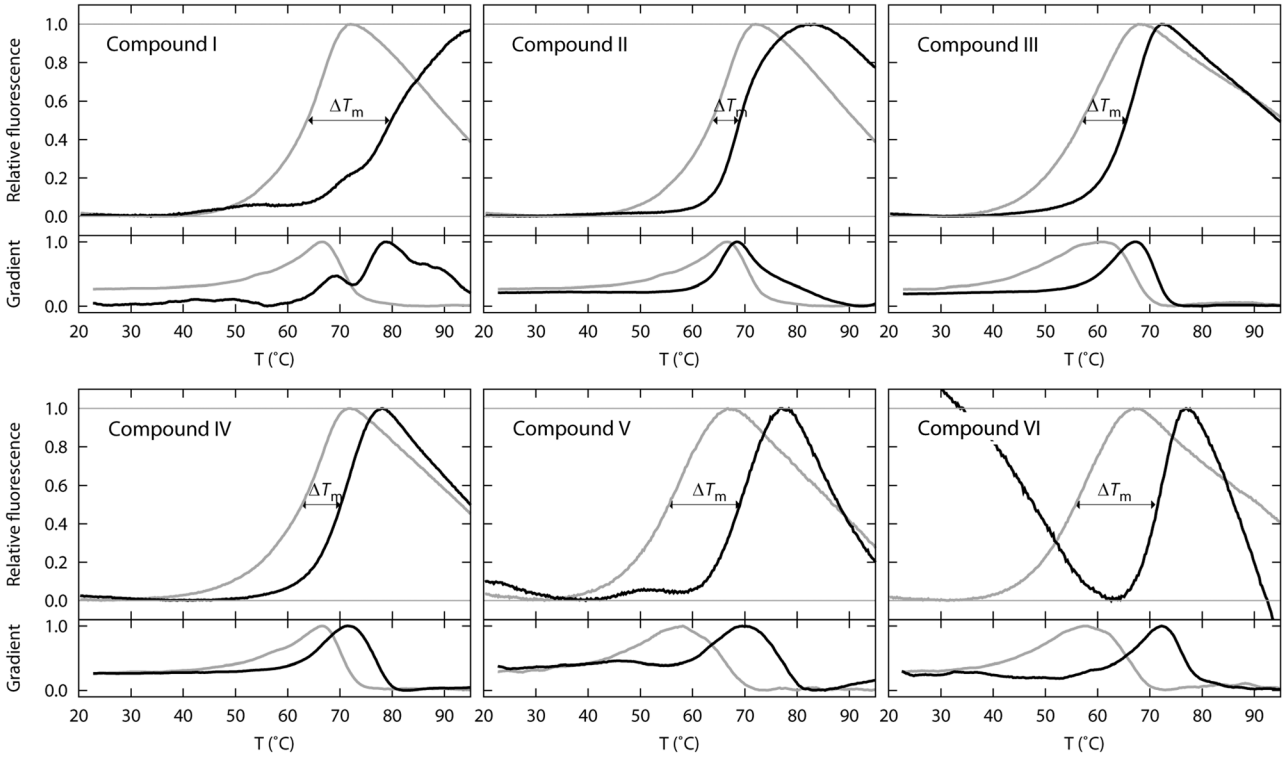

Figure 1. Differential scanning fluorimetry profiles for six candidate pharmacological chaperones. Thermal denaturation profiles of purified wild-type ATR (0.086 mg/ml) (fluorescence at 610 nm vs. temperature [°C]). In grey, curve for ATR incubated with DMSO (final concentration 2%); in black, purified ATR incubated with 0.04 mg/ml of compounds I–VI. The melting temperature (T_m) was taken as the temperature at which the maximum fluorescence was achieved; ΔT_m was calculated as the difference between the T_m in the presence of a ligand and T_m in the presence of DMSO. The lower figure for each graph represents the data without scaling.

and encephalopathy, or a milder late-onset form usually diagnosed during infancy that has a less serious neurological outcome. While there is currently no cure for the disease, therapeutic options, including the dietary restriction of substrates, aim to reduce methylmalonic acid production and improve the clinical outcome. Pharmacological cobalamin supplementation is part of the usual treatment, although only 40% of patients show any biochemical response to it, and in many cases neurological manifestations persist. In those that do respond, significant improvements in clinical condition, growth and metabolic variables have been reported, although the levels of toxic metabolites never normalize (1).

Efforts are now being directed towards exploring alternative therapies based on identifying new targets in the context of personalized medicine. Understanding the molecular mechanisms of pathogenesis underlying genetic defects can help guide the design and development of new therapeutic approaches. Several studies have shown that many human diseases are caused by loss-of-function mutations that impair the correct folding of affected proteins (11–13). Over the past decade, pharmacological chaperones have emerged as novel therapeutic tools for rescuing misfolded proteins by stimulating and preserving their correct folding (14,15). Pharmacological chaperones are small, cell-permeable molecules that specifically bind and stabilize target proteins. Pharmacological chaperones have been investigated as a potential treatment for many genetic disorders that result from misfolded and/or unstable proteins, and proof-of-concept studies have been described for several human diseases such as lysosomal disorders, phenylketonuria and cystic fibrosis (12,16–19).

In a previous study, we reported the characterization of two mutations in the *MMAB* gene, p.Ile96Thr and p.Arg191Trp, both of which are associated with reduced ATR stability and residual activity (20). The aim of the present work was to identify compounds with pharmacological chaperone potential for ATR. We demonstrate that *N*-{[(4-chlorophenyl)carbamothioyl] amino}-2-phenylacetamide, here after referred to as compound V, enhanced the stability of wild-type and p.Ile96Thr mutant ATR. It also increased the residual activity of ATR in patient-derived fibroblasts harboring the latter mutation. The effect of compound V on the stabilization of recombinant wild-type and mutant ATR both as isolated recombinant protein and in patient-derived fibroblasts is further increased when tested simultaneously with cobalamin. Finally, oral loading of compound V in wild-type mice resulted in an increase in ATR stability in the liver and brain (disease-relevant organs).

RESULTS

High-throughput screening for pharmacological chaperones

A subset of 2000 compounds from the MyriaScreen Diversity Collection was screened by differential scanning fluorimetry (DSF). Data analysis revealed a group of six compounds that shifted the T_m of ATR between 6.0 and 17°C. These six compounds (I–VI) were selected for further studies (Figs 1 and 2).

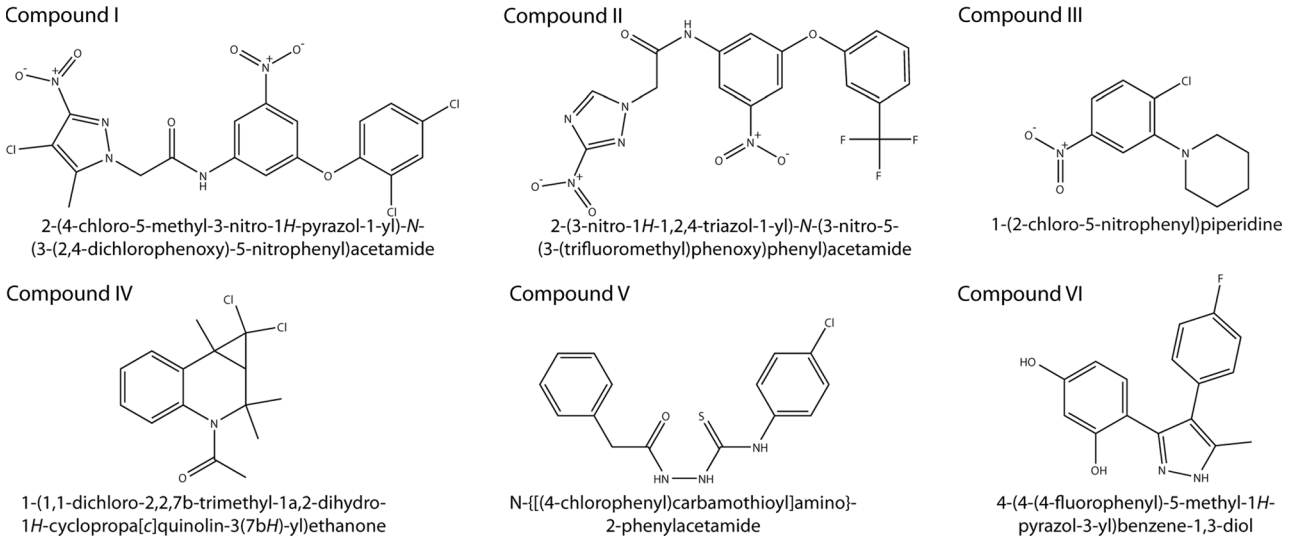

Figure 2. Chemical structures and IUPAC names of the selected compounds. Six compounds, named I to VI, were found to stabilize ATR protein in a high-throughput screening of 2000 compounds.

Table 1. Thermal stabilization in the presence of compounds I–VI from DSF screening, and relative stability of wild-type and p.Ile96Thr ATR in the presence of compounds as measured by quantitative immunoblotting[a]

	ΔT_m (°C)	Wild-type 40 μM	80 μM	p.Ile96Thr 40 μM	80 μM
DMSO[b]	—	1.0	1.0	1.0	1.0
Compound I	16.1	1.8 ± 0.4 (*)	1.6 ± 1.2	0.8 ± 0.3	2.3 ± 1.3
Compound II	5.4	2 ± 1	ND	1.3 ± 0.1	ND
Compound III	8.5	0.7	0.9 ± 0.4	1.9 ± 0.5	2.1 ± 0.6(**)
Compound IV	7.4	1.0 ± 0.2	3.4 ± 0.4(****)	2.0 ± 0.6	2.2 ± 0.1(***)
Compound V	13.6	ND	1.4 ± 1.0	1.6 ± 1.2	**3 ± 1** (**)
Compound VI	15.7	4 ± 2 (*)	**6.2 ± 0.5**(****)	2.1 ± 0.1 (****)	1.7 ± 0.2(**)

Bold figures highlight the most important effect of compounds V and VI.
ND, not determined.
[a]Data obtained with bacterial extracts prepared from cultures grown in the presence of 40 or 80 μM of compounds I–VI, as described in Materials and Methods.
[b]Data represent the mean ± SD of at least two independent determinations. In all cases the appropriate DMSO control was used and taken as the reference value (stability = 1) for the bacterial cultures grown in the presence of the compounds.
*$P < 0.05$.
**$P < 0.01$.
***$P < 0.005$.
****$P < 0.001$.

ATR stability and activity in the presence of hit compounds

To determine whether compounds I–VI acted as pharmacological chaperones, their effect on the stability of wild-type ATR and the p.IleI96Thr mutant was studied. Table 1 summarizes the quantification of ATR by western blot analysis of the bacterial lysates grown in the presence of the potential chaperones. Compounds I–VI increased or tended to increase the steady-state levels of expressed wild-type and/or mutant ATR (Table 1) indicating an increase in ATR stability. Compound V (80 μM) had the largest effect on the mutant (Table 1). Compound VI was the most effective in stabilizing the wild-type type ATR (Table 1). Based on these results, compounds V and VI were selected for further studies.

The effect of compounds V and VI was then analyzed by measuring the activity of the lysates of bacterial cultures expressing wild-type and mutants (p.Ile96Thr and p.Arg191Trp), grown in the presence of 100 μM compounds. While no effect could be observed for compound VI, in either wild-type or mutant extracts, the activity in the lysates of bacterial cultures grown with compound V increased 1.5-fold for wild-type and 8-fold for the destabilizing mutation p.Ile96Thr. For the p.Arg191Trp mutant, which is also unstable, no quantifiable enzyme activity could be measured in the lysates of cultures grown without compound V, but some activity could be detected in its presence (data not shown).

A clear stabilizing effect of the p.Ile96Thr by compound V was observed in the time-dependent quantification of mutant

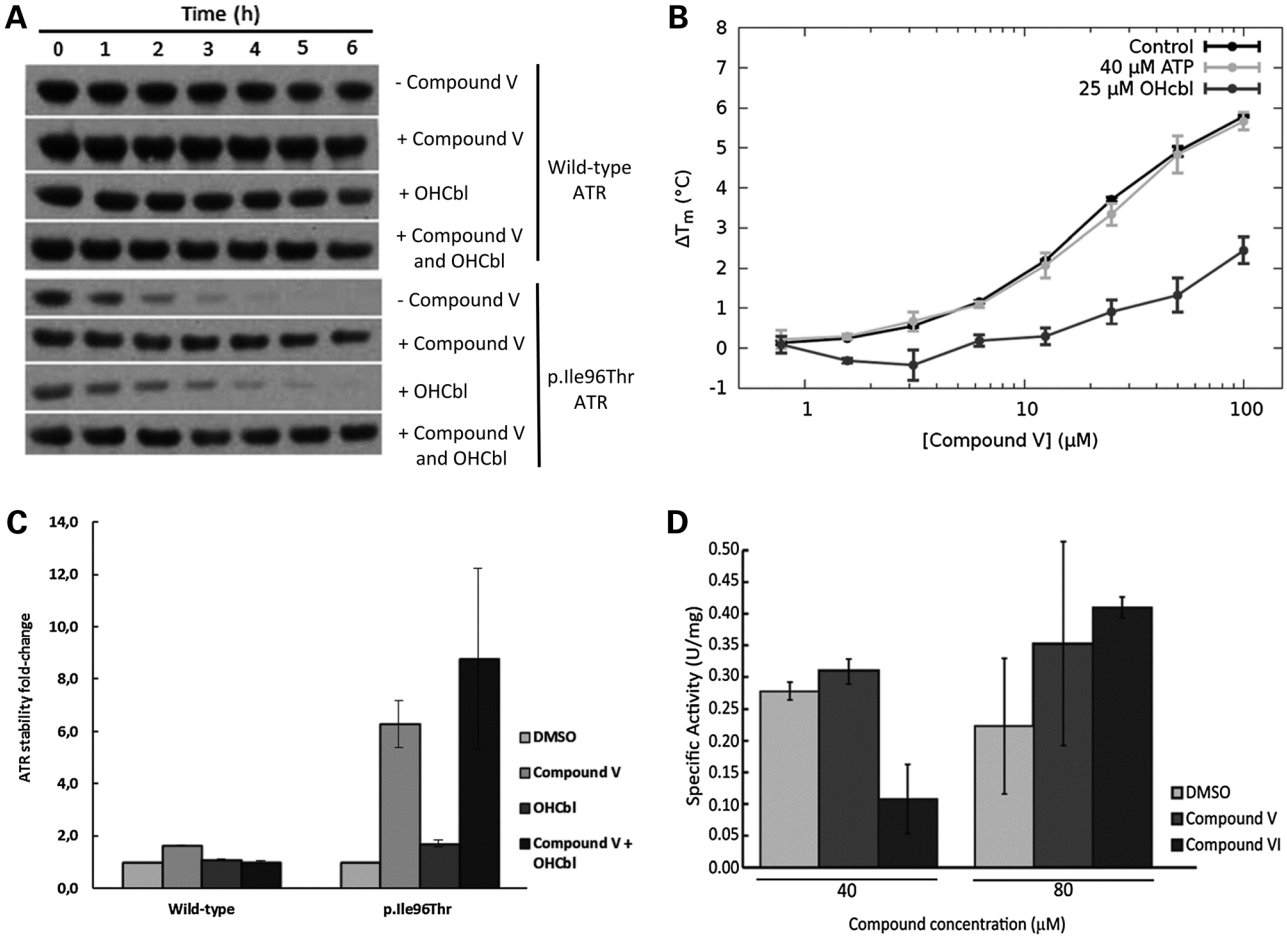

Figure 3. Effect of compounds V, VI and cobalamin on ATR stability and activity. (**A**) Effect of compound V on p.Ile96Thr ATR protein stability**.** Bacteria expressing wild-type or p.Ile96Thr mutant ATR were incubated with 80 μM compound V (final DMSO concentration 0.2%) or the equivalent amount of the vehicle (0.2% DMSO) or with 1 μg/ml (0.7 μM) of OHCbl or both. Crude cell extracts from cultures expressing wild-type or p.Ile96Thr ATR were incubated at 37°C, and aliquots were removed at different times. The aliquots were loaded onto SDS–PAGE gels and the protein was immunodetected by western blotting. Proteins were quantified by laser densitometry as the percentage density of each protein relative to its density at time 0. Compound-treated samples were compared with the DMSO-treated sample. (**B**) Quantification of the effect of compound V and/or OHCbl on stability of wild-type ATR and mutant p.Ile96Thr ATR. (**C**) Concentration-dependent stabilization of ATR by compound V and effect of OHCbl and ATP. The stabilization of ATR in the presence of compound V (0–200 μM) in the absence of OHcbl (black solid line, circles) and in the presence of OHCbl at 3 μM (dark grey solid line, triangles) and 12 μM (light grey solid line, squares) or 40 μM ATP (dotted line, squares). See main text for estimated K_d values for compound V binding. (**D**) Specific activity was measured using purified wild-type ATR from bacteria with 40 or 80 μM of either compound V or VI or the equivalent volume of DMSO (final DMSO concentration 0.4 or 0.8%). $^{*}P < 0.05$, $^{**}P < 0.01$.

protein in the bacterial lysates (Fig. 3A and B). Similar time-course experiments were performed with lysates from bacterial cultures grown in the presence of 1 μg/ml (0.7 μM) OHCbl, which did not have any stabilizing effect on the expressed wild-type and only slight on mutant protein (Fig. 3A and B). Interestingly, the combined addition of compound V and OHCbl showed a slightly increased stabilizing effect of the mutant p.Ile96Thr compared with compound V alone (Fig. 3A and B).

The combined effect of compound V and OHCbl was further analyzed using isolated recombinant wild-type ATR protein. We first measured the concentration-dependent thermal stabilization of ATR by OHcbl using DSF. Concentrations up to 25 μM OHCbl did not affect the thermal stability of the protein, and similar unfolding curves as for the controls (shown in Fig. 1) were obtained. But higher concentrations of OHCbl destabilized ATR slightly (1.5°C) and gave poor curves due to quenching of fluorescence. Titration with compound V (0–200 μM) in the absence of OHCbl showed that ATR is thermally stabilized by the compound at concentrations approximately >2 μM (Fig. 3C), and by analyzing the effect of the ligand on the T_m of ATR as described by Cooper and McAuley-Hecht (21), we estimated a $K_d = 7.4 \pm 0.4$ μM for compound V. In the presence of 0.75 μM OHCbl, this K_d was not affected, but higher concentrations of the substrate increased the affinity of compound V ($K_d = 5.4 \pm 0.5$ μM with 3 μM OHCbl and $K_d = 5.5 \pm 0.4$ with 12 μM), resulting in increased stabilization at similar concentrations of the compound (Fig. 3C). Comparatively, ATP, which had a negligible effect on the T_m for ATR denaturation up to 200 μM, did not have any effect on the concentration-dependent stabilization by compound V (Fig. 3C). The affinity of ATR for compound V appears comparable to the apparent K_m values for ATP (6.4 ± 0.4 μM) and 3.7 ± 0.5 μM for cobalamin (22).

Given that pharmacological chaperones can act as enzyme inhibitors if they resemble the natural substrates (23), we tested the effect of compound V on the activity of recombinant ATR. The specific activity of purified recombinant human ATR was 0.23 ± 0.04 U/mg at the standard assay conditions. In the presence of 40 μM of compound V, the activity remained comparable to that of control samples (0.27 ± 0.02 U/mg) (Fig. 3D). Comparatively, with 40 μM of compound VI, another of the initial hit compounds, the specific activity decreased to 0.09 ± 0.05 U/mg, suggesting that compound VI, but not V might be inhibitory. At concentrations of 80 μM, no inhibitory effect was again obtained for compound V (specific activity of 0.30 ± 0.14 U/mg). For compound VI at 80 μM, the inhibition observed at lower concentration appears reversed, suggesting a complex pattern of stability and activity effects for this inhibitory potential pharmacological chaperone.

Given that compound V showed a clear stabilizing effect on wild-type and mutant ATR and did not seem to be inhibitory, it was selected for further testing on cellular and animal models.

Recovery of residual activity in a cellular disease model

The therapeutic potential of compound V was further evaluated by its ability to increase total cellular ATR activity using patient-derived transformed fibroblasts. Its effect at 40 and 80 μM on the propionate oxidation metabolic pathway was assessed using immortalized dermal fibroblasts from a patient bearing the mutations p.Ile96Thr and p.Ser174fs (20) incubated for 48 and 72 h with the compound. [^{14}C]-propionate uptake was quantified as an indirect measurement of ATR activity. Incubation with compound V at 80 μM for 48 h induced a slight increase in the residual activity (data not shown), while 72 h of treatment significantly increased ATR activity (5.4-fold). Indeed, it reached control range levels. An effect due to DMSO was ruled out since residual activity in the presence or absence of DMSO was comparable. In the same way as described earlier, the effect of compound V and OHCbl on the activity and stability of ATR was assessed. According to the results obtained with the patient-derived fibroblasts, OHCbl increased the incorporation of ^{14}C propionate (3.5-fold). ^{14}C propionate incorporation was further stimulated (~17-fold) when compound V and OHCbl (1 μg/ml) were simultaneously present (Fig. 4A). The levels of mitochondrial ATR protein were also slightly increased when both compound V and OHcbl were added (Fig. 4B).

Supplementation with compound V to mice: effect on liver and brain ATR

In addition to *in vitro* and *ex vivo* studies, experiments with whole organisms are pivotal for determining a drug's pharmacokinetics to assess whether it is adequately absorbed, distributed and excreted. To this end, the effect of compound V on the stability of endogenous ATR was examined in a wild-type mouse strain since a *cblB* mouse model is currently unavailable. Two doses (0.25 and 5 mg/kg/day) of compound V were administered orally every day for 12 days. No secondary effects of compound exposure (such as weight loss, automutilation, tumors, abnormal movements, etc.) were observed. The results showed an increase in the amount of immunoquantified ATR at the 5 mg/kg/day dose in liver and brain, two disease-relevant organs (Fig. 5), supporting the stabilizing effect of compound V *in vivo*.

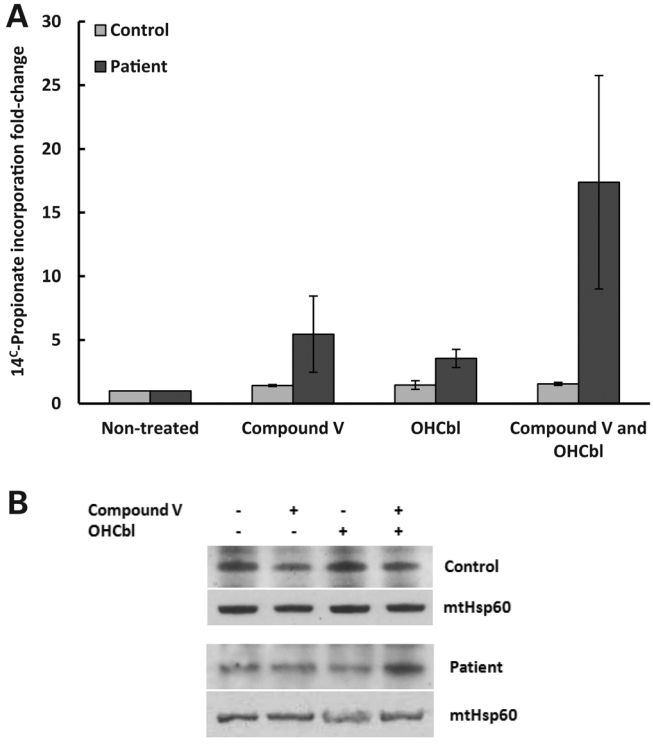

Figure 4. Effect of compound V and cobalamin in a cellular disease model. Immortalized patient (harboring the mutations p.Ile96Thr/p.Ser174fs) and healthy-derived fibroblasts were incubated in the presence of 80 μM of compound V or the equivalent volume of DMSO (0.1 or 0.2%), and in the presence of 1 μg/ml of cobalamin. After 72 h, ATR activity was indirectly measured via [^{14}C]-propionate incorporation into acid-precipitable material in intact cells grown in basal medium. (**B**) Western blot analysis for ATR protein using mitochondria isolated from healthy and patient-derived fibroblasts. The cells were treated for 72 h with 80 μM of compound V or 1 μg/ml of OHCbl or both substances. Mitochondrial Hsp60 was used as a protein control loading.

Molecular docking

The molecular docking of compound V (24,25) resulted in 49 clusters being identified in eight different pockets of the protein. The top-score cluster had a significantly lower FullFitness (26) than the others. This binding site is formed by residues at the C-terminal end of each subunit in the trimeric ATR (residues 228–240), and the loop 165–175, close to residue Phe170, which has been reported as a potential candidate residue for binding the hydrophobic surfaces of cobalamin (9). The site is distant from the ATP binding site (Fig. 6A). In this conformation, compound V could be able to form three hydrogen bonds with the backbone amide of Ala169 and the carboxyl acid side chain of Glu235, making it a favorable binding site (Fig. 6B). The location of this binding pocket is consistent with the results obtained by DSF on the synergistic stabilizing effect of OHCbl and compound V and the absence of effect by ATP (Fig. 3C). Thus, binding of OHCbl and compound V to their respective adjacent sites might lead to a greater packing and conformational stability of this part of the protein, and notably the loop 165–175, than obtained by compound V binding alone.

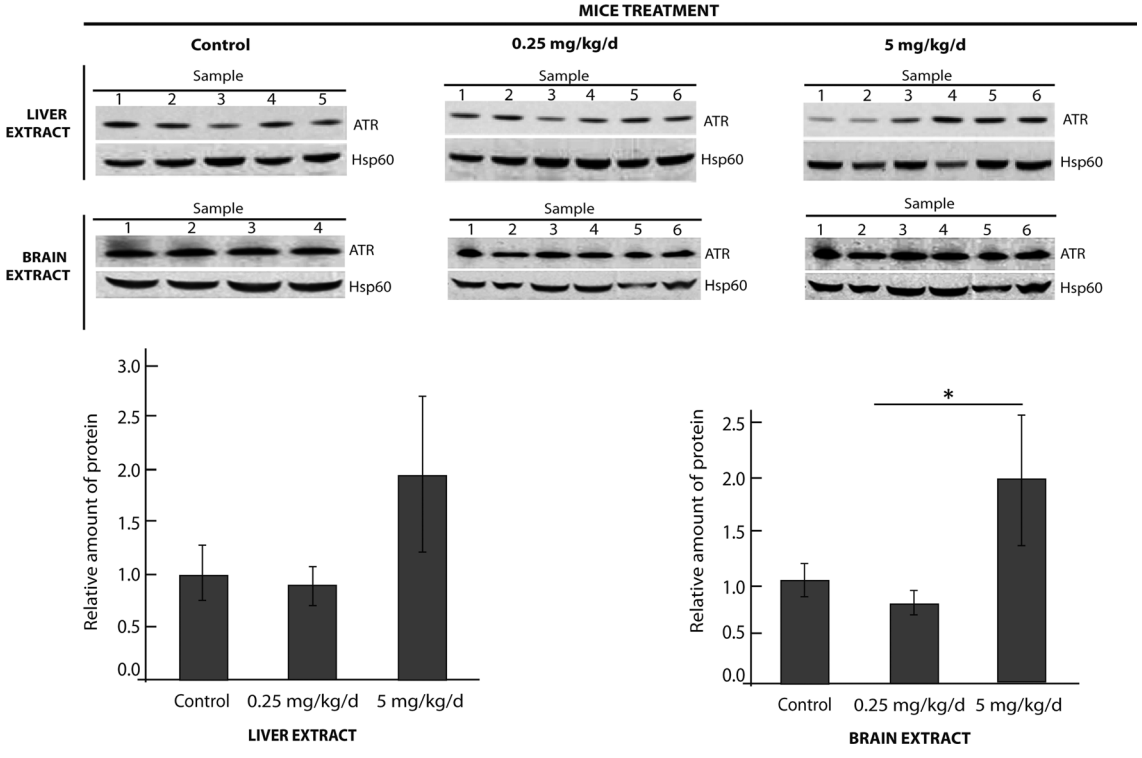

Figure 5. Effect of compound V in wild-type mice. Two groups of six wild-type C57BL/6 mice were orally treated for 12 days with 0.25 mg/kg/day or 5 mg/kg/day of compound V. The control animals (five mice) were treated with 10% DMSO in a 9% glucose solution, i.e. the vehicle for compound V administration. After treatment, whole liver and whole brain extracts were prepared and ATR protein levels detected by immunoblotting (represented as the mean ± SD for each group). $^*P < 0.05$.

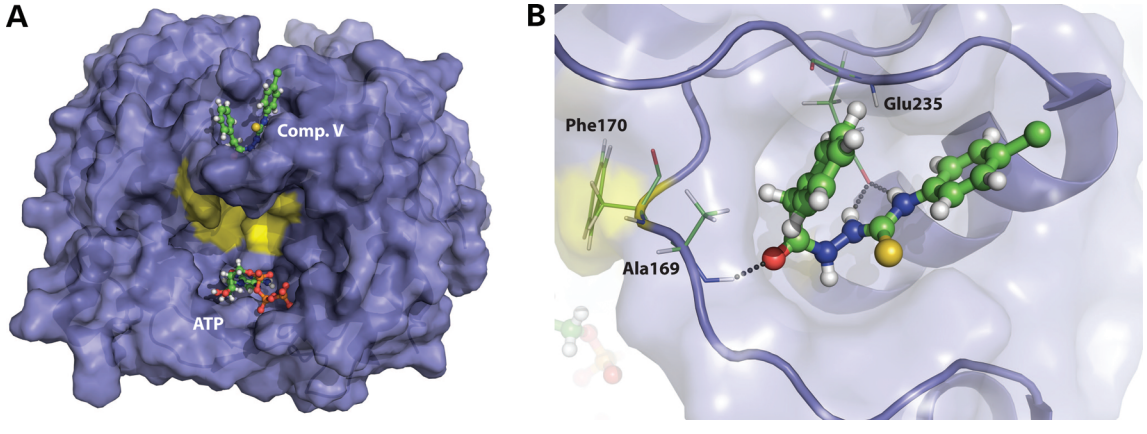

Figure 6. Proposed binding site of compound V. (**A**) Overview of ATR (PDB ID 2IDX) showing the location of the proposed binding site for compound V in one of the protein subunits (top score position from SwissDock with highest FullFitness) (26), the location of ATP, and the residues proposed to interact with cobalamin (yellow). (**B**) A detailed view of the proposed binding site of compound V (ball-and-stick). The residues Ala169 and Glu235 are shown with sticks and the potential hydrogen bonds to compound V with dotted lines. Phe170, which is implicated in cobalamin binding, is also shown.

DISCUSSION

Research into understanding how missense mutations trigger protein degradation is a growing field, the goal of which is to find new therapeutic options for protein misfolding diseases (27). Particular efforts have been directed towards the use of drugs that increase the amount of native-state protein (12,15) through increasing its stability and reducing the degradation of mutated but biologically active protein. Such research could lead to new orphan drugs for treating rare diseases within the context of personalized medicine (12,17,18,28–30). In the present study, we searched for compounds that enhance ATR enzyme stability, opening up the possibility of a new therapeutic strategy for the treatment of MMA cblB, which envisions a tailored therapy for patients harboring destabilizing mutations that could be used in combination with MMA conventional treatment.

Combinations of *in vitro*, *ex vivo* and *in vivo* approaches were used successfully in the search for compounds capable of stabilizing the ATR protein. DSF-based high-throughput screening

(HTS) identified compounds that stabilized purified recombinant wild-type ATR and the p.Ile96Thr mutant to different degrees. One of these compounds, compound V, also stabilized the p.Ile96Thr protein *ex vivo*, and was associated with a dose-dependent increase in ATR activity in the patient-derived cell line bearing the mutations p.Ile96Thr/-p.Ser174fs (20). No inhibitory effects of the compounds on the purified ATR protein were observed. A broad concentration window for compound V administration could be used for increasing a patient ATR activity up to the therapeutic range and is therefore available for a future therapeutic trial in selected cblB patients (18,31).

The promising preliminary results obtained with compound V with the rare destabilizing mutations p.Ile96Thr and p.Arg191 Trp (20) open up the possibility of analyzing the response of other misfolding mutations of ATR (9,31,32). An *in vitro* evaluation of compound V effects is needed to determine which patients it might be beneficial for.

The efficacies of the potential pharmacological chaperones found by HTS were varied (Table 1) and it is possible that their co-administration might lead to synergistic effects, increasing the residual activity of mutant ATR, and combinations of the hit compounds could be tested for each mutation background. While the threshold for clinical efficiency in MMA is unknown, small increases in residual activity (5–10%) might be sufficient to attenuate a severe clinical phenotype (17,18,32). The synergistic effect of OHCbl and compound V on the activity and stability of ATR is noteworthy. The results suggest that vitamin B_{12} administrated alone is not a natural chaperone; no increase in protein was detected in any experiment, and the vitamin did not cause any increase in the T_m of recombinant wild-type ATR, as seen by DSF. Nevertheless, wild-type ATR is indeed stabilized in the presence of both substances, as well as the mutant enzyme in the bacterial and cellular model. The modeled structure of compound V bound to ATR, adjacent to the proposed cobalamine site (Fig. 6), appears to support the synergistic effect of both substances.

The present study suggests a possible clinical application for pharmacological chaperones in the treatment of MMA *cblB* type. However, putative toxic effects of compound V need to be assessed in an appropriate *cblB* animal model (33,34). The proof-of-concept work performed in the present study made use of wild-type mice since no available ATR-deficient mouse model carrying missense alleles was available. The results obtained in these mice *in vivo* suggest that compound V is efficiently absorbed and transported to tissues that are affected in MMA and that it crosses the cellular and mitochondrial membranes and increases ATR stability at a relatively low dose (5 mg/kg/day).

The ultimate goal in MMA treatment research is to prevent, or slow, the development of symptoms of the disease, including metabolic instability, strokes and kidney failure. Currently there is some controversy regarding the source of neurological dysfunction: it might be caused by methylmalonic acid produced in the neurons and/or glia in brain, or by it being made elsewhere in the body and being transported across the blood–brain barrier (BBB) (35). If the brain is responsible for its production, a pharmacological chaperone would have to cross the BBB to be effective. The results obtained with mouse brain extracts are very encouraging since they suggest that compound V could cross the BBB.

In conclusion, the present work identifies a potential pharmacological chaperone (compound V) with *in vitro* efficacy in patient-derived fibroblasts carrying the p.Ile96Thr mutant protein and in wild-type mice. It is therefore a good candidate for therapeutic trials in selected *cblB* patients. Further, the excellent effects of cobalamin—reported over decades—in the treatment of *cblB* MMA patients might be improved by co-administration of compound V. Compound V might also be subjected to chemical modification to enhance its effectiveness; this warrants further investigation.

MATERIALS AND METHODS

Compounds tested for pharmacological chaperone potential

The library of small compounds tested in this study was the commercially available MyriaScreen Diversity Collection (Sigma-Aldrich, St Louis, MO, USA), where the compounds are dissolved to a final concentration of 2 mg/ml in 100% DMSO. The hit compounds from the screening were consecutively ordered from Sigma-Aldrich, prepared at concentrations of 10 mM in 100% DMSO and stored at −20°C, and their chemical structure confirmed by HPLC-MS/MS and NMR spectroscopy.

All experiments presented in this study were performed by the addition of compound dissolved in DMSO to the different assays and parallel control experiments were carried out maintaining the same concentration of DMSO (but without compound).

ATR expression, preparation of bacterial crude extracts and protein purification

Human ATR was expressed in *Escherichia coli* (BL21Star™ DE3 One Shot Cells) transformed with the NL173 plasmid. This plasmid, which is based on the pET41a vector, encoded either wild-type or mutant (p.Ile96Thr or p.Arg191Trp) ATR lacking the mitochondrial targeting sequence (20). Protein expression was induced with 1 mM IPTG; 5 h after induction the cells were harvested by centrifugation (4°C, 6000 rpm for 10 min) and frozen at −70°C until needed. Cell pellets were resuspended in 50 mM potassium phosphate buffer pH 8, 100 mM NaCl, 1 mM DTT, 1 × Complete Mini, EDTA-free Protease Inhibitor Cocktail (Roche Applied Sciences, Indianapolis, IN, USA), 1 mM EDTA, 0.05 mg/ml DNAse and 0.3 mg/ml lysozyme. After 1 h, the cell suspension was sonicated and centrifuged (4°C, 13 000 rpm for 15 min) to obtain the crude soluble cell extract, which was diluted to 1 mg/ml. This crude extract was used in protein stabilization studies and in crude bacterial extract activity assays. For further purification of ATR, the extract was subjected to ammonium sulfate precipitation and subsequent anion-exchange chromatography using a HiTrap Sepharose Q column (GE Healthcare, Buckinghamshire, UK) as previously described (36). In all purification steps, the protein concentration was determined by the Bradford assay (Bio-Rad Laboratories, Munchen, Germany). Fractions eluted from the Sepharose Q column were subjected to SDS–PAGE to identify those enriched in ATR. Purified ATR was centrifuged at 10 000*g* for 10 min at 4°C to precipitate aggregates, and then loaded onto a Superdex 200 HiLoad 16/60 size-exclusion chromatography column (GE Healthcare). The elution peak corresponding to the trimeric ATR form was recovered and used for

further experiments. Pure protein concentration was estimated by measuring the absorbance at 280 nm in a Nanodrop spectrophotometer (Thermo Scientific) using the theoretical molar extinction coefficient (16 305 M^{-1} cm^{-1}) estimated from the amino acid composition for ATR.

High-throughput screening for pharmacological chaperones

Ligand-induced ATR stabilization was assessed by an HTS protocol using DSF (37), monitoring the thermal denaturation of purified ATR in the presence of the extrinsic fluorescent probe SYPRO Orange (Sigma-Aldrich). Protein solutions containing 0.086 mg/ml of ATR (3.2 μM ATR subunit) in 20 mM Na-Hepes, pH 7.0, 200 mM NaCl and 5× SYPRO Orange, were dispensed (49 μl) into 96-well PCR plates (LightCycler480 Multiwell Plate 96, Roche). One microliter of each potential chaperone compound dissolved in DMSO was added to each well to produce final concentrations of 0.04 mg/ml compound and 2% DMSO. Plates were incubated at room temperature for 30 min before loading into a Light Cycler 480 (Roche Applied Science, Indianapolis, IN, USA) for thermal denaturation. Control experiments with 2% DMSO were routinely performed. Unfolding curves were registered from 20 to 99°C, at a scan rate of 2°C/min. The increase in SYPRO Orange fluorescence intensity associated with protein unfolding ($\lambda_{excitation}$ = 465 nm, $\lambda_{emission}$ = 610 nm) was monitored as a measure of thermal denaturation. Unfolding curves were recorded from 20 to 95°C, at a scan rate of 2°C/min. The experimental unfolding curves were smoothed, normalized and analyzed using in-house software. The midpoint melting temperature (T_m) was calculated as the temperature at which half the protein is in the unfolded state. A compound qualified as a 'hit' if it increased the T_m of the protein by ≥6°C.

The concentration-dependent stabilization of ATR 0.15 mg/ml (6.35 μM ATR subunit) by ATP and hydroxocobalamin (OHCbl) (0–200 μM) was carried out using DSF at otherwise similar sample preparation, pre-incubation and scanning conditions as in the HTS protocol. Following this experiment, thermal stabilization titrations with compound V (0–200 μM) were carried out in the presence or absence of either 40 μM ATP or 0.75, 3 and 12 μM of OHCbl.

Effect of the compounds on ATR stability in a prokaryotic expression system

ATR stability was assessed as previously described (20). Basically, ATR expression was induced with 1 mM IPTG in 10 ml *E. coli* LB cultures for 5 h in the presence of 40 or 80 μM compound dissolved in DMSO (final concentration of DMSO 0.1 or 0.2%, respectively) or the corresponding concentration of DMSO. To determine a possible synergistic effect of compound V and OHCbl on ATR stability, the same experiment was performed in the presence of 1 μg/ml (0.7 μM), of OHcbl a concentration commonly used to stimulate cells to incorporate ^{14}C propionate. Additionally, *E. coli* were cultured for 5 h in the presence of 80 μM of compound V dissolved in DMSO added together with OHCbl dissolved in water. The crude extracts, prepared as described earlier, were diluted to 1 mg protein/ml. Aliquots of equal amounts of total protein were incubated at 37°C, and equal sample volumes were removed at different times for immediate analysis by SDS–PAGE or frozen until gel loading.

Enzyme activity assays

ATR activity was measured as described by Johnson *et al*. (38) with minor modifications. Briefly, 1 ml of reaction mixture (200 mM Tris–HCl pH 8.0, 1.6 mM KH_2PO_4, 2.8 mM $MgCl_2$ and 100 mM KCl) was dispensed into cuvettes and kept at 37°C. Specific activity was measured with 40 μM ATP and 60 μM OHCbl (Sigma-Aldrich). In indicated experiments, 0–100 μM of compound V or VI were added to the reaction mixture. After titanium (III) citrate (30 μL) was added, the reaction was started by the addition of 10 μg of purified wild-type ATR. Alternatively, 50–100 μg of crude extracts from bacterial cultures expressing wild-type, p.Ile96Thr or p.Arg191Trp, grown in the presence of 0–100 μM of compound V or VI, were used to start the reaction. Anaerobic procedures were followed in the preparation of the reaction mix, the protein solution, compound solutions and the titanium (III) citrate solution. The reduction in absorbance at 388 nm was monitored to calculate the concentration of AdoCbl, with ΔA_{388} taken as 24.9 cm^{-1} mM^{-1}, and specific activity was expressed as μmol of product generated per minute and milligram of protein (U/mg). Experiments were performed in triplicate.

Biochemical data on the p.Ile96Thr-bearing patient and biochemical chaperone analysis in patient fibroblasts

The patient with the genotype c.287T>C/c.584G>A (p.Ile96Thr/p.Ser174fs) has been described earlier (20). This patient was placed under protein restriction, carnitine supplementation and oral OHCbl administration (5 ml/day). During therapy, the patient showed >1000 mmol/mol creatinine, plasma C3 levels of ∼10 μM and normal plasma odd-chain fatty-acid levels (<0.4%). Urine methylmalonic acid varied (<200–800 mmol/mol creatinine). A dermal fibroblast cell line from this patient and healthy control fibroblasts were stably transformed with pBabe retroviral vector (kindly provided by Dr J.A. Enriquez, *Centro Nacional de Enfermedades Cardiovasculares,* Madrid). 5×10^5 transformed cells were plated and grown at 37°C for 24 h in MEM medium supplemented with 2 mM glutamine, 10% fetal bovine serum and antibiotics. After treatment, the culture medium was discarded and replaced with fresh medium containing 40 or 80 μM of compound V for 48 or 72 h, or the equivalent volume of DMSO for controls. After this time, cell lines were grown for 18 h in the presence of [^{14}C]-propionate, and were harvested by trypsinization, followed by centrifugation, and were used to determine ATR activity, which was indirectly measured by [^{14}C]-propionate incorporation into acid-precipitable material in intact cells grown in basal medium (39). Assays were performed in triplicate and results were examined statistically using an *F*-test analysis of variance followed by a one-tailed, paired *t*-test. Significance was set at $P < 0.05$.

Alternatively, mitochondrial isolation from cell pellets was performed using anti-TOM22 MicroBeads (Mitochondrial Isolation Kit, Miltenyi Biotec, Bergisch Gladbach, Germany). Briefly, 8.0×10^5 cells from a healthy control and patient immortalized fibroblasts were seeded in T75 flasks and incubated overnight at 37°C, and then for 72 h with 80 μM of compound V, 1 μg/ml of OHCbl or both. The cells were harvested

by trypsinization and the mitochondria isolated following the manufacturer's protocol. Mitochondrial pellets were resuspended in 50 μL of storage buffer.

Animal studies

Seventeen female 12-week-old wild-type mice (C57BL/6J) were purchased from Harlan Laboratories (Harlan Laboratories Inc., Indianapolis, IN, USA). These were housed under standard conditions in compliance with European Community Guidelines (Directive 86/609/EEC) at the *Centro de Biología Molecular Severo Ochoa*, and maintained at a temperature of 22 ± 1°C under a 12 h/12 h light/dark cycle. All had *ad libitum* access to food and water and were handled in strict accordance with national and institutional animal welfare guidelines. Two groups of six animals (23–25 g) were orally loaded with a 25 μl suspension containing either 0.25 or 5 mg/ml/day of compound V in 10% DMSO plus 9% glucose for 12 days. The control group was treated only with the 10% DMSO and 9% glucose. Approximately, 30 min after the last dose, the animals were sacrificed using CO_2. The livers and brains were rapidly removed and divided into two equal parts, one of which was frozen in liquid nitrogen for further studies. Fresh liver extracts were prepared in phosphate buffered saline with protease inhibitors; fresh brain extracts were prepared in RIPPA buffer [50 mM Tris–HCl, pH 7.4, 1% Triton, 150 mM NaCl, 1 mM EDTA, 1 mM NaF, 1 mM Na_3VO_4, 1× Complete Mini EDTA-free Protease Inhibitor Cocktail (Roche Applied Sciences) and 0.25% Na-deoxycholate]. These samples were homogenized using a Tissue Lyser II (QIAGEN, Hilden, Germany) and the extracts clarified by centrifugation at 13 000 rpm for 30 min at 4°C. The supernatants were stored at −70°C prior to SDS–PAGE and immunoblotting analyses.

SDS–PAGE and immunoblotting

Samples were loaded onto pre-cast polyacrylamide NuPAGE SDS–PAGE Bis–Tris 10% gels in the case of bacterial crude extract or 4–12% gels for the murine tissue extracts (75 μg of liver or 150 μg of total brain extract) and separated using NuPAGE SDS MES running buffer (Life Technologies, Grand Island, NY, USA). Proteins were transferred to a nitrocellulose transfer membrane using the iBLOT gel Device System (Life Technologies). Poinceau staining was used to monitor equal protein loading. Immunodetection was performed using commercially available anti-ATR antibodies (ProteinTech Group, Inc., Chicago, IL, USA) as primary antibodies (diluted 1:1000 for the bacterial crude extracts, and 1:500 for the mouse tissue extracts). The secondary antibody used was conjugated goat-anti-mouse IgG-horseradish peroxidase (1:10 000 for bacterial extracts and 1:5000 for mouse tissue extracts) (Santa Cruz Biotechnology Inc., Santa Cruz, CA, USA). The mouse tissue extract membranes were also immune stained with a polyclonal antibody against mitochondrial Hsp60 (1:10 000). Signals were visualized using the Enhanced Chemiluminescence System (GE Healthcare, Munich, Germany) and the relative amount of protein determined using a GS-800 calibrated densitometer running Quantity One software (BioRad, Hercules, CA, USA). The prokaryotic stability experiments were performed in triplicate and were statistically examined using the *F*-test analysis of variance followed by a one-tailed paired *t*-test. Significance was set at $P < 0.05$.

Molecular docking

To identify potential binding sites of compound V, we performed an automated molecular-docking procedure using the web-based SwissDock program (24,25). The docking was performed using the 'Accurate' parameter at otherwise default parameters, with no region of interest defined (blind docking).

WEB RESOURCES

http://www.ncbi.nlm.nih.gov/omim.

ACKNOWLEDGEMENTS

We thank Carmen Gherasim (University of Michigan Medical School) for assistance with the measurement of ATR activity.

Conflict of Interest statement. None declared.

FUNDING

This work was funded by grants from the Fondo de Investigaciones Sanitarias (PI10/00455 to B.P.), the Fundación Ramón Areces to B.P., MITOLAB (S2010/BMD-2402 to B.P.), the Research Council of Norway (nr. 185181 to A.M.), the KG Jebsen Foundation, the Western Norway Health Authority (nr. 911618 to A.M.), Novo Seeds (Novo Nordisk Foundation to A.M.) and the National Institutes of Health (DK45776 to R.B.). A.J.F. was supported by a grant from the Instituto de Salud Carlos III. S.B. was supported by a grant from Fundação para a Ciência e Tecnologia of Portugal (SFRH/BD/45753/2008). An institutional grant from the Fundación Ramón Areces to the Centro de Biología Molecular Severo Ochoa is gratefully acknowledged.

REFERENCES

1. Fowler, B., Leonard, J.V. and Baumgartner, M.R. (2008) Causes of and diagnostic approach to methylmalonic acidurias. *J. Inherit. Metab. Dis.*, **31**, 350–360.
2. Coelho, D., Kim, J.C., Miousse, I.R., Fung, S., du Moulin, M., Buers, I., Suormala, T., Burda, P., Frapolli, M., Stucki, M. *et al.* (2012) Mutations in ABCD4 cause a new inborn error of vitamin B(12) metabolism. *Nat. Genet.*, **44**, 1152–1155.
3. Coelho, D., Suormala, T., Stucki, M., Lerner-Ellis, J.P., Rosenblatt, D.S., Newbold, R.F., Baumgartner, M.R. and Fowler, B. (2008) Gene identification for the cblD defect of vitamin B12 metabolism. *N. Engl. J. Med.*, **358**, 1454–1464.
4. Rutsch, F., Gailus, S., Miousse, I.R., Suormala, T., Sagne, C., Toliat, M.R., Nurnberg, G., Wittkampf, T., Buers, I., Sharifi, A. *et al.* (2009) Identification of a putative lysosomal cobalamin exporter altered in the cblF defect of vitamin B12 metabolism. *Nat. Genet.*, **41**, 234–239.
5. Banerjee, R., Gherasim, C. and Padovani, D. (2009) The tinker, tailor, soldier in intracellular B12 trafficking. *Curr. Opin. Chem. Biol.*, **13**, 477–484.
6. Froese, D.S., Healy, S., McDonald, M., Kochan, G., Oppermann, U., Niesen, F.H. and Gravel, R.A. (2010) Thermolability of mutant MMACHC protein in the vitamin B12-responsive cblC disorder. *Mol. Genet. Metab.*, **100**, 29–36.
7. Padovani, D., Labunska, T., Palfey, B.A., Ballou, D.P. and Banerjee, R. (2008) Adenosyltransferase tailors and delivers coenzyme B12. *Nat. Chem. Biol.*, **4**, 194–196.

RESEARCH ARTICLE

Human Mutation

OFFICIAL JOURNAL
HGVS
HUMAN GENOME VARIATION SOCIETY
www.hgvs.org

Pseudoexon Exclusion by Antisense Therapy in 6-Pyruvoyl-Tetrahydropterin Synthase Deficiency

Sandra Brasil,[1,2] Hiu Man Viecelli,[3] David Meili,[3] Anahita Rassi,[3] Lourdes R. Desviat,[1] Belen Pérez,[1] Magdalena Ugarte,[1*†] and Beat Thöny[3*]

[1]*Centro de Diagnóstico de Enfermedades Moleculares, Centro de Biología Molecular, Centro de Investigación Biomédica en Red de Enfermedades Raras (CIBERER), Madrid, Universidad Autónoma de Madrid, Spain;* [2]*Metabolism & Genetics Group, Research Institute for Medicines and Pharmaceuticals Sciences (iMed.UL), Faculty of Pharmacy, University of Lisbon, Portugal;* [3]*Division of Clinical Chemistry and Biochemistry and Children's Research Center (CRC), Department of Paediatrics, University Children's Hospital Zurich, Switzerland*

Communicated by Haig H. Kazazian, Jr.

Received 1 October 2010; accepted revised manuscript 21 April 2011.
Published online 3 May 2011 in Wiley Online Library (www.wiley.com/humanmutation). DOI 10.1002/humu.21529

ABSTRACT: Antisense oligonucleotide therapy to modulate splicing mutations in inherited diseases is emerging as a treatment option also for metabolic defects. In this article, we report the effect of cellular antisense therapy to suppress pseudoexon activation in primary dermal fibroblasts from patients with mutations in the *PTS* gene encoding 6-pyruvoyltetrahydropterin synthase (PTPS), which leads to tetrahydrobiopterin and monoamine neurotransmitter deficiency. Pathogenic inclusion of SINE or LINE-derived cryptic exons in different PTPS patients due to the intronic mutations c.84−322A>T, c.163+695_163+751del57, or c.164−712A>T was demonstrated by transcript analysis in fibroblasts and minigene ex vivo assays. Antisense morpholino oligonucleotides (AMOs) directed to the pseudoexons 3′ or 5′ splice sites were designed with the aim of preventing the pathological pseudoexon inclusion. At the time of AMO transfection, we investigated patients' cells for correct *PTS*-mRNA splicing and functional recovery of the PTPS protein. Transcriptional profiling after 24 hr posttransfection revealed a dose- and sequence-specific recovery of normal splicing. Furthermore, PTPS enzyme activity in all three patients' fibroblasts and the pterin profile were close to normal values after antisense treatment. Our results demonstrate proof-of-concept for pseudoexon exclusion therapy using AMO in inherited metabolic disease.

Additional Supporting Information may be found in the online version of this article.

*Correspondence to: Magdalena Ugarte, Centro de Diagnóstico de Enfermedades Moleculares, Centro de Biología Molecular "Severo Ochoa," Nicolas Cabrera, 1, Universidad Autonoma de Madrid, Campus de Cantoblanco 28049, Madrid, Spain. E-mail: mugarte@cbm.uam.es or or Beat Thöny, Division of Clinical Chemistry and Biochemistry, Department of Pediatrics, University of Zürich, Steinwiesstrasse 75, CH-8032 Zürich, Switzerland. E-mail: beat.thony@kispi.uzh.ch

Contract grant sponsor: Fundaçao para a Ciencia e Tecnologia from Portugal; Contract grant number: SFRH/BD/45753/2008 (to S.B.); Contract grant sponsor: Comisión Interministerial de Ciencia y Tecnología; Contract grant number: SAF2007-61350 (to L.R.D. and B.P.); Contract grant sponsor: Fondo de Investigaciones Sanitarias; Contract grant number: PI10/00455 (to B.P); Contract grant sponsors: Institutional grant from the Fundación Ramón Areces to the Centro de Biología Molecular Severo Ochoa (to B.P., L.R.D., S.B., and M.U.); The Swiss National Science Foundation (to B.T.).

Hum Mutat 32:1019–1027, 2011. © 2011 Wiley-Liss, Inc.

KEY WORDS: alternative splicing; antisense oligonucleotides; pseudoexons; splicing therapy; tetrahydrobiopterin deficiency

Introduction

Pseudoexon inclusion is emerging as a common disease-causing mechanism in many human disorders. Most pathological pseudoexon inclusion events are originated from intronic mutations creating a new 5′ or 3′ splice site followed by the subsequent selection of weaker opportunistic acceptor or donor site sequences [Dhir and Buratti, 2010]. In addition, other common mechanisms for intronic insertion activation involve the creation/deletion of splicing regulatory sequences or genomic rearrangements, that is, gross deletions or genomic inversions. Many of these new exons in our genome are transposable sequence elements derived from short or long interspersed nuclear elements (SINEs or LINES, respectively), with primarily SINE-*Alu* sequences as a prominent source of new exons in the eukaryotic transcriptome [Vorechovsky, 2010]. Several examples of this pathogenic mechanism have been reported in human genetic disorders such as cystic fibrosis, ataxia telangiestasia, and several inherited metabolic disorders, including organic acidemias, phosphomanomutase deficiency, and 6-pyruvoyltetrahydropterin synthase deficiency [Perez et al., 2010].

Previously, we described two new disease-causing mutations that improve the branch site of a LINE-2 element or the polypyrimidine tract of an antisense *Alu* sequence in the *PTS* gene encoding 6-pyruvoyltetrahydropterin synthase (PTPS; MIM♯ 261640) [Meili et al., 2009]. PTPS catalyzes the second reaction in the three-step biosynthesis of tetrahydrobiopterin (BH_4) from GTP and is encoded by the *PTS* gene located in chromosome 11q22.3–q23.3. BH_4 is the natural cofactor for aromatic amino acid hydroxylases, nitric oxide synthases, and glycerol ether monooxygenase [Werner et al., 2011]. The most common form of BH_4 deficiency is due to the autosomal recessive PTPS deficiency. Patients present with elevated levels of neopterin, low levels of biopterin, hyperphenylalaninemia, and monoamine neurotransmitter deficiency in the central nervous system (CNS) [Thöny and Blau, 2006]. Early diagnosis and treatment to control hyperphenylalaninemia and also correction of neurotransmitter deficiency in the CNS is associated with better outcome of the

disease [Jaggi et al., 2008]. Oral administration of BH_4 is effective to control peripheral hyperphenylalaninemia, but BH_4 passes ineffectively through the blood–brain barrier. Thus, L-dopa and 5-hydroxytryptophan, the precursors for the catecholamines and serotonin, respectively, also have to be administrated to normalize monoamine neurotransmitters in the CNS. Patients can have the typical/severe form with hyperphenylalaninemia and abnormal CSF neurotransmitters or the less common atypical/peripheral form with minor or no changes in neurotransmitter levels and less significant or transient hyperphenylalaninemia [Jaggi et al., 2008; Longo, 2009; Shintaku, 2002]. More than 64 different mutations have been reported to date (HGMD® professional release 2010) associated with the severe or the milder forms of PTPS deficiency [Thöny and Blau, 2006]. Although this treatment is effective in most cases, it is believed that alternative strategies to improve the current life-long dependency from BH_4 and monoamine neurotransmitter precursors should be pursued.

Splice modulation therapy by manipulation of premessenger RNA splicing is a promising therapy for genetic diseases [Wood et al., 2007]. Therapeutic strategies based on antisense oligonucleotide (AON) chemistry have been employed in Duchenne muscular dystrophy (DMD) to induce mutant exon skipping to avoid aberrant pseudoexon inclusion [Wood et al., 2010]. Mutations causing exonization of deep intronic sequences are more common than previously thought, and antisense strategies have been employed to rescue the splicing process [Dhir and Buratti, 2010; Perez et al., 2010]. AONs bind by complementarity to the pre-mRNA, and steric hindrance, which inhibits the recruitment of splicing factors to the targeted splicing *cis*-elements, forces the spliceosomal machinery to use the natural splicing sites [Wood et al., 2007]. Based on the pioneering work with antisense-mediated modulation in the *CTFR* and β-globin genes [Friedman et al., 1999a; Suwanmanee et al., 2002], several aberrant splicing processes have been successfully restored in various cellular disease models [Friedman et al., 1999b; Lacerra et al., 2000; Perez et al., 2009]. Some of these antisense approaches for splicing intervention have been tested already in animal models [Alter et al., 2006], and a human clinical phase III trial for DMD has been launched as well [Kinali et al., 2009; van Deutekom et al., 2007]. The induction of skipping a specific exon bearing a nonsense change in DMD in an attempt to rescue a internally shorter but partially functional dystrophin, has been shown to be promising and safe both in The Netherlands and the United Kingdom [Aartsma-Rus et al., 2009].

This work aims at developing a cellular splice-modulation antisense therapy to suppress pseudoexon activation in primary dermal fibroblasts from PTPS-deficient patients who have been identified with intronic mutations causing exonization. Whereas two *PTS* mutations were reported before (c.84−322A>T and c.163+695_163+751del57; the latter originally reported as c.163_164ins45) [Meili et al., 2009] we included identification and functional analysis as well as ex vivo minigene assays of a new intronic sequence variant (c.164−712A>T), which activates insertion of the antisense *Alu* exon located in intron 2. Although antisense therapy using AMO for BH_4-deficient patients with intronic exonization mutations in the *PTS* gene is far from clinical application, our results demonstrate proof of concept for pseudoexon exclusion therapy in inherited metabolic disease.

Materials and Methods

Metabolic Analysis of *PTPS*-Deficient Patients

The study includes primary dermal fibroblasts from the three PTPS patients: MD96, MD130, and MD335. MD96 with the mild form, and MD130 with the severe form of PTPS deficiency were described elsewhere [Meili et al., 2009] (with ID363 and ID503 in the International Database of tetrahydrobiopterin deficiencies BIODEF, http://www.bh4.org). Patient MD335 was identified recently with the severe form of PTPS deficiency and had an elevated blood Phe value (668 μmol/l), elevated neopterin (50 mmol/mol creatinin), and no detectable biopterin (<0.01 mmol/l) in urine, and PTPS enzyme activity of 0.22 μU/mg protein in primary dermal fibroblasts. Analysis of biogenic amines in the cerebral spinal fluid (CSF) of patient MD335 (ID622 in BIODEF) revealed very low homovanillic acid (56 nmol/l) and 5-hydroxyindolacetic acid (85.1 nmol/l; for reference values see [Blau et al., 2002; Bonafe et al., 2001]).

Mutation Analysis of the *PTS* Gene

Mutation analysis was carried out with cDNA and genomic DNA samples prepared from primary fibroblasts and/or whole blood. Total RNA was isolated using the RNeasy Mini Kit (Qiagen, Chatsworth, CA) and the first-strand cDNA was synthesized with the AMV Reverse Transcription System (Promega, Madison, WI) and primer PTPS-53 (5′-TTT CAA TAA ATA GGC ACT CC-3′). Amplification of the *PTS* cDNA was carried out with primers PTPS-53 and PTPS-54 (5′-ATG AGC ACG GAA GGT GGT G-3′). Primers and polymerase chain reaction (PCR) conditions for amplification and DNA sequence analysis of exons 1–6 and intron 2 are available upon request. Mutation designation is according to the official mutation nomenclature (http://www.hgvs.org/mutnomen/). Reference accession numbers for normal alleles: L76259.1 for human genomic DNA; M97655.1 for human cDNA (cDNA numbering starts with 1 at A at the ATG start codon). To validate nomenclature of mutations we used the program Mutalyzer 2.0 β-2 (http://www.mutalyzer.nl/2.0).

Patient MD96 was found to be homozygous for the nucleotide change c.84−322A>T (g.2666A>T), and MD130 is compound heterozygous for the changes c.393delA (g.7901delA) and c.163+695_163+751del57 (originally reported as c.163_164ins45; g.3762_3818del57.

In primary dermal fibroblasts we found for MD96 an insertion of a LINE2 sequence of 79 bp between exon 1 and 2 (r.83_84ins79). Fibroblasts from MD130 presented a larger cDNA fragment containing a 45-nucleotide insertion (r.163_164ins45) resulting from a maternal deletion located 20 nt upstream of an antisense *Alu* sequence (c.163+695_163+751del57) [Meili et al., 2009]. Splice scores of the natural and cryptic donor and acceptor sites were determined using the analysis tools from Berkeley Drosophila Genome Project (BDGP server: http://www.fruitfly.org/).

Transcriptional Profile and Ex Vivo Minigene Analysis

Splicing reporter plasmid encompassing *PTS* exons 2 to 4 (described in [Meili et al., 2009]) was used as a template. Mutation c.164−712A>T from patient MD335 was introduced with the QuikChange II XL Kit (Agilent Technologies, Santa Clara, CA) using primer 5′-CCT CCC AGG TTC GTG CGA TTC TCC AGC-3′ and its reverse complement. Variant minigenes containing mutations c.164−714C>A and c.164−715T>A were generated by site-directed mutagenesis using primers 5′-CTC CAC CTC CCA GGT ACG AGC GAT TCT CC-3′ and 5′-CTC CAC CTC CCA GGT ACG TAG AGC GAT TCT CC-3′, respectively, and their reverse complement. COS-1 cells were transfected in triplicates using 2.25-μg plasmid DNA and 8.5 μl lipofectamine LTX according to the manufacturer's instructions (Invitrogen,

Carlsbad, CA). Cells were harvested by trypsinization after 24 hr. Total RNA was extracted using the QIAamp RNA Blood Mini Kit (Qiagen, Hilden, Germany). RNA was reverse transcribed and amplified using vector-specific primers PL3 (5′-GGG AGA CCC AAG CTG GCT A-3′) and PL4b (5′-AGT CGA GGC TGA TCA GCG G-3′) and OneStep RT-PCR Kit (Qiagen) with the following cycling conditions: 30 min at 50°C, 15 min at 95°C, 40 cycles of 30 sec at 95°C, 30 sec at 55°C, 1 min at 72°C, followed by 10 min at 72°C. PCR products were separated on agarose and sequenced to confirm their identity.

Antisense Morpholino Oligonucleotide Treatment

Patients and control dermal fibroblasts were cultured in MEM containing 10% fetal bovine serum, 100 U/ml penicillin, 100 μg/ml streptomycin, and 2 mM glutamine. Cells were passaged by trypsinization and studied at a passage number ranging from 6–23. Cultures were kept at 37°C in humidified air containing 5% CO_2.

The 25-mer AMO were designed, synthesized, and purified by Gene Tools (Philomath, OR) and were targeted to donor or acceptor cryptic splice sites in the pre-mRNA. The sequences of the three AMOs are: PTS-AMO1 5′- AGT GCC TAC AAT GTA ACA GGC AAG T-3′, PTS-AMO2 5′-AGG CTG GAG AAT CGC TCG AAC CTG G-3′, and PTS-AMO3 5′-AGG CTG GAG AAT CGC ACG AAC CTG G-3′. As a negative control, a standard 25-mer Morpholino control oligonucleotide provided by Gene Tools was used (5′-CCT CTT ACC TCA GTT ACA ATT TAT A-3′). As a delivery reagent, Endo-Porter was used following the manufacturer's recommendations as previously described (Gene Tools; www.gene-tools.com) [Ugarte et al., 2007]. After transfection with 20 and 30 μM of the corresponding AMO, cells were harvested at 24 hr and mRNA was isolated using the MagnaPure system following the manufacturer's protocol (Roche Applied Sciences, Indianapolis, IN). The cell lines were incubated with cycloheximide 0.75–1 mg/ml 4–6 hr prior to cell harvest. For PCR amplification of transcript from MD96 and MD130 cell lines 5′-TAT GGA GGA GGC GAT TAT GC-3′ and 5′-TTT CAA TAA ATA GGC ACT CC-3′ were used as forward and reverse primer, respectively. To exclude amplification from the allele bearing the c.163+2T>G mutation in the mRNA from MD335, a forward specific primer located in the exon 1 and exon 2 junction was used (5′-CCG ATT GTA CAG TAA ATT TCT AA-3′).

Different amounts of antisense Morpholinos, PTS-AMO1, and PTS-AMO3, that were covalently linked to Vivo-Porter (also supplied by Gene Tools) were added directly to the cultured primary dermal fibroblast cells (VIVO-AMO1 and VIVO-AMO3). Conventional RT-PCR for splice analysis was performed as described above.

PTPS Activity, Pterin Quantification, and Protein Immunodetection

The patients' fibroblast cells were treated with 30 μM of AMOs during 48 and 72 hr, and the activity levels were determined as described elsewhere [Bonafe et al., 2001]. To induce expression of the GTPCH enzyme, a confluent cell monolayer in 75-cm^2 plates was stimulated with a cytokine cocktail containing 1,250 U of recombinant human interferon-γ (IFN-γ) and 500 U of tumor necrosis factor α (TNF-α), and incubated for 24–96 hr. At the same time the cells were treated with 30 μM of the corresponding AMO and harvested 48, 72, and 96 hs after transfection. Cells grown for 96 hr were transfected twice with the AMOs. After incubation, cells were harvested by trypsinization, counted to determine the cell number, washed with phosphate-buffered saline, and kept at −70°C until analyzed for neopterin and biopterin.

Cytokine-stimulated cells from a confluent 75-cm^2 plate were lysed in 150 μl of lysis buffer (100 mM Tris-HCl, pH 8.0, 2.5 mM EDTA, 300 mM KCl, and 10% glycerin) by freezing and thawing six times. Lysate was centrifuged at 15,000 × *g* for 15 min at 4°C. A volume of 100 μl of supernatant was oxidized with 6 μl of 1 M HCl and 20 μl of a 10 g/l iodine solution for 30 min at room temperature in the dark. The remaining supernatant was used for determination of protein concentration using the Bradford reagent (Bio-Rad, Munich, Germany). The oxidation reaction was stopped by the addition of 20 μl of 10 g/l ascorbic acid (freshly prepared). To adjust the pH to 8.0–9.0, 10 ml of dephosphorylation buffer (1 M Tris-HCl pH 9.6 containing 80 mM $MgCl_2$) was added to the sample with alkaline phosphatase (20 U) to desphosphorylate the neopterin triphosphate. The sample was incubated at 37°C for 60 min. The reaction was stopped by acidification to pH 2.0 with 7 μl of 2 M HCl. The sample was deproteinized using a low protein binding centrifugal filter (VWR, West Chester, PA) and analyzed by high-performance liquid chromatography (HPLC). The intracellular concentrations of neopterin and biopterin after cytokine stimulation are expressed as pmol per mg of protein [Bonafe et al., 2001; Werner et al., 1996].

For Western blot analysis patient's fibroblasts from one confluent 75-cm^2 plate were treated with the corresponding AMO. After 48 hr cells were harvested by trypsinization and protein concentration was determined using the Bradford reagent (Bio-Rad, Munich, Germany). Equal amounts of protein crude extracts were loaded on a 4–12% NuPAGE® Novex® Bis-Tris precast gel (Invitrogen, Carlsbad, CA). After electrophoresis, proteins were transferred to a nitrocellulose membrane (iBlot® Gel Transfer Stacks, Regular) in an iBlot® Gel transfer device (Invitrogen) for 7 min. Poinceau staining was used to monitor equal loading of protein. Immunodetection was carried out using antihuman PTPS polyclonal antibody SZ28 (1:500 diluted) [Elzaouk et al., 2004] followed by a second antibody (conjugated goat antirabbit IgG horseradish peroxidase, diluted 1:10,000; Santa Cruz Biotechnology Inc., Santa Cruz, CA). The detection was made using the Enhanced Chemiluminescence System (GE Healthcare, Buckinghamshire, UK).

Results

Identification of a Novel Exonization Mutation Leading to Inclusion of the Antisense *Alu* Sequence in Intron 2 of the *PTS* Gene

Patient MD335 was identified by newborn screening for hyperphenylalaninemia and later diagnosed for the severe form of PTPS deficiency based on urinary pterins, monoamine neurotransmitter deficiency in CSF, and PTPS enzyme activity in primary fibroblasts (see also Materials and Methods; ID622 in BIODEF, http://www.bh4.org). Subsequent fibroblast-cDNA and genomic DNA analyses revealed two compound heterozygous mutations in the *PTS* gene intron 2, a T>G transversion at c.163+2T>G (g.3069T7>G), and an A>T transversion at position c.164−712A>T (g.3887A>T). The transcriptional profile in primary dermal fibroblasts from patient MD335 and his parents is shown in Figure 1A. The intronic c.163+2T>G mutation, which was inherited from the mother (MD336), is located in the 5′ splice site of intron 2 (IVS2+2T>G) and generates three distinct shorter *PTS*-mRNA transcripts or cDNA-fragments

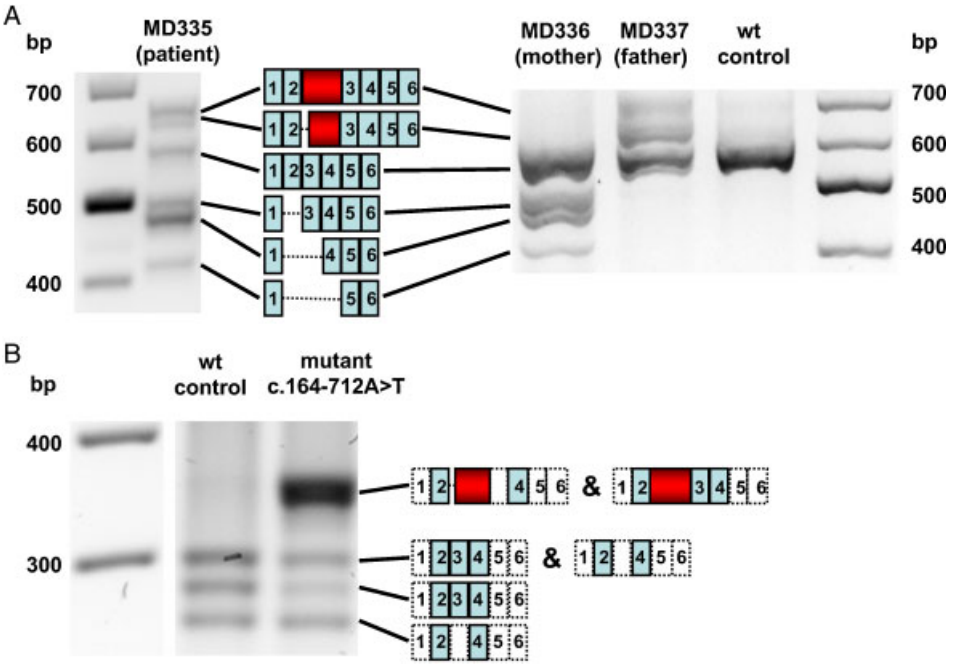

Figure 1. Transcriptional profiling of fibroblasts derived from patient MD335 and functional analysis of the splicing mutation c.164−712A>T using a minigene assay. **A:** RT-PCR pattern and subsequent sequence analysis of the amplified products obtained from patient's fibroblast. Individual bands were validated by DNA sequence analysis. As shown from analyzing the parents' expression profile for the *PTS*-mRNA, the two larger bands correspond to the insertion of the longer (70 nt) or shorter (45 nt) version of the antisense *Alu* sequence using the identical 5′ splice donor, but two different 3′ splice acceptor sites (for details, see also [Meili et al., 2009]). The paternal mutation c.164−712A>T was identified based on computation methods to be located in the "putative exonic splicing silencer," or PESS, 5′ from the antisense *Alu* sequence in intron 2 of the *PTS* gene. The shorter bands correspond to skipping of different exons due to the maternal mutation c.163+2T>G, located in the 5′ splice site of intron 2. **B:** Result of the ex vivo splicing assay for minigene constructs with wild-type and the corresponding c.164−712A>T mutation from patient MD355. The A>T transversion produces in the minigene vector produces in our assay an additional and very prominent upper band, which turns out to contain the 70-bp antisense *Alu* sequence with or without exon 3. Furthermore, we could not rule out that a low percentage of this upper band contained in addition the shorter 45-bp version of the antisense *Alu* fragment. [Color figures can be viewed in the online issue, which is available at www.wiley.com/humanmutation.]

corresponding to skipping of exon 2, exons 2–3, and exons 2–4. The deep intronic mutation c.164−712A>T, inherited from the father (MD337), was identified based on computation methods to be located in the "putative exonic splicing silencer" site, or PESS, 5′ from the antisense *Alu* sequence in intron 2 of the *PTS* gene [Meili et al., 2009]. As shown below, this intronic A>T transversion leads to the inclusion of a similar antisense *Alu* exon, which was retained in the *PTS*-mRNA from patient MD130. However, in MD335 we found besides the known 45-nt pseudoexon, a longer 70-nt fragment, that is, the 45-nt fragment from MD130 extended at the 5′ side by 25 nt. The 3′ splice acceptor site contains at least two conserved 3′ AG dinucleotides, the more upstream being the predicted "natural" *Alu* exon and 70-nt downstream the corresponding 5′ GT splice site, which is identical to the pseudoexon 5′ site in MD130 [Meili et al., 2009]. Using minigene assays with COS1 cells that were transfected with corresponding splicing reporter plasmids, the c.164−712A>T mutation is responsible for exonization and inclusion of primarily the 70 nt antisense *Alu* sequence (see Fig. 1B).

In the following, the 5′ GT splice site was analyzed in more detail, as mutation c.164−712A>T located in a putative splicing silencer element might effect at the same time complementarity to U1 snRNA, and it was reported that extensive complementarity to U1 snRNA exerts to some extend a dominant effect for 5′ splice site selection [Roca et al., 2005]. A schematic representation of base pairing between the 5′ splice site of the pseudoexon and the U1 sequence is shown in Figure 2A. In an attempt to address this point and by taking into account that the 5′ splice site motif consists of nine partially conserved nucleotides at the exon–intron boundary, the last three nucleotides of the upstream exon and the first six nucleotides of the intron, we tested the two additional mutations c.164−714C>A and c.164−715T>A in our minigene assay. As shown in Figure 2B, mutation c.164–715T>A appeared to be even more efficient in splicing of the 70-bp pseudoexon compared to mutation c.164−712A>T. On the other hand, the minigene construct containing the c.164−714C>A alteration was similar to the wild-type control and did not lead to pseudoexon inclusion. In addition, a shorter band corresponding to insertion of the 45-bp pseudoexon was weakly detectable also for construct c.164−715T>A. In conclusion, changing positions +3 or +6 downstream of the pseudoexon not only improved complementary to U1 snRNA but also strengthened the 5′ splice site.

Reversion of the Splicing Defect and Restoration of *PTPS* Enzymatic Activity Using Antisense Therapy

In the following, we investigated three deep intronic changes c.84−322A>T, c.163+695_163+751del57, and c.164−712A>T, which are responsible for splicing defects and exonization in the *PTS* gene found in patients MD96, MD130, and MD335, respectively. Whereas the heterozygous mutation c.164−712A>T in patient MD335 was newly identified (plus mutation c.163+2T>G), the homozygous c.84−322A>T transversion in MD96 and the heterozygous deletion c.163+695_163+751del57 in

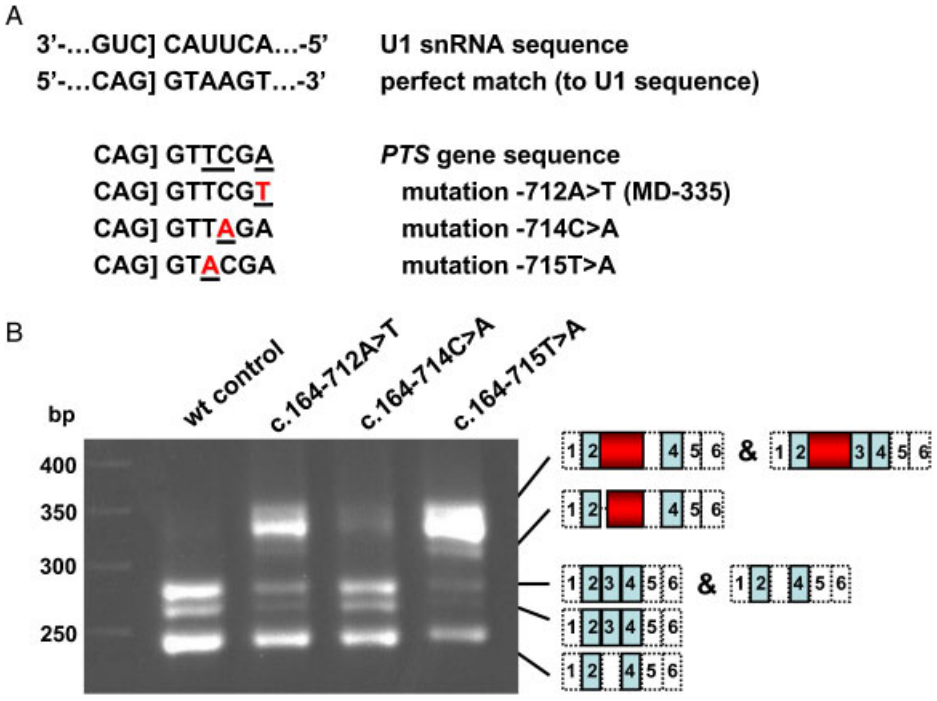

Figure 2. Result of the ex vivo splicing in the minigene assay using constructs with wild-type sequences, the mutation c.164−712A>T from patient MD355, and the changes c.164−714C>A and c.164−715T>A. **A:** Schematic representation of base pairing between the 5′ splice site of the pseudoexon and the U1 snRNA sequence, plus the different minigene constructions tested. The 5′ splice motive consists of nine partially conserved nucleotides at the exon–inton boundary, and differences between the *PTS* gene sequence and the "perfect match" to the U1 sequence are underlined; also underlined and in red/gray are the changes to match the "perfect" sequence. **B:** RT-PCR profile of the ex vivo splicing assay from the different minigene constructs. The mutations c.164−712A>T and c.164−715T>A produced in our assay an additional and very prominent upper band, which turns out to contain the 70-bp antisense *Alu* sequence with or without exon 3. Construct c.164−715T>A generated a shorter but very faint band corresponding the 45 bp pseudoexon. [Color figures can be viewed in the online issue, which is available at www.wiley.com/humanmutation.]

MD130 (plus c.393delA) were described previously, and lead to the insertion of a LINE-2 element in exon 1 and exonization of a shortened, 45-nt version, of the antisense *Alu* sequence in exon 2, respectively [Meili et al., 2009]. To determine if either the pathological insertions of a LINE-2 fragment in MD96, or the two variants of the antisense *Alu* in MD130 and MD335 can be suppressed to rescue PTPS activity in patients' fibroblasts, the possibility of redirecting transcript processing by AMOs was explored. AMOs were targeted to the 3′ (PTS-AMO1) and 5′ cryptic splice sites (PTS-AMO2 and PTS-AMO3) to block access of the splicing machinery to the pseudoexonic regions in the pre-mRNA. Because the mutation c.164−712A>T in MD335 leads to the use of the same 5′ splice donor site as for the mutation c.163+695_163+751del57 in MD130, the same AMO was used for treatment (PTS-AMO2). Fibroblasts were transfected with two different concentrations of AMOs 20 and 30 μM for a 24-hr period, followed by transcriptional profiling analysis. The results showed that the splicing process was restored in all three cases (Fig. 3), even when MD335 fibroblasts were transfected with AMO2 (MD130), which differ in a single nucleotide (data not shown). Correctly spliced mRNA was obtained 24 hr after transfection in a dose-dependent fashion. In all three cases, the upper band containing the intronic insertion disappeared even though the cells were cultured with cycloheximide to avoid mRNA degradation. The identity of the cDNA fragments obtained was confirmed by sequence analysis, and for MD130 we were able to confirm the presence of mutation c.393delA in heterozygous state after AMO treatment. When all three patient cells were transfected with a scrambled morpholino, the splicing process did neither influence nor rescue the erroneous splicing pattern (see Supp. Fig. S1).

A recent development of a new transporter structure that is thought to provide effective in vivo delivery of morpholino antisense oligomers into a wide variety of tissues are the Vivo-Morpholino complexes, conjugates of an octa-guanidine dendrimer covalently linked to the morpholino oligo [Li and Morcos, 2008]. In a set of parallel experiments we wanted to test such Vivo-Morpholinos to confirm whether the splicing correction is comparable to AMO treatment under cell culture conditions. As shown in Figure 4, the AMO transporter-conjugates VIVO-AMO1 and VIVO-AMO3 corrected the erroneous splicing in MD96 and MD335 cells, respectively. Due to the poor growth behavior of the primary dermal fibroblasts from MD130, we were not able to include results from this patient. In conclusion, we found no significant differences under cell culture conditions between the use of AMO and the transporter-conjugated Vivo-Morpholinos as the delivery reagent.

To test whether suppression of missplicing resulted not only in the production of a normal *PTS*-mRNA, but also in functional PTPS protein, we analyzed enzyme activity and recovery of the pterin profile. Patients' fibroblasts were treated with 30 μM of AMO during 48 and 72 hr, and activity levels were determined. As shown in Figure 5A, PTPS activity was rescued in all three fibroblast cell lines after AMO treatment for 48 and 72 hr. We observed recovery of the activity in the range of normal levels for primary dermal fibroblasts, which is between 0.4 and 1.6 μU/mg [Bonafe et al., 2001]. Although PTPS activity increased to control levels 48 hr after transfection, enzyme activities in all three cases were somewhat lowered 72 hr after treatment (Fig. 5A). Using the specific antibody SZ28 against PTPS protein [Elzaouk et al., 2004],

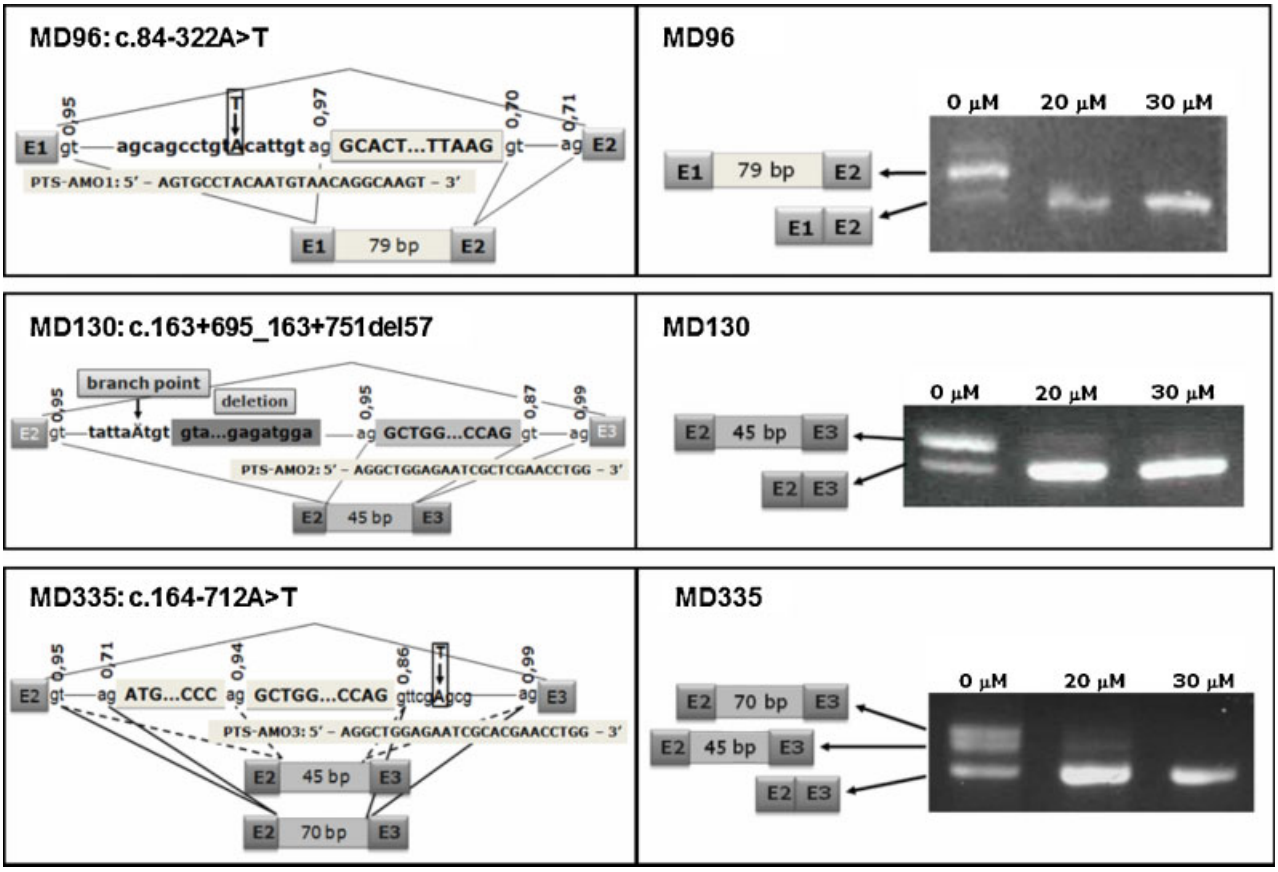

Figure 3. Splicing therapy using antisense AMOs to avoid pseudoexon inclusion in primary dermal fibroblast from PTPS-deficient patients. The left panels show the schematics of the splicing patterns with the regions of the *PTS* gene where the splicing mutations were found in patients MD96, MD130, and MD335. The numbers indicate the splicing scores calculated with BDGP software (http://www.fruitfly.org/). The sequence of the three different AMOs used are depicted. The right panels show transcriptional profiling analyses by conventional RT-PCR of fibroblasts derived from patients MD96, MD130, and MD335, treated (20 and 30 µM) or untreated (0 µM) with the corresponding AMOs (PTS-AMO1, PTS-AMO2, PTS-AMO3).

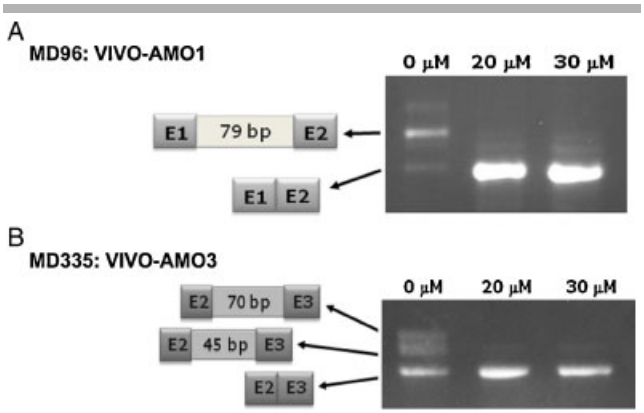

Figure 4. RT-PCR pattern of fibroblasts derived from patients MD96 (**A**) and MD335 (**B**) untreated (0 µM) and treated (20 µM and 30 µM) with two different concentrations of Vivo-Morpholinos (VIVO-AMOs). To identify the PCR fragments indicated, DNA sequence analysis was performed.

we were able to detect protein recovery in all three primary patients' cells after 48 hr of treatment in (Fig. 5B).

Quantification of pterin levels in the patients' fibroblasts was performed after cells were treated with 30 µM of the corresponding AMO. Because GTPCH is not expressed in dermal fibroblasts but can be induced upon cotreatment with TNF-α and INF-γ, AMO therapy was done simultaneously with cytokine stimulation [Bonafe et al., 2001]. After 48, 72, or 96 hr of in the presence of the AMOs, neopterin levels decreased and biopterin increased to variable degrees, depending on the cell line, but all fibroblast cells normalized their pterin profile in a time and cell-dependent manner (Table 1). The best recovery was obtained in cells from patient MD96 after 96 hr posttreatment and following two consecutive transfections. As mentioned above, MD96 is homozygous for the splicing mutation, whereas MD130 and MD335 are both carrying a second mutant allele that cannot be corrected by the pseudoexon exclusion approach. Therefore, it is not unexpected the AMO correction of cells from MD96 resulted in a better recovery due to this dosage effect.

Discussion

Extensive RNA-based diagnosing in addition to genomic DNA mutation analysis of human genetic disorders allows identification of several deep intronic mutations that may cause splicing mutations including exonization of pseudoexon sequences. In addition, treating patient's cells with nonsense-mediated mRNA decay (NMD) inhibitors and subsequent transcript profiling analysis allows comprehensive diagnosis and identification of these elusive mutations. Such a strategy not only improves genetic diagnosis but may also provide the rationale to tailor a specific genetic treatment.

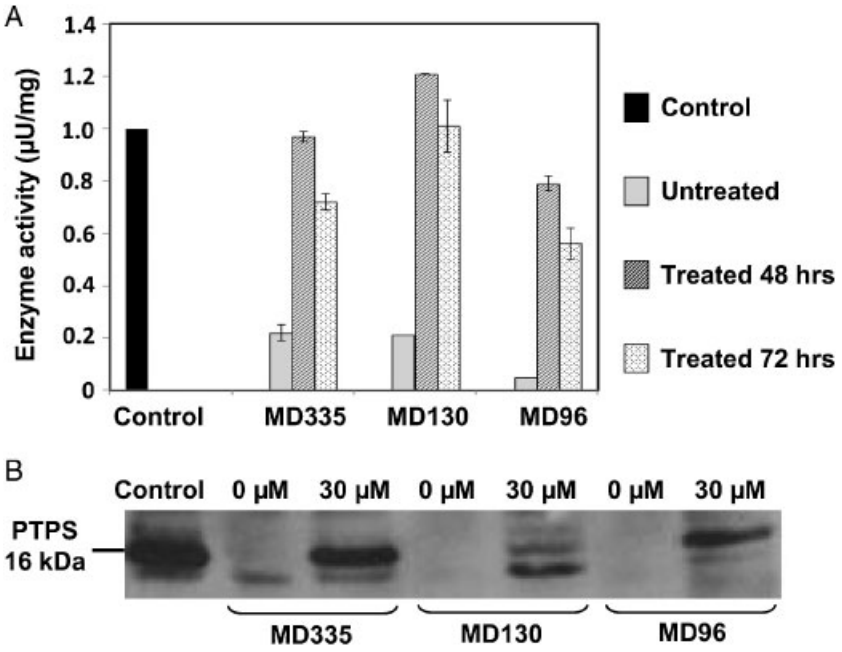

Figure 5. Restoration of PTPS enzyme activity and protein expression in primary patients' fibroblasts. **A:** Functional correction of PTPS activity after treatment. The activity was assayed in primary dermal fibroblasts derived from a healthy control subject and from patients MD96, MD130, and MD335, treated for 48 or 72 hr. **B:** PTPS protein expression in control and in MD96, MD130, and MD335-derived fibroblasts treated (30 μM) or untreated with corresponding AMOs.

Table 1. Neopterin and Biopterin Levels in Antisense AMO-Treated Fibroblasts Derived from Three Different PTPS-Deficient Patients

Patient	Time of treatment (hr)	Neopterin (pmol/mg)	Biopterin (pmol/mg)	Neopterin fold activation	Biopterin fold activation	N/B ratio
MD-96	0	281.16	0.40	–	–	703
	48	75.88	14.17	3.71	35.05	5.35
	72	57.84	32.91	1.31	2.32	1.76
	96	**15.61**	**26.86**	**3.71**	**0.82**	**0.58**
MD-130[a]	0	378.23	0.51	–	–	741.60
	48	**243.32**	**5.53**	**1.55**	**10.84**	**44.00**
MD-335	0	235.37	1.48	–	–	159.49
	48	123.23	8.98	1.91	6.09	13.72
	72	38.46	9.52	3.20	1.06	4.04
	96	**6.50**	**2.09**	**5.92**	**0.22**	**3.12**
Control[b]	48–72	11.42	45.85	–	–	0.25
Patient (U)[c]	Untreated	45 nmol/l	0 nmol/l	–	–	–
	Treated	34 nmol/l	25 nmol/l	–	–	1.36

[a]The assay was performed only 48 hr posttransfection due to the poor growth behavior of the primary fibroblasts.
[b]Neopterin and biopterin in control fibroblasts.
[c]Neopterin and biopterin in patient's urine before and 24 hr after an oral loading test with 20 mg/kg synthetic BH4. Neopterin and biopterin in control urine are 5–22 mmol/l and 4–10 mmol/l, respectively; ratio 1.25–2.2 [Blau et al., 2003].

Transposable sequences are prone to have nucleotide changes activating the creation of new exons in the genome [Vorechovsky, 2010]. These sequences in addition to playing an essential role in gene evolution are associated to Mendelian diseases, and to date, several examples have been described with pathological effect [Dhir and Buratti, 2010]. In the *PTS* gene two different changes have been reported previously [Meili et al., 2009], and herein we present one additional case of pseudoexon inclusion in intron 2. All three mutations, which are deep intronic DNA alterations, activate the insertion of transposable elements present in the *PTS* gene, an antisense *Alu* sequence in exon 2 or a LINE-2 in exon 1. Knowing that pseudoexon sequences are present in an intron, one should take into account that deep intronic alterations in such a region have the potential to be pathogenic mutations, and they must be included in the genetic diagnosis of the disease.

An interesting observation of the mutation analysis is the identification of two different deep intronic mutations, c.163+695_163+751del57 (MD130) and c.164−712A>T (MD335), resulting in exonization of the same peudoexon but with different 3′ splice sites, resulting in inclusion of either a 45- or 70-bp fragment. As discussed before, the deletion mutation introduced a favorable branch point sequence in the optimal distance from the pseudoexon 3′ splice site, and at the same time removed an upstream AG dinucleotide required for the 3′ splice site repression on normal alleles [Meili et al., 2009]. Furthermore, this intronic deletion lacks the most upstream pseudoexon 3′ splice site, thus

leading to the shorter 45-bp pseudoexon insertion. A different mechanism is responsible for exoniziation of the same *Alu*Sq sequence by the intronic mutation c.164−712A>T. Here a change at position +6, but also at position +3 as shown by in vitro minigene assay with mutation c.164−715T>A, seems to strengthen the pseudoexon 5′ splice site, thus improving complementarity to U1 snRNA (see Fig. 2). Both mutations, c.164−712A>T and c.164−715T>A, predominantly activate the inclusion of the 70-bp pseudoexon and to a much lesser extent inclusion of the 45-bp pseudoexon even though this internal 3′ splice site has a higher splice score than the selected one. It is clear that the consensus motifs are by themselves insufficient to completely define the splice site, and other parameters such as splicing regulatory-elements may modulate the alternative splicing process, determining which 3′ splice site should be used [Andresen and Krainer, 2009].

Considering the increasing knowledge at the molecular level of the diseases, treatment is moving toward an increasing personalized therapy. It is well known that this kind of mutation represents an excellent example for mutation-specific therapies. Recently, antisense therapy has been applied successfully in several inherited metabolic disease cellular models [Dhir and Buratti, 2010; Perez et al., 2010] and in view of this, we report new examples of successful rescue of an aberrant splicing process by pseudoexon insertions. Specifically, we could demonstrate in cells derived from three individual PTPS deficient patients carrying three different mutations that two short antisense oligonucleotides can suppress the aberrant splicing process of the *PTS* pre-mRNA. Moreover, normal mRNA processing and recovery of the PTPS enzyme activity was achieved. Although the amount of PTPS protein was not comparable to control levels based on Western blot quantification, enzyme activity was in the normal range even for the compound heterozygous PTPS-deficient cells from MD335 and MD130. In any case, the results suggest that moderate increases in PTPS enzyme are sufficient to achieve a therapeutic effect in a recessive disorder, as has been described in other genetic disorders such as methylmalonic aciduria, propionic acidemia, and phosphomannomutase deficiency [Perez et al., 2009; Ugarte et al., 2007; Vega et al., 2009]. This finding has also been described in the PCCA knock-out animal model treated with a liver-specific transgene, which allowed prolonged survival of the animal even though PCCA protein activity was rather low [Miyazaki et al., 2001].

The recovery appears to be sequence-, dose-, as well as cell-specific. The fact that pterin levels after treatment are different in the three individual primary dermal fibroblasts may reflect subtle variations in the levels of pseudoexon insertion and could also contribute to patient's phenotype. It can be envisaged that some levels of normal transcript might exist depending on the deep intronic mutations as described in patient MD96 [Meili et al., 2009], but also for other disorders [Gurvich et al., 2008], resulting in a milder phenotype. It is worth noting that the best functional recovery was obtained after extended treatment for 96 hr in either cell derived from MD96 and from MD335, whereas the result obtained in the severely effected patient MD130-derived cells was less efficient. In any case, in all three PTPS fibroblasts, the neopterin/biopterin ratio was improved significantly, even though the pterin profile was not completely normalized.

All functional results presented here establish a proof of principle for the application of AMO treatment in the PTPS-affected patients as has been demonstrated in other inherited metabolic disorders [Perez et al., 2010]. In any case, the clinical exploitation of antisense therapy as well as interfering-based therapies will depend on safe and effective in vivo delivery to target tissue that should be assayed using animal models, such as mice or zebra fish, to check the biodistribution of antisense oligonucleotides [Alter et al., 2006; Madsen et al., 2008]. An Interesting approach would also be the generation of induced pluripotent stem (iPS) cells as they will provide a valuable experimental platform with potential value for cell therapy application [Raya et al., 2009].

In addition to all other complications in developing a new drug, within neurological disorders one must consider the blood–brain barrier (BBB). Interesting, attempts to cross the barrier by large polar structures have been reported with successful recovery of the function assessed [Aouadi et al., 2009; Ivanova et al., 2008; Kumar et al., 2007]. Using polymeric nanoparticles, as has been used in the present studies and also in Li and Morcos [2008], cell-penetrating peptides, or PEGylated immunoliposomes [Pardridge, 2010] to encapsulate the nucleic acid cargo, a modest delivery of siRNA into the adult mice brain [Li and Morcos, 2008] has been achieved as well as phosphorothiolate oligonucleotide by intravenous administration in an Alzheimer's model [Banks, 2008; Banks et al., 2001]. These encouraging results should stimulate investigations on the development of a safe and effective vehicle to deliver antisense therapeutic molecules.

In conclusion, this work represents an example of a genetic splicing disorder with the potential to be treated with antisense therapy. Furthermore, the future novel methods—such as, for instance, the use of Vivo-Morpholinos, which show great promise for optimal delivery of antisense drugs to the brain or other organs—should be investigated in an attempt to improve splice correction therapy for a broad range of genetic disorders.

Acknowledgments

We thank N. Blau for valuable discussion.

References

Aartsma-Rus A, van Vliet L, Hirschi M, Janson AA, Heemskerk H, de Winter CL, de Kimpe S, van Deutekom JC, t Hoen PA, van Ommen GJ. 2009. Guidelines for antisense oligonucleotide design and insight into splice-modulating mechanisms. Mol Ther 17:548–553.

Alter J, Lou F, Rabinowitz A, Yin H, Rosenfeld J, Wilton SD, Partridge TA, Lu QL. 2006. Systemic delivery of morpholino oligonucleotide restores dystrophin expression bodywide and improves dystrophic pathology. Nat Med 12:175–177.

Andresen B, Krainer AR. 2009. When the genetic code is not enough. How sequence variations can affect pre-mRNA splicing and cause (complex) disease. In: Al-Chalabi A, Alamassy L, editors. Genetics of complex human diseases. Cold Spring Harbor, NY: Cold Spring Harbor Laboratory Press. p 165–182.

Aouadi M, Tesz GJ, Nicoloro SM, Wang M, Chouinard M, Soto E, Ostroff GR, Czech MP. 2009. Orally delivered siRNA targeting macrophage Map4k4 suppresses systemic inflammation. Nature 458:1180–1184.

Banks WA. 2008. Developing drugs that can cross the blood–brain barrier: applications to Alzheimer's disease. BMC Neurosci 9(Suppl 3):S2.

Banks WA, Farr SA, Butt W, Kumar VB, Franko MW, Morley JE. 2001. Delivery across the blood–brain barrier of antisense directed against amyloid beta: reversal of learning and memory deficits in mice overexpressing amyloid precursor protein. J Pharmacol Exp Ther 297:1113–1121.

Blau N, Bonafe L, Blaskovics ME. 2002. Disorders of phenylalanine and tetrahydrobiopterin metabolism. In: Blau N, Duran M, Blaskovics ME, Gibson KM, editors. Physician's guide to the laboratory diagnosis of metabolic diseases. 2nd ed. Berlin: Springer. p 89–106.

Blau N, Duran M, Blaskovics ME, Gibson KM. 2003. Physician's guide to the laboratory diagnosis of metabolic diseases. 2nd ed. Berlin: Springer.

Bonafe L, Thöny B, Leimbacher W, Kierat L, Blau N. 2001. Diagnosis of dopa-responsive dystonia and other tetrahydrobiopterin disorders by the study of biopterin metabolism in fibroblasts. Clin Chem 47:477–485.

Dhir A, Buratti E. 2010. Alternative splicing: role of pseudoexons in human disease and potential therapeutic strategies. FEBS J 277:841–855.

Elzaouk L, Laufs S, Heerklotz D, Leimbacher W, Blau N, Resibois A, Thony B. 2004. Nuclear localization of tetrahydrobiopterin biosynthetic enzymes. Biochim Biophys Acta 1670:56–68.

Friedman G, Goldschmidt N, Friedlander Y, Ben-Yehuda A, Selhub J, Babaey S, Mendel M, Kidron M, Bar-On H. 1999a. A common mutation A1298C in human methylenetetrahydrofolate reductase gene: association with plasma total homocysteine and folate concentrations. J Nutr 129:1656–1661.

Friedman KJ, Kole J, Cohn JA, Knowles MR, Silverman LM, Kole R. 1999b. Correction of aberrant splicing of the cystic fibrosis transmembrane conductance regulator (CFTR) gene by antisense oligonucleotides. J Biol Chem 274: 36193–36199.

Gurvich OL, Tuohy TM, Howard MT, Finkel RS, Medne L, Anderson CB, Weiss RB, Wilton SD, Flanigan KM. 2008. DMD pseudoexon mutations: splicing efficiency, phenotype, and potential therapy. Ann Neurol 63:81–89.

Ivanova GD, Arzumanov A, Abes R, Yin H, Wood MJ, Lebleu B, Gait MJ. 2008. Improved cell–penetrating peptide–PNA conjugates for splicing redirection in HeLa cells and exon skipping in mdx mouse muscle. Nucleic Acids Res 36: 6418–6428.

Jaggi L, Zurfluh MR, Schuler A, Ponzone A, Porta F, Fiori L, Giovannini M, Santer R, Hoffmann GF, Ibel H, Wendel U, Ballhausen D, Baumgartner MR, Blau N. 2008. Outcome and long-term follow-up of 36 patients with tetrahydrobiopterin deficiency. Mol Genet Metab 93:295–305.

Kinali M, Arechavala-Gomeza V, Feng L, Cirak S, Hunt D, Adkin C, Guglieri M, Ashton E, Abbs S, Nihoyannopoulos P, Garralda ME, Rutherford M, McCulley C, Popplewell L, Graham IR, Dickson G, Wood MJ, Wells DJ, Wilton SD, Kole R, Straub V, Bushby K, Sewry C, Morgan JE, Muntoni F. 2009. Local restoration of dystrophin expression with the morpholino oligomer AVI-4658 in Duchenne muscular dystrophy: a single-blind, placebo-controlled, dose-escalation, proof-of-concept study. Lancet Neurol 8:918–928.

Kumar P, Wu H, McBride JL, Jung KE, Kim MH, Davidson BL, Lee SK, Shankar P, Manjunath N. 2007. Transvascular delivery of small interfering RNA to the central nervous system. Nature 448:39–43.

Lacerra G, Sierakowska H, Carestia C, Fucharoen S, Summerton J, Weller D, Kole R. 2000. Restoration of hemoglobin A synthesis in erythroid cells from peripheral blood of thalassemic patients. Proc Natl Acad Sci USA 97:9591–9596.

Li YF, Morcos PA. 2008. Design and synthesis of dendritic molecular transporter that achieves efficient in vivo delivery of morpholino antisense oligo. Bioconjug Chem 19:1464–1470.

Longo N. 2009. Disorders of biopterin metabolism. J Inherit Metab Dis 32:333–342.

Madsen EC, Morcos PA, Mendelsohn BA, Gitlin JD. 2008. In vivo correction of a Menkes disease model using antisense oligonucleotides. Proc Natl Acad Sci USA 105:3909–3914.

Meili D, Kralovicova J, Zagalak J, Bonafe L, Fiori L, Blau N, Thony B, Vorechovsky I. 2009. Disease-causing mutations improving the branch site and polypyrimidine tract: pseudoexon activation of LINE-2 and antisense Alu lacking the poly(T)-tail. Hum Mutat 30:823–831.

Miyazaki T, Ohura T, Kobayashi M, Shigematsu Y, Yamaguchi S, Suzuki Y, Hata I, Aoki Y, Yang X, Minjares C, Haruta I, Uto H, Ito Y, Müller U. 2001. Fatal propionic acidemia in mice lacking propionyl-CoA carboxylase and its rescue by postnatal, liver-specific supplementation via a transgene. J Biol Chem 276:35995–35999.

Pardridge WM. 2010. Preparation of Trojan horse liposomes (THLs) for gene transfer across the blood-brain barrier. Cold Spring Harb Protoc 2010:pdb prot5407.

Perez B, Rincon A, Jorge-Finnigan A, Richard E, Merinero B, Ugarte M, Desviat LR. 2009. Pseudoexon exclusion by antisense therapy in methylmalonic aciduria (MMAuria). Hum Mutat 30:1676–1682.

Perez B, Rodriguez-Pascau L, Vilageliu L, Grinberg D, Ugarte M, Desviat LR. 2010. Present and future of antisense therapy for splicing modulation in inherited metabolic disease. J Inherit Metab Dis 33:397–403.

Raya A, Rodriguez-Piza I, Guenechea G, Vassena R, Navarro S, Barrero MJ, Consiglio A, Castella M, Rio P, Sleep E, González F, Tiscornia G, Garreta E, Aasen T, Veiga A, Verma IM, Surrallés J, Bueren J, Izpisúa Belmonte JC. 2009. Disease-corrected haematopoietic progenitors from Fanconi anaemia induced pluripotent stem cells. Nature 460:53–59.

Roca X, Sachidanandam R, Krainer AR. 2005. Determinants of the inherent strength of human 5′ splice sites. RNA 11:683–698.

Shintaku H. 2002. Disorders of tetrahydrobiopterin metabolism and their treatment. Curr Drug Metab 3:123–131.

Suwanmanee T, Sierakowska H, Fucharoen S, Kole R. 2002. Repair of a splicing defect in erythroid cells from patients with beta-thalassemia/HbE disorder. Mol Ther 6: 718–726.

Thöny B, Blau N. 2006. Mutations in the BH4-metabolizing genes GTP cyclohydrolase I, 6-pyruvoyl-tetrahydropterin synthase, sepiapterin reductase, carbinolamine-4a-dehydratase, and dihydropteridine reductase. Hum Mutat 27: 870–878.

Ugarte M, Aguado C, Desviat LR, Sanchez-Alcudia R, Rincon A, Perez B. 2007. Propionic and methylmalonic acidemia: antisense therapeutics for intronic variations causing aberrantly spliced messenger RNA. Am J Hum Genet 81

van Deutekom JC, Janson AA, Ginjaar IB, Frankhuizen WS, Aartsma-Rus A, Bremmer-Bout M, den Dunnen JT, Koop K, van der Kooi AJ, Goemans NM, de Kimpe SJ, Ekhart PF, Venneker EH, Platenburg GJ, Verschuuren JJ, van Ommen GJ. 2007. Local dystrophin restoration with antisense oligonucleotide PRO051. N Engl J Med 357:2677–2686.

Vega AI, Perez-Cerda C, Desviat LR, Matthijs G, Ugarte M, Perez B. 2009. Functional analysis of three splicing mutations identified in the PMM2 gene: toward a new therapy for congenital disorder of glycosylation type Ia. Hum Mutat 30: 795–803.

Vorechovsky I. 2010. Transposable elements in disease-associated cryptic exons. Hum Genet 127:135–154.

Werner ER, Blau NBT. 2011. Tetrahydrobiopterin: biochemistry and pathophysiology. Biochem J (in press).

Werner ER, Werner-Felmayer G, Wachter H. 1996. High-performance liquid chromatographic methods for the quantification of tetrahydrobiopterin biosynthetic enzymes. J Chromatogr B Biomed Appl 684:51–58.

Wood M, Yin H, McClorey G. 2007. Modulating the expression of disease genes with RNA-based therapy. PLoS Genet 3:e109.

Wood MJ, Gait MJ, Yin H. 2010. RNA-targeted splice-correction therapy for neuromuscular disease. Brain 133(Pt 4):957–972.

8. Dobson, C.M., Wai, T., Leclerc, D., Wilson, A., Wu, X., Dore, C., Hudson, T., Rosenblatt, D.S. and Gravel, R.A. (2002) Identification of the gene responsible for the cblA complementation group of vitamin B12-responsive methylmalonic acidemia based on analysis of prokaryotic gene arrangements. *Proc. Natl Acad. Sci. USA*, **99**, 15554–15559.
9. Schubert, H.L. and Hill, C.P. (2006) Structure of ATP-Bound Human ATP:Cobalamin Adenosyltransferase. *Biochemistry*, **45**, 15188–15196.
10. Fenton, W.A., Gravel, R.A. and Rosenberg, L.E. (2001) In Scriver, C.R., Beaudet, A.L., Sly, W. and Valle, D. (eds), *The Metabolic and Molecular Bases of Inherited Disease*. McGraw-Hill, New York, pp. 2165–2190.
11. Gregersen, N., Bross, P., Vang, S. and Christensen, J.H. (2006) Protein misfolding and human disease. *Annu. Rev. Genomics. Hum. Genet.*, **7**, 103–124.
12. Martinez, A., Calvo, A.C., Teigen, K. and Pey, A.L. (2008) Rescuing proteins of low kinetic stability by chaperones and natural ligands phenylketonuria, a case study. *Prog. Mol. Biol. Transl. Sci.*, **83**, 89–134.
13. Cheung, J.C. and Deber, C.M. (2008) Misfolding of the cystic fibrosis transmembrane conductance regulator and disease. *Biochemistry*, **47**, 1465–1473.
14. Loo, T.W. and Clarke, D.M. (2007) Chemical and pharmacological chaperones as new therapeutic agents. *Expert Rev. Mol. Med.*, **9**, 1–18.
15. Conn, P.M. and Janovick, J.A. (2009) Drug development and the cellular quality control system. *Trends Pharmacol. Sci.*, **30**, 228–233.
16. Bonnefont, J.P., Bastin, J., Laforet, P., Aubey, F., Mogenet, A., Romano, S., Ricquier, D., Gobin-Limballe, S., Vassault, A., Behin, A. *et al.* (2010) Long-term follow-up of bezafibrate treatment in patients with the myopathic form of carnitine palmitoyltransferase 2 deficiency. *Clin. Pharmacol. Therap.*, **88**, 101–108.
17. Parenti, G., Zuppaldi, A., Gabriela Pittis, M., Rosaria Tuzzi, M., Annunziata, I., Meroni, G., Porto, C., Donaudy, F., Rossi, B., Rossi, M. *et al.* (2007) Pharmacological enhancement of mutated alpha-glucosidase activity in fibroblasts from patients with Pompe disease. *Mol. Ther.*, **15**, 508–514.
18. Benjamin, E.R., Khanna, R., Schilling, A., Flanagan, J.J., Pellegrino, L.J., Brignol, N., Lun, Y., Guillen, D., Ranes, B.E., Frascella, M. *et al.* (2012) Co-administration with the pharmacological chaperone AT1001 increases recombinant human alpha-galactosidase A tissue uptake and improves substrate reduction in Fabry mice. *Mol. Ther.*, **20**, 717–726.
19. Santos-Sierra, S., Kirchmair, J., Perna, A.M., Reiss, D., Kemter, K., Roschinger, W., Glossmann, H., Gersting, S.W., Muntau, A.C., Wolber, G. *et al.* (2012) Novel pharmacological chaperones that correct phenylketonuria in mice. *Hum. Mol. Genet.*, **21**, 1877–1887.
20. Jorge-Finnigan, A., Aguado, C., Sanchez-Alcudia, R., Abia, D., Richard, E., Merinero, B., Gamez, A., Banerjee, R., Desviat, L.R., Ugarte, M. *et al.* (2010) Functional and structural analysis of five mutations identified in methylmalonic aciduria cblB type. *Hum. Mutat.*, **31**, 1033–1042.
21. Cooper, A. and McAuley-Hecht, K.E. (1993) Microcalorimetry and the molecular recognition of peptides and proteins. *Philos. Trans. R. Soc. A*, **345**, 23–35.
22. Zhang, J., Dobson, C.M., Wu, X., Lerner-Ellis, J., Rosenblatt, D.S. and Gravel, R.A. (2006) Impact of cblB mutations on the function of ATP:cob(I)alamin adenosyltransferase in disorders of vitamin B12 metabolism. *Mol. Genet. Metab.*, **87**, 315–322.
23. Valenzano, K.J., Khanna, R., Powe, A.C., Boyd, R., Lee, G., Flanagan, J.J. and Benjamin, E.R. (2011) Identification and characterization of pharmacological chaperones to correct enzyme deficiencies in lysosomal storage disorders. *Assay. Drug Dev. Technol.*, **9**, 213–235.
24. Grosdidier, A., Zoete, V. and Michielin, O. (2011) SwissDock, a protein-small molecule docking web service based on EADock DSS. *Nucleic Acids Res.*, **39**, W270–W277.
25. Grosdidier, A., Zoete, V. and Michielin, O. (2011) Fast docking using the CHARMM force field with EADock DSS. *J. Comput. Chem.*, **32**, 2149–2159.
26. Grosdidier, A., Zoete, V. and Michielin, O. (2007) EADock: docking of small molecules into protein active sites with a multiobjective evolutionary optimization. *Proteins*, **67**, 1010–1025.
27. Wong, E. and Cuervo, A.M. Integration of clearance mechanisms: the proteasome and autophagy. *Cold Spring Harbor Perspect. Biol.*, **2**, a006734.
28. Calvo, A.C., Scherer, T., Pey, A.L., Ying, M., Winge, I., McKinney, J., Haavik, J., Thony, B. and Martinez, A. (2010) Effect of pharmacological chaperones on brain tyrosine hydroxylase and tryptophan hydroxylase 2. *J. Neurochem.*, **114**, 853–863.
29. Lee, W.C., Kang, D., Causevic, E., Herdt, A.R., Eckman, E.A. and Eckman, C.B. (2010) Molecular characterization of mutations that cause globoid cell leukodystrophy and pharmacological rescue using small molecule chemical chaperones. *J. Neurosci.*, **30**, 5489–5497.
30. Khanna, R., Benjamin, E., Pellegrino, L., Schilling, A., Rigat, B., Soska, R., Nafar, H., Ranes, B., Feng, J., Lun, Y. *et al.* (2010) The pharmacological chaperone isofagomine increases the activity of the Gaucher disease L444P mutant form of beta-glucosidase. *The FEBS J.*, **277**, 1618–1638.
31. Benjamin, E.R., Flanagan, J.J., Schilling, A., Chang, H.H., Agarwal, L., Katz, E., Wu, X., Pine, C., Wustman, B., Desnick, R.J. *et al.* (2009) The pharmacological chaperone 1-deoxygalactonojirimycin increases alpha-galactosidase A levels in Fabry patient cell lines. *J. Inherit. Metab. Dis.*, **32**, 424–440.
32. Fan, C. and Bobik, T.A. (2008) Functional characterization and mutation analysis of human ATP:Cob(I)alamin adenosyltransferase. *Biochemistry*, **47**, 2806–2813.
33. Klotz, U. (2007) The role of pharmacogenetics in the metabolism of antiepileptic drugs: pharmacokinetic and therapeutic implications. *Clin. Pharmacokinet.*, **46**, 271–279.
34. Dawood, S. and Leyland-Jones, B. (2009) Pharmacology and pharmacogenetics of chemotherapeutic agents. *Cancer Invest.*, **27**, 482–488.
35. Ballhausen, D., Mittaz, L., Boulat, O., Bonafe, L. and Braissant, O. (2009) Evidence for catabolic pathway of propionate metabolism in CNS: expression pattern of methylmalonyl-CoA mutase and propionyl-CoA carboxylase alpha-subunit in developing and adult rat brain. *Neuroscience*, **164**, 578–587.
36. Leal, N.A., Olteanu, H., Banerjee, R. and Bobik, T.A. (2004) Human ATP:Cob(I)alamin adenosyltransferase and its interaction with methionine synthase reductase. *J. Biol. Chem.*, **279**, 47536–47542.
37. Niesen, F.H., Berglund, H. and Vedadi, M. (2007) The use of differential scanning fluorimetry to detect ligand interactions that promote protein stability. *Nat. Protocols*, **2**, 2212–2221.
38. Johnson, C.L., Pechonick, E., Park, S.D., Havemann, G.D., Leal, N.A. and Bobik, T.A. (2001) Functional genomic, biochemical, and genetic characterization of the Salmonella pduO gene, an ATP:cob(I)alamin adenosyltransferase gene. *J. Bacteriol.*, **183**, 1577–1584.
39. Perez-Cerda, C., Merinero, B., Sanz, P., Jimenez, A., Garcia, M.J., Urbon, A., Diaz Recasens, J., Ramos, C., Ayuso, C. and Ugarte, M. (1989) Successful first trimester diagnosis in a pregnancy at risk for propionic acidaemia. *J. Inherit. Metab. Dis.*, **12**(Suppl. 2), 274–276.